

~~CLASSIFIED~~

AD 287 406

*Reproduced
by the*

SERVICES TECHNICAL INFORMATION AGENCY
ARLINGTON HALL STATION
ARLINGTON, VA, VIRGINIA



~~UNCLASSIFIED~~

Best Available Copy

NOTICE: When government or other drawings, specifications or other data are used for any purpose other than in connection with a definitely related government procurement operation, the U. S. Government thereby incurs no responsibility, nor any obligation whatsoever; and the fact that the Government may have formulated, furnished, or in any way supplied the said drawings, specifications, or other data is not to be regarded by implication or otherwise as in any manner licensing the holder or any other person or corporation, or conveying any rights or permission to manufacture, use or sell any patented invention that may in any way be related thereto.

287 406

287 406



Research Report

**Infrared Absorption by Carbon Dioxide, Water Vapor,
and Minor Atmospheric Constituents**

Best Available Copy

**Best
Available
Copy**



Research Report

Infrared Absorption by Carbon Dioxide, Water Vapor, and Minor Atmospheric Constituents

**DARRELL E. BURCH, DAVID GRYVNAK,
EDGAR B. SINGLETON, WILBUR L. FRANCE,
AND DUDLEY WILLIAMS
OHIO STATE UNIVERSITY
CONTRACT AF 19(604)-2633**

OPTICAL PHYSICS LABORATORY PROJECT 1960

AIR FORCE CAMBRIDGE RESEARCH LABORATORIES, OFFICE OF AEROSPACE RESEARCH, UNITED STATES AIR FORCE, FORT RUSSELL, ALABAMA

PREFACE

In 1955 GRL published Geophysical Research Papers No. 40, which has appeared originally as an Ohio State University contract report, to make a very useful study available to a wider audience. This report contained the results by J. N. Howard, D. E. Burch, and D. Williams at the Ohio State University of their studies on long path length infrared absorption of water vapor and carbon dioxide. This report was almost a unique source for this type of data and was and still is in great demand.

Shortly after that time Dr. Howard left the Ohio State group, but Dr. Burch and others continued these infrared studies, extending them to other atmospheric constituents such as N_2O , CH_4 , and CO and to smaller concentrations and lower pressure conditions more appropriate to higher altitudes. In addition part of the above work was repeated with better spectral resolution. The results of this work under contract AF19(604)-2633 with the Ohio State University were brought out in three contract reports: AFCRL-TN-60-674, AFCRL 255, and AFCRL 412. The demand for these reports has exhausted the supply. They are now being published as a single paper in the AFCRL Research Report series for wider dissemination.

ABSTRACT

This report presents results of studies concerned with the absorption of infrared radiation by various atmospheric gases. It places under one cover three previously published contractor reports on (1) absorption by nitrous oxide, carbon monoxide, and methane; (2) absorption by carbon dioxide, and (3) absorption by water vapor and nitrous oxide.

CONTENTS

	<u>Page</u>
A Absorption by Nitrous Oxide, Carbon Monoxide and Methane	1
B Absorption by Chlorine Dioxide	131
C Absorption by Water Vapor and Nitrous Oxide	147

PART A

**ABSORPTION BY NITROUS OXIDE, CARBON MONOXIDE
AND METHANE**

by

Darrell E. Curch and Dudley Williams

CONTENTS-PART A

	<u>Page</u>
LIST OF FIGURES	
List of Figures	vii
I. INTRODUCTION	1
II. THEORY	4
A. LORENTZIAN LINES	5
B. ABSORPTION BANDS	9
C. BAND IDENTITIES	12
III. EXPERIMENTAL METHODS	13
A. SPECTROGRAPHS, ABSORPTION CELLS, AND GAS-HANDLING EQUIPMENT	13
B. MEASUREMENT OF TOTAL ABSORPTION	12
C. ERRORS AND ACCURACY	16
D. UNITS	20
E. DETERMINATION OF SELF-RESCAINTING COEFFICIENTS	20
IV. TREATMENT OF DATA	24
V. EXPERIMENTAL RESULTS FOR THE 2224 cm^{-1} H_2O BAND	26
A. ABSORPTION CURVES	26
B. TOTAL ABSORPTION AS A FUNCTION OF ABSORBER CONCENTRATION AND EQUIVALENT PRESSURE	30
C. BAND INTENSITY	42
D. EMPIRICAL EQUATIONS: LIMITATIONS	34
E. COMPARISON OF RESULTS WITH THE PREDICTIONS BASED ON ELIASZER BAND MODEL	48
F. FLUORIDE TESTS OF ELIASZER MODEL: ABSORPTION AT P-MAX. AND P-MAX.	52

CONTENTS (CONT'D)-PART A

	Page
VI. THE FUNDAMENTAL AND FIRST OVERTONE BANDS OF CARBON MONOXIDE	61
A. THE 2143 cm^{-1} CO BANDS	61
B. THE 4260 cm^{-1} CO BAND	83
VII. THE 3020 , 1306 , AND 1550 cm^{-1} CH_4 BANDS	91
VIII. SUMMARY	113
BIBLIOGRAPHY	143
APPENDIX I. ADSORPTION EFFECTS	145

LIST OF TABLES-PART A

<u>Table No.</u>		<u>Page</u>
1	Materials	115
2	Self-Broadening Coefficients for Minor Atmospheric Gases	116
3	Data for the 2224 cm^{-1} N_2O Band	117
4	Data for the 2143 cm^{-1} CO Band	124
5	Data for the 4260 cm^{-1} CO Band	130
6	Data for the CH_4 Bands	132
7	Summary of Empirical Constants	141
8	Summary of Band Intensities	142

LIST OF FIGURES-PART A

Figure No.		Page
1	Two views of the Perkin-Elmer Model 521 spectrometer with dual long-path cells and gas-handling system.	15
2	Design of short absorption cells.	17
3	The self-broadening coefficient b for the 2224 cm^{-1} H_2O band.	22
4	Spectra of the 2224 cm^{-1} H_2O band.	27
5	Spectra of the 2224 cm^{-1} H_2O band.	29
6	Spectra of the 2224 cm^{-1} H_2O band.	31
7	Spectra of the 2224 cm^{-1} H_2O band.	31
8	Spectra of the 2224 cm^{-1} H_2O band.	32
9	Spectra of the 2224 cm^{-1} H_2O band.	33
10	Spectra of the 2224 cm^{-1} H_2O band.	34
11	Spectra of the 2224 cm^{-1} H_2O band.	35
12	The total absorption of the 2224 cm^{-1} H_2O band versus equivalent pressure for samples having constant values of absorber concentration.	37
13	The total absorption of the 2224 cm^{-1} H_2O band versus equivalent pressure for samples whose values of absorber concentration are proportional to the equivalent pressure.	39
14	The total absorption of the 2224 cm^{-1} H_2O band versus absorber concentration.	41

LIST OF FIGURES-PART A

<u>Figure No.</u>		<u>Page</u>
1	Two views of the Perkin-Elmer Model 21 spectrometer with dual long-path cells and gas-handling system.	14
2	Design of short absorption cells.	17
3	The self-broadening coefficient B for the 2224 cm^{-1} H_2O band.	22
4	Spectra of the 2224 cm^{-1} H_2O band.	27
5	Spectra of the 2224 cm^{-1} H_2O band.	29
6	Spectra of the 2224 cm^{-1} H_2O band.	30
7	Spectra of the 2224 cm^{-1} H_2O band.	31
8	Spectra of the 2224 cm^{-1} H_2O band.	32
9	Spectra of the 2224 cm^{-1} H_2O band.	33
10	Spectra of the 2224 cm^{-1} H_2O band.	34
11	Spectra of the 2224 cm^{-1} H_2O band.	35
12	The total absorption of the 2224 cm^{-1} H_2O band versus equivalent pressure for samples having constant values of absorber concentration.	37
13	The total absorption of the 2224 cm^{-1} H_2O band versus equivalent pressure for samples whose values of absorber concentration are proportional to the equivalent pressure.	39
14	The total absorption of the 2224 cm^{-1} H_2O band versus absorber concentration.	41

Figure No.	LIST OF FIGURES (Cont'd.)-1 RTA	Page
15	The total absorption of the 2224 cm^{-1} H_2O band versus wP_g .	52
16	The total absorption of the 2224 cm^{-1} H_2O band versus wP_g .	53
17	The percent absorption at 2240 cm^{-1} versus equivalent pressure for samples having constant values of absorber concentration.	53
18	The percent absorption at 2240 cm^{-1} versus equivalent pressure for samples whose values of absorber concentration are proportional to the equivalent pressure.	54
19	The percent absorption at 2240 cm^{-1} versus wP_g .	55
20	The percent absorption at 2213 cm^{-1} versus equivalent pressure for samples having constant values of absorber concentration.	57
21	The percent absorption at 2213 cm^{-1} versus equivalent pressure for samples whose values of absorber concentration are proportional to the equivalent pressure.	58
22	The percent absorption at 2213 cm^{-1} versus wP_g .	59
23	Spectra of the 2143 cm^{-1} CO band.	60
24	Spectra of the 2143 cm^{-1} CO band.	63
25	Spectra of the 2143 cm^{-1} CO band.	64
26	Spectra of the 2143 cm^{-1} CO band.	65
27	Spectra of the 2143 cm^{-1} CO band.	66
28	Spectra of the 2143 cm^{-1} CO band.	67
29	Spectra of the 2143 cm^{-1} CO band.	68
30	The total absorption of the 2143 cm^{-1} CO band versus equivalent pressure for samples having constant values of absorber concentration.	70

Figure No.

LIST OF FIGURES (CONT.)-PART A

Page

31	The total absorption of the 2143 cm^{-1} CO band versus equivalent pressure for samples whose values of absorber concentration are proportional to the equivalent pressure.	72
32	The total absorption of the 2143 cm^{-1} CO band versus absorber concentration.	73
33	The total absorption of the 2143 cm^{-1} CO band versus $\text{vP}_e^{0.6}$.	75
34	The total absorption of the 2143 cm^{-1} CO band versus vP_e .	77
35	The percent absorption at 2168 cm^{-1} versus equivalent pressure.	79
36	The percent absorption at 2168 cm^{-1} versus vP_e .	81
37	The percent absorption at 2116 cm^{-1} versus equivalent pressure.	82
38	The percent absorption at 2116 cm^{-1} versus vP_e .	84
39	Spectra of the 4260 cm^{-1} CO band.	85
40	Spectra of the 4260 cm^{-1} CO band.	86
41	The total absorption of the 4260 cm^{-1} CO band versus equivalent pressure.	88
42	The total absorption of the 4260 cm^{-1} CO band versus absorber concentration.	90
43	Spectra of the 3080 cm^{-1} CH_4 band.	92
44	Spectra of the 3080 cm^{-1} CH_4 band.	93
45	Spectra of the 3080 cm^{-1} CH_4 band.	94
46	Spectra of the 3080 cm^{-1} CH_4 band.	95
47	Spectra of the 1306 cm^{-1} CH_4 band.	96
48	Spectra of the 1306 cm^{-1} CH_4 band.	97

LIST OF FIGURES (Cont'd)-PART A

<u>Figure No.</u>		<u>Page</u>
49	Spectra of the 1306 cm^{-1} and 1550 cm^{-1} CH_4 bands.	90
50	Spectra of the 1306 cm^{-1} and 1550 cm^{-1} CH_4 bands.	91
51	Spectra of the 1306 cm^{-1} and 1550 cm^{-1} CH_4 bands.	100
52	The total absorption of the 3020 cm^{-1} CH_4 band versus equivalent pressure.	102
53	The total absorption of the 3020 cm^{-1} CH_4 band versus absorber concentration.	104
54	The total absorption of the 1306 cm^{-1} CH_4 band versus equivalent pressure.	105
55	The total absorption of the 1306 cm^{-1} CH_4 band versus absorber concentration.	107
56	The total absorption of the 1550 cm^{-1} CH_4 band.	108
57	The total absorption of the 3020 cm^{-1} CH_4 band versus $vP_e^{0.4}$.	110
58	The total absorption of the 1306 cm^{-1} CH_4 band versus $vP_e^{0.6}$.	112

ABSORPTION BY NITROUS OXIDE, CARBON MONOXIDE AND METHANE

I. INTRODUCTION

A detailed knowledge of the infrared transmission of planetary atmospheres is of importance to space physics in connection with studies of heat balances and with the possible development of infrared probing and signaling systems. During the past three-quarters of a century numerous studies of infrared transmission of the earth's atmosphere have been made. Molecular absorption in the atmosphere is caused chiefly by water vapor, carbon dioxide, and ozone, but the presence of small quantities of nitrous oxide, carbon monoxide, and methane also results in significant absorption; molecular oxygen also has absorption bands in the very near infrared. Infrared radiation undergoes attenuation by particles of fog, haze, and smoke in the atmosphere; this type of attenuation, as well as uncontrollable factors such as temperature and humidity, makes it difficult to obtain quantitative data on true molecular absorption in field studies. Hence, laboratory studies of "synthetic atmospheres" seem desirable even in telluric atmospheric work, and provide a powerful method of investigating absorption in the atmospheres of other planets.

The absorption of near infrared radiation by atmospheric gases results chiefly from transitions between the rotation-vibration energy levels of molecules; absorption in the far infrared is produced by transitions between rotational levels. The observed transmission by clean samples of atmospheric gases is therefore a function of frequency ν . If $I_0(\nu)$ represents the intensity of a beam of incident radiation as measured by a monochromator set for frequency ν in the vicinity of an absorption band, it is found that the intensity $I(\nu)$ of the radiation after passage through a sample consisting of a mixture of gases is less than $I_0(\nu)$. The ratio $T(\nu) = I(\nu)/I_0(\nu)$ is called the measured transmission of the gas sample at frequency ν and is expressed either as a fraction or a percentage. The measured fractional absorption at frequency ν is given by $A(\nu) = 1 - T(\nu)$; $A(\nu)$ may also be stated as a percentage. It is found that the measured absorption $A(\nu)$ depends on such factors as the total number of absorbing molecules per cross-sectional area of the beam, denoted by \bar{v} and called the absorber concentration or optical density; the partial pressure p of the absorbing gas, the total pressure P , which includes the partial pressure of absorbing and nonabsorbing gases; the absolute temperature T of the sample; and the effective slitwidth of the monochromator.

In 1948 Chapman and Howard¹ of this department began a laboratory study of the absorption of water vapor and carbon dioxide samples containing various amounts of nonabsorbing gases. The gas samples were enclosed in a multiple-traversal cell giving a maximum path length of several meters; the temperature of the gas samples could be elevated by electrical heating of the entire cell. In 1953 Howard, Burch, and Williams² (hereafter referred to as HBW), also of this laboratory, extended the earlier studies of water vapor and carbon dioxide to longer path lengths by the use of a 22-meter multiple-traversal absorption cell, in which absorption paths as great as 100 meters could be obtained. The work reported by HBW was done with gases at room temperature.

In these earlier studies it was verified that although the measured values of $A(\nu)$ for a given sample and given path length are strongly dependent upon the slitwidth, the integral

$$\int_{\nu_1}^{\nu_2} A(\nu) d\nu \quad \text{Total Absorption} \quad (1)$$

is independent of slitwidth provided the limits ν_1 and ν_2 are chosen to include an entire absorption band; the validity of this statement is discussed in some detail by HEW. The integral (1) is called the total absorption of the absorption band defined by the limits ν_1 and ν_2 and is expressed in frequency units; other authors have referred to the integral (1) as the equivalent band width of the absorption, since the same integral can be considered as applying to an equivalent band having complete absorption over a frequency interval

$$\Delta\nu = \int_{\nu_1}^{\nu_2} A(\nu) d\nu$$

The work of Chapman and Howard and of HEW was directed toward the determination of the total absorptions of various infrared bands of water vapor and carbon dioxide mixed with nitrogen as functions of absorber concentration c , partial pressure p of the absorbing gas, total pressure P , and absolute temperature T . The functional relationships between total absorption and the parameters listed were given by tables, by suitable graphs, and by empirical equations applicable to certain restricted ranges of total absorption for each band.

The present research program includes (i) further studies of absorption by water vapor and carbon dioxide with an extension to spectral regions and to ranges of c , p , P , and T not covered in earlier studies, and (ii) studies of the infrared absorption produced by the minor atmospheric constituents nitrous oxide, carbon monoxide, and methane. The purpose of the investigation is to establish the functional relationship

$$\int_{\nu_1}^{\nu_2} A(\nu) d\nu = f(c, p, P, T) \quad (2)$$

for various regions of characteristic absorption. The functional relation will, as in the earlier reports, be given by tables, graphs, and empirical equations. It is hoped that the results of the investigation will prove useful in the following cases:

- (a) predictions of absorption for known paths through known absorbing mixtures;

(b) determination of atmospheric composition by measurements of the transmission of infrared radiation along known path lengths in the atmosphere; and

(c) test of the various theories that have been proposed to account for absorption phenomena.

The results obtained in the present research program will be given in three reports as follows:

REPORT I (present): Absorption by nitrous oxide in the $2000-1200\text{ cm}^{-1}$ region; absorption by carbon monoxide in the region of its fundamental (2143 cm^{-1}) band and its first overtone (4286 cm^{-1}) band; absorption of methane bands at 3020 cm^{-1} , 1550 cm^{-1} , and 1306 cm^{-1} .

REPORT II: Absorption by carbon dioxide bands at 2100 cm^{-1} , at 1600 cm^{-1} , at 1275 cm^{-1} , at 920 cm^{-1} , at 1064 cm^{-1} , and in the range $875-450\text{ cm}^{-1}$.

FINAL REPORT: Absorption by water vapor in the region of its vibration-rotation bands at 1595 cm^{-1} and near 3700 cm^{-1} , and in the region of its pure rotational band in the range $400-1000\text{ cm}^{-1}$; absorption by nitrous oxide bands at 189 cm^{-1} , 1067 cm^{-1} , 1285 cm^{-1} , 2461 cm^{-1} , and 2469 cm^{-1} ; a study of the relative effects of various foreign gases on the total absorption of several infrared bands.

A portion of the data on the H_2O , CO , and CO_2 bands were reported previously in a Ph.D. dissertation by one of us¹. However, additional data which are included in Reports I and II were not included in the previous work. As a result of these additional data some of the empirical relations which were derived have been modified slightly.

11. THEORY

Theories of absorption are based on an exponential law of absorption which was proposed by Lambert nearly two hundred years ago on the basis of studies of absorption of light by liquids, and was later elaborated by Beer. According to the Lambert law, the fractional absorption $A'(\nu)$ for monochromatic radiation of frequency ν is given by the expression

$$A'(\nu) = 1 - e^{-k(\nu)c} \quad (3)$$

where $k(\nu)$ is the absorption coefficient for the absorbing material and c is the absorber concentration. Beer's elaboration of the law was concerned with a mixture of absorbing materials. According to Beer's law

$$k(\nu) = C_1\epsilon_1 + C_2\epsilon_2 + C_3\epsilon_3 \dots \quad (4)$$

where C_1, C_2, C_3, \dots are the concentrations of the various components and $\epsilon_1, \epsilon_2, \epsilon_3, \dots$ are characteristic constants called "extinction coefficients" for the various components. Beer's law is based on the assumption that each absorbing molecule absorbs radiation independently of every other molecule.

Various early evidences of the failure of Beer's law for infrared absorption of gases are discussed by EBM. The failure of Beer's law can be traced to two sources.

(1) In the first place, spectrographs have finite slitwidths and therefore direct measurement of $A'(\nu)$ is impossible, since truly monochromatic radiation is not being measured. In the case of broad, relatively structureless bands observed for liquids, the measured absorption $A(\nu)$ approaches $A'(\nu)$; it was this close correspondence of $A(\nu)$ and $A'(\nu)$ that led Lambert and Beer to the formulation of their laws. The infrared spectrum of a gas consists of bands composed of individual lines with resulting rapid variations of $A'(\nu)$ with ν . With line widths that are usually narrow as compared with the spectral interval $\Delta\nu$ passed by a monochromator or spectrograph set to pass radiation of frequency ν , the measured $A(\nu)$ is not usually a close approximation of $A'(\nu)$. Thus, it is not surprising that there is apparent failure of the simple absorption laws (3) and (4) if in a test measured absorption $A(\nu)$ is used to replace $A'(\nu)$ in (3). However, the simple laws fail for a more fundamental reason even when more sophisticated comparisons of theory and experiment are made.

- (11) As indicated above, Beer's law is based on the assumption that the absorption of each molecule is independent of every other molecule. This assumption is not justified for the case in which the absorbing molecule experiences collisions with other molecules, since molecular collisions result in appreciable broadening of the spectral lines.

Even in the case of noninteracting molecules, spectral lines have finite natural widths related to the uncertainty principle which predicts an uncertainty ΔE in an energy level related to the lifetime Δt of the molecule in the level by the relation $\Delta E \Delta t \approx \hbar$; since Δt is limited for all excited levels, all spectral lines involving transitions between ground states and excited states would be expected to have an uncertainty in frequency $\Delta \nu = \Delta E/h \approx 1/\Delta t$. Natural broadening is independent of effect external to the molecule. Usually natural broadening is negligible as compared with line broadening due to the Doppler effect, which is related to the temperature of the gas sample and produces noticeable effects when absorption of gases at very low pressures is measured. Doppler broadening is independent of pressure. The contributions of natural widths and Doppler broadening to the total widths of spectral lines are usually negligible as compared with contributions produced by the large electric fields that act during molecular collisions. The frequency of molecular collisions is related to pressure and hence the total line widths are related to pressure except at extremely low pressures. Broadening of lines beyond the widths attributable to natural widths and the Doppler effect is usually referred to as "pressure broadening", a term which includes effects attributable to collision damping, to pressure shifts, and to Stark effects produced by "close approaches" between molecules. The present work deals primarily with studies of collision broadening, since the range of pressures does not extend to the enormous pressures required to produce asymmetry shifts, Stark shifts, and enforced dipole effects. Collision broadening is usually encountered when the times between collisions are large compared with the times spent in collision; the other effects are encountered when time spent in collisions is large and involves radiation absorbed during collisions.

A. LORENTZIAN LINES

Although the experimental results obtained in the present investigation are not dependent upon assumptions as to the actual shapes of spectral lines, it is convenient for purposes of discussion to assume a line shape first proposed by Lorentz and found to give a satisfactory approximation to actual line shapes over the fairly wide range of pressures in which "collision damping" or "collision broadening" is encountered. The expression for the absorption coefficient proposed by Lorentz is

$$K(\nu) = \frac{S}{\pi} \frac{\alpha}{(\nu - \nu_0)^2 + \alpha^2} \quad (5)$$

where the line strength $S = \int_{-\infty}^{\infty} A(\nu) d\nu$ and x is the halfwidth of the line at half the maximum value of $A(\nu)$. The line strength of a given collision-broadened line is a constant for a given temperature and is related to probabilities of transitions between the initial and final energy levels of the absorbing molecule and to the relative populations of these levels. The half-width Δ is related to the pressure, the absolute temperature, and the types of molecules in the gas sample.

Ladenberg and Reiche⁴ have shown that with the value of $x(\nu)$ in (5) substituted in (4) the integral

$$\int A(\nu) d\nu = \int \left(1 - e^{-2x(\nu)\nu} \right) d\nu \quad (6)$$

can be evaluated in terms of S , Δ , and ν provided the limits of integration include the entire absorption associated with a given line. Thus, on the assumption that with appropriate limits of integration $\int A(\nu) d\nu = \int A(\nu) d\nu$, it is possible to obtain experimental tests of Ladenberg and Reiche's theoretical results. Their results indicate that

$$\int A(\nu) d\nu = S \operatorname{erf}(x)$$

where $x = S\nu/\Delta$, and

$$\operatorname{erf}(x) = 1 - e^{-x^2} \left[\frac{2}{\pi} \int_0^x \frac{e^{-t^2}}{t} dt \right] \quad (7)$$

where $\int_0^x \frac{e^{-t^2}}{t} dt$ and $\int_0^x \frac{e^{-t^2}}{t} dt$ are the Dawson functions of order 0 and 1, respectively.

Although Eq. (7) is a rather involved expression, Elsasser⁵ has adapted two approximations which can be readily used to determine the total absorption of single lines under certain limiting conditions:

$$\int A(\nu) d\nu = S\nu \quad \text{for small } x \quad (\text{weak lines}) \quad (8)$$

and

$$\int A(\nu) d\nu = \sqrt{S\nu} \quad \text{for large } x \quad (\text{strong lines}) \quad (9)$$

Equations (8) and (9) imply predictions that are susceptible to experimental tests. The line strength S can be satisfactorily related to spectroscopic quantities that can be measured.

As indicated earlier, the line strength S' of a collision-broadened line is a constant at a given temperature. The absorber concentration at a given temperature is directly proportional to the product of the partial pressure p and the absorption path length $w \cdot \text{cm}$. The relation between the half-width and the pressure, temperature, and composition of the sample is somewhat more involved.

The half-width α of a collision-broadened spectral line is proportional to the collision frequency F . From kinetic theory it can be shown that the half-width is given by the relation

$$\alpha = \frac{F}{2\pi} = \frac{1}{4\pi} \sum_i N_i [D_{0,i}]^2 \left[2kT \left(\frac{1}{M_0} + \frac{1}{M_i} \right) \right]^{1/2} \quad (10)$$

where N_i is the number of molecules of the i -th type per unit volume, $D_{0,i}$ is the sum of the optical collision diameters of the absorbing molecule and a molecule of the i -th type, k is Boltzmann's constant, T is the absolute temperature, M_0 is the mass of the absorbing molecule, and M_i is the mass of a molecule of the i -th type.

The dependence of α on pressure P can readily be determined for a given mixture of gases in which the ratios of the partial pressures of the components are the same for all values of the total pressure. Recalling that the partial pressure p_i of gas of the i -th type is given by $p_i = N_i kT$ and assuming that collision diameters are independent of temperature, one can readily show that for a given mixture of gases the half-width of a collision-broadened absorption line can be written

$$\alpha = \alpha_0 (P/P_0) \sqrt{T_0/T} \quad (11)$$

where α_0 is the half-width of the line under standard conditions P_0 and T_0 ; at a given temperature, the half-width α would be expected to be directly proportional to the total pressure P .

Substitution of the value of α given by (11) in relations (8) and (9) leads to the following predictions for a given mixture of gases at a given temperature:

$$\int A(\nu) d\nu \sim \epsilon \nu \sim \alpha P l \quad \text{For small } \alpha \quad (\text{weak line}) \quad (8')$$

$$\int A(\nu) d\nu \sim \sqrt{\epsilon P \nu} \sim \sqrt{\epsilon P_0 \nu} \quad \text{For large } \alpha \quad (\text{strong line}) \quad (9')$$

Equations (3') and (3'') assume a very simple form for the special case of a sample consisting of a single absorbing gas with no admixture of other gases, since for this special case $p = 1$ and the equations become:

$$\int A(\nu) d\nu = \sqrt{\pi} \omega \sqrt{S P} \quad \text{for small } x \quad (\text{weak line}) \quad (8')$$

$$\int A(\nu) d\nu = \sqrt{\pi} \omega \sqrt{S} \quad \text{for large } x \quad (\text{strong line}) \quad (9')$$

The expressions of total absorption given in (3') and (3'') apply to the very limited situation in which a given mixture of gases is studied at various conditions of total pressure. In other situations it is necessary to compare total absorption of mixtures of different proportions of absorbing and non-absorbing gases. The appearance of $D_{a,i}$ and $D_{b,i}$ in (10) indicates that different gases have different "broadening" effects on spectral lines. Since most of the gas samples employed in the experimental work consisted of binary mixtures of absorbing gases and nitrogen, which was used as a nonabsorbing "broadening gas", it is desirable to consider (10) for the special case of a binary mixture of an absorbing gas a and a broadening gas b . The summation in (10) will in this case have two terms: a self-broadening term in which $i = a$, and a second term for the effects of broadening by the inert gas $i = b$. Equation (10) assumes the form

$$\alpha = \frac{1}{4\pi} \left(\frac{2\pi\nu}{c} \right)^{1/2} \left\{ D_{a,a} (C_{a,a})^2 \left[\frac{p_a}{p_b} \right]^{1/2} + D_{b,b} (C_{b,b})^2 \left[\frac{p_b}{p_a} \right]^{1/2} \right\} \quad (10')$$

Substitution for $D_{a,i}$ and $D_{b,i}$ in terms of the partial pressures p_a and p_b gives

$$\alpha = \frac{1}{4\pi} \left(\frac{2\pi\nu}{c} \right)^{1/2} \left\{ C_{a,a} p_a + C_{a,b} p_b \right\} \quad (12)$$

where $C_{a,a}$ and $C_{a,b}$ are constants involving the optical collision diameters and masses of absorbing and broadening gases. Recalling that the total pressure $P = p_a + p_b$, one may write an expression for α in terms of P and p_a by rewriting (12) in the form

$$\begin{aligned} \alpha &= \frac{1}{4\pi} \left(\frac{2\pi\nu}{c} \right)^{1/2} C_{a,b} \left\{ (C_{a,a}/C_{a,b}) + \left(\frac{C_{a,a}}{C_{a,b}} - 1 \right) \frac{p_a}{P} \right\} \\ &= \frac{1}{4\pi} \left(\frac{2\pi\nu}{c} \right)^{1/2} C_{a,b} \left\{ P + (P-1)p_a \right\} \quad (13) \end{aligned}$$

where $B = C_{a,a}/C_{a,p}$ is called the self-broadening coefficient of the absorbing gas and represents the ratio of the "self-broadening ability" of the absorbing gas to the "broadening ability" of the nonabsorbing gas. Methods of determining B for various absorbing gases relative to N_2 will be described later. The term in brackets in (13) is called the equivalent pressure P_e of the gas sample,

$$P_e = P + (B - 1)p \quad (14)$$

where P is the measured total pressure of the sample and p is the partial pressure of the absorbing gas. The predictions embodied in (8') and (9') should be fulfilled by a mixture of gases provided P is replaced by appropriate equivalent pressure P_e . It should be remarked that the theory presented thus far might be expected to apply to lines whose width is determined primarily by collision broadening; it is not applicable to extremely low pressures, for which natural widths and Doppler broadening are of primary importance, nor to extremely high pressures, at which absorption during collisions or "close approaches" leads to Stark effects and asymmetrical pressure shifts.

B. ABSORPTION BANDS

In order to extend the theory to include total absorption of entire bands it is necessary to consider the spacings and intensities of the individual lines. If there is overlapping of the spectral lines so that more than one line contributes to the absorption at frequency ν , $A'(\nu)$ is still given by eq. (4) if the value of $k(\nu)$ used is the sum of the $k(\nu)$ for each of the individual lines. Equation (6) also yields the total absorption of an entire band if the proper value of $k(\nu)$ is used. For the simple case of no overlapping of the lines, the total absorption of a band can be treated as the sum of the total absorptions of each of the lines.

In order to make theoretical calculations of the dependence of total absorption of an entire band on pressure and absorber concentration, it is usually necessary to make some assumptions about the spacings and intensities of the individual lines. Two different idealized band models have received general recognition:

- (a) A band consisting of an infinite array of equally intense, equally spaced lines has been treated by Gladstone;⁵
- (b) A disordered band, usually referred to as the statistical model, which is composed of lines whose positions occur at random and whose intensities can be represented by a probability distribution, has been worked out independently by Gouy⁶ and by Meyer.⁷

Plass⁶ has recently discussed in detail these two models as well as a third:

- (c) The random Elsasser model which is composed of several groups of lines each of which individually forms an Elsasser band, but where these groups are superposed to give a nearly random spacing.

The report by Plass also includes curves which relate absorption to absorber concentration and pressure for the three different band models.

Of course, no real band is exactly represented by any of these theoretical models. But it was demonstrated in the NBS report that at 15 μ the general dependence of the total absorption on w and P_e for CO_2 bands can be explained by the Elsasser model*. It was also demonstrated that the absorption by H_2O bands is similar to that of a statistical band model. It is not surprising that the absorption by CO_2 is best explained by an Elsasser band, since the changes in the intensities, half-widths, and spacings of the lines are gradual over the bands. The intensities and spacing of the H_2O lines vary almost at random over the band, and the absorption is therefore similar to that of the statistical model.

Exact theoretical expressions for total absorption of even the idealized band models are complex. However, Plass⁶ has discussed three different approximations for each of the three band models listed above. Each approximation permits the absorption to be expressed in terms of elementary functions and is valid over a considerable range of pressure and absorber concentration. These three approximations are: (i) strong-line approximation; (ii) weak-line approximation; and (iii) non-overlapping approximation. Methods (i) and (ii) are valid regardless of whether or not the spectral lines overlap, and method (iii) is valid whether or not the absorption lines are weak or strong.

(i) The strong-line approximation is valid when there is virtually complete absorption near the centers of the strongest lines, and an increase in either w or P_e results in increased absorption in the wings of the lines only. The requirement for the validity of the strong line approximation is given in Eq. (9) and corresponds to large values of w and small values of P_e . For the case of no overlapping of the lines the total absorption of a band can be treated as the sum of the total absorptions of all of the lines, and for strong lines the total absorption of the band is seen from Eqs. (9), (13), and (14) to be proportional to $(wP_e)^{1/2}$. The range of values of w and P_e over which this relationship is valid is referred to as the square-root region. When there is overlapping of the lines the total absorption no longer follows a simple square-root dependence; however, the

*The definition of P_e in this report differs from the equivalent pressure employed by NBS.

total absorption is still a function of the product wP_0 . The distinguishing feature of the strong line approximation is that the total absorption can be expressed as a function of the single variable wP_0 . The distinction between the square-root dependence encountered for strong non-overlapping lines and the more general strong-line approximation with reference to entire bands is emphasized; the square-root dependence can be considered as a special case of the strong-line approximation, and is valid only when the spectral lines do not overlap appreciably.

(ii) The weak-line approximation is valid when the absorption is small at all frequencies in the band, including those near the centers of the strongest absorption lines. The requirement for the validity of the weak-line approximation with reference to an entire band is similar to the requirement for the weak-line approximation for a single line given in Eq. (8). This requirement is satisfied in the case of small values of y and large values of P_0 . The total absorption of a given band is a function of y only; however, the simple linear relationship given by Eq. (9) is not valid in the case of over-lapping.

(iii) The non-overlapping approximation is valid when there is not appreciable overlapping of the lines; and the total absorption is given by Eq. (7) with the contribution of all the individual lines added together.

It is possible to test the usefulness of a given band model by comparing the results of total absorption measurements with the theoretical predictions for ranges of values of y and P_0 over which the strong-line approximation is expected to be valid. The strong-line approximation is useful for testing different band models since the total absorption depends on the distribution of the strengths of the lines as well as upon the arrangement of the spectral lines, and is quite different for different band models. However, the weak-line approximation and the non-overlapping approximation cannot be used to test different band models since the total absorption is virtually independent of the line spacing and the distribution of the strengths of the lines.

Of the gases treated in the present report, CO and H₂O are linear molecules whose absorption bands are composed of lines having gradually changing intensity and spacing. The structure of these bands is best approximated by an Elsasser model; and it is therefore useful to compare the H₂O and CO data in the present study with results based on the Elsasser theoretical model for values of y and P_0 for which the strong-line approximation would be expected to be valid.

It will be shown below in the discussion of each of the bands involved that the Elsasser model is sufficient to predict, in a general way, the dependence of total absorption on absorber concentration and

pressure. However, it will be seen that the experimentally observed effect of increasing pressure is significantly less than that predicted for an Elsasser band for certain values of ν and P_0 .

C. BAND INTENSITIES

One quantity of fundamental importance in studies of molecular spectra is a quantity called band strength or band intensity, $\int k(\nu) d\nu$, a quantity analogous to the line strength defined in connection with (5) except for the fact that the limits of integration are chosen to include an entire band. If $\int k(\nu) d\nu$ is known for a vibration-rotation band, basic information concerning transition moments appropriate to transitions between vibrational levels can be obtained; the value of $\int k(\nu) d\nu$ also depends upon the population differences between the lower and upper levels and is therefore also a function of temperature.

From the data on total absorption to be presented later in the report, it is sometimes possible to determine a value of band intensity for the various bands to be investigated. This quantity can be evaluated from total absorption measurements provided $k(\nu)\nu \ll 1$ for all frequencies included in absorption. Under this condition, an integral similar to (6) but with the limits of integration chosen to include an entire band becomes

$$\int A(\nu) d\nu = \nu \int k(\nu) d\nu \quad (6')$$

for $k(\nu)\nu \ll 1$ throughout the entire band. Since $\int A(\nu) d\nu$ and ν can both be measured, the band intensity $\int k(\nu) d\nu$ can be determined. The choice of absorber concentrations and pressure for which (6') applies will be discussed later in some detail.

III. EXPERIMENTAL METHODS

A. SPECTROGRAPHS, ABSORPTION CELLS, AND GAS-HANDLING EQUIPMENT

In the present study, a double-beam, single-pass Perkin-Elmer Model 21 spectrometer with NaCl prism was employed for frequencies between 4000 cm^{-1} and 670 cm^{-1} . This spectrograph was equipped with a drive mechanism and recorder which provided a direct plot of $A(\nu)$ vs. ν on the recorder chart. In Fig. 1 are shown two views of the Model 21 with dual long-path cells designed and constructed specifically for it by Perkin-Elmer. In the upper part of the figure the sample cell housing has been removed to show the multiple-reflection system which utilizes the White¹⁰ principle. The two cells, which extend from either side of the spectrometer, are identical and are arranged so that they may be used simultaneously, one in the sample beam and one in the reference beam. In the lower part of the figure the sample cell housing is shown in place; the cell housing is designed to hold vacuum and gauge pressures up to 100 pounds per square inch. A portable gas-handling system which was constructed for the present investigation is shown in both views and is discussed below.

Each cell has a base path of one meter, and can be adjusted to 40 traversals or any smaller number divisible by four. The cell housing must be removed in order to adjust the number of traversals. Although electrical heating coils around the cell housing are capable of heating the cells to approximately 100°C , the data included in the present study were obtained with the samples near 30°C .

Very little effort is involved in changing from the dual long-path cells to conventional short sample cells, or vice versa. In order to use the long-path cells a set of kinematically mounted optics fits into the sampling space between the cells and directs the radiation into the cell and from the cell to the monochromator. These optics, which are not visible in Fig. 1, can be easily removed when short cells are to be used.

The main body of the gas-handling system shown in Fig. 1 and also the packless miniature valves were made of AISI 316 stainless steel which would withstand high pressures and would also allow the possible future use of many gases which are corrosive to carbon steel and nonferrous metals. One of six outlet valves was connected to the sample cell, one to the reference cell, and any of the other four could be connected to cylinders of gas being used. The pressure in the system was recorded by one of four different gauges designed for different pressure ranges. A Wallace and Tiernan absolute pressure gauge was used in the pressure range between 1 and 50 mm Hg. This gauge is calibrated from 0 to 50 mm Hg and is designed to have an accuracy of one part in 100 provided the "zero" is properly adjusted. A McLeod gauge was used for absolute pressures less than 1.5 mm Hg and also served as a check of the readings.

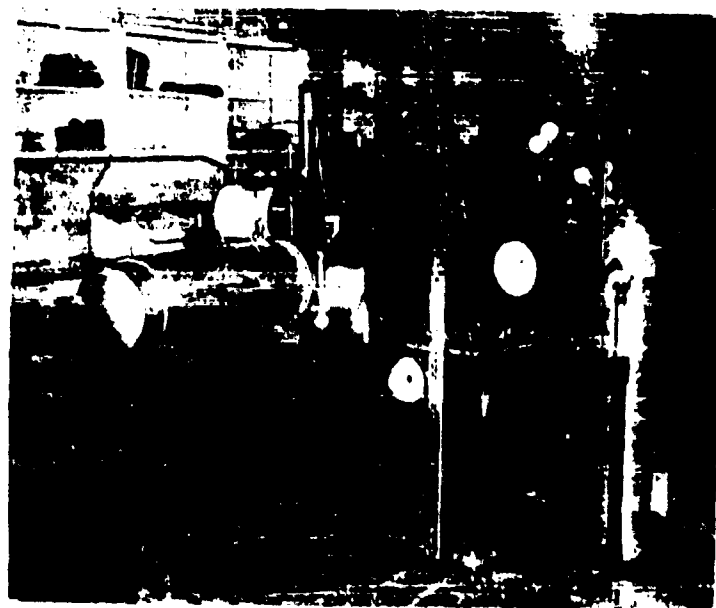
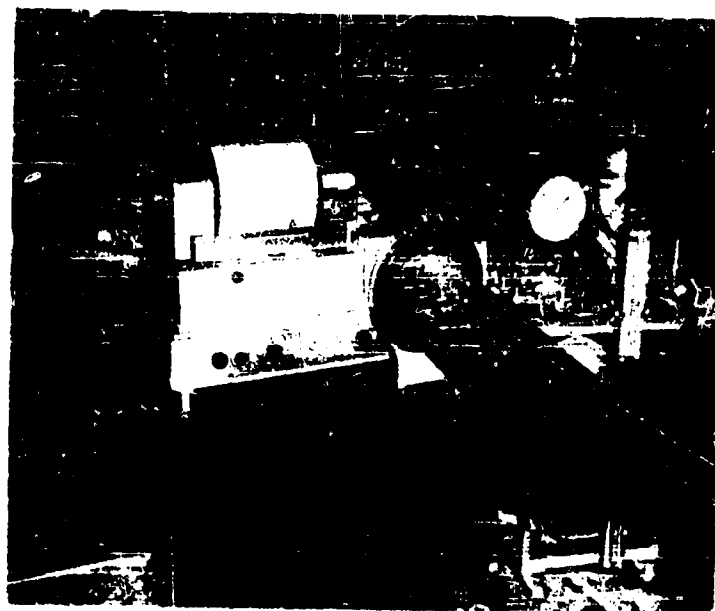


Fig. 1. Two views of the Perkin-Elmer Model 21 spectrometer with dual long-path cells and gas-handling system

of the Wallace and Tiernan gauge at low pressures. A simple "U"-tube manometer served to measure pressures in the range from 50 mm Hg to one atmosphere. An Ashcroft "Duragauge", which is a Bourdon tube-type pressure gauge, was used in the higher pressure range. The Ashcroft gauge is also constructed from AISI 316 stainless steel and is calibrated for gauge pressures between 0 and 100 pounds per square inch in steps of one pound per square inch.

Before introducing a sample into the sample cell, the entire gas-handling system was evacuated, the reference cell was closed off, and the absorbing gas was added to the system and to the sample cell at the desired pressure. The valve to the sample cell was then closed. In order to produce a sample with the same absorber concentration but greater total pressure, nitrogen was added to the sample. Before the nitrogen was introduced, the gas-handling system (excluding the sample cell) was evacuated in order to prevent more absorber from being forced into the cell. Nitrogen was then added to the system to a pressure slightly greater than that in the cell before the valve was opened; more nitrogen was then added to the sample cell until the desired pressure was reached. This procedure was followed in order to reduce the flow of absorber from the cell back into the rest of the system. To produce a sample of still higher total pressure, more nitrogen was added to the system, without evacuating it; the valve between the main system and the sample cell was then opened and nitrogen added to the desired pressure. This procedure could be repeated several times to measure the total absorption of a series of samples having the same absorber concentration and varying total pressure.

In order to reduce the chance of the absorber diffusing from the sample cell back through the valve, the valve was kept open for the minimum time required to allow the pressure to come to equilibrium. It is probable that most of the absorber which did in some way get out of the cell would remain for several minutes in the 3-foot length of small tubing which connected the cell to the rest of the system. When more nitrogen was added, most of this absorber would be forced back into the cell, and any losses of this type would not be cumulative. It was found that the observed absorption of a sample of low absorber partial pressure with nitrogen added to a high pressure in one step agreed well with a similar sample in which the nitrogen was added by several successive steps, thus indicating that leakage of the absorber through the valve was negligible.

When samples containing two gases were being studied, it was essential that the gases be thoroughly mixed to ensure that the proper amount of absorber was contained in the radiation path. One might expect that as nitrogen was being added to a sample, the absorber would tend to move to the part of the cell away from the entrance; and, until the gases became uniformly mixed, by thermal motion or otherwise, a false absorption reading would be obtained. It was assumed that a uniform gas mixture had been obtained when the absorption of the sample had

reached a constant value. The mixing problem was investigated for each of the different absorption cells used.

A fan has been built in the Perkin-Elmer long-path cells to speed up mixing. Without the fan several minutes are required for mixing of samples at high pressures; however, only a few seconds are required for mixing when the fan is used. The fan blade is connected to a shaft which extends through a rotating vacuum seal to a small electric motor outside the cell. The motor, which is mounted above the sample cell, can be seen in the lower portion of Fig. 1. The necessity for forced mixing probably arises from the fact that the cantilever, which holds one of the mirrors inside the cell and is visible in the upper portion of Fig. 1 divides the cell into two chambers. Diffusion from one of these chambers to the other apparently occurs rather slowly.

Figure 2 is a drawing which illustrates the construction of two short cells which were used, one 1.55 cm and the other 6.35 cm long. The synthetic buna-N "O" ring between the window and the cell body serves as the seal, and the windows are held in place by brass end plates joined by threaded brass rods. The grooves for the "O" rings are not deep enough to allow metal-to-window contact; this reduces any local stresses caused by irregularities in the windows or metal which might tend to crack the windows. An "O" ring between the end plate and window serves as a cushion and is directly opposite the "O" ring seal. This makes it possible to hold the windows on firmly without producing appreciable shearing stress. The short cells can be used for vacuum and for gauge pressures up to 60 psig. Grooves were milled in one endplate which fits into a receptacle provided on the spectrometer directly in front of the entrance slit. Two NaCl windows were put in the reference beam to correct for the attenuation by the cell windows.

It was found that mixing was essentially complete in the short cells within a few seconds. However, a few minutes were required for mixing in a somewhat similar cell different from the type shown in Fig. 2 in that the valve was joined to the main body of the cell by approximately two inches of tubing. The valve was soldered directly to the cells used in the later work. It is probable that the rather long mixing time for the first type of cell was caused by the fact that diffusion through the small-bore tubing to the valve took place very slowly.

Studies of the 4260 cm^{-1} CO band were made with a Perkin-Elmer Model 99 spectrometer with a LiF prism. A Nernst glower served as a radiation source and a thermocouple was used as the detector. The signal was amplified by a Perkin-Elmer Model 177 amplifier and the spectrum displayed by a Leeds and Northrup Speedomax Recorder. A multiple-pass cell with a White¹⁰ optical system and external adjustments was used with the Model 99 spectrometer. The base length of the cell is 1.5 meters and paths as long as 40 meters were used, although paths twice this great can be obtained. The body of the cell is steel, the end plates aluminum, and the windows NaCl. Total pressures are limited to atmospheric and less.

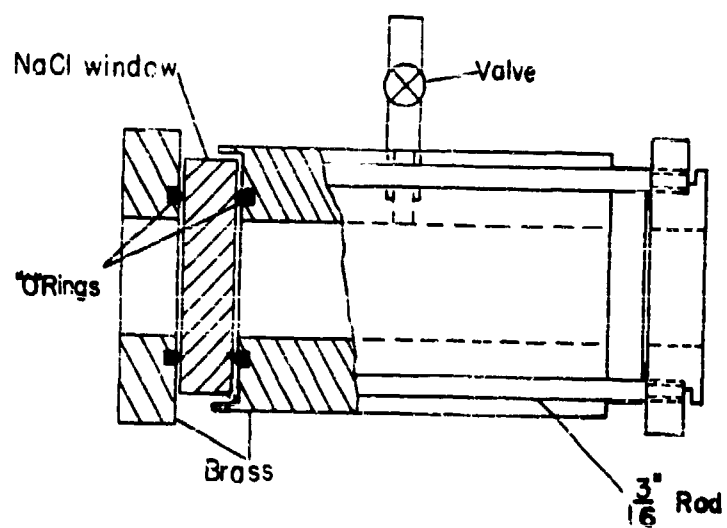


Fig. 2. Design of short absorption cells

Absorption measurements with the multiple-pass cell used in the study of the 4260 cm^{-1} CO band indicate that mixing is complete within several seconds after nitrogen is introduced; therefore, forced mixing was not necessary.

B. MEASUREMENT OF TOTAL ABSORPTION

The total absorption of the samples studied with the Model 21 spectrometer was easily determined by measuring the area under each recorded spectrum with a compensating polar planimeter. The abscissa was linear in frequency ν and the ordinate was linear in fractional absorption $A(\nu)$; therefore the area under the absorption curve was proportional to the total absorption. In some cases slight corrections had to be made for scattered light and for differences in deflection corresponding to zero absorption. Such differences were caused by unequal attenuation in the sample and reference beams by the instrument and by the atmospheric gases within the instrument. These effects were easily corrected so that negligible error in the measurement of total absorption was caused by them.

Spectra of the 4260 cm^{-1} band obtained with the Model 99 spectrometer were replotted before being measured. An "envelope" spectrum was obtained with the cell evacuated, and was superimposed on each sample spectrum. The envelope spectrum served as the zero percent absorption curve and the spectrum was replotted on a scale whose ordinate was linear in fractional absorption. The area under the replotted curve was then measured and multiplied by an appropriate "normalizing factor" to determine the total absorption. This process of replotting the spectra has been discussed in detail by BEW².

C. ERRORS AND ACCURACY

The possible sources of error in a study such as this may be divided into three categories:

- (i) errors in sampling of the gases (in determining the amount of absorbing gas and nitrogen in the cell),
- (ii) errors arising from inaccurate recording by the spectrometer due to noise, drift, and non-linearity in the detection-amplification-recording system,
- (iii) errors in measuring the recorded spectra.

1. Sampling Errors

The major source of error in sampling is the effect of absorption of the gases on the cell walls; the problems involved are discussed in great detail in Appendix I. Another source of sampling error involves the accuracy with which the pressures of the samples were measured. With the system of four gauges mentioned above it was possible to measure pressures greater than 10 mm Hg to 1% with a somewhat greater error for smaller samples. Improper mixing of the absorber with nitrogen would give rise to error; however, this error is believed to be negligible, as mentioned earlier, since care was taken to ensure sufficient mixing.

Errors in the recorded spectra might arise from absorption by an impurity in the same spectral region as the absorption band being studied. Small amounts of CO_2 which were present in the H_2O and CO gases produced slight absorption on the high-frequency side of the 2224 cm^{-1} H_2O band and the 2143 cm^{-1} CO band. By recording spectra of CO_2 samples having approximately the same absorption as the CO_2 impurity, it was possible to estimate the CO_2 absorption and to correct the spectra in the region where both the absorbing gas and the CO_2 produce absorption. A similar correction for absorption by H_2O impurity in the CH_4 was also made. This type of correction was necessary only for samples of large absorber concentration and was easily made to yield an error of less than 1% in the total absorption except in the case of the 1550 cm^{-1} CdH_2 band, for which the error is somewhat larger. No absorption by impurities in the region of the CO 4260 cm^{-1} band was found.

The approximate purities of the gases used in the present study are listed along with the major impurities in Table 1.

2. Recording Errors

Errors in recording the spectra arise from the usual noise and from other variations due to faulty instrument operation. These variations can cause a misinterpretation of the apparent location of the zero absorption curve. Errors of this sort are particularly noticeable in spectra with low total absorption and are estimated to be $\pm 5\%$ for total absorption less than 10 cm^{-1} . The percentage error decreases for greater absorption and is approximately $\pm 2\%$ for values of total absorption greater than 10 cm^{-1} .

3. Errors in Measurement of Records

Repeated measurements indicate that a careful operator can measure the area under an absorption curve with a precision of less than $\pm 1\%$.

It is estimated that the over-all error does not exceed $\pm 10\%$ for values of total absorption less than 10 cm^{-1} and is less than $\pm 5\%$ if the total absorption is greater than 10 cm^{-1} .

D. UNITS

In the present study all values of partial pressure, total pressure, and equivalent pressure are expressed in units of mm Hg absolute. Tabulated values of partial pressure of the absorbing gas represent the partial pressure of the gas as it comes from the cylinder without correcting for the purity.

Values of absorber concentration \underline{v} are expressed in terms of a unit called the atmos cm , and are given by the product of the absorber path length in cm and the partial pressure of the absorbing gas in atmospheres, corrected to standard temperature. The purity of the absorbing gas is taken into account in calculating values of \underline{v} .

Since values of absorber concentration are expressed units of atmos cm , it follows from (6') that the units of band intensity $\int k(\nu) d\nu$ are $\text{atmos}^{-1} \text{cm}^{-2}$. It is emphasized that values of band intensity are based on values of \underline{v} which were corrected to standard temperature. The observed values of $\int k(\nu) d\nu$ will be compared later to results of other workers which are expressed in units of $\text{atmos}^{-1} \text{cm}^{-1} \text{sec}^{-1}$. When these units are used the numerical value differs by a factor of \underline{c} , the speed of light.

E. DETERMINATION OF SELF-BROADENING COEFFICIENTS

In Section II the concept of equivalent pressure was introduced and was expressed in (14) in terms of a self-broadening coefficient B , which can be expressed as

$$B = \left[\frac{2M_a}{M_a + M_b} \right]^{1/2} \left[\frac{D_{a,a}}{D_{a,b}} \right]^2$$

in terms of the symbols introduced earlier. The experimental determination of B involves a study of the transmission of radiation through cells of different length in which the absorber concentration \underline{v} is the same. The sample in the short cell, called the "reference cell", consists of a pure sample of the absorbing gas at pressure p ; for this cell $p_{\text{ref}} = p$ and the equivalent pressure is given by

$$P_e = B p_{\text{ref}} \quad (\text{Reference Cell}). \quad (16)$$

The sample in the longer cell, called the "sample cell", initially consists of a sample of the pure absorber at the partial pressure p required to produce an absorber concentration α equal to that in the reference cell. Initially, the absorption of radiation in the sample cell is considerably less than that in the reference cell, since the partial pressure and total pressure are less than those in the shorter reference cell. Various amounts of nitrogen are then added to the reference cell corresponding to equivalent pressures

$$P_0 = P_0 + P_b \quad (\text{Sample Cell}) \quad (17)$$

where p_b is the partial pressure of the broadening gas. For the situation in which the absorptions in sample and reference cells are most nearly equal, it is assumed that the values of P_0 in (16) and (17) are equal. The value of the self-broadening coefficient can then be determined from the relation

$$B = \frac{P_b}{p^{\text{ref}} - p} \quad (18)$$

where p^{ref} is the partial pressure of the absorbing gas in the short reference cell and p and p_b , respectively, are the partial pressures of the absorbing and broadening gases in the longer sample cell when the absorptions in the two cells are equal.

The value of B was determined for all except the 4260 cm^{-1} CO band by making use of the double-beam feature of the Model 21 spectrometer, with the 6.35-cm cell in the sample beam and the 1.55-cm cell in the reference beam. The method used to determine B for the 4260 cm^{-1} band is described below in the discussion of the results obtained for this band. The same absorber concentration was added to both cells by making the ratio of the partial pressures of absorbing gas in the two cells inversely proportional to the cell lengths. The pressure in the sample cell was then increased in small intervals by adding N_2 and the spectrum was scanned for each sample. The spectrometer recorded the ratio of the transmission of the sample cell $T(\text{sam.})$ to the transmission of the reference cell $T(\text{ref.})$

Typical spectral comparisons which were obtained in this manner for the 2224 cm^{-1} N_2O band are shown in part I of Fig. 3 for various values of total pressure in the sample cell. The dashed line at $T(\text{sam.})/T(\text{ref.}) = 1.00$ represents the recorder pen position when the two beams were "balanced": i.e., the transmissions of both samples were the same. It is seen that the ratio of the transmissions decreased with increasing pressure in the sample cell as would be expected, and that some of the spectra occur above

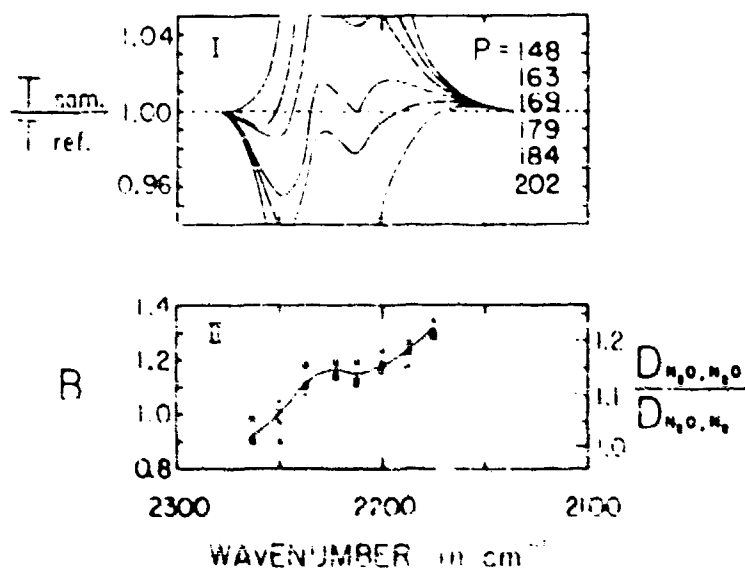


Fig. 3. The self-broadening coefficient B for the 2224 cm^{-1} H_2O band. Part I: Spectra obtained with $v = 0.30$ atmos cm in both reference and sample cells, total pressure in reference cell = 164 mm Hg. Total pressure in sample cell for each spectrum is indicated. Part II: Plot of B and collision cross section ratio. The four different sets of points correspond to the results of the spectra shown in Part I as well as to three other sets of samples having different values of absorber concentration.

the balance line for some frequencies and below the line for others. Therefore the total pressure corresponding to balance was not the same for all frequencies. The pressure corresponding to balance for any given frequency was determined by interpolating between the two successive curves which occur on opposite sides of the balance line.

Since the value of p_0 corresponding to equal transmission of the cells was found to vary with frequency, it is apparent that the value of B varies throughout the band. Points corresponding to the experimentally determined value of B were plotted against frequency in Part II of Fig. 3.

The ratio of collision cross sections is shown by the right-hand scale in Part II of Fig. 3. This quantity is included only as a matter of interest and for future comparison. It is related to the more important quantity, B , by Eq. (15).

The present study deals primarily with total absorption rather than with the absorption at certain frequencies. It was therefore desirable to obtain a nominal value of B which could be used for an entire band. The nominal value was arrived at by taking a "weighted average" value of B over the frequency limits of the band, with extra weight given to the frequency ranges which contribute most of the absorption. The values of B determined for each band, which are listed in Table 2, are believed accurate to 10% as an "effective" value for the entire bands.

The experimental results reported in Sections V - VII indicate that the total absorption never has a dependence on equivalent pressure P_0 which is greater than approximately $P_0^{0.45}$. Therefore a relative error of 6% in B would not give rise to a relative error greater than 2 or 3% in the calculation of total absorption from the empirical equations to be presented later. This maximum error would occur only for samples containing the absorbing gas alone; the error would decrease for samples containing N_2 and would vanish in the case of infinite dilution. The nominal values of B given in Table 1 are therefore sufficiently accurate for the present purpose, which is to make it possible to account for the different broadening ability of different gases.

The final report on this research program will contain detailed information on the dependence of B with frequency for each of the absorption bands discussed in the present study, as well as for other absorption bands discussed in subsequent reports. Information will also be given which concerns the relative broadening abilities of several inert gases; N_2 , O_2 , A , Ne , and He . Singleton¹¹ of this laboratory, as well as several earlier investigators, has found that unambiguous values of B can be determined and that the determined values are actually independent of pressure for the pressure range covered in this report. This result indicates that the effective collision cross sections of molecules are essentially independent of pressure over the range of pressures and for gases used in the present study.

It was shown in the HEW report that the broadening ability of air is very nearly the same as that of N_2 . Therefore the values of equivalent pressure which are used in the present study would approximate the total pressure in an atmospheric path, provided the partial pressure of the absorbing gas is small in comparison with atmospheric pressure.

IV. TREATMENT OF DATA

When the study of a given absorption band or region was started, it was found desirable to select some definite slit program for the spectrometer and to take all data with the same program. On the Model 21 spectrometer it is possible to scan the spectrum of a band with the slitwidth constant or to use a slit programming mechanism which automatically adjusts the slits continuously as the spectrum is being scanned. Although the total absorption $\int A(\nu) d\nu$ is independent of slitwidth or of slit program, there are occasions when it is desirable to compare $A(\nu)$ for some definite frequency for different samples; this would be impossible unless all data are taken with the same slit program. However, since the datum of primary importance in the present work is $\int A(\nu) d\nu$, it is not necessary to work with narrow slits; it is desirable to work with slits sufficiently wide to give large values of signal-to-noise ratio even for the largest values of total absorption. Another practical reason for the use of wide slits is that the process of planimetry of spectral recordings is easier for bands not exhibiting rotational fine structure; for nearly every band studied, it would have been possible to obtain more detailed information concerning band shape had this information been important to the investigation.

Once a program for the slits had been selected, a large number of spectra were recorded. These spectra provided data on $\int A(\nu) d\nu$ for extremely wide ranges of absorber concentration w , partial pressure p , and total pressure P --including, of course, pure samples of the absorbing gas, for which case $p = P$. The values of total absorption for various cell lengths, absorber concentrations, equivalent pressure, etc., are organized in tabular form for use in tests of theoretical predictions; it is hoped that these tabulations will prove useful to theorists.

One type of relationship important to nearly all current theories is the relationship between absorption and pressure. In order to establish this relationship from the data obtained in the present work, a set of logarithmic plots of total absorption $\int A(\nu) d\nu$ as a function of equivalent pressure P_e is then made for various values of absorber concentration w . From the slopes of the curves, the relationship between $\int A(\nu) d\nu$ and P_e can be obtained, usually it is found possible to show that $\int A(\nu) d\nu \sim P_e^n$, where n usually does not have the value of 0.5 that would be expected on the basis of (9) for a square-root approximation even in situations where this approximation might be expected to apply.

Another set of logarithmic plots is then prepared giving $\int A(\nu) d\nu$ as function of absorber concentration w for various values of equivalent

pressure P_e . From the slopes of the resulting curves, it is possible to determine the relation between $\int A(\nu) d\nu$ and ν . It is usually found that $\int A(\nu) d\nu \sim \nu^m$ where $m \approx 0.5$ in cases in which the square-root approximation might be expected to apply.

The next step in attempting to establish experimental relationships between $\int A(\nu) d\nu$ and sample parameters is to make logarithmic plots of $\int A(\nu) d\nu$ as a function of νP_e^a . From the resulting plots it is frequently possible to obtain empirical equations relating total absorption to pertinent sample parameters for certain definite ranges of values of total absorption and equivalent pressure. It is usually possible to obtain empirical equations of the form

$$\int A(\nu) d\nu = c [\nu P_e^a]^b \quad (19)$$

where c , a , and b are empirical constants with b approximately equal to 0.5. Such equations are valid for intermediate values of $\int A(\nu) d\nu$ and P_e for which strong but not seriously overlapping lines might be expected throughout most parts of the band.

For large values of $\int A(\nu) d\nu$ it is found that the central portions of the absorption band represent a spectral region of nearly complete absorption. Further increase in ν or P_e results merely in growth of $A(\nu)$ in the wings of the band. For this situation, the total band absorption can be expressed by equations of the form

$$\int A(\nu) d\nu = C + D \log (\nu P_e^a) \quad (20)$$

where C , D , and a are empirical constants.

It is rather difficult to derive satisfactory empirical equations for extremely small values of $\int A(\nu) d\nu$ and P_e . Under certain circumstances $\int A(\nu) d\nu$ is found to be nearly independent of P_e , a result indicating that Doppler broadening is the dominant influence on line width; under other conditions $\int A(\nu) d\nu$ may vary linearly with ν as predicted by (8) for small values of $x = S\nu/2\pi\lambda$.

Although total absorption is the quantity that is independent of slitwidth, it is sometimes desirable to compare the measured values of $A(\nu)$ at certain points of interest in absorption bands in order to compare experimental results with predictions based on various theoretical band models. Measured values of $A(\nu)$ near regions of maximum absorption in the P and R-branches are examples of regions where theoretical predictions can sometimes be checked. It should be emphasized again that $A(\nu)$ is dependent on effective slitwidth; comparisons of $A(\nu)$ obtained with different effective slitwidths are meaningless.

The treatment of data and the development of empirical relations will be discussed in some detail in the following section--along with a comparison of observed results and theoretical predictions. Many details will be omitted in later Sections.

V. EXPERIMENTAL RESULTS FOR THE 2224 cm^{-1} N_2O BAND

The ν_3 fundamental band of N_2O which has its center at 2224 cm^{-1} occurs in the "atmospheric window" which lies between the strong 2350 cm^{-1} CO_2 band and the 1595 cm^{-1} H_2O band. The major portion of the absorption by N_2O in this spectral region is due to the ν_3 fundamental of the common isotope $\text{N}_2^{14}\text{O}^{16}$. However, there is absorption by the less common isotopes as well as by at least one weak band ($\nu_1+\nu_2-\nu_1$) described by Thompson and Williams¹². For the sake of simplicity in the present report, all these bands together will be referred to as the 2224 cm^{-1} N_2O band.

Although the concentration of nitrous oxide in the earth's atmosphere near ground level is only approximately three parts in ten million¹³, this band gives rise to a major portion of the atmospheric absorption in the region where it occurs. A knowledge of the absorption of this band is therefore important in the calculation of the transmission of radiation in the "atmospheric window" in which it occurs. The contribution of this band to the heat balance of the earth's atmosphere is negligible since the major portion of the solar radiation occurs at higher frequencies and most of the radiation emitted by the earth's surface occurs at lower frequencies.

More than 200 spectra were obtained by using the double-beam Model 21 spectrometer with absorption cell lengths of 1.55, 6.35, 400, 800, and 1600 cm. Different combinations of N_2O and N_2 were used to provide absorber concentrations from 0.00016 to 76.4 atmos cm and total pressures from 1 to 3000 mm Hg. All spectra were obtained with slit widths corresponding to approximately 25 cm^{-1} and with the cell temperature near 30°C.

A. ABSORPTION CURVES

Tracings of spectra of some of the samples having the largest absorber concentration are shown in the left-hand portion of Fig. 4. A slight growth of the band as a result of increasing the pressure with N_2 is illustrated by these spectra; and the band limits, beyond which there is negligible absorption for even the largest samples, are indicated by the limits of the spectra. A few spectra of samples containing still larger values of absorber concentration were obtained but have not been included since very little additional information could be obtained from them. It is shown below in the discussion of Figs. 12 and 14 that there is little increase in the total absorption of the band for larger

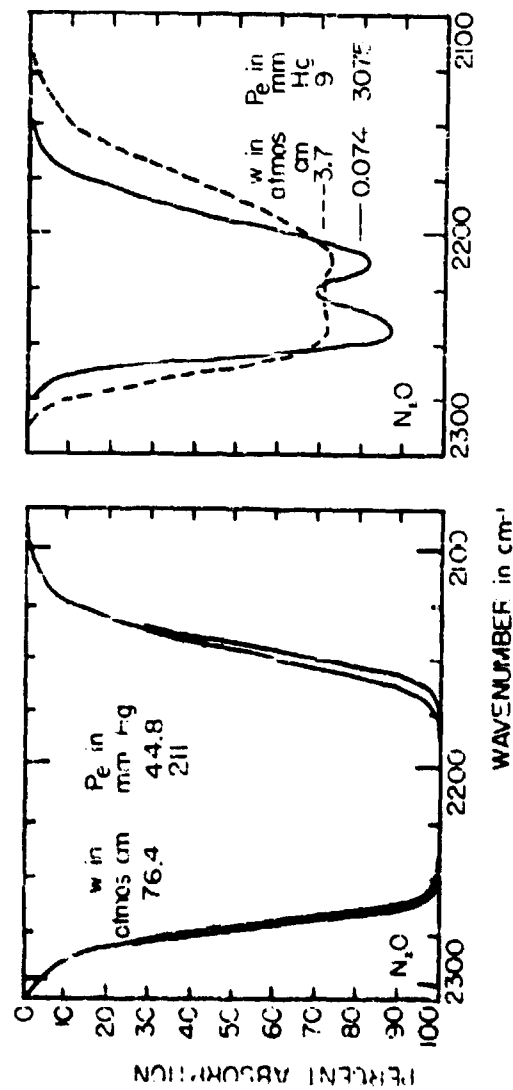


Fig. 4. Spectra of the 2224 cm^{-1} N_2O band.

values of absorption cross-sections. The values of the cross-sections are given in Table I. The values of the cross-sections are given in Table I. The values of the cross-sections are given in Table I.

The typical curves for the γ -ray spectra of the various materials having different values of μ and ρ are shown approximately equal and unabsorbed. It is noted that the values of the γ -ray spectra curves are quite different even though the spectral lines of the absorbers are the same. This is a typical case of the different portions of the γ -ray spectra of the absorbers and the γ -ray spectra of the absorbers. The γ -ray spectra of the absorbers are shown in Figure 1. The γ -ray spectra of the absorbers are shown in Figure 1. The γ -ray spectra of the absorbers are shown in Figure 1.

Other representative spectra were shown and discussed in Figure 2. The γ -ray spectra were superimposed in groups as shown in order to illustrate the effect of pressure broadening. In general, spectra are in groups corresponding to constant values of absorber concentration and different pressures. However, spectra of several samples were combined without maintaining constant values of different pressures. There is an attempt to group the resulting curves in any systematic fashion.

It was mentioned previously that one of the major sources of error in the present treatment of the line of the spectrum curve corresponding to zero absorption. By grouping the spectra as in Fig. 2, it was possible to observe the effect of the shape of the line and of the γ -ray spectra of the absorbers. The γ -ray spectra of the absorbers are shown in Figure 1. The γ -ray spectra of the absorbers are shown in Figure 1. The γ -ray spectra of the absorbers are shown in Figure 1.

Many of the spectra were obtained with the detector which operated at a voltage of 1000 V. The voltage value of the detector of these spectra was adjusted to give the normal reading of percent absorption.

It is noted that spectra of many of the samples which had low absorption in the range of the γ -ray spectra were shown. The γ -ray spectra of the absorbers are shown in Figure 1. The γ -ray spectra of the absorbers are shown in Figure 1. The γ -ray spectra of the absorbers are shown in Figure 1.

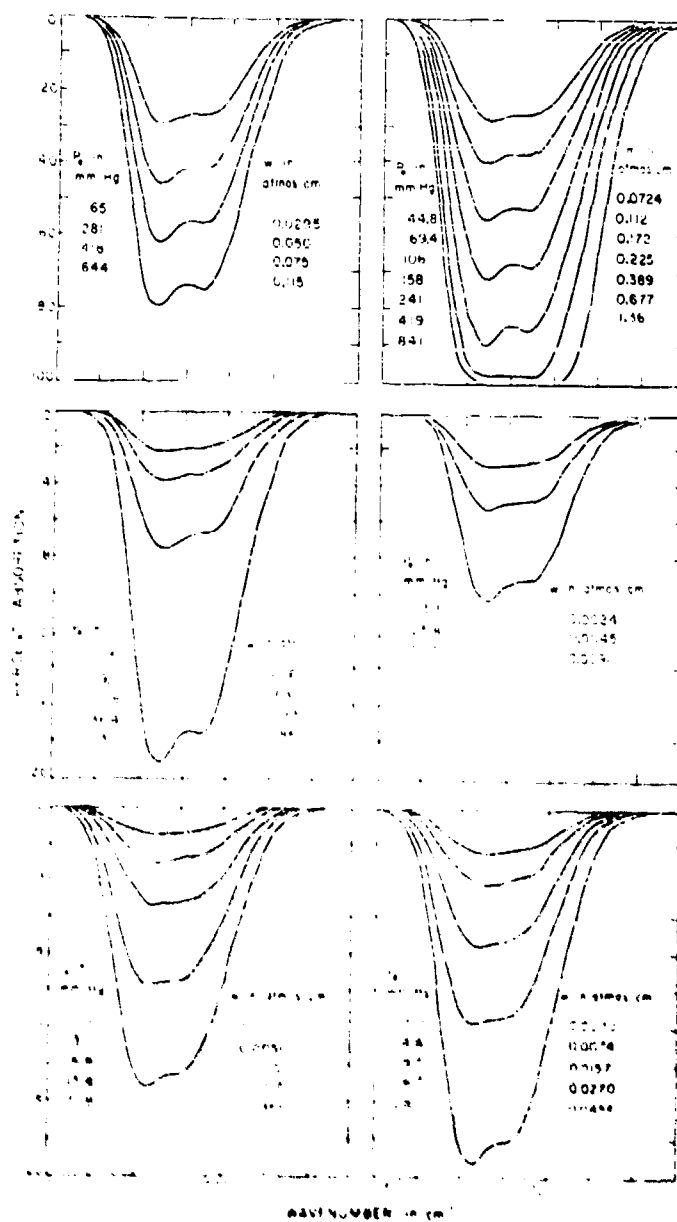


Fig. 5. Spectrum of the 220-cm⁻¹ H₂O band.

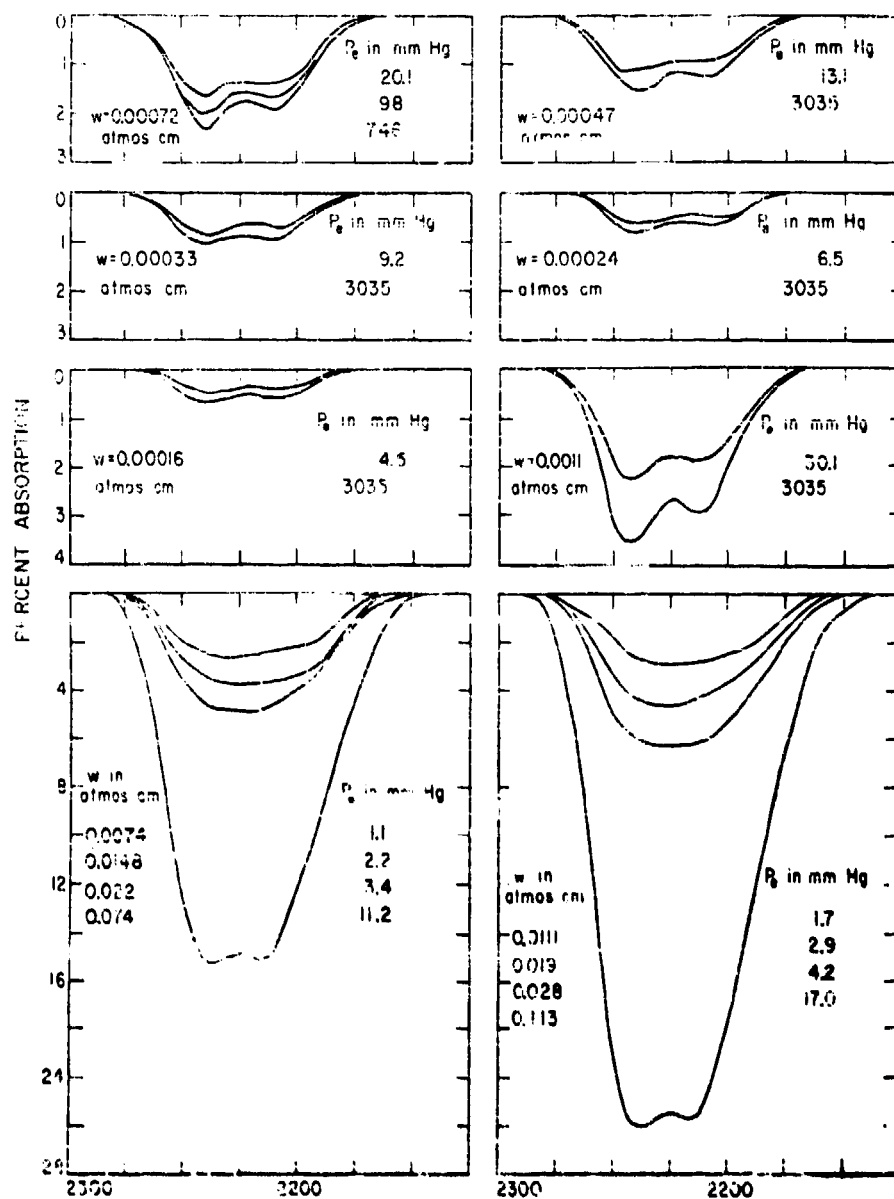


Fig. 6. Spectra of the 2224 cm^{-1} N_2O band.

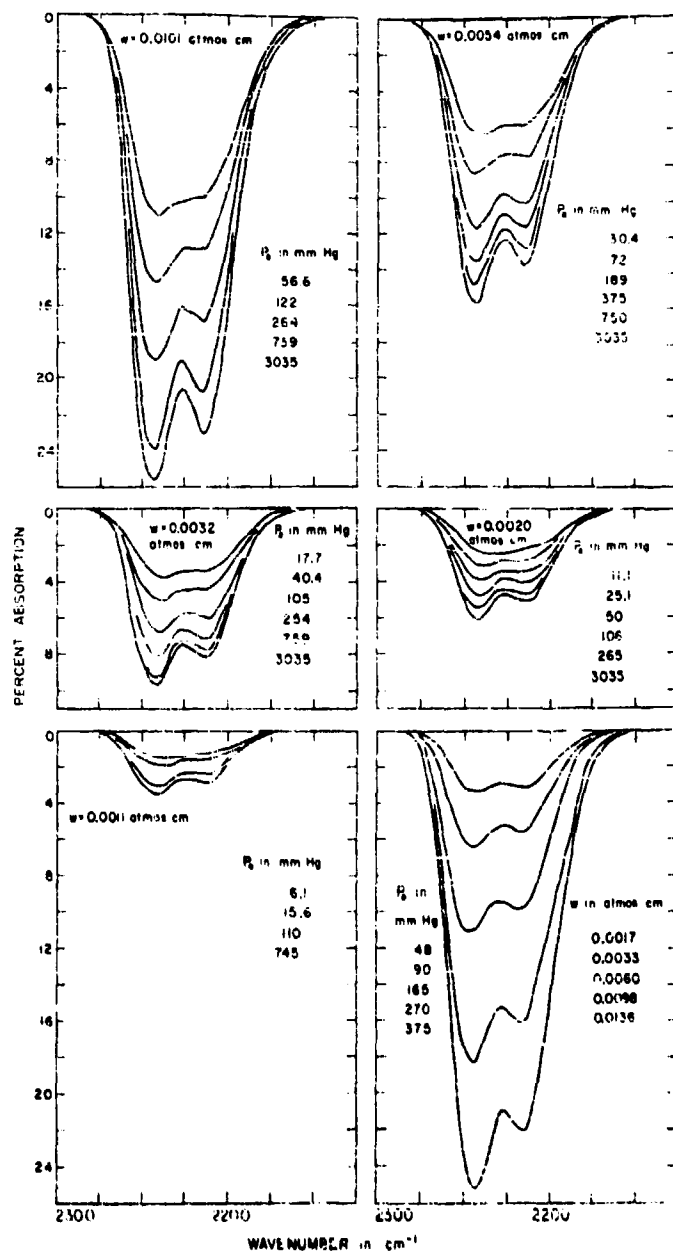


Fig. 7. Spectra of the 2224 cm⁻¹ NdO band.

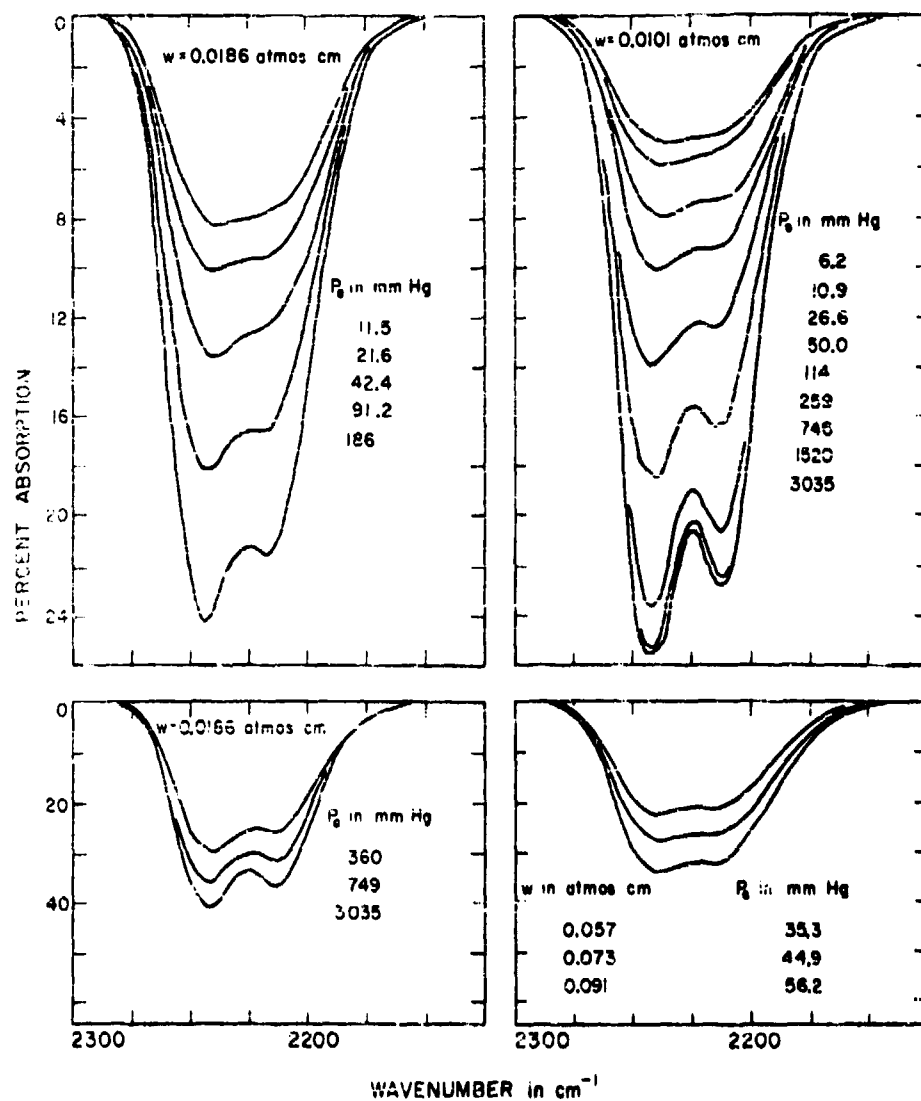


Fig. 8. Spectra of the 2224 cm⁻¹ H₂O band.

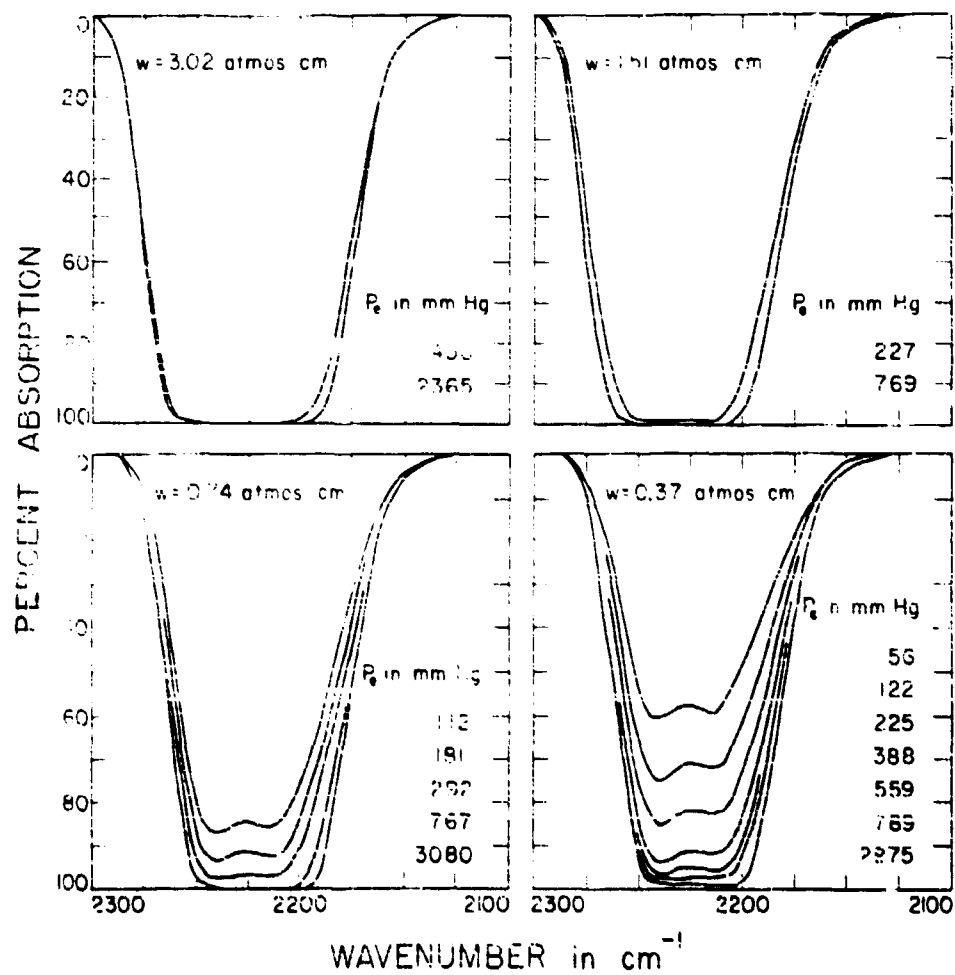
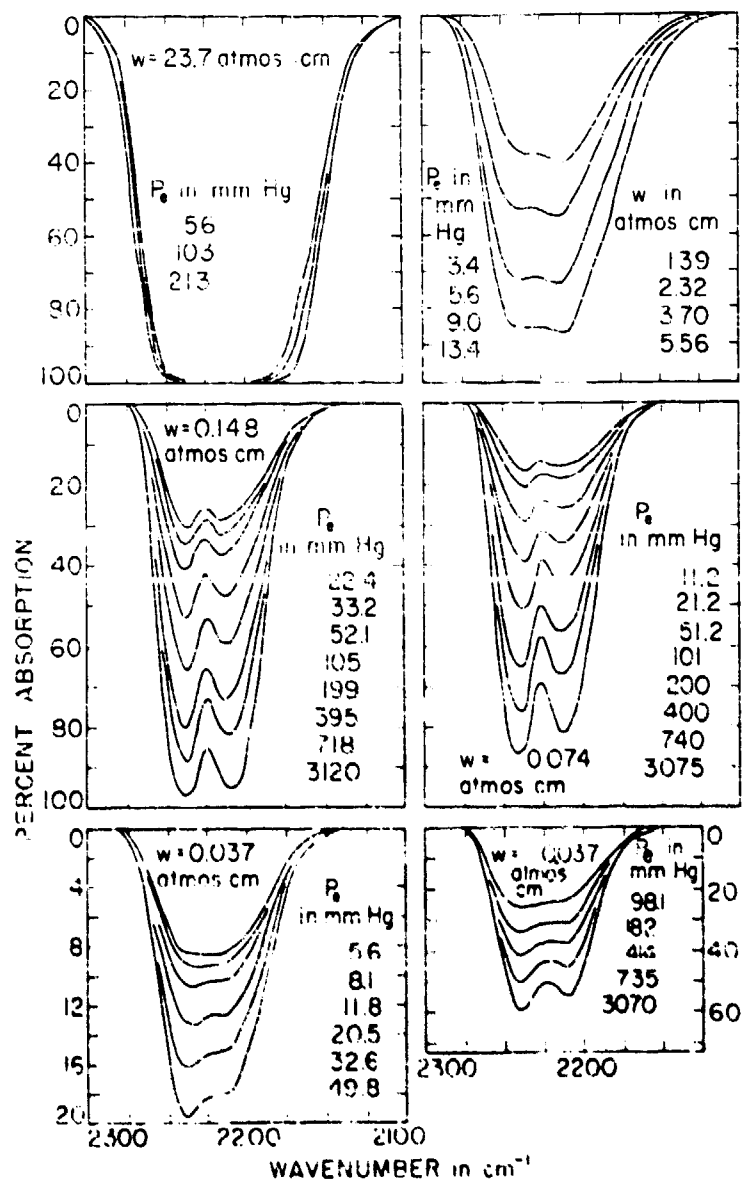


Fig. 9. Spectrum of the 2224 cm^{-1} N_2O band.



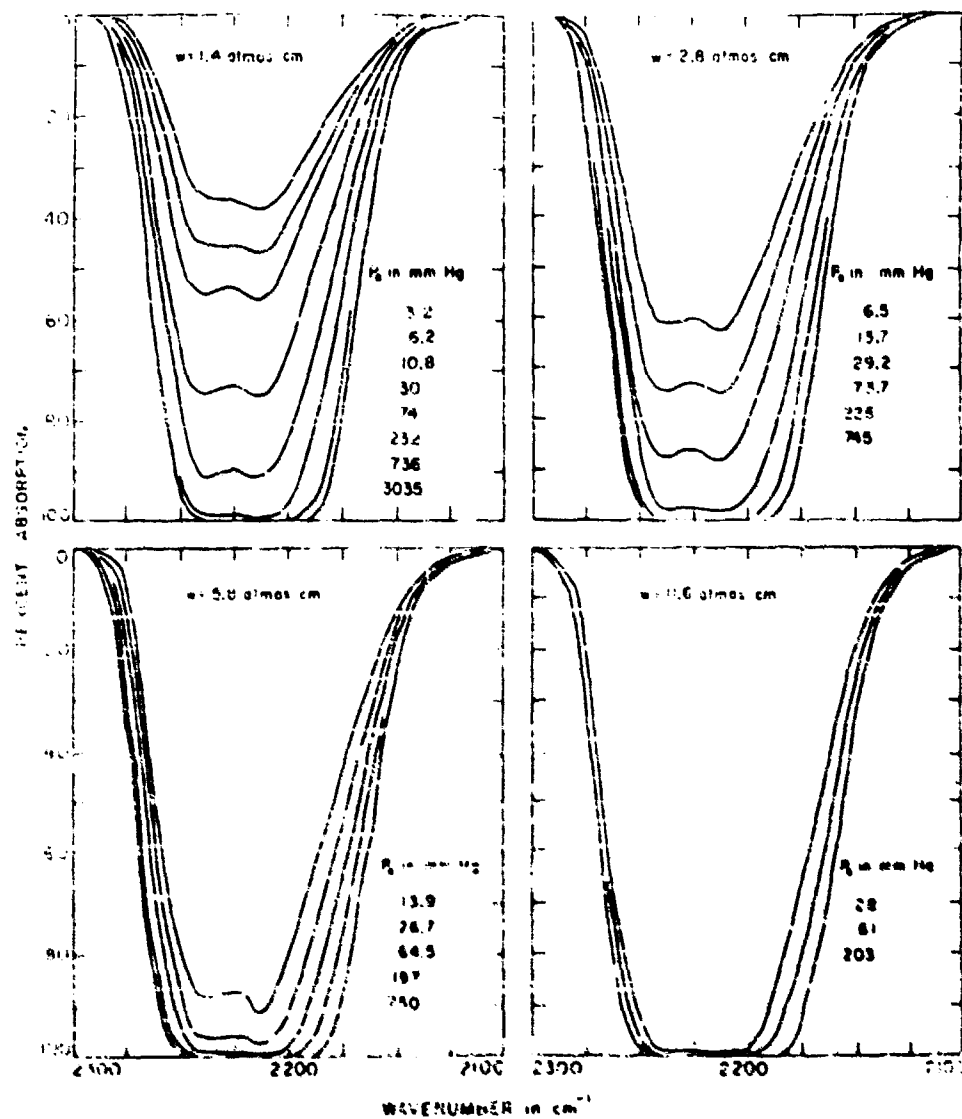


FIG. 1. Spectra of the D_2O band.

Sections of many of the spectra have been omitted to prevent over-crowding of the figures, but as much of each spectrum as could be presented clearly was included. The percent transmission of the samples in the spectral regions where segments were omitted can easily be estimated by interpolation between adjacent absorption curves.

All of the experimental results obtained for the 2224 cm^{-1} H_2O band are summarized in Table 3. The absorber concentration v and equivalent pressure P_e for each sample are shown. The equivalent pressure P_e was calculated from the total pressure P and the H_2O partial pressure p by the simple equation

$$P_e = P + 0.12 p \quad (21)$$

in accordance with Eq. (14) and Table 2.

Values of the total absorption as well as the observed percent absorption at 2240 cm^{-1} and 2213 cm^{-1} are tabulated. These two frequencies correspond to the maximum absorption in the R- and P-branches, respectively. Remarks concerning the sampling procedure are included in the right-hand column of the table.

B. TOTAL ABSORPTION AS A FUNCTION OF ABSORBER CONCENTRATION AND EQUIVALENT PRESSURE

Many of the results summarized in Table 3 are plotted on a logarithmic scale in Fig. 11 with total absorption shown as a function of the equivalent pressure P_e . Each curve corresponds to a given absorber concentration v and shows the effect of increasing the equivalent pressure by adding H_2 . The "path" refers to the length of the absorption cell. The points marked α which occur at the lower ends of curves A through F represent results obtained for samples of H_2O alone. The other points on a given curve give results for samples containing the same amount of H_2O , but with different amounts of H_2 added. The points on the lower ends of curves G, H, and I represent results for samples made from previously mixed H_2O and H_2 ; on these curves there are no points which represent total absorption due to H_2O alone.

The parts of curves D and E corresponding to high equivalent pressures are omitted from the figure for purposes of clarity. If curves D and E had been extended to higher pressures they would be found to be within 1% of the value of total absorption expected from an extrapolation to larger absorber concentrations based on curves F, G and H.

There is a general increase of the slopes of the curves with increasingly high pressures, indicating a decrease in the dependence of

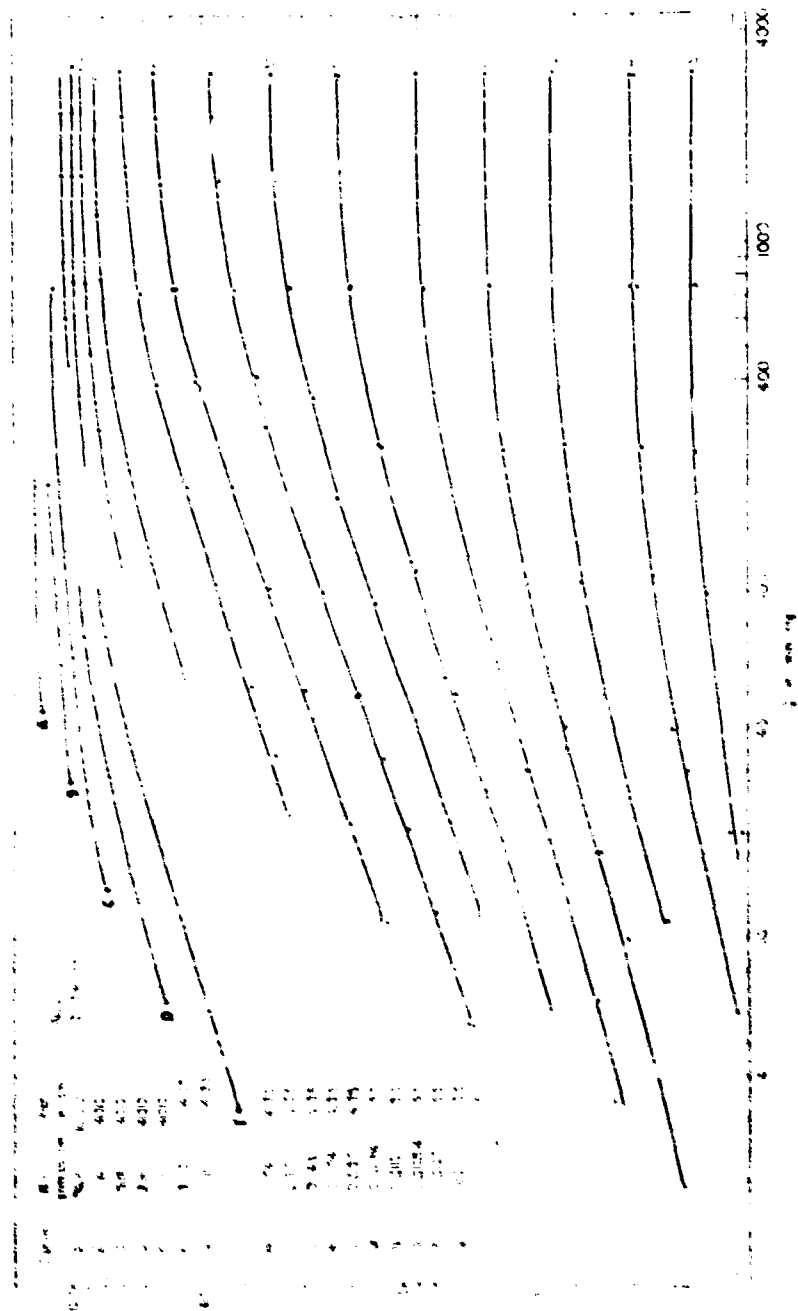


Fig. 12. The total absorption of the 22.4 μm N_2O band
 was constant pressure for samples having
 constant values of absorber concentration.

total absorption on equivalent pressure. This "saturation phenomenon" can be explained on the basis of the change in line shape with pressure. As the pressure increases, the half-width of a spectral line increases and the absorption coefficient $k(\nu)$ increases in the wings and decreases near the center of the line. For pressures sufficiently high that the line half-width is approximately equal to the spacing d between the lines, the fine structure of a band diminishes and further increases in pressure have but little effect on total absorption. Goody and Womell¹⁴ have shown that the half-width $\alpha = d$ for N_2O bands at a pressure of approximately 4100 mm Hg (5.4 atmospheres), where α and d are necessarily averaged over the entire band. One would therefore not expect the total absorption to change appreciably with pressure in the higher-pressure ranges used in the present study.

It is seen from Fig. 12 that the value of P_0 above which the total absorption increases only slightly with increasing pressure is greater for larger values of absorber concentration than for smaller values. In the case of large ν , the decrease of $k(\nu)$ near the line centers which occurs with increasing pressure does not appreciably decrease the absorption $A'(\nu)$ at these frequencies since $k(\nu)\nu$ is still sufficiently large that the absorption remains essentially complete at the line centers. However, in the case of small ν , a lower pressure P_0 is sufficient to reduce $k(\nu)\nu$ near the line centers to a value such that the decrease in absorption near the line centers with increasing pressure is approximately the same as the increase in absorption in the wings of the line. There is therefore little or no net increase in total absorption with increasing pressure.

Curves J through O have approximately the same slope for values of pressure below 200 mm Hg. The slopes of any of the curves in this region have a maximum value of approximately 0.38 and an average of approximately 0.37. Thus it is possible to express the total absorption as some function of the absorber concentration ν times $P_0^{0.37}$ for values ν and P_0 represented by these curves.

That the variation of the total absorption with changes in ν and P_0 becomes very slight for large values of ν and P_0 is illustrated by the crowding of the curves in the upper right-hand corner of Fig. 12. This result is due to the fact that $k(\nu)\nu \gg 1$ for most frequencies within the band, and hence the total absorption as given by Eq. (6), changes very slowly as ν and P_0 change. Inspection of the spectra of samples with large ν and P_0 , such as those in Figs. 10 and 11, which are represented by the points in the upper right portion of Fig. 12, reveals that absorption is complete near the band center and that the growth of the band with increasing ν and P_0 is slight and occurs in the wings.

In Fig. 13 are five curves relating the total absorption to the equivalent pressure. The curves of Fig. 13 are different from those of Fig. 12 in that those in Fig. 13 do not correspond to constant values of absorber concentration. Curves A, B, and C correspond to samples of

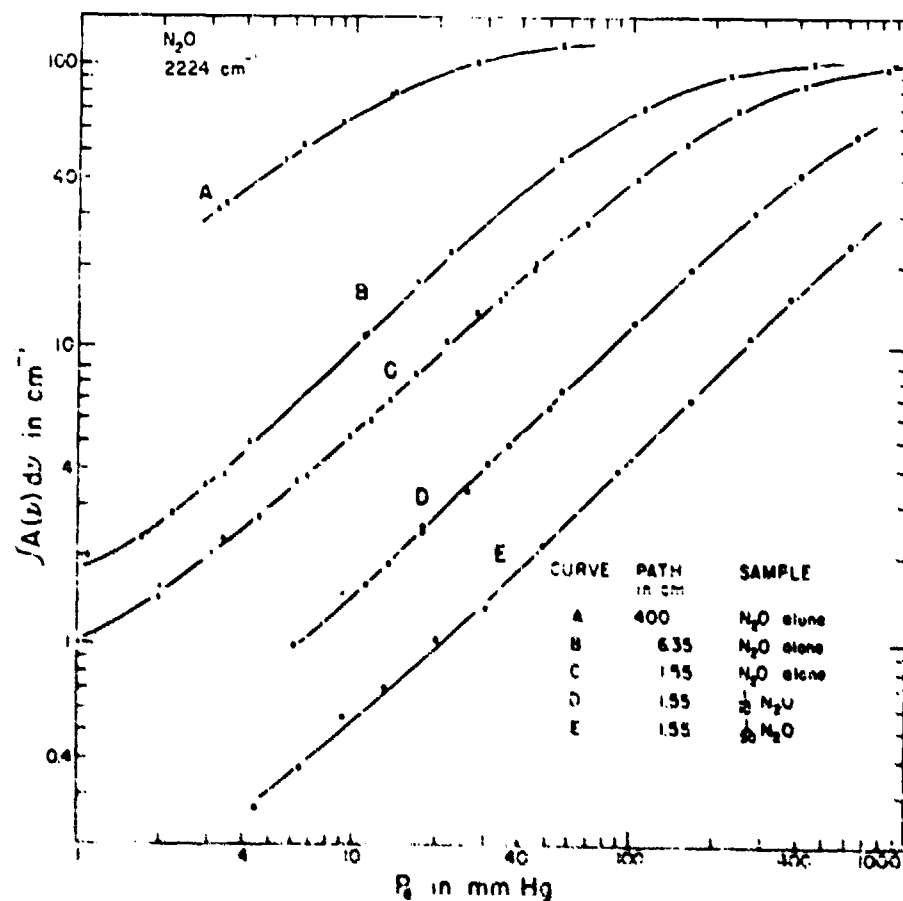


Fig. 13. The total absorption of the 2224 cm^{-1} N_2O band versus equivalent pressure for samples whose values of absorber concentration are proportional to the equivalent pressure.

H₂O alone in the absorption cell, and the absorber concentration \bar{v} is therefore proportional to P_0 . The ratio of \bar{v} to P_0 for the three curves is different because of the different cell path lengths. Curve D corresponds to samples composed of a mixture of one part H₂O to nine H₂ (by volume), and E corresponds to a mixture of one part H₂O to 49 parts H₂. For curves D and E, \bar{v} is also proportional to P_0 as for curves A, B, and C, but the two quantities are related by a different proportionality constant as a result of the different dilution with H₂. Figure 13 contains points corresponding to several of the samples represented in Fig. 12 as well as several other samples which are not represented in Fig. 12 because they do not belong to a group of samples having the same value of \bar{v} .

The slopes of curves A, B, and C are seen to decrease, as in the case of the curves of Fig. 12, for large values of \bar{v} and P_0 . This "saturation", of course, occurs for smaller pressures for the longer paths since the values of \bar{v} are greater; the maximum values of \bar{v} are not sufficiently large to produce saturation in curves D and E.

It is noted that curves B, C, D, and E of Fig. 13 have regions which are approximately linear over a rather wide range of values of equivalent pressure greater than 10 mm Hg. The linear portions of these curves have slopes of approximately 0.91, which is considerably greater than the slope of the linear regions of the curves in Fig. 12. The increase in slope is, of course, due to the fact that \bar{v} increases with P_0 in the curves of Fig. 13, whereas \bar{v} is constant for each curve of Fig. 12. The slope of 0.91 indicates that, for the values of \bar{v} and P_0 covered by the linear portion of these curves,

$$\int A(\bar{v}) d\bar{v} = c \bar{v}^n P_0^m \quad (22)$$

where $m + n = 0.91$ and c is a constant. It was shown in the discussion of Fig. 12 that the total absorption is proportional to $P_0^{0.57}$ over a considerable range of values of \bar{v} and P_0 . This result indicates that the constant n defined immediately above equals 0.57, and m therefore equals approximately 0.54. It will be shown in the discussion of Fig. 14 that the total absorption is, in fact, approximately proportional to $P_0^{0.54}$ over the same range of values of \bar{v} and P_0 as are represented by the linear portions of the curves of Fig. 12 and 13.

It is noted that the slopes of curves A, C, D and E of Fig. 13 decrease toward lower values of P_0 , for P_0 less than approximately 10 mm Hg. This decrease in slope toward lower pressures cannot be explained on the basis of a band consisting of lines having the Lorentz shape given by Eq. 1. The decrease in slope is attributed to Doppler broadening of the lines. Similar deviation from the expected behavior of a band composed of Lorentz lines were observed by Goody and Vornholt¹⁴ in a study of the 1161 and 1185 cm⁻¹ H₂O bands and were attributed to

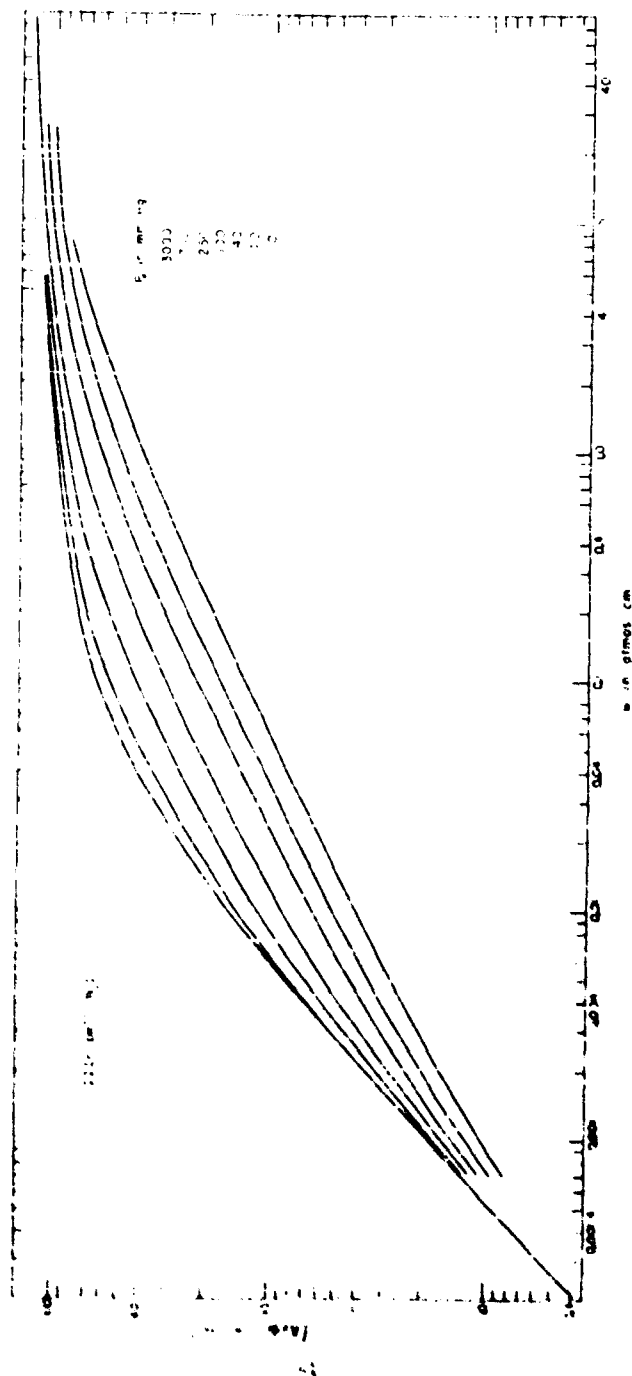


Fig. 14. The total absorption of the 222 cm^{-1} N_2O band versus absorber concentration

Doppler broadening. Benedict¹⁵ et al have also shown that the contribution of Doppler broadening to the absorption of a line or band becomes important at pressures less than approximately 10 mm Hg, causing the absorption to be larger than expected from the Lorentz theory. These results are confirmed in the present study.

There are also indications of a decrease in the slopes of a few of the curves in Fig. 12 at values of P_0 less than approximately 10 mm Hg. However, these curves include only a few points at lower pressures, and any explanation of the effects of Doppler broadening based on these curves alone would hardly be conclusive.

In order to illustrate the dependence of total absorption upon absorber concentration v , values were taken from Figs. 12 and 13 and plotted on a logarithmic scale in Fig. 14. Each curve corresponds to a constant value of equivalent pressure indicated in order from top to bottom. From the curves of Fig. 14 it is possible to determine the total absorption of any sample for which the values of absorber concentration and equivalent pressure fall within the range covered. For samples having values of equivalent pressure which lie between values corresponding to the curves, it is possible to interpolate. The points were omitted in order that readings from the curves might be made more readily. Each curve was drawn over the range of absorber concentrations covered by the data.

C. BAND INTENSITY

The lower portion of the uppermost curve in Fig. 14 which corresponds to an equivalent pressure of 3000 mm Hg is seen to be linear with a slope of approximately one, thus indicating a linear dependence on v . The linear dependence on v can be explained on the basis of Eq. (5) for samples such that $k(v)v \ll 1$ for all frequencies. Under this condition Eq. (6) can be written as

$$\int k(v)dv = v \int k(v)dv. \quad (6')$$

where $\int k(v)dv$ is the band intensity.

The condition $k(v)v \ll 1$ is attained by keeping v very small with P_0 sufficiently large so that $k(v)$ is small, even near the centers of the spectral lines. The condition of large P_0 and small v are satisfied for the linear region of the top curve in Fig. 14. From Eq. (6') the linear dependence on v is obvious, and it is apparent that the value of the quantity $\int k(v)dv$ can be determined graphically from the absorption curves of samples represented by the linear portion of the curve.

At the intercept of the uppermost curve of Fig. 14 with the ordinate axis, $\int A(\nu) d\nu = 0.37 \text{ cm}^{-1}$ and $\bar{\nu} = 2 \times 10^{-4} \text{ atmos cm}$. Substitution of these values into Eq. (6') yields a value of

$$\int k(\nu) d\nu = 1850 \text{ atmos}^{-1} \text{ cm}^{-2} \quad (23)$$

for the band intensity of the $2224 \text{ cm}^{-1} \text{ H}_2\text{O}$ band.

The value of $\int k(\nu) d\nu$ given by Eq. (23) can be compared to values of this quantity which have been published by other workers. The results of three other workers are as follows.

Observer	$k(\nu) d\nu$ in $\text{atmos}^{-1} \text{ cm}^{-2}$
Thorndike and Wells ¹⁶	1867
Callomon, McKean and Thompson ¹⁷	1617
Eggers and Crawford ¹⁸	1650

In order to find the value of $\int \nu(\nu) d\nu$ by the method employed in the present study, the approximation that $k(\nu)/\nu \ll 1$ for all ν must be valid, a requirement which is satisfied by small values of ν and values of P_0 sufficiently large so that $k(\nu)$ is small, even near the centers of the lines. Under these conditions the lines of the band are said to be "completely broadened" and the total absorption is independent of pressure.

Without data which include sufficiently wide ranges of ν and P_0 , it is difficult to be sure that the conditions of small ν and large P_0 are sufficiently well satisfied so that the approximation $k(\nu)/\nu \ll 1$ is valid. Some question has arisen concerning the results of Thorndike and Wells, which were mentioned above, with regard to this approximation¹⁷. However, in the present study sufficient data are available which indicate that the approximation is indeed valid.

The left-hand portions of the upper three curves, which correspond to values of $P_0 > 250 \text{ mm Hg}$, converge. Therefore one concludes that for the value of $\bar{\nu} = 2 \times 10^{-4} \text{ atmos cm}$ used to calculate $\int k(\nu) d\nu$, the value of $P_0 = 3000 \text{ mm Hg}$ used was sufficiently large to produce complete broadening.

The requirement that ν be small is apparently satisfied since the lower portion of the upper curve of Fig. 14 is linear with a slope of very nearly unity. It therefore seems that the accuracy of the value given by Eq. (23) depends more on the accuracy with which the spectra were measured and the accuracy to which $\bar{\nu}$ was determined rather than on the validity of the approximation that $k(\nu)/\nu \ll 1$.

The spectra which correspond to the portion of the curve in Fig. 14 from which the reading was taken were recorded with the ordinate scale expanded by a factor of ten. Three spectra were obtained for each sample and the average was used. The short absorption cell (1.55 cm) was used in order to produce small values of absorber concentration y without using extremely small partial pressures of N_2O . In order to improve the accuracy of determining y , the N_2O was admitted to the cell in the form of a mixture of N_2O and N_2 . This procedure made it possible to deal with pressures sufficiently large that they could be measured with greater accuracy. Consideration of the total absorption measurements indicated that the value of $\int A(y) dy$ given by (23) is accurate to $\pm 10\%$.

D. EMPIRICAL EQUATIONS: LIMITATIONS

The curves of Fig. 14 are seen to converge at the lowest and highest values of y , but the five lower curves are nearly linear and parallel over a wide range of y near the centers of the curves. The slope of the linear portions of the curves was found to be approximately 0.53, thus indicating that the total absorption is proportional to $y^{0.53}$. The range of values of y and P_0 for which $\int A(y) dy$ is proportional to $y^{0.53}$ is approximately the same as the range for which $\int A(y) dy$ was found to be proportional to $P_0^{0.57}$ in the discussion of Fig. 12. For values of y and P_0 which are represented by the linear portions of the curves of Figs. 12 and 14, these results indicate that

$$\int A(y) dy = c y^{0.53} P_0^{0.57} = [y P_0^{0.7}]^{0.53}, \quad (24)$$

where c is a constant. The result in Eq. (24) is seen to be in good agreement with Eq. (22), which is based on Fig. 13. It is recalled that the curves of Fig. 13 are based on data obtained from samples of N_2O alone and samples of N_2O and N_2 which were mixed before being introduced to the cell. Most of the curves of Figs. 12 and 14 are based on data obtained from samples formed by adding N_2 to the absorption cell after the N_2O had been introduced. The good agreement between the results of Fig. 13 and those of Figs. 12 and 14 therefore indicates that very little error in sampling was introduced in the process of adding N_2 to the samples.

From Figs. 12, 13, and 14 it is seen that a very complex function would be required to relate the total absorption to y and P_0 for all values of these parameters. Several experimenters have succeeded in using simple expressions, but these were only valid for limited values of y and P_0 , as in the case of Eq. (24).

In the JNM report, two different types of equations were used. A "weak fit" equation of the form

$$\int A(\nu) d\nu = c \nu^{1/2} P_e^k \quad (25)$$

was used for small values of total absorption, and a "strong fit" of the form

$$\int A(\nu) d\nu = C + D \log \nu + K \log P_e \quad (26)$$

was used for larger values of total absorption above a certain value called a determining value.

Values for the constants c , k , C , D , and K as well as the determining value were chosen for each band to give the best fit with the data. Equations (25) and (26) were intended only as empirical equations with the constants having no particular physical or theoretical significance. Since the data presented in the present report cover much wider ranges of both ν and P_e than those covered by HBW, it is of interest to use these new data to determine the regions for which equations of the form given by (25) and (26) are valid. It is of equal interest to demonstrate the short-comings of such empirical equations and to point out the danger involved in using them to extrapolate to values of ν and P_e not included by the data from which they were derived.

Equation (24) indicates that the total absorption is a function of the product $\nu P_e^{0.7}$, at least for certain values of ν and P_e . In order to check the usefulness of a function of $\nu P_e^{0.7}$ for all the data obtained and to illustrate its deficiencies, the curves of Fig. 15 have been drawn. Each curve corresponds to a given value of P_e as indicated. The points shown in Fig. 15 do not represent actual samples, but correspond to values taken from the curves of Figs. 12 and 13. Since each curve corresponds to a given value of equivalent pressure it has the same shape as the corresponding curve in Fig. 14, but the relative positions of the curves are shifted along the abscissa. Some of the curves were not extended over the full range since several curves would be so close as to not be distinguishable. Although the complete curves were not included, all the points were included and indicate where the curves would occur.

If the total absorption were a function of only the product $\nu P_e^{0.7}$ for all values of ν and P_e , the curves of Fig. 15 would all coincide. It is not surprising that the curve corresponding to $P_e = 3000$ mm Hg occurs well to the right of the others since the fine structure of the band is nearly smoothed out at this high pressure and the effects of increasing the pressure are small as indicated in Fig. 12.

It is interesting to note that the curves corresponding to $P_e \leq 250$ mm Hg occur relatively close together for values of $\nu P_e^{0.7}$ greater than approximately 0.5 (atmos cm) (mm Hg) $^{0.7}$, a result indicating that over

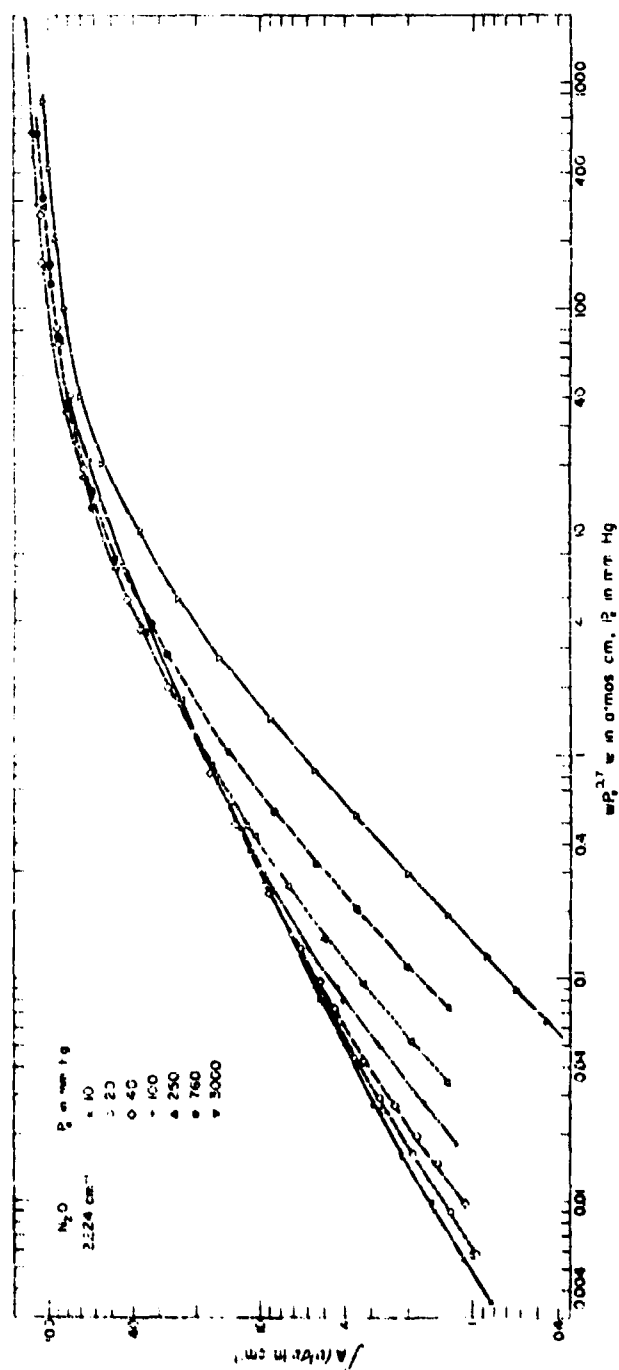


Fig. 15. The total absorption of the $2224 \text{ cm}^{-1} \text{ N}_2\text{O}$ band versus $\nu_{\text{F}_2}^{17}$.

this region of values of v and P_g the total absorption could be approximated by a function of $vP_g^{0.7}$. The curve corresponding to 760 mm Hg also converges with the lower pressure curves for values of $vP_g^{0.7}$ greater than approximately 3, but this curve falls definitely below the others for smaller values of $vP_g^{0.7}$.

The lower portions of the curves diverge, with the curves for higher pressures and lower absorber concentration falling below the curves for lower pressure and higher values of absorber concentration. This result is expected on the basis of the lower curves of Fig. 12, for which the value of absorber concentration is small and the increase in total absorption with increasing pressure is slight.

The points corresponding to all the values of P_g except 3000 mm Hg occur close together in the rather flat upper portion of the curves of Fig. 15. It should be noted that the closeness of these points does not necessarily indicate that the values of the exponent (0.7) to which P_g is raised has been determined accurately for the values of v and P_g represented by these points. Since a change in the exponent would cause only a relative horizontal shifting of the curves of Fig. 15, the value of the exponent could be changed considerably without appreciably altering the ordinates of the rather flat portions of the curves.

The upper portion of the curve corresponding to 10 mm Hg crosses the curves of higher pressure (except 3000 mm Hg) and falls below them. This indicates that for these points the exponent of P_g should be somewhat greater than 0.7. Thus, one concludes that 0.7 is low for some values of v and P_g and too large for others, but it is a nominal value which can be used satisfactorily over rather wide ranges without introducing serious error.

From Fig. 15, it is a simple matter to determine graphically some simple empirical functions of the product $vP_g^{0.7}$, and to determine the values of v and P_g for which each function is valid.

The middle portions of these curves which are nearly linear can be represented by the following equation:

$$\begin{aligned} \text{for} \quad & \int A(v)dv = 19.0 \, v \left[P_g^{0.7} \right]^{0.53} \\ \text{and} \quad & 10 < \int A(v)dv < 45 \, \text{cm}^{-1}, \\ & 10 < P_g < 250 \, \text{mm Hg}. \end{aligned} \quad (27)$$

Equation (27) is the same as Eq. (24) except the constant c of (P_g) has been evaluated from the curves of Fig. 15 and substituted into the latter equation.

For larger values of total absorption the following equation, which is similar to the strong fit (26) of HEM, has been derived.

$$\begin{aligned} \int A(\nu) d\nu &= 15 + 40 \log (wP_0^{0.7}), \\ \text{for } 45 &< \int A(\nu) d\nu < 120 \text{ cm}^{-1}, \\ \text{and } 10 &< P_0 < 760 \text{ mm Hg.} \end{aligned} \quad (28)$$

Values of total absorption calculated by use of Eqs. (27) and (28) are believed to be accurate to approximately $\pm 10\%$.

Several investigators have used functions of wP_0^a to represent data which included values of w and P_0 covering much smaller ranges than in the present study. Therefore, the limitations of the use of such functions were not illustrated so vividly as in the present study. It should be emphasized that empirical equations involving a function of wP_0^a cannot be used for small values of w/P_0 or for high pressures. It is, therefore, suggested that caution should be used when applying the equations listed in the HEM report to samples that are smaller than those from which the equations were derived.

K. COMPARISON OF RESULTS WITH THE PREDICTIONS BASED ON ELIASZER BAND MODEL

It is recalled from Section II that for certain values of w and P_0 the strong-line approximation of the Eliaszer band model is valid and the total absorption is a function of wP_0 . However, it has been shown in the previous section that a function of $wP_0^{0.7}$ fits the 2224 cm^{-1} H_2O data over rather wide ranges of values of the parameters. It is therefore of interest to show the relationship between the total absorption of the 2224 cm^{-1} H_2O band and the product wP_0 .

In order to show this relationship graphically, the logarithm of the total absorption was plotted in Fig. 14 against the logarithm of wP_0 for the different pressures indicated. The points shown in Fig. 14 do not correspond to samples actually measured, but to values taken from the curves of Figs. 12 and 13. By this procedure it was possible to obtain sets of points which correspond to a given value of P_0 as was done for Figs. 14 and 15. Since each curve corresponds to a given value of equivalent pressure, it has the same shape as the corresponding curves in Figs. 14 and 15, but the relative positions of the curves are shifted along the abscissa.

The different curves corresponding to values of $P_0 \leq 200 \text{ mm Hg}$ occur very close together in the region corresponding to wP_0 greater

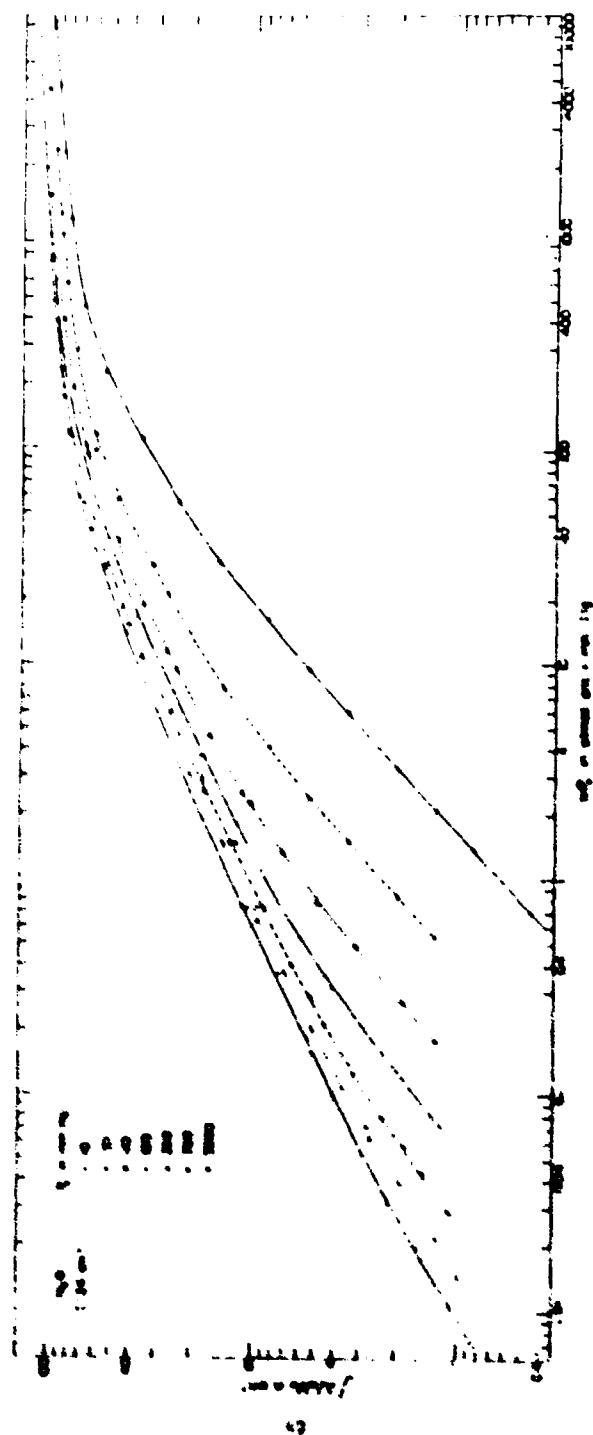


Fig. 16. The total absorption of the $2226 \text{ cm}^{-1} \text{ H}_2\text{O}$ band versus w .

than approximately 500 atmos cm x cm Hg. This result indicates that it is possible to relate the total absorption to the variable νP_e for the values of ν and P_e which are involved. However, this result is somewhat inconclusive, since it was shown in Fig. 15 that the total absorption of samples involving the same values of ν and P_e could also be related to the variable $\nu P_e^{0.7}$. In the discussion of Fig. 15 it was pointed out that for these samples the absorption is nearly complete, and that the total absorption of the band increases only slightly with increasing ν or P_e . The total absorption can therefore be satisfactorily related to a function of νP_e^a , and the value of the exponent a can be varied considerably.

The curves are separated considerably for values of ν and P_e for which the absorption is still increasing with either ν or P_e . This result, of course, indicates that the total absorption cannot be satisfactorily related to the single variable νP_e . However, it is of interest to look in particular at the regions of the curves of Fig. 16 for which the strong-line approximation would be valid if the absorption band being studied could in fact be represented by an Elsasser band.

The regions of the curves which are to be investigated can be determined from curves and equations given by Plasse⁹ for the region of validity of the strong-line approximation for an Elsasser band. Before the present data, which are given in terms of the parameters ν and P_e , can be compared to the theoretical predictions, it is necessary to relate ν and P_e to the dimensionless quantities x and β which serve as the variables in the theoretical equations.

As indicated in Section II, the quantity x is given by

$$x = \frac{8\nu}{2\pi\alpha} ; \quad (29)$$

the parameter β is given by

$$\beta = \frac{2\pi\nu}{d} \quad (30)$$

where d is the frequency separation of adjacent absorption lines. For a given band, β is proportional to α , which in turn is proportional to P_e (Eq. 14); therefore it is necessary to find the constant relating the two quantities β and P_e . The value of the proportionality constant can be determined by using values of α and d for an N_2O band, taken from an article by Goody and Wormell¹⁴ mentioned previously. The value used for d was 0.04 cm^{-1} , and α was assumed to be proportional to P_e and equal to 0.15 cm^{-1} at a pressure of one atmosphere. Therefore it can be shown that $\beta = 1$ corresponds to $P_e = 600$ for N_2O .

$$\beta = P_e/600 \quad (31)$$

where P_0 is expressed in mm Hg.

By using Eq. (11) and applying the conditions given by Plasz, the validity of the strong-line approximation of an Elsasser band, it is possible to determine regions of the curves of Fig. 16 over which one would expect the total absorption to be a function of the variable νP_0 , accurate to $\pm 5\%$.

For example, for $P_0 \leq 250$ mm Hg, the total absorption is a function of νP_0 accurate to $\pm 5\%$ for values of $\int A(\nu) d\nu$ greater than approximately 60 cm^{-1} , and the relative error should decrease as the total absorption increases. At the value of νP_0 for which the curve of Fig. 16 corresponding to 250 mm Hg gives a value of $\int A(\nu) d\nu$ equal to 60 cm^{-1} , the curve corresponding to 10 mm Hg reads approximately 74 cm^{-1} . Thus it is seen that the total absorption cannot be represented, with an accuracy of 5% , as a function of the single variable νP_0 for the values of ν and P_0 predicted by the Elsasser band model. The error is seen to be more nearly 20% than 5% . Similar deviations from the predicted strong-line dependence were found for other values of P_0 .

As just indicated, the dependence of the total absorption of this band on ν and P_0 cannot be described by a simple Elsasser band, and can be described by a simple empirical equation only over limited ranges of P_0 and ν . However, the total absorption could possibly be described in terms of a "random Elsasser model" made up of two or more Elsasser bands of different intensities. Such an analysis of the 9.6μ ozone band has been made by Plasz⁹.

From the previous discussion it can be concluded that the total absorption of the 2224 cm^{-1} N_2O band is less dependent upon P_0 than upon ν for essentially all values of ν and P_0 . This is in contrast to an Elsasser band for which the strong-line approximation is valid over a considerable range of values of ν and P_0 , and the total absorption has the same dependence on both ν and P_0 .

The low dependence upon pressure as compared with an Elsasser band can be explained, qualitatively at least, from the fact that the spectral lines are not all of equal intensity as assumed for an Elsasser band. Much of the band where the lines are weak, for which (8) is approximately valid, and where the effect of increasing pressure is small while the effect of increasing absorber concentration is large. Unless all the lines of the band are strong, the effect of increasing pressure will always be less than the effect of increasing absorber concentration, which is the result observed in the present study.

F. FURTHER TESTS OF ELSASSER MODEL:
ABSORPTION AT R-MAX. AND P-MAX.

Since it is probable that the absorption by weak lines in the wings of the band contributes to the deviation of the total absorption from a strong-line dependence, it is of interest to investigate the absorption $A(\nu)$ at the frequencies of maximum absorption in the R- and P-branches, where the strong-line approximation might be expected to apply. These two frequencies will hereafter be referred to as R-max. and P-max. respectively.

The major portion of the absorption observed at these frequencies arises from the spectral lines whose centers occur within the spectral interval passed by the spectrometer. If one could assume that all the lines in this interval were evenly spaced and had the same half-width and line strength, one would expect that for a certain range of values of ν and P_0 , the absorption would show the strong-line dependence predicted by an Elsasser model. However, it was mentioned above that the spectral region under investigation contains weak bands as well as the strong fundamental band. Therefore a portion of the absorption observed at frequencies of peak absorption is due to weak lines whose centers occur within the spectral interval of the spectrometer. The effect of these weak lines would be to cause the observed absorption to deviate somewhat from the strong-line dependence.

There is also a contribution to the absorption by the wings of spectral lines whose centers occur outside the spectral interval passed by the spectrometer. However, as was discussed in Section II in connection with the strong-line approximation, the absorption by the wings of a line has a strong-line dependence. Therefore, the absorption by lines whose centers are outside the spectral interval passed by the spectrometer would not be expected to cause the observed absorption to deviate from the strong-line dependence.

The values of the absorption $A(2240 \text{ cm}^{-1})$ and $A(2213 \text{ cm}^{-1})$, the frequencies corresponding to R-max. and P-max., respectively, have been tabulated for each spectrum in Table 2. The frequency of the regions of maximum absorption shifted very slightly as the shape of the band changed for different values of ν and P_0 , but the difference between the maximum absorption and that at the two frequencies listed is very slight, since the slope of the absorption curves is small near these frequencies. Some of the absorption curves, such as those in Fig. 5, do not have two distinct absorption maxima, but for such spectra the value of percent absorption was measured at the two frequencies designated.

The values of absorption $A(2240 \text{ cm}^{-1})$ of several of the samples are plotted against the equivalent pressure in Fig. 17. Each curve corresponds to a given value of ν as indicated, with "x's" corresponding to samples of H_2O alone and the dots corresponding to samples having H_2 added to the H_2O . The curves have the same general features as those in Fig. 12,

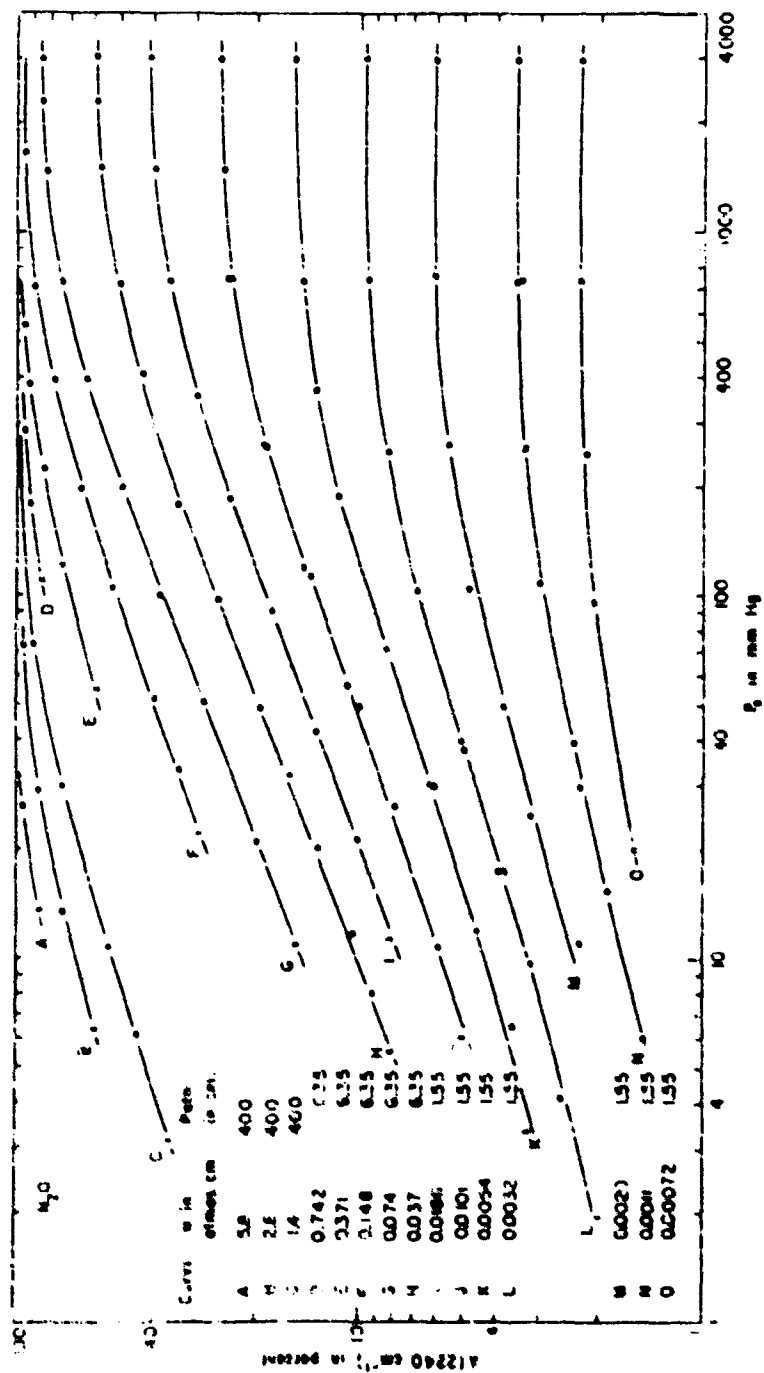


Fig. 17. The percent absorption at 2240 cm^{-1} versus equivalent pressure for samples having constant mass of absorber concentration.

in which the total absorption was plotted against P_0 . The slopes of the curves decrease at high values of equivalent pressure and the curves converge at 100% absorption for large values of v and P_0 . Several of the curves have portions for $10 \text{ mm Hg} < P_0 < 200 \text{ mm Hg}$ which are nearly linear and approximately parallel. The slope of these portions of the curves is approximately 0.41, indicating that the absorption is proportional to $P_0^{0.41}$. It is noted that the $P_0^{0.41}$ dependence is significantly less than the $P_0^{0.5}$ dependence which is associated with the well-known square-root approximation.

There seems to be a slight decrease in the slope of curves K and L at equivalent pressures less than six or eight mm Hg; this decrease in slope probably corresponds to additional absorption resulting from Doppler broadening.

The absorption $A(2240 \text{ cm}^{-1})$ at H-branch maximum was plotted in Fig. 18 against P_0 for the samples for which total absorption is plotted in Fig. 15. These curves differ from those in Fig. 17 in that each curve in Fig. 18 does not correspond to a given value of v , but v increases in proportion to P_0 . In each sample v is proportional to P_0 , but the ratio v/P_0 is smaller for the sample represented by each successive curve. Curves B, C, D, and E are seen to have nearly linear portions of slopes approximately 0.92, with decreasing slope for larger values of P_0 for which overlapping of the lines becomes significant. The linear portions of the curves suggest that the absorption is proportional to $v^a P_0^b$ where the sum of the exponents a and b is approximately 0.92. This result is to be compared with the predicted square-root region over which the absorption is proportional to $v^{0.5} P_0^{0.5}$. The decrease in slope of curves B, C, D, and E at pressures below 6-8 mm Hg is undoubtedly due to Doppler broadening, as in the curves of total absorption in Figs. 12 and 13.

As stated earlier, the absorption can be represented by the single variable vP_0 for values of v and P_0 for which the strong-line approximation is valid. In order to show the dependence of the observed absorption on the variable vP_0 , values of absorption $A(2240 \text{ cm}^{-1})$ were taken from the curves of Figs. 17 and 18 and plotted as a function of vP_0 in Fig. 19, where each curve corresponds to a given value of equivalent pressure. The features of these curves are similar to those of Fig. 16 in which the ordinate represents total absorption rather than percent absorption at a fixed frequency. Validity of the strong-line approximation would, of course, be represented in Fig. 19 by a coincidence of the curves corresponding to the different pressures. As in the case of Fig. 16, which is similar except that total absorption is plotted as the ordinate, most of the curves corresponding to higher pressures occur to the right of and below the curves corresponding to lower pressures. The curves corresponding to lower pressures tend to converge for large values of v , a result indicating that for these values of v and P_0 the total absorption could be expressed by a strong-line approximation.

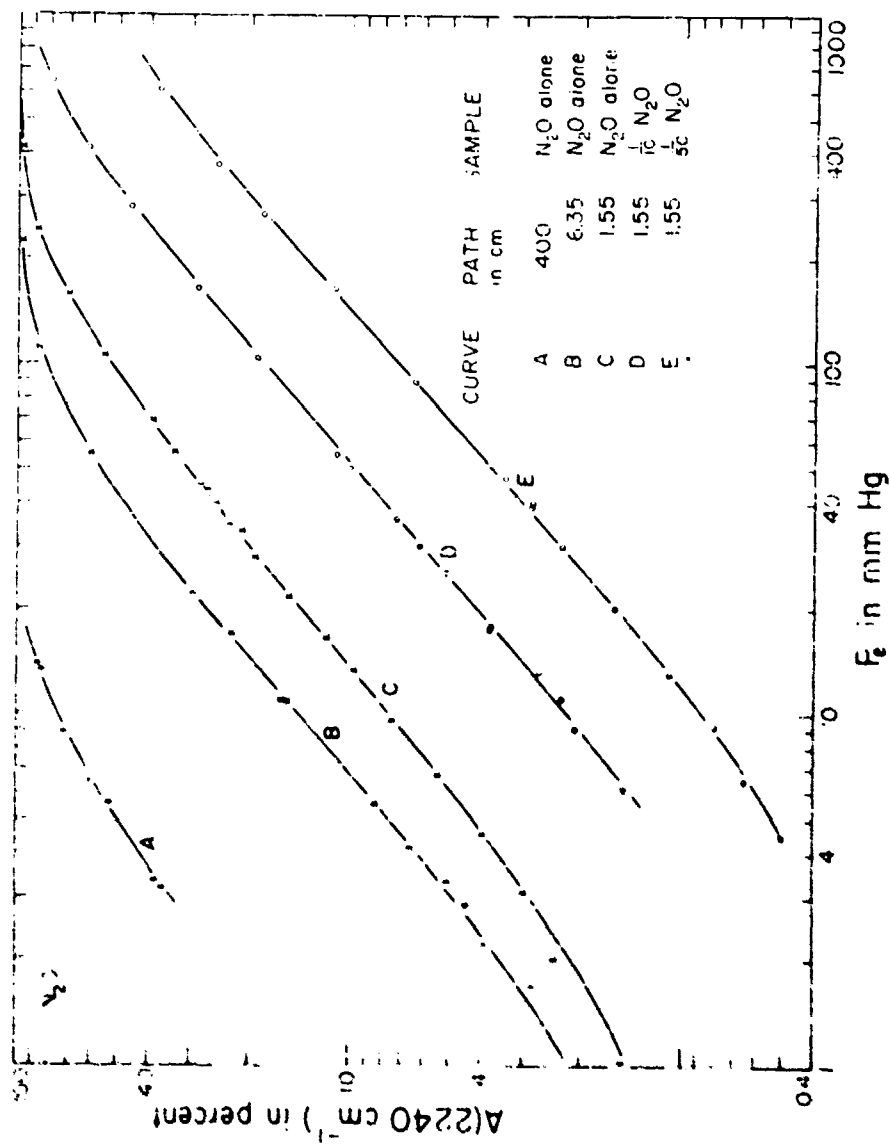


Fig. 16. The percent absorption $\pm 2240 \text{ cm}^{-1}$ versus equivalent pressure for samples whose values of absorber concentration are proportional to the equivalent pressure.

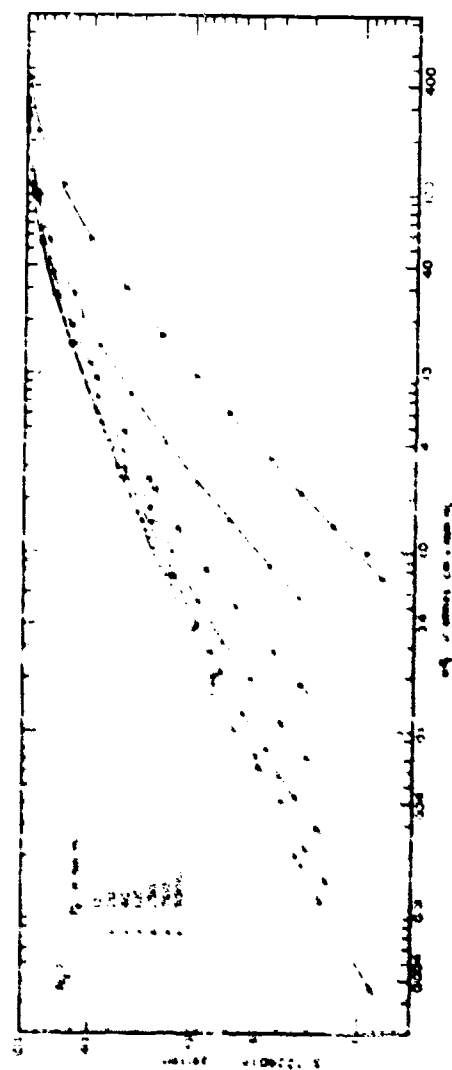


Fig. 12. The percent absorption L-22-C nm⁻¹ versus μ

The three curves corresponding to values of P_0 equal to 10, 20, and 40 mm Hg contain portions which are nearly straight with a slope whose value is approximately 0.50. This result corresponds to the well-known square-root dependence on ν ; however, it is apparent from these curves that the dependence on P_0 is less than square-root since the curves corresponding to higher pressures occur to the right of those corresponding to lower pressures. It is also recalled from the discussion of Fig. 17 that the maximum dependence on P_0 is only approximately $P_0^{0.41}$.

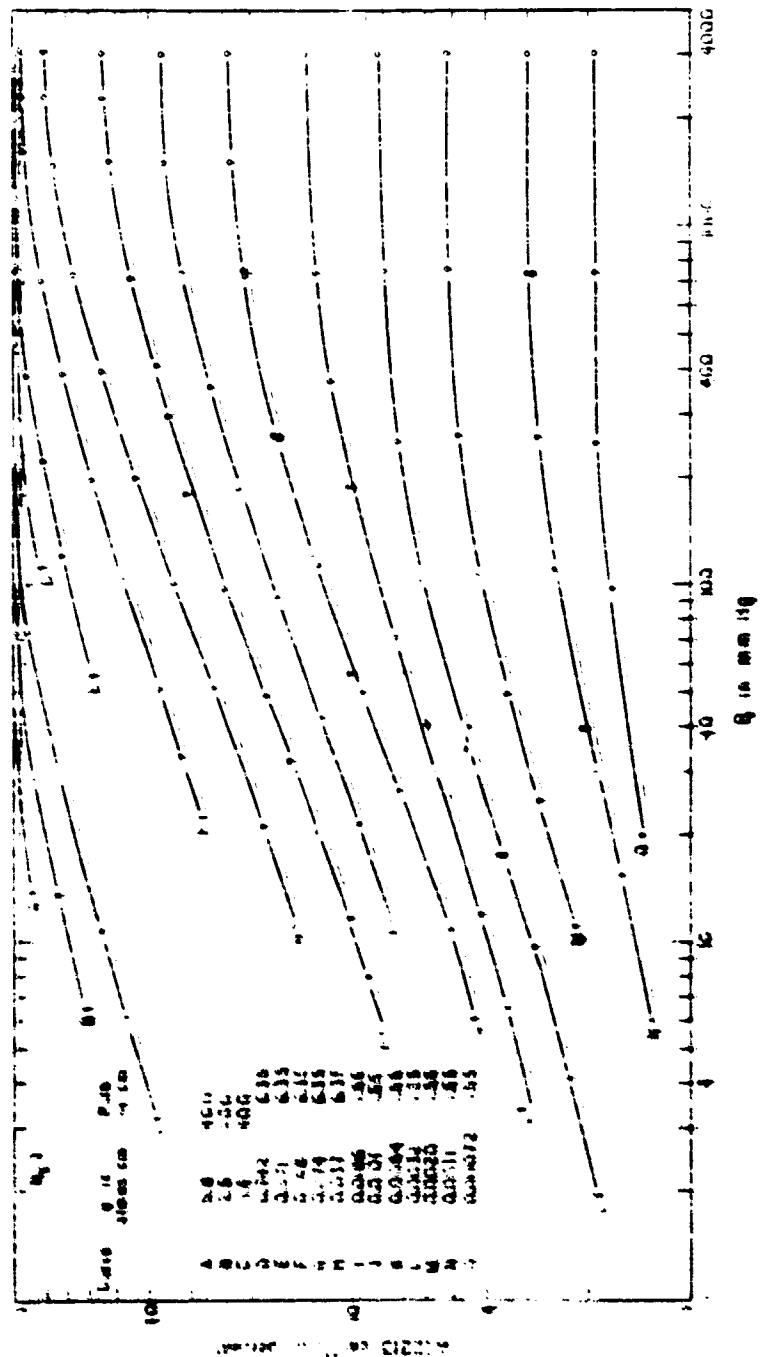
It is noted that the $\nu^{0.50} P_0^{0.41}$ dependence which is found from Figs. 17 and 19 is consistent with the result of Fig. 18, which indicated that the absorption was proportional to $\nu^m P_0^n$ where $m + n = 0.92$.

Curves similar to those in Figs. 17, 18, and 19 were drawn for the absorption $A(2217 \text{ cm}^{-1})$, the frequency corresponding to maximum absorption in the F-branch. The features of the curves of Fig. 20 are similar to the corresponding curves of Fig. 17; the slope of the straight portions of the curves of Fig. 20 is approximately 0.38, which is slightly less than the value 0.41 obtained in Fig. 17. This result indicates that the maximum dependence on pressure is slightly less for the peak absorption in the F-branch than in the R-branch.

The curves of Fig. 21 are also similar to the curves of the corresponding Fig. 18 which represents the R-branch absorption. The slopes of the straight portions of the curves in Figs. 18 and 21 are essentially the same, 0.92. Similarly, the features of the curves of Fig. 22 are like those of Fig. 19; however, the slope of the straight portions of the curves of Fig. 22 seems to be slightly greater (0.52 instead of 0.50), although this small difference is hardly significant.

Figures 19 and 22 indicate that the absorption can be represented by the strong-line approximation only for small values of P_0 and very large values of ν . For smaller values of ν such that the absorption is proportional to $\nu^{0.5}$ the dependence on P_0 is significantly less, and the strong-line approximation is no longer valid. It is of interest to compare the curves of Figs. 19 and 22 with theoretical results based on an Einstein band in the same manner as was done with the curves of Fig. 16. It was possible to make such a comparison by assuming the relationship between β and P_0 that is given by Eq. (31) and applying the conditions given by Eqs. 9 for the validity of the strong-line approximation.

For example, if $P_0 \leq 150$ mm Hg, the absorption of an Einstein band can be expressed as a function of νP_0 within $\pm 1\%$ for values of absorption greater than approximately 4%. In comparing this with the curves of Fig. 19, it is found that the absorption $A(2260 \text{ cm}^{-1})$ equals approximately 4% at $P_0 = 250$ mm Hg for the same value of νP_0 which gives a value of 50% absorption on the 10 mm Hg curve. Thus there is an observed relative difference of 1% as compared with the value of 4% based on



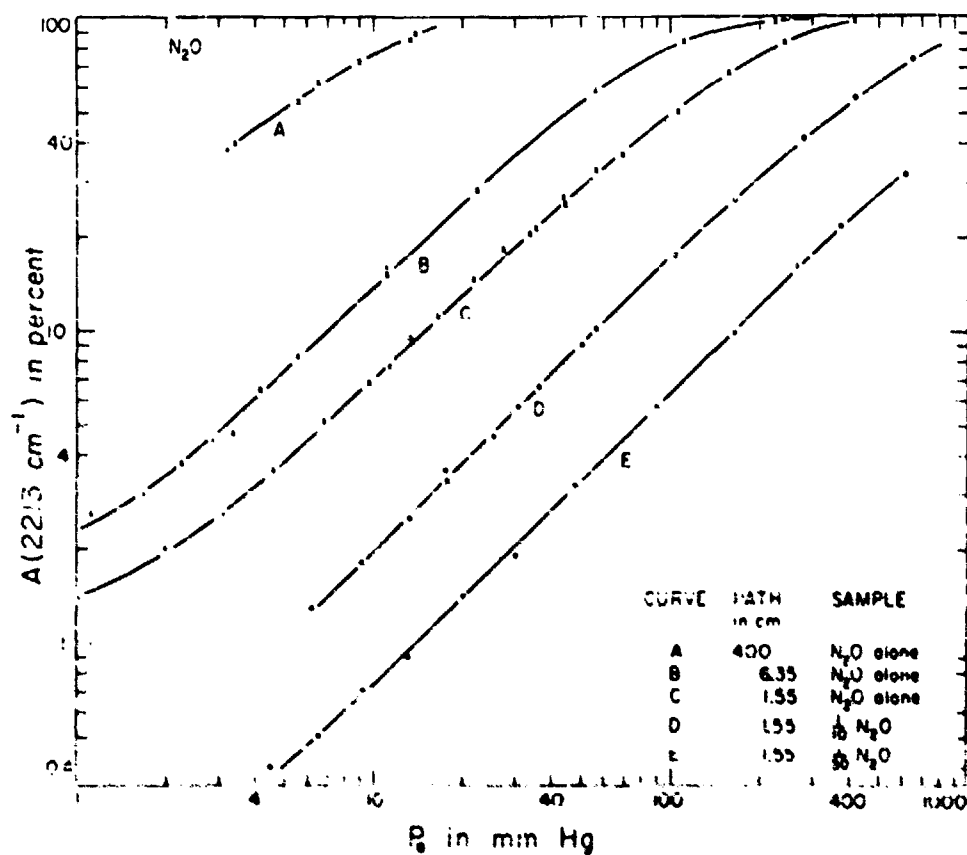


Fig. 21. The percent absorption at 2213 cm^{-1} versus equivalent pressure for samples whose values of absorber concentration are proportional to the equivalent pressure

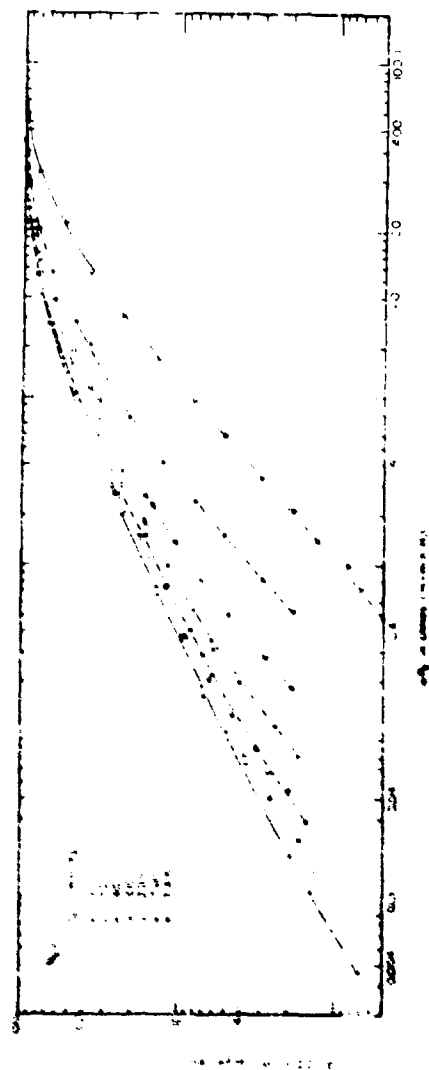


Fig. 22. The percent absorption at 2213 cm^{-1} versus Fe

the Elsasser model. Similar readings from the curves of Fig. 22 which represent $A(2213 \text{ cm}^{-1})$ indicate an even greater deviation from the predicted values.

If P_0 is restricted to lower values, such as 100 mm Hg or less, Plasse⁹ has shown that theory based on the Elsasser model predicts that the strong-line approximation is accurate to $\pm 5\%$ for absorption greater than approximately 20%. Inspection of Fig. 19 shows that there is approximately 20% relative difference between the readings of the two curves corresponding to 10 mm Hg and 100 mm Hg in the region where $A(2240 \text{ cm}^{-1})$ equals approximately 20%.

On the basis of these comparisons it can be concluded that the absorption at frequencies of maximum absorption in the P- and R-branches cannot be accurately represented by a strong-line approximation. It seems improbable that an error in the value of the constant relating K_0 to μ in (11) could account for the deviation of the observed results from the predicted behavior. It can be shown that if the constant in Eq. (51) were in error by as much as a factor of two, the data would still show deviation from the strong-line approximation for smaller values of K_0 than those predicted.

It is of interest to compare the results of Figs. 19 and 22, which deal with absorption $A(\nu)$ at certain frequencies, with those of Fig. 16 which deals with total absorption $\int A(\nu)d\nu$; the curves representing absorption approach a very definite upper limit of 100%. But the curves representing total absorption tend to indicate a small increase with increasing values of ν , for even the larger samples, as a result of the continuing growth in the wings of the band. The curves which correspond to the lower values of pressure in all three of these figures all contain portions which are nearly straight with slopes of approximately 0.5. Thus, the total absorption as well as percent of absorption increases approximately as the square root of absorber concentration for certain ranges of values of ν and P_0 . Similar comparison of Figs. 17, 17', and 20 indicates that the maximum dependence on P_0 is not greatly different for total absorption than for percent absorption. The maximum dependence of total absorption on P_0 was found to be approximately $P_0^{0.57}$, while a dependence of $P_0^{0.47}$ and $P_0^{0.46}$ was observed for the absorption at R-max. and P-max. respectively.

It was suggested earlier that the absorption by weak lines in the wings of the band might be one of the factors accounting for the fact that the total absorption did not show a square-root dependence on P_0 . However, it is seen that the absorption at R-max. and P-max., which is unaffected by absorption in the wings of the band, showed only a slightly greater dependence on P_0 than did the total absorption. It is possible, therefore, that the failure of either of these quantities, percent absorption or total absorption, to exhibit strong-line properties is due largely to the weak bands which are superimposed on the strong fundamental band.

By considering the difference between the growth of weak lines and the growth of strong lines with increasing pressure, it is possible to give a qualitative explanation of the greatly different shapes of the absorption curves shown in the right-hand portion of Fig. 4.

It has been shown that the absorption at R-max. and P-max. has a rather large dependence on P_0 over fairly wide ranges of values of y and P_0 . It is therefore possible for a sample of low absorber concentration and high pressure to produce greater absorption than a sample of much greater absorber concentration but low pressure. This is the case for the spectra in Fig. 4; the sample having the smaller value of absorber concentration and higher pressure shows greater absorption at R-max. and P-max. than does the sample of larger absorber concentration and lower pressure. However, the lines in the wings of the band are much weaker and grow less rapidly with increasing pressure. The absorption in the wings of the band is therefore less for the sample having the smaller value of absorber concentration, in spite of its higher pressure.

VI. THE FUNDAMENTAL AND FIRST OVERTONE BAND OF CARBON MONOXIDE

A. THE 2143 cm^{-1} CO BAND

Migotti¹⁹ identified CO as a permanent atmospheric constituent from solar spectra obtained at Columbus, Ohio; and several investigators, including Shaw²⁰, have since made studies of the CO content in the atmosphere and found a concentration of approximately 0.1 atoms cm per air mass. One air mass is an atmospheric path containing the same amount of air as a vertical path through the entire atmosphere.

The fundamental band of CO occurs near the ν_1 H_2O band in the atmospheric window which lies between the strong 2350 cm^{-1} CO_2 band and the 1995 cm^{-1} H_2O band. The major portion of the absorption by CO in this spectral region is due to the fundamental vibration-rotation band of the common isotope $^{12}\text{C}^{16}\text{O}$. Other isotopic bands occur in this spectral region, as do some difference bands which are very weak for samples at room temperature. In the present report all these absorption bands together are referred to as the 2143 cm^{-1} CO band.

Approximately 160 spectra of the CO band were obtained in the present study by using the double-beam spectrometer along with absorption cells of lengths 4.55, 6.35, and 400 cm. Different combinations of CO and H_2 were used to provide values of absorber concentration from 9.6×10^{-4} to 45.6 atoms cm and total pressures from approximately 3 to 3000 mm Hg.

Tracings of a large number of absorption curves are shown in Figs. 23-29, where they appear in groups. The values of absorber concentration y and equivalent pressure P_0 of the sample corresponding to each

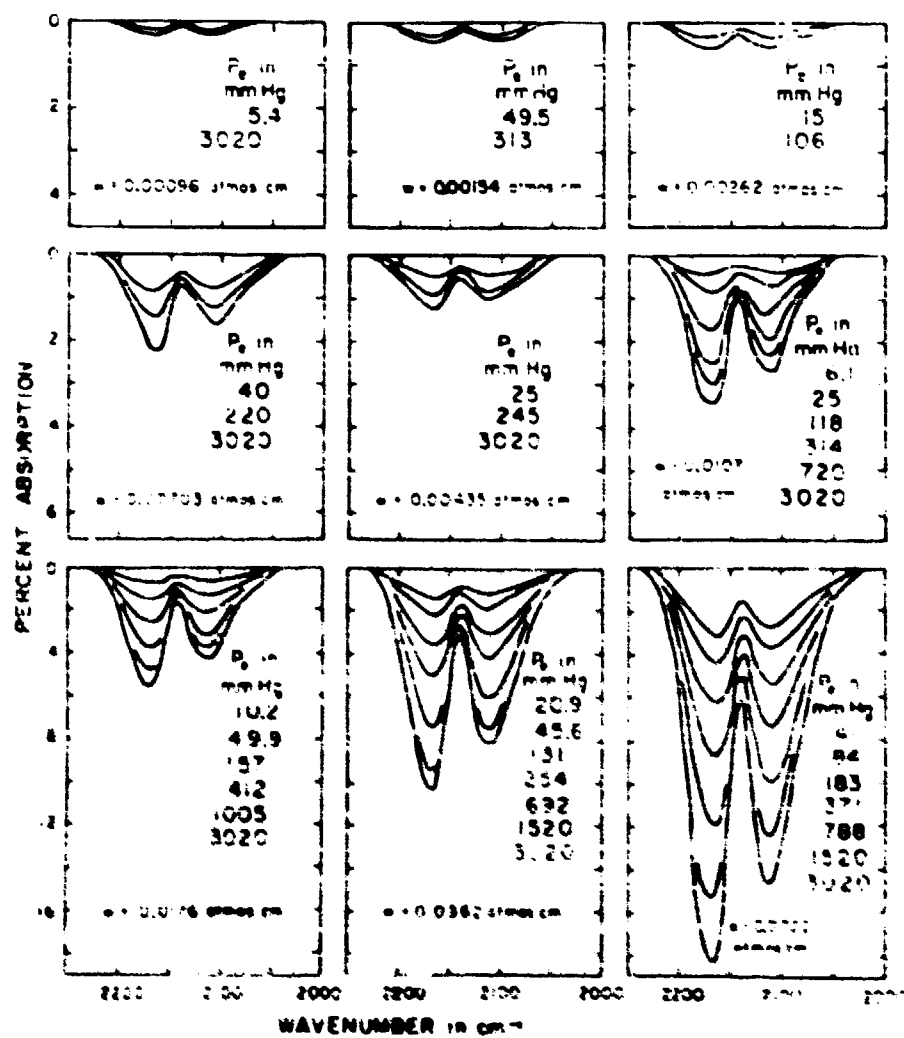


Fig. 25. Spectrum of the 2143 cm⁻¹ CO band

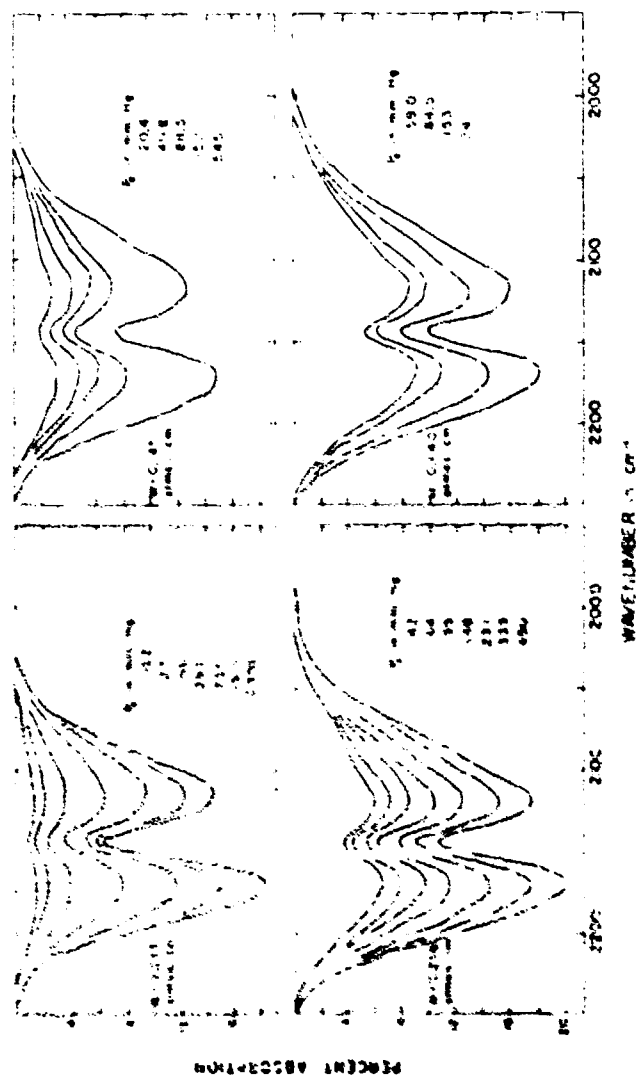


FIG. 16. Spectra of the 21-5 cm⁻¹ C₂ and



Fig. 2. Spectra of the 2145 cm⁻¹ band.

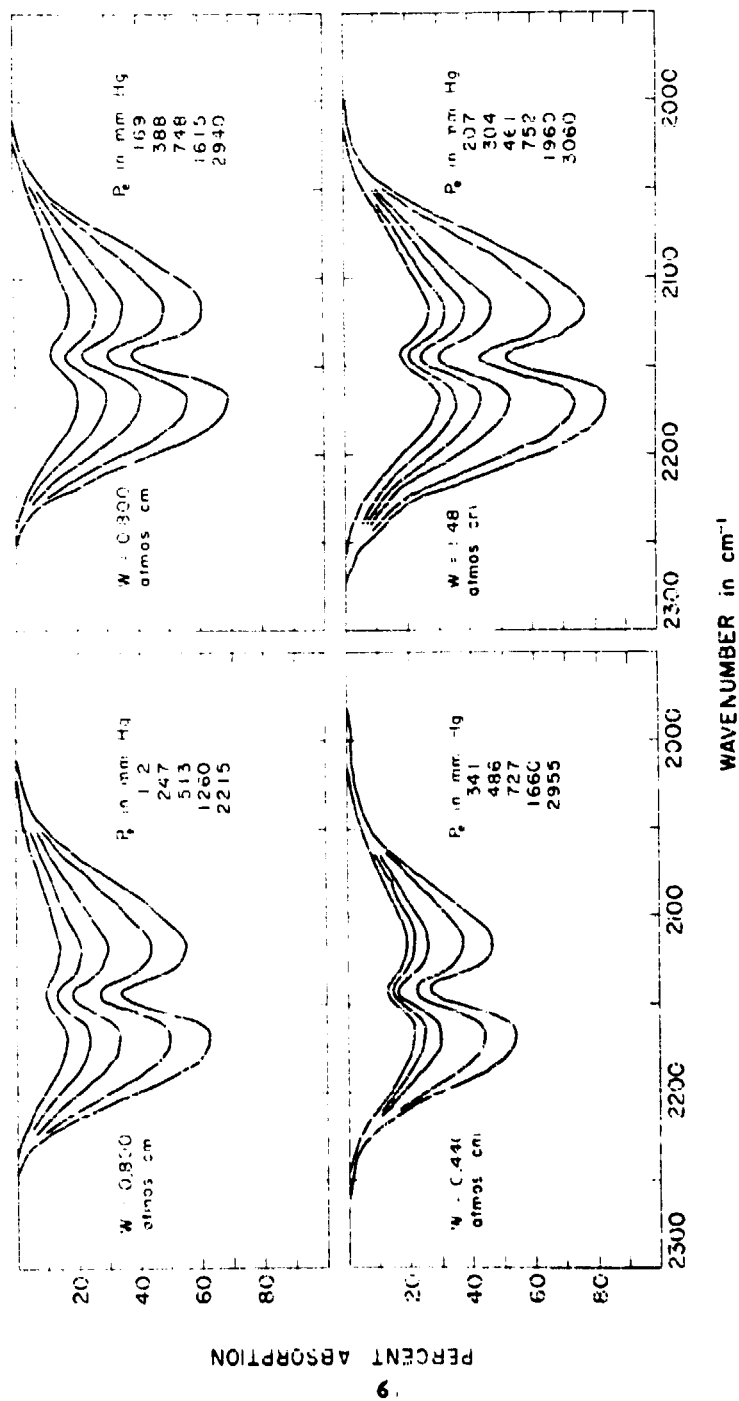


Fig. 26. Spectra of the 2142 cm^{-1} band

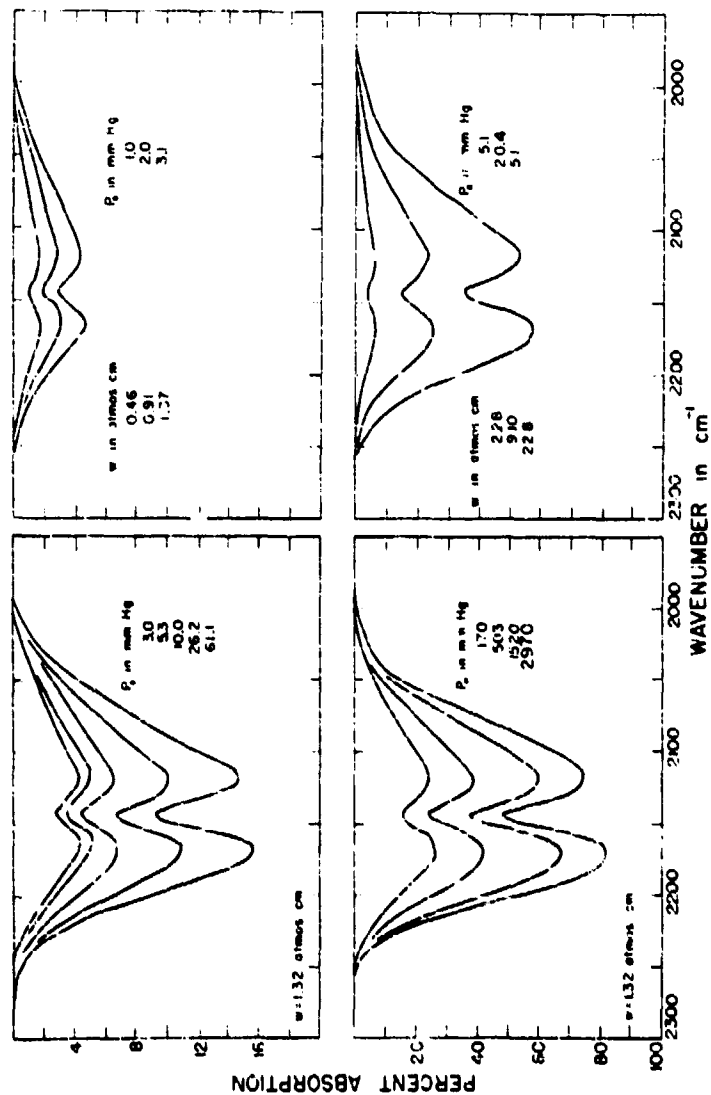


Fig. 27. Spectra of the 2143 cm⁻¹ CO band

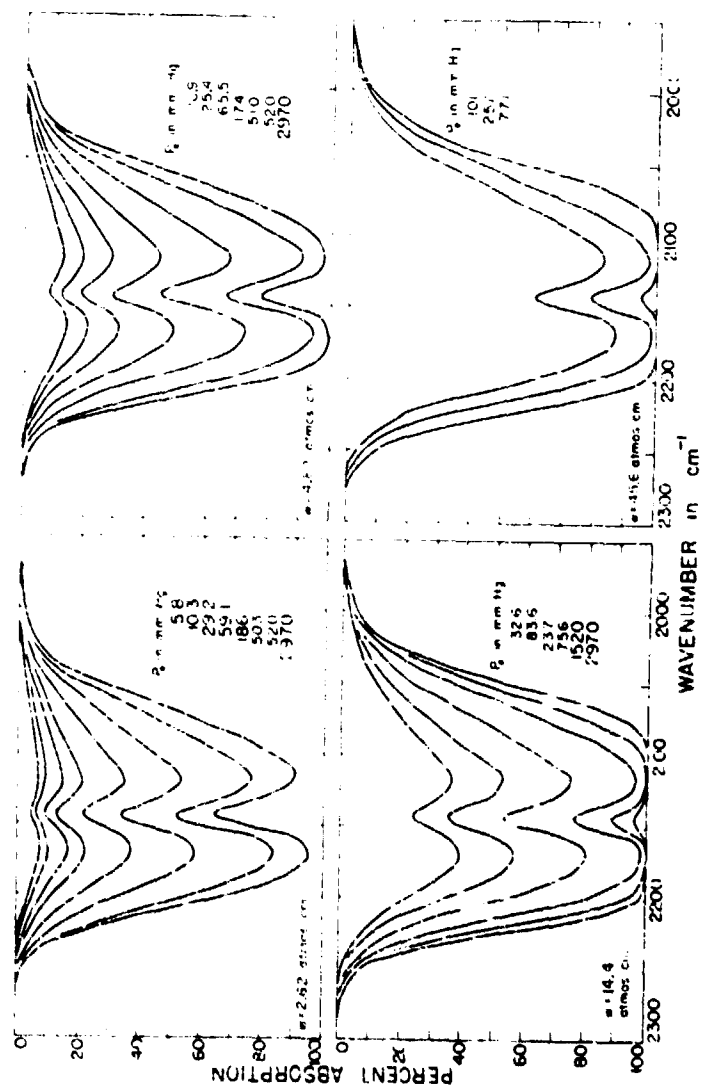


Fig. 28. Spectra of the 2143 cm^{-1} CO band

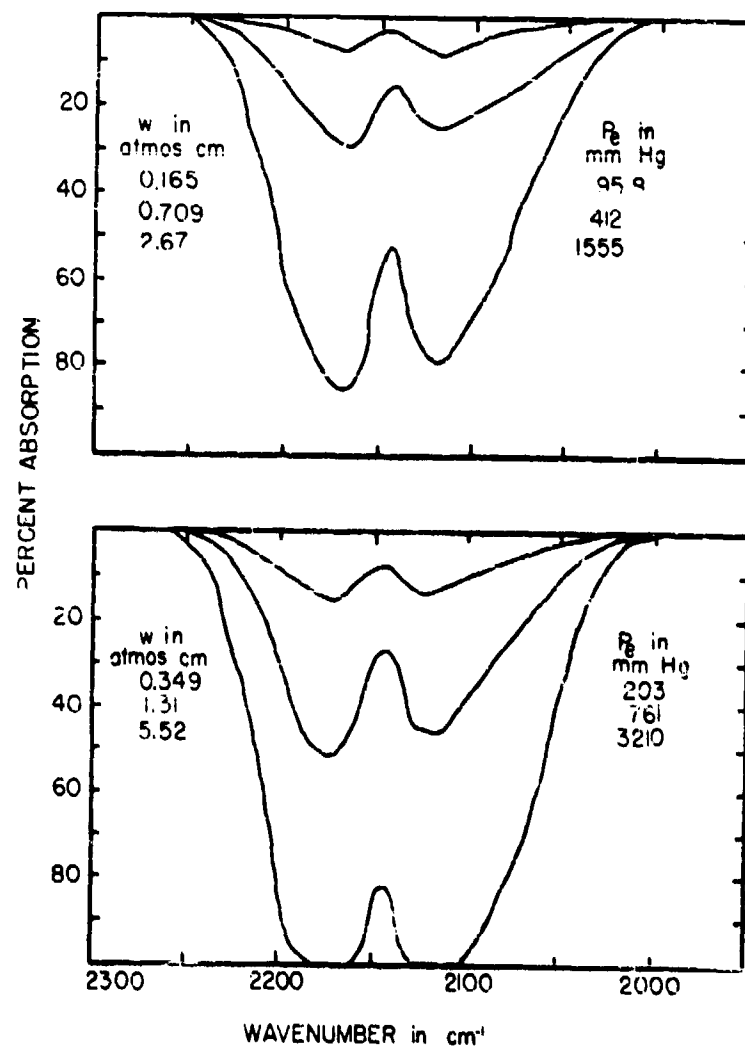


Fig. 29. Spectra of the 2145 cm^{-1} CO band.

spectrum appear with each group. All the spectra were obtained with the same spectrometer slit width, which corresponded to approximately 25 cm^{-1} .

All of the data for the 2143 cm^{-1} CO band included in the present report are collected in Table 4. The absorber concentration v and equivalent pressure P_e for each sample are shown. The value of the equivalent pressure P_e was calculated from the total pressure P and the CO partial pressure p by the equation

$$P_e = P + 0.02p, \quad (32)$$

in accordance with Eq. (14) and Table 1.

Included in Table 4 are the values of total band absorption $\int A(v) dv$ along with the observed percent of absorptions $A(2116 \text{ cm}^{-1})$ and $A(2168 \text{ cm}^{-1})$ corresponding in good approximation to the absorption maxima in the P- and R-branches of the band, respectively.

Many of the total absorption data listed in Table 4 are plotted in Fig. 30 with the total absorption presented as a function of the equivalent pressure. Each curve corresponds to a given value of absorber concentration and shows the effect of increasing the total pressure by adding N_2 . Curves F, G, H, and I correspond to values of absorber concentration which occur in the same range as the values corresponding to curves B, C, D, and E. These two sets of curves represent samples which were obtained by using two absorption cells of quite different length and with quite different values of CO partial pressure. Since these two sets of curves represent approximately the same range of values of absorber concentration, it is possible to compare the total absorption of a sample in the 6.35-cm cell with that of a sample in the 400-cm cell which has the same, or nearly the same, values of v and P_e . Such comparisons can be seen to indicate that the results are consistent to approximately 15%.

The general features of the curves of Fig. 30 are the same as those of the corresponding curves for the 2224 cm^{-1} H_2O band which were shown in Fig. 12. The variation of the total absorption with changes in v and P_e becomes very slight for large values of v and P_e . This result is illustrated by the crowding of the curves in the upper right-hand corner, and is due to the fact that $k(v)v \gg 1$ for most frequencies within the band, and the total absorption changes slowly.

There is a general decrease of the slope of the curves towards higher pressures as a result of the change in the shape of the spectral lines which was described in connection with Fig. 12. However, the decrease in slope is less pronounced for the CO curves in Fig. 30 than for the H_2O curves in Fig. 12; this result can be explained by the fact

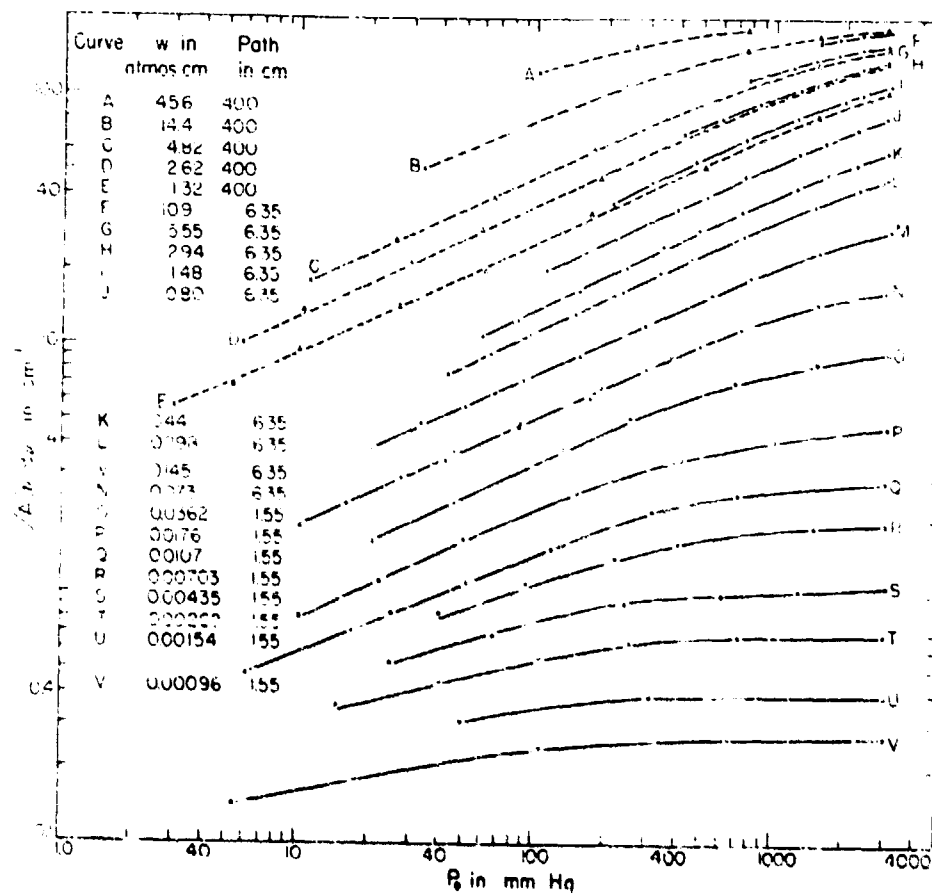


Fig. 10. The total absorption of the 2143 cm^{-1} CO band versus equivalent pressure for samples having constant values of absorber concentration

that the quantity $p = \alpha d/d$ is less for CO than for N_2O at the same pressure. By using an average value of $d = 3.8 \text{ cm}^{-1}$ and $\alpha = 0.08 \text{ cm}^{-1}$ reported by Shaw¹⁹ at a P_e of 760 mm Hg, it is easily shown that $\alpha = 1$ corresponds to P_e equal to approximately 5750 mm Hg. It is recalled that for N_2O , $\beta = 1$ for P_e equal to approximately 680 mm Hg. The dependence of total absorption on P_e therefore starts decreasing at a smaller value of P_e for the N_2O band than for the CO band. Therefore the structure of the CO band would be less "smeared" than that of the N_2O band at the maximum values of P_e used in the present study.

Several of the curves of Fig. 30 contain portions which are nearly straight and parallel to each other. The slope of the straight portions of these curves is approximately 0.44. This result indicates that the total absorption is proportional to $P_e^{0.44}$ for samples whose values of P_e and y are within the range represented by the straight portions of the curves.

In Fig. 31 are three curves relating the total absorption to the equivalent pressure. The curves of Fig. 31 are different from those of Fig. 30 in that those in Fig. 31 do not correspond to constant values of absorber concentration. The curves of Fig. 31 correspond to samples of CO alone in the absorption cell, and the absorber concentration y is therefore proportional to P_e .

The features of Fig. 31 are similar to the corresponding Fig. 13 for the 2224 cm^{-1} N_2O band. There is a decrease in the slope of curve A at low pressures as a result of Doppler broadening, and at large values of y and P_e as absorption becomes nearly complete. The curves of Fig. 31 have straight portions with a slope of approximately 0.98. For values of y and P_e represented by the straight portions of the curves, the total absorption is therefore proportional to $y^m P_e^n$ where $m + n = 0.98$. It was shown previously in the discussion of Fig. 30 that the total absorption was proportional to $P_e^{0.44}$. Therefore $n = 0.44$, and $m = 0.98 - 0.44 = 0.54$. It is accordingly to be expected that the total absorption is proportional to $y^{0.54} P_e^{0.44}$. This result is confirmed below in the discussion of Fig. 33, where the ranges of values of y and P_e for which this simple relationship is valid will be determined.

In order to determine the dependence of total absorption upon absorber concentration y , values were taken from Fig. 30 and 31 and plotted in Fig. 32, in which each curve corresponds to a constant value of equivalent pressure as indicated in order from top to bottom.

The lower portion of the uppermost curve, which corresponds to an equivalent pressure of 3000 mm Hg, is linear with a slope of approximately 1. From this portion of the curve it is possible to determine directly the value of the band intensity $\int k(\nu) d\nu$ in the same manner as was done for the 2224 cm^{-1} N_2O band.

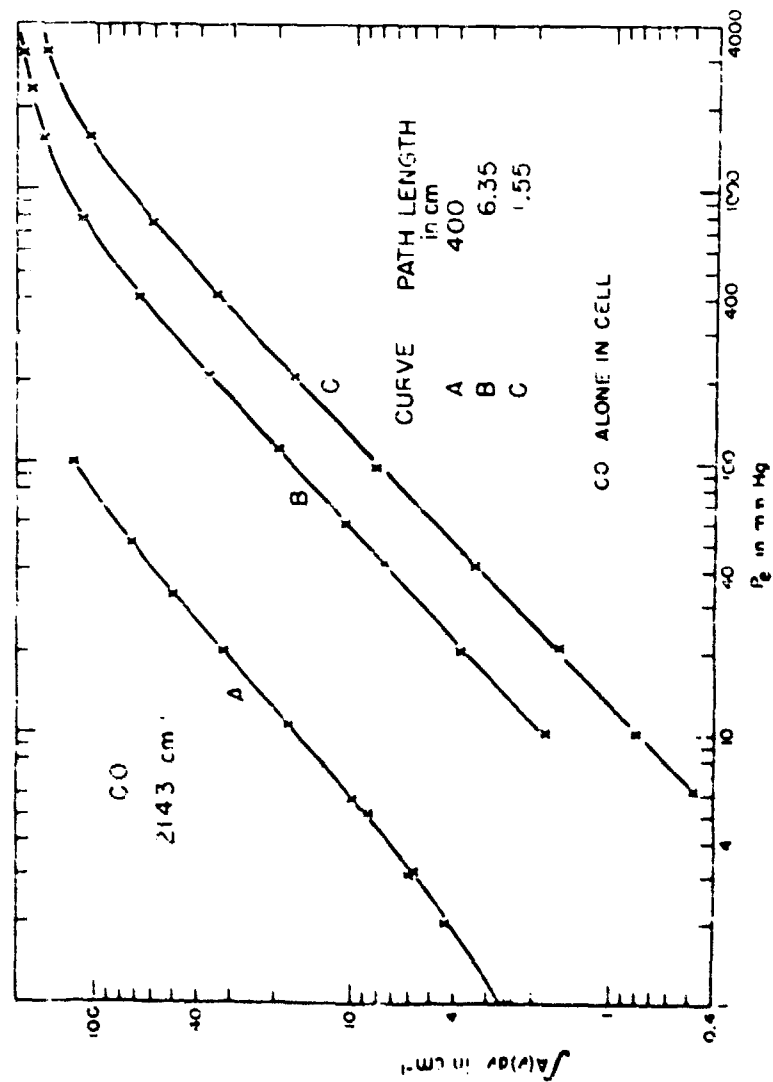


Fig. 35. The total absorption of the 2143 cm⁻¹ CO band versus equivalent pressure for samples whose values of absorber concentration are proportional to the equivalent pressure.

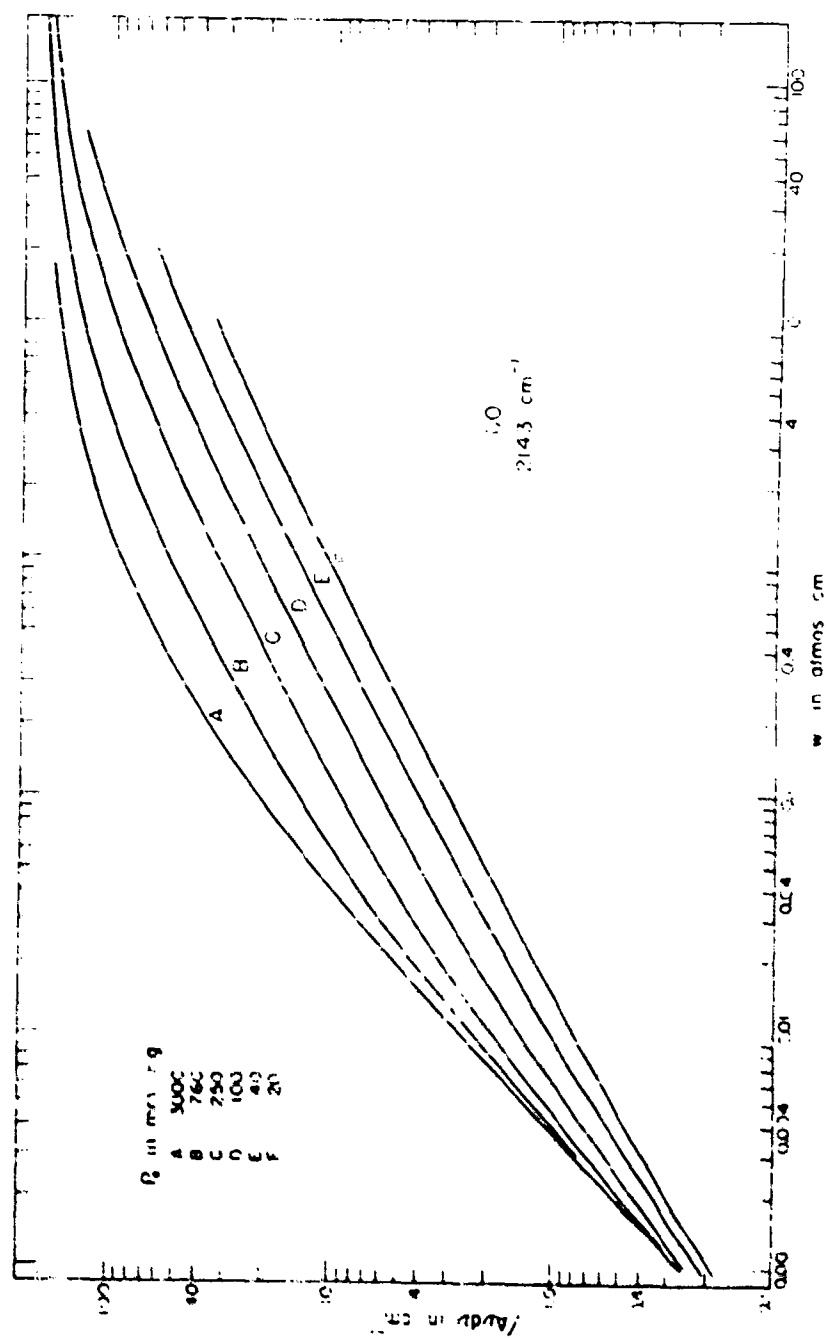


Fig. 36. The total absorption of CO₂ at 2143 cm⁻¹ and
versus absorber concentration.

The value determined for the 2143 cm^{-1} CO band is

$$\int k(\nu) d\nu = 260 \text{ atmos}^{-1} \text{ cm}^{-2}, \quad (33)$$

This value, which is believed to be accurate to within $\pm 10\%$, can be compared to the value of $237 \text{ atmos}^{-1} \text{ cm}^{-2}$ reported by Penner and Weber²¹, and apparently not corrected to STP. If the values of ν in Fig. 32 had not been corrected to standard temperature, a value of $\int k(\nu) d\nu = 235 \text{ atmos}^{-1} \text{ cm}^{-2}$ would have been obtained. The difference between this value and that of Penner and Weber is within the limits of experimental error.

From the curve of Fig. 32 it is possible to determine the total absorption of any sample whose values of absorber concentration and equivalent pressure fall within the range covered. However, it is possible to derive empirical equations which relate total absorption to the parameters ν and P_0 and make it possible to estimate total absorption without the use of the curves of Fig. 32.

The curves of Fig. 32 converge at the lowest and highest values of ν , but the five lower curves are nearly linear and parallel over a wide range of ν near the centers of the curves. The slope of the linear portions of the curves is approximately 0.55, thus indicating that the total absorption is proportional to $\nu^{0.55}$. The range of values of ν and P_0 for which $\int A(\nu) d\nu$ is proportional to $\nu^{0.55}$ is approximately the same as the range for which $\int A(\nu) d\nu$ was found to be proportional to $P_0^{0.44}$. In the discussion of Fig. 31 it was suggested that the total absorption was proportional to $\nu^{0.56} P_0^{0.44}$. The values of the exponent of ν which were derived from two different sets of curves are consistent within the limits of experimental error. The curves of Fig. 31 correspond only to samples of CO alone, while the curves of Fig. 32 are based on samples of CO alone as well as samples of CO mixed with N_2 .

Since, for certain values of ν and P_0 , the total absorption is proportional to $\nu^{0.55} P_0^{0.44} = (\nu P_0^{0.8})^{0.55}$, it is of interest to investigate the range of values of ν and P_0 for which the total absorption might be expressed as a function of $\nu P_0^{0.8}$. In order to check the possibility of using such a function and to illustrate the deviations of the data from it, the curves of Fig. 32 were plotted with the total absorption against the variable $\nu P_0^{0.8}$. Each curve corresponds to a given value of P_0 as indicated. The points shown do not represent actual samples but correspond to values taken from the curves of Figs. 30 and 31.

If the total absorption were a function of the product $\nu P_0^{0.8}$ for all values of ν and P_0 , the curves of Fig. 33 would all coincide. It is seen that there is a rather wide region over which the curves corresponding to $P_0 \leq 240 \text{ mm Hg}$ are nearly coincident. From the curves it is easy to show that

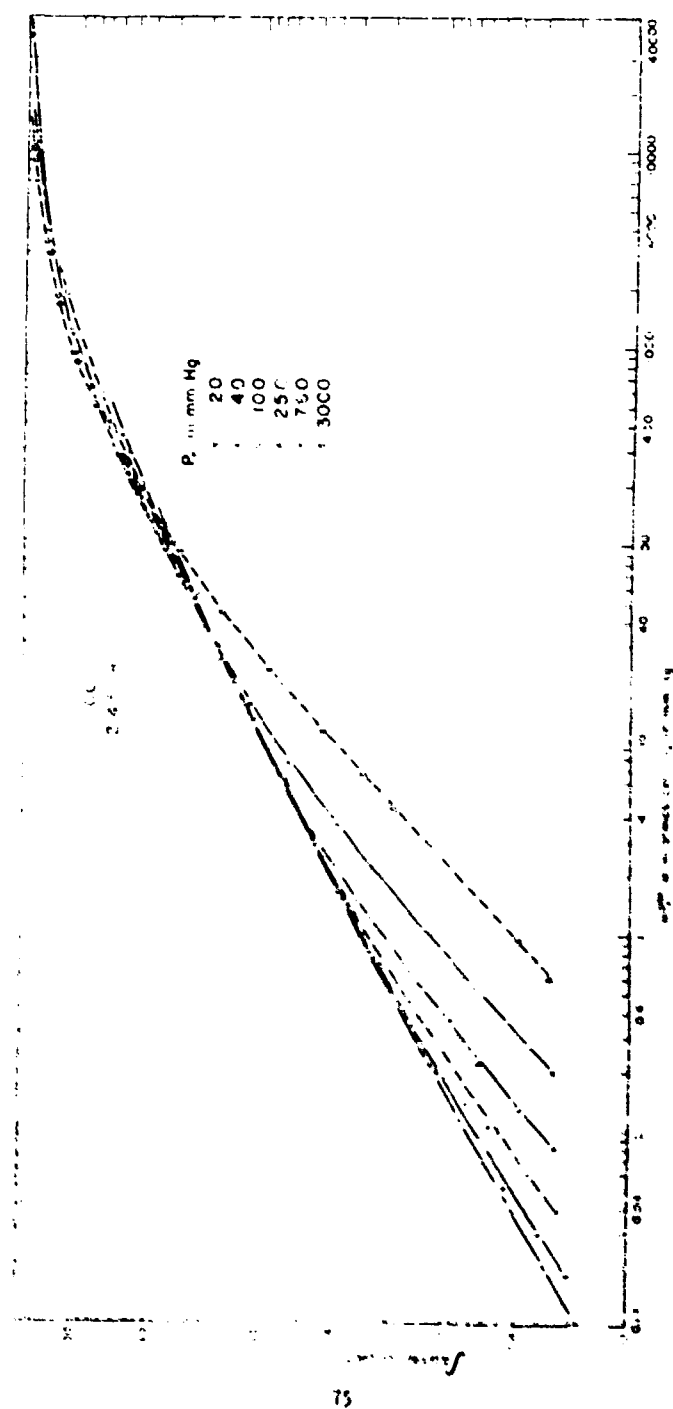


Fig. 55. The total absorption of the 2143 cm^{-1} CO band versus P , 0.5

$$\int A(v)dv = 2.75 (vP_0^{0.8})^{0.55}, \quad (34)$$

for

$$4 < \int A(v)dv < 40 \text{ cm}^{-1} \text{ if } 20 < P_0 < 250 \text{ mm Hg}$$

and for

$$10 < \int A(v)dv < 40 \text{ cm}^{-1} \text{ if } 20 < P_0 < 760 \text{ mm Hg}.$$

In the lower left-hand portion of Fig. 33 the curves corresponding to high pressures fall to the right of the curves corresponding to lower pressures. This result is consistent with the results of the corresponding Fig. 15 for the H_2O band and indicates that a function of $vP_0^{0.8}$ gives too much weight to the equivalent pressure. The data corresponding to the curves in the lower left portion of the figure could therefore be more accurately represented by a function of vP_0^a , where a is less than 0.8. In the upper right portion of Fig. 33 the curves corresponding to high pressures fall to the left of, or above, the curves corresponding to low pressures. Some of the curves corresponding to lower pressures do not extend to the right-hand portion of the figure; however, it is apparent that if they were extrapolated they would fall below the curves corresponding to higher pressures. The data represented by the right-hand portion of the figure could thus be more accurately represented by a function of vP_0^a , where a is greater than 0.8.

Thus, the total absorption can be represented by a function of $vP_0^{0.8}$ over certain values of v and P_0 , but such a function gives too much weight to P_0 for samples having large values of P_0 and small values of v . For larger values of v such a function gives too little weight to P_0 . This latter result would be expected on the basis of the requirement: for the strong-line approximation, which gives the total absorption as a function of vP_0 , and is valid for large v and small P_0 .

In order to show the relationship between the total absorption and the variable vP_0 , these parameters were plotted in Fig. 34 for the different values of the pressures indicated. Over the major portion of Fig. 34 the curves corresponding to high pressures lie to the right of the curves corresponding to lower pressures. This result is, of course, to be expected on the basis of Fig. 33. However, in the upper right-hand portion of Fig. 34 the curves tend to converge. The curves corresponding to the lower pressures, 20, 40, and 100 mm Hg, do not extend as far to the right as do the curves corresponding to the higher pressures. Therefore, one can only estimate where the low-pressure curves would occur relative to the high-pressure curves in the right-hand portion of the figure, but it would appear that if the low-pressure curves were extrapolated, they would nearly converge with the high-pressure curves.

Complete convergence of the curves in Fig. 34 would indicate validity of the strong-line approximation. On the basis of the curves experimentally obtained, it can be concluded that the strong-line approximation is valid only for values of v so large that the absorption of the band is nearly complete and the dependence of total absorption on both v and P_0 is small.

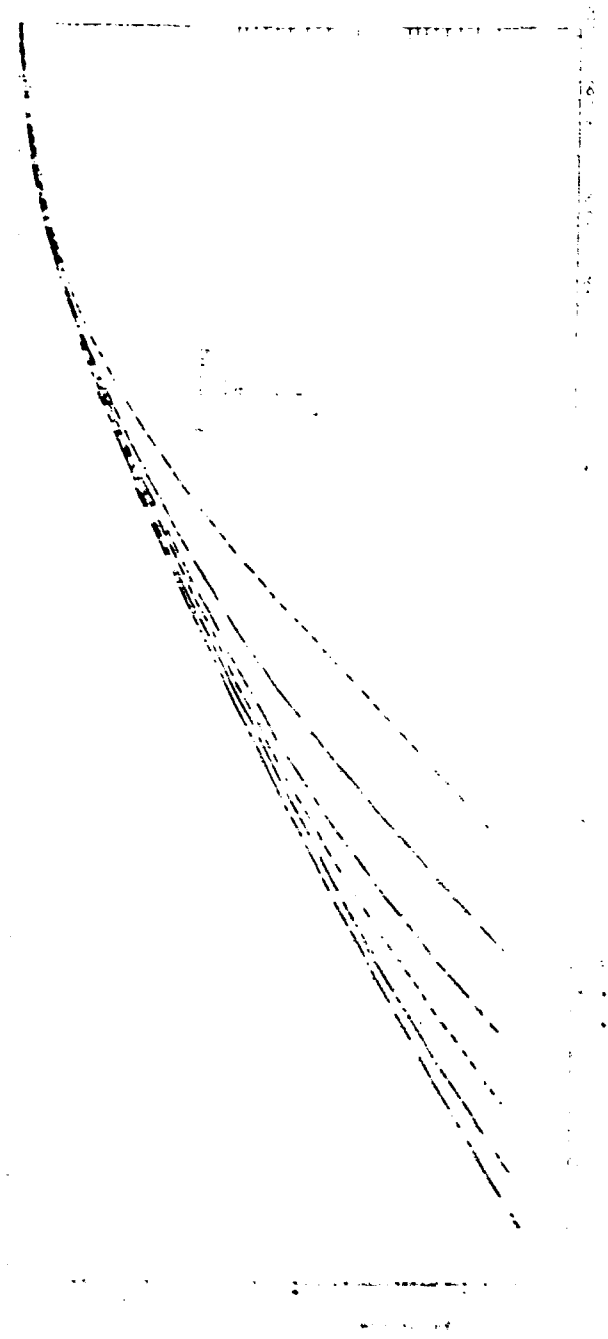


Fig. 10. The effect of wavelength on the transmittance of a solution of a certain substance.

If one is willing to allow as much as 10-15% error, it is possible to derive from the curves of Fig. 34 some rather simple equations which relate total absorption to the variable νP_0 for values of $\int A(\nu) d\nu$ not included by Eq. (34). The empirical equations which have been derived, and the region of validity for each is as follows:

$$\begin{aligned} & \int A(\nu) d\nu = 3.20 (\nu P_0)^{0.43}, \\ \text{for} & \quad 40 < \int A(\nu) d\nu < 120 \text{ cm}^{-1}, \\ \text{and} & \quad 20 < P_0 < 760 \text{ mm Hg.} \end{aligned} \quad (35)$$

$$\begin{aligned} & \int A(\nu) d\nu = 10.7 + 6.1 \log(\nu P_0), \\ \text{for} & \quad 120 < \int A(\nu) d\nu < 210 \text{ cm}^{-1}, \\ \text{and} & \quad 20 < P_0 < 3000 \text{ mm Hg.} \end{aligned} \quad (36)$$

It is emphasized that the total absorption of a given sample can be determined more accurately from the curves of Fig. 32 than from the empirical equations, which are included so that it might be possible to make determinations without the use of the curves. The empirical Eqs. (34), (35), and (36) are seen to be useful over rather wide ranges of values of ν and P_0 ; and they are believed to give values of $\int A(\nu) d\nu$ accurate to within 10% except for values of ν and P_0 near the limits of the region of validity, where $\int A(\nu) d\nu$ given by the equations may be in error by as much as 15%.

It is noted that Eqs. (35) and (36) have the form expected on the basis of a strong-line approximation, i.e., the total absorption is a function of the product νP_0 ; however, neither of these equations nor Eq. (34) corresponds to the square-root relation, which should apply in the special case of the strong-line approximation with no overlapping of the spectral lines. For the square-root approximation the total absorption is proportional to $\nu^{0.5}$ and $P_0^{0.5}$, but the maximum dependence on P_0 which was observed was $P_0^{0.44}$. The same qualitative explanation of the invalidity of the square-root relation given in the discussion of the H_2O band also applies to the CO band.

The absorptions at R-mn. and P-mn. have been investigated in a manner similar to the method used for the H_2O band. The values of observed absorption $A(2168 \text{ cm}^{-1})$ at R-mn. for a major portion of the spectra are plotted in Fig. 35 against the equivalent pressure. Each curve represents a given value of absorber concentration as indicated. It is noted that several of the curves have portions which are nearly straight with slope equal to approximately 0.46, indicating that the

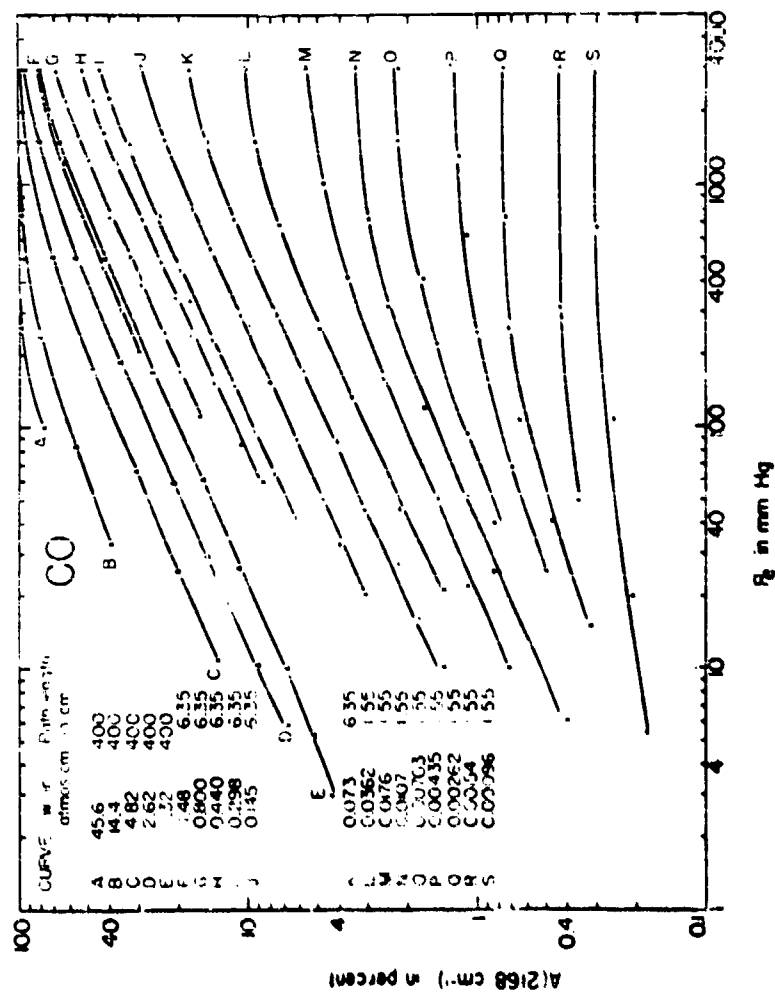


Fig. 35. The percent absorption at 2168 cm^{-1} versus equivalent pressure.

absorption is proportional to $P^{0.48}$, which is nearly equal to the $P^{0.5}$ dependence associated with the square-root approximation. The other features of the curves of Fig. 35 are similar to those of Figs. 17 and 20 which were described previously.

Values of percent absorption were taken from the curves of Fig. 35 and plotted in Fig. 36 with the variable wP_e as the abscissa. Each curve represents a given value of equivalent pressure, and validity of the strong-line approximation would be illustrated by a coincidence of the different curves. Portions of some of the curves were omitted from the figure to avoid overcrowding; however, points were included which indicate where the curves would occur if they had been included. It is noted that the four upper curves corresponding to the lower pressures are nearly coincident over a wide range of values of the variable wP_e . These four curves also contain portions which are nearly straight with a slope of approximately 0.51, indicating a $w^{0.51}$ dependence.

The results of these measurements can be compared to the absorption $A(2145 \text{ cm}^{-1})$ at P-max. In Fig. 37 are plotted the values of $A(2145 \text{ cm}^{-1})$ against equivalent pressure P_e , where each curve represents a given value of absorber concentration. The gross features of the curves of Fig. 37 are, of course, similar to those of Fig. 35 which represent the absorption at R-max. The straight portions of the curves of Fig. 37 have a slope of approximately 0.45, which is slightly less than the value of 0.48 in Fig. 35.

Values were taken from Fig. 37 and plotted in Fig. 38 with wP_e as the abscissa. For the largest values of wP_e the curves converge and approach 100% absorption. The straight portions of the curves have a slope of approximately 0.42 as compared with 0.51 for the curves of Fig. 36.

Thus, for certain values of w and P_e , the absorption at P-max. and R-max. for the 2145 cm^{-1} CO band shows a dependence on these parameters which is only slightly different from the square-root dependence for which the absorption is proportional to $w^{0.5} P_e^{0.5}$. As in the case of the absorption at R-max. and P-max. of the 2204 cm^{-1} H_2O band, the maximum dependence on P_e is somewhat less than the $P_e^{0.5}$ dependence associated with the square-root approximation. However, the deviation from the square-root dependence is considerably less for the CO band than for the H_2O band. It was pointed out in the discussion of the H_2O band that the absence of a square-root dependence on pressure could be attributed to the weak lines which occur along with the strong lines of the strong fundamental band. It is well known from high-resolution spectra that there are fewer weak lines in the CO band than in the H_2O band. It is therefore not surprising that the deviation of the CO absorption from the square-root dependence is less than for the H_2O absorption.

It is further noted that the deviation from the square-root dependence of the absorption at P-max. is greater than at R-max. for the CO band.

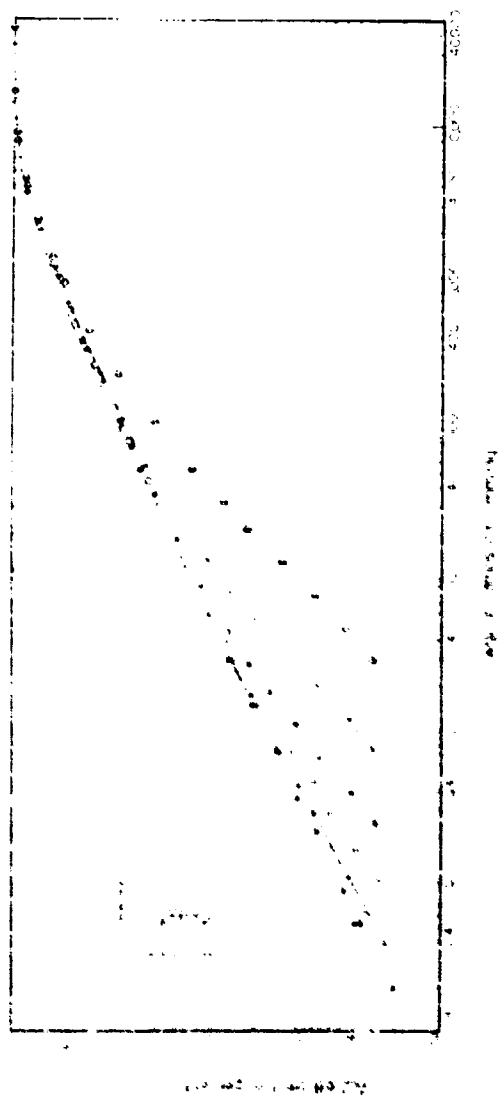


Fig. 10. The percent absorption at 2160 cm⁻¹ versus wt%.

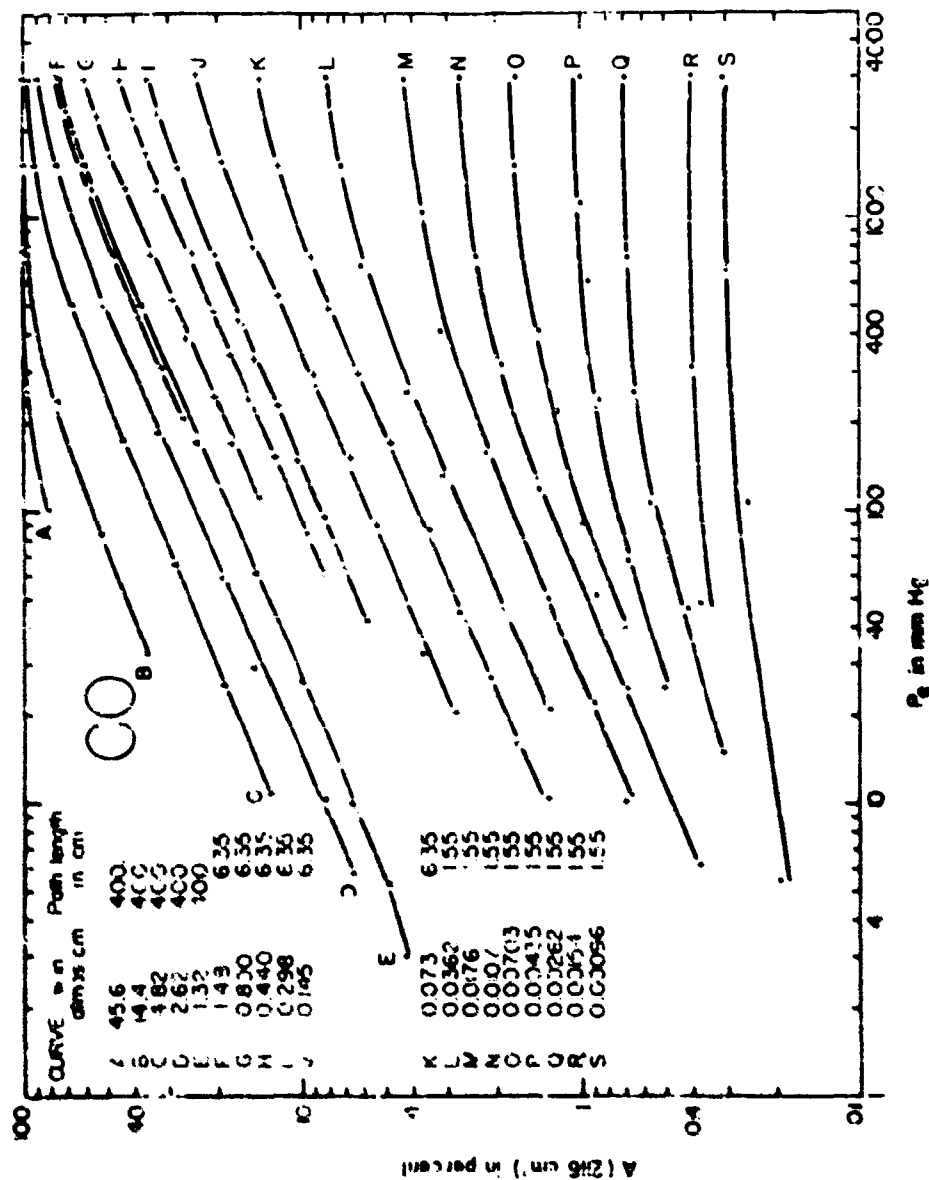


Fig. 37. The percent absorption at 215 cm^{-1} versus equivalent pressure

Although the difference in dependence on P_e is small ($P_e^{0.45}$ compared with $P_e^{0.40}$), it is believed to be significant. Further evidence of the difference can be seen by comparing the straight portions of the four upper curves of Fig. 36 with the corresponding curves of Fig. 38. The curves of Fig. 36 occur considerably closer together than do those of Fig. 38; the difference in spacing indicates that the strong-line approximation is more nearly valid for R-max. than for P-max. This result can undoubtedly be explained by the presence of rather prominent lines of the isotopic band $C^{13}O$ near P-max.; the lines of this isotopic band are much weaker near R-max. and therefore give rise to less deviation from the square root dependence. The difference in the relative strengths of the isotopic lines in the two different spectral intervals is well known from high-resolution spectra and is a result of the shift of the band center of the $C^{13}O$ band relative to the center of the band of the more common isotope.

Comparison of the straight portions of the four upper curves of Fig. 36, which relates $\int A(\nu) d\nu$ to νP_e , with the corresponding curves of Figs. 36 and 38 also indicates that the square root approximation is more valid for the absorption at R-max. and P-max. than for the total absorption. This result can undoubtedly be explained by the fact that the weak lines near the wings of the band contribute to the total absorption but not to the absorption at R-max. and P-max.

B. THE 4260 cm^{-1} CO BAND

The CO overtone band at 4260 cm^{-1} was investigated by using a double-pass, single-beam Model 99 Perkin-Elmer spectrometer with a LiF prism. A deuterium glow served as the source and a thermocouple as the detector. External adjustments on the multiple-traverse cell which was used, made it possible to record spectra of each sample at 4, 6, 16 and 32 traverses corresponding to path lengths of 625, 1250, 2500, and 5000 cm, respectively. The spectra were replotted on a linear scale of percent absorption versus wavenumber, and the total absorption was determined from the area under each spectrum.

Drawings of several of the replotted spectra are shown in Figs. 39 and 40; the spectral slitwidth of the spectrometer was between 15 and 20 cm^{-1} .

Table 1 lists the absorption parameters and the total absorption for all of the spectra obtained. The cell was at room temperature, which varied by approximately 1°C during the course of the experiment.

In order to determine the value of P_e for each sample it was first necessary to determine the value of the self-broadening coefficient B in Eq. (14). Since the spectrometer used for this portion of the study was not a double-beam type instrument, it was not possible to determine the value of B by the method described previously for the 2124 cm^{-1} $^{12}\text{C}^{16}\text{O}$ and 2143 cm^{-1} CO bands. The method of determining B for this band made

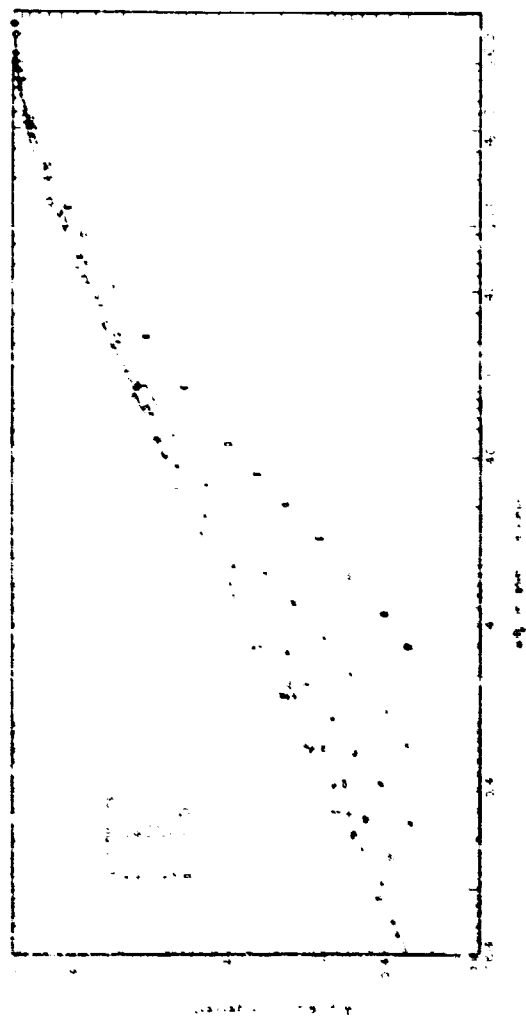


Fig. 13. The percent absorption at 211 cm^{-1} versus wPc

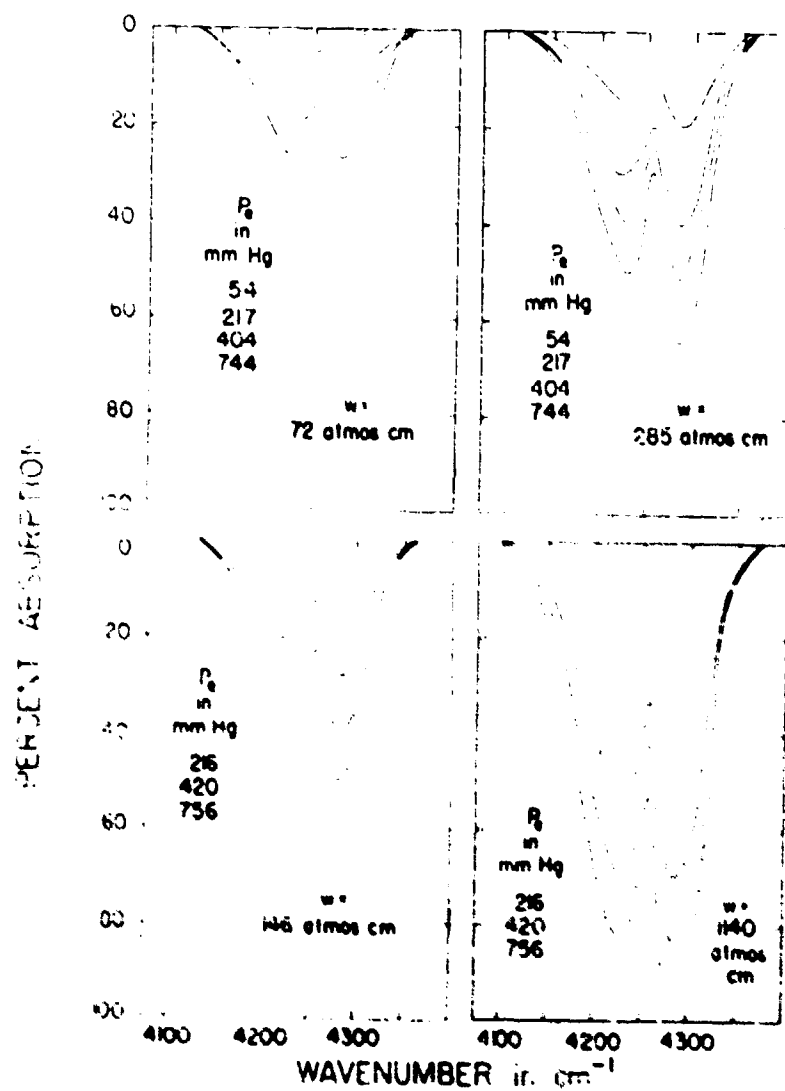


Fig. 1. The effect of the pressure on the 20 band.

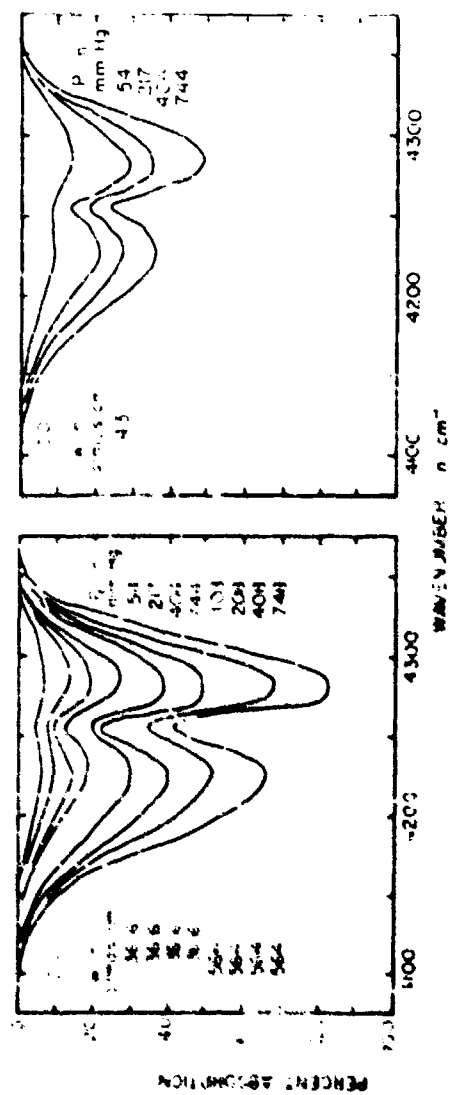


Fig. 10. Spectra of the 4260 cm^{-1} band

use of the fact that several different samples which were studied contained approximately the same absorber concentration at different path lengths. For example, an absorber concentration of approximately 143 atmos cm was obtained with path lengths of 625, 1252, and 2445 cm by using different partial pressures of CO in the absorption cell. Spectra of each of these samples were obtained at different values of total pressure which were produced by adding N_2 . The different samples, which contained the same absorber concentration but different partial pressures of CO, necessarily required different amounts of N_2 in order to produce the same total absorption. By comparing the different values of CO partial pressure and N_2 partial pressure required to produce the same total absorption by samples having the same absorber concentration, it was possible to determine the value of B according to Eq. (15). Approximately 20 separate calculations, which involved a large portion of the data obtained for the 4260 cm^{-1} CO band, were made. These calculations yielded a value of $B = 1.00$, which is believed accurate to 46%. In accordance with Eq. (14) the value of P_0 was determined by

$$P_0 = P + 0.06 p, \quad (17)$$

where P is the total pressure and p is the partial pressure of CO.

The value of $B = 1.00$ is somewhat larger than the value of 1.00 determined for the fundamental CO band. The two values differ by slightly less than the maximum experimental error; however, it would not be surprising to find a significant difference in B for different bands of the same gas since variations were found within the 2224 cm^{-1} H_2O and the 2143 cm^{-1} CO bands. The method used to determine the value of B for the 4260 cm^{-1} CO band did not make it possible to detect small variations of B within the band.

The data for the 4260 cm^{-1} CO band are shown in Fig. 41 with total absorption plotted as a function of equivalent pressure. The top and bottom curves represent single values of absorber concentration. Each of the other curves correspond to an approximately constant value of absorber concentration; the values indicated at the left of each curve indicate the maximum and minimum values of absorber concentration represented by that curve. The Δ 's represent samples of CO alone, while the "O"s represent samples composed of both CO and N_2 .

Figure 41 relates the same parameters as does Fig. 30 for the fundamental CO band. However, Fig. 41 does not represent nearly as wide a range of values of v and P_0 as does Fig. 30. Therefore, some of the definite features of Fig. 30 are not present in Fig. 41, such as the decrease in slope at small values of P_0 as a result of Doppler broadening and at large values of P_0 as a result of overlapping of the spectral lines. The crowding of the curves in the upper right-hand corner also does not occur in Fig. 41, since the largest values of v and P_0 were not

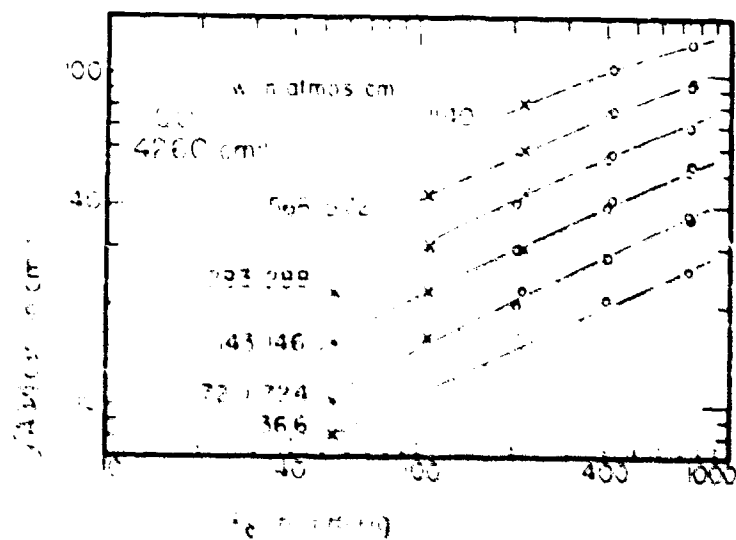


Fig. 10. The total absorption of the 4260 cm⁻¹ band versus equivalent pressure.

sufficiently large to produce complete absorption over the band.

In order to show the dependence of total absorption on y , values were taken from the curves of Fig. 41 and plotted in Fig. 42 for the four different values of P_0 indicated. This figure is similar to Fig. 32, which was drawn for the fundamental CO band; but as in the case of Fig. 41, this figure does not contain all of the features of Fig. 32 because of the much smaller range of values of y and P_0 which are represented.

By comparing the points in Fig. 42 with the curves of Fig. 32, it was found that at a given equivalent pressure the total absorption of the 2145 cm^{-1} band was very nearly the same as the total absorption of the 4260 cm^{-1} band at the same equivalent pressure but with the value of absorber concentration 150 times as great. In fact, each of the curves of Fig. 42 was drawn by tracing the curve of Fig. 32 corresponding to the same value of P_0 but with the value of y different by a factor of 150. It is noted that the experimental points fit nicely the traced curves. This direct tracing of the curves with the value of the abscissa different by a constant factor was possible, of course, because of the fact that the abscissae are logarithmic. The curve in Fig. 42 which corresponds to an equivalent pressure of 50 mm Hg was not traced from Fig. 32, as were the other three curves, since Fig. 32 does not contain a curve corresponding to this pressure. The curve corresponding to 50 mm Hg in Fig. 42 was therefore drawn from another similar curve which corresponds to 50 mm Hg for the 2145 cm^{-1} band but is not included in this report.

The total absorption of the 4260 cm^{-1} band for samples in the "linear region" (6') cannot be determined from the curves of Fig. 42 since the largest values of P_0 were not sufficiently large, nor was the smallest value of y sufficiently small. However, Penner and Weber²¹ investigated the total absorption of both bands in the linear region and found that the value of $\epsilon(\nu)\nu$ for the fundamental band was approximately 145 times that of the overtone band. The total absorption of the overtone in the linear region is therefore the same as that of the fundamental with the value of absorber concentration $1/145$ as great.

The factor of 145 is within the limits of experimental error of the factor of 150, which was observed for a different range of values y and P_0 . Since the two bands are similar with regard to line shape, line spacing, and relative line strengths within the band, it is probably true that the total absorption of the weaker overtone band can be determined from the curves of Fig. 3, which deals with the fundamental band, by using the same value of P_0 and a value of y which is $145/150$ times that of the sample whose total absorption is being determined. Equations (14), (15), and (16) could probably also be applied satisfactorily by using 145 in the equation wherever y appears.

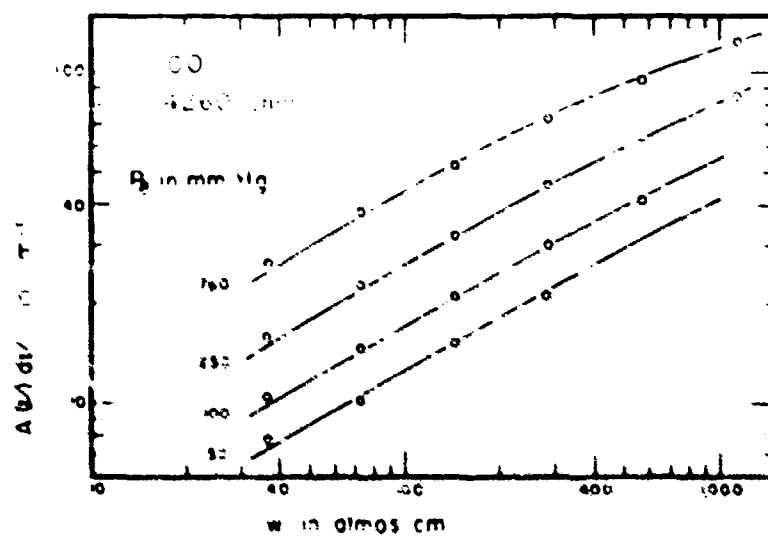


Fig. 10. The total desorption of CO from the polymer and
versus weight concentration.

VII. THE 3400, 1550, AND 1300 cm^{-1} CH_4 BANDS

It has been known for quite some time that CH_4 occurs in rather large quantities in the atmospheres of the planets Jupiter, Saturn, Uranus, and Neptune. Not until 1949 was CH_4 discovered by Megret²⁰ to be a permanent constituent of the earth's atmosphere; the average abundance has since been found to be approximately 1.0 parts per million by volume.

Approximately 150 absorption spectra of CH_4 were obtained in the spectral region from 3400 - 700 cm^{-1} . Absorption path lengths of 6.35, 400, and 1500 cm were used to obtain values of absorber concentration from 0.015 to 188 atmos cm. Values of total pressure were varied from approximately 5 to 3000 mm Hg.

Virtually all of the absorption occurs in two different intervals, one between 3400 and 2200 cm^{-1} , and the other between 1750 and 1100 cm^{-1} . Tracings of many of the spectra of the high-frequency region are presented in Figs. 43-46 and spectra of the low frequency region are shown in Figs. 47-51. Portions of some of the spectra were omitted from the figures to prevent overcrowding, and it was necessary to correct small portions of some of the absorption curves for overlapping absorption by CO_2 and H_2O , which occurred as impurities in the CH_4 and in the air in the optical path of the spectrometer. For some of the samples containing very large values of absorber concentration, the CH_4 absorption extended into the region of the 2350 cm^{-1} CO_2 band, and because of the CO_2 impurity in the CH_4 it was necessary to correct for CO_2 absorption between 2450 and 2200 cm^{-1} . It was also necessary to correct for spurious H_2O absorption in the region between 1750 and 1500 cm^{-1} for samples of large v . The effective slit width varied throughout each absorption curve with an average value of approximately 25 cm^{-1} in the high-frequency region and 10 cm^{-1} in the low-frequency region.

For purposes of analysis the 1750 - 1100 cm^{-1} region was divided into 2 regions at 1555 cm^{-1} . For identification purposes the high-frequency region is referred to as the 1550 cm^{-1} band and the low-frequency region as the 1300 cm^{-1} band, since these two frequencies correspond to the centers of the two stronger bands in the region. Similarly the spectral region from 3400 - 2200 cm^{-1} is referred to as the 3020 cm^{-1} band. Since the region referred to as the 1550 cm^{-1} band occurs in the region of the water vapor absorption, the accuracy of the traced spectra and the values of $\int A(v)dv$ for this band are somewhat less than for the other bands.

The CH_4 data corrected for spurious absorption are given in Table 7, which includes values of $\int A(v)dv$ for all three bands for the listed values of v and P_0 . The value of the self-broadening coefficient B was found to be 1.40 for the 3400 cm^{-1} band and 1.38 for the 1300 cm^{-1} band. It was not possible to obtain an accurate measurement of B for the 1550 cm^{-1}

VII. THE 3020, 1500, AND 1300 cm^{-1} CH_4 BANDS

It has been known for quite some time that CH_4 occurs in rather large quantities in the atmospheres of the planets Jupiter, Saturn, Uranus, and Neptune. Not until 1948 was CH_4 discovered by Migotte²² to be a permanent constituent of the earth's atmosphere; the average abundance has since been found to be approximately 1.6 parts per million by volume.

Approximately 150 absorption spectra of CH_4 were obtained in the spectral region from 3400 - 700 cm^{-1} . Absorption path lengths of 6.35, 400, and 1500 cm were used to obtain values of absorber concentration from 0.015 to 188 atmos cm. Values of total pressure were varied from approximately 5 to 3000 mm Hg.

Virtually all of the absorption occurs in two different intervals, one between 3400 and 2200 cm^{-1} , and the other between 1750 and 1100 cm^{-1} . Tracings of many of the spectra of the high-frequency region are presented in Figs. 43-46 and spectra of the low frequency region are shown in Figs. 47-51. Portions of some of the spectra were omitted from the figures to prevent overcrowding, and it was necessary to correct small portions of some of the absorption curves for overlapping absorption by CO_2 and H_2O , which occurred as impurities in the CH_4 and in the air in the optical path of the spectrometer. For some of the samples containing very large values of absorber concentration, the CH_4 absorption extended into the region of the 2350 cm^{-1} CO_2 band, and because of the CO_2 impurity in the CH_4 it was necessary to correct for CO_2 absorption between 2450 and 2200 cm^{-1} . It was also necessary to correct for spurious H_2O absorption in the region between 1750 and 1500 cm^{-1} for samples of large v . The effective slit width varied throughout each absorption curve with an average value of approximately 25 cm^{-1} in the high-frequency region and 10 cm^{-1} in the low-frequency region.

For purposes of analysis the 1750 - 1100 cm^{-1} region was divided into 2 regions at 1535 cm^{-1} . For identification purposes the high-frequency region is referred to as the 1550 cm^{-1} band and the low-frequency region as the 1300 cm^{-1} band, since these two frequencies correspond to the centers of the two stronger bands in the region. Similarly the spectral region from 3400 - 2200 cm^{-1} is referred to as the 3020 cm^{-1} band. Since the region referred to as the 1550 cm^{-1} band occurs in the region of the water vapor absorption, the accuracy of the traced spectra and the values of $\int A(v)dv$ for this band are somewhat less than for the other bands.

The CH_4 data corrected for spurious absorption are given in Table 5, which includes values of $\int A(v)dv$ for all three bands for the listed values of v and P_0 . The value of the self-broadening coefficient B was found to be 1.30 for the 3020 cm^{-1} band and 1.38 for the 1300 cm^{-1} band. It was not possible to obtain an accurate measurement of B for the 1550 cm^{-1}

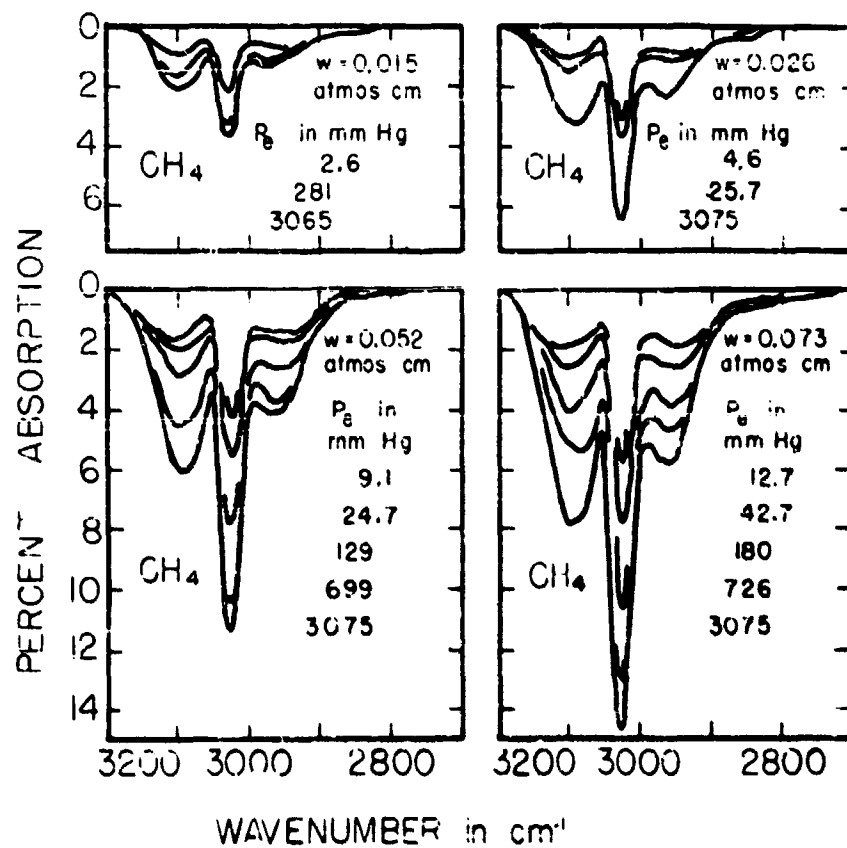


Fig. 45. Spectra of the 3000 cm^{-1} CH_4 band

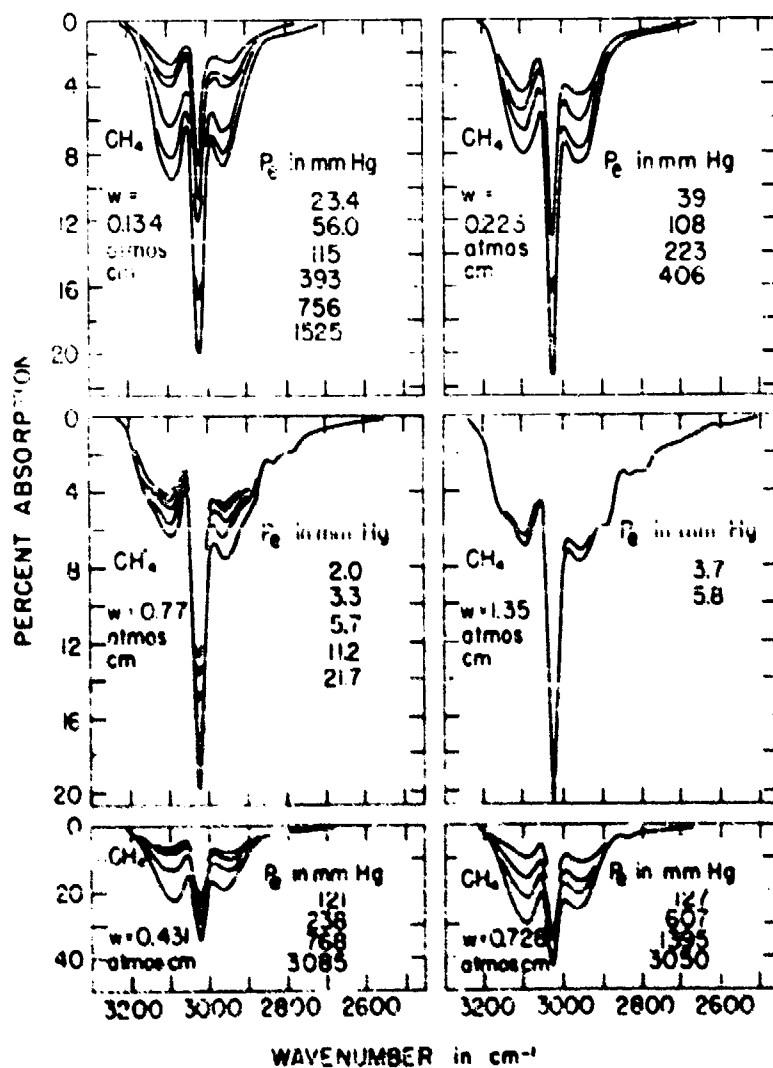


Fig. 44. Spectra of the 3000 cm⁻¹ CH₄ band

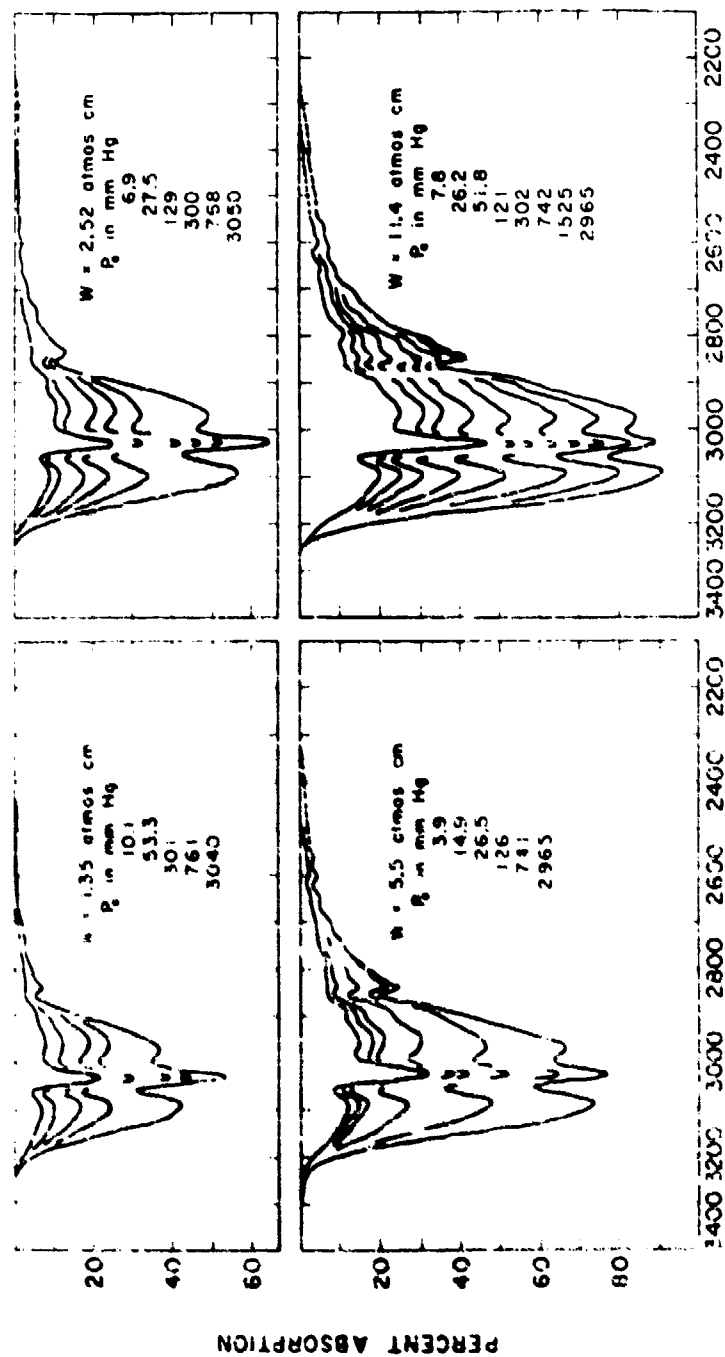
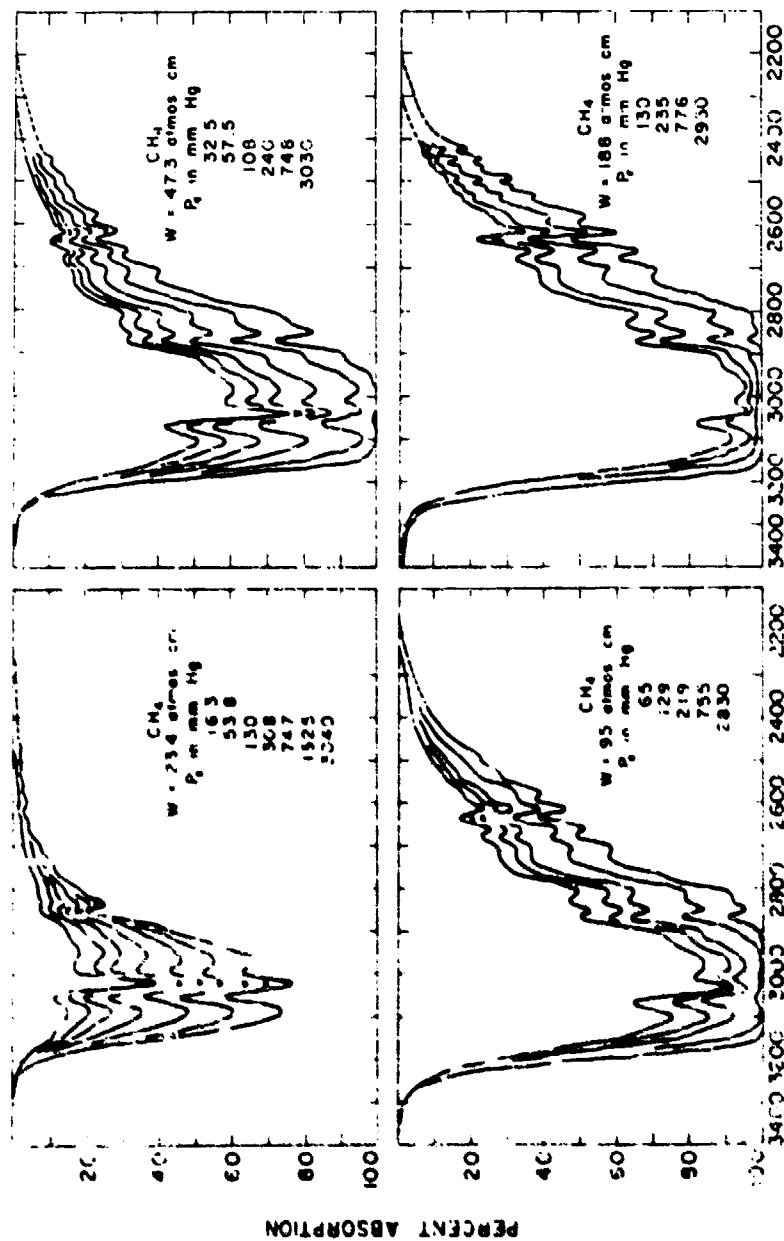


Fig. 4. Variation of the 1000 and 1100 bands



WAVENUMBER in cm⁻¹

Fig. 1. Infrared spectra of CH₄ at various pressures and path lengths.

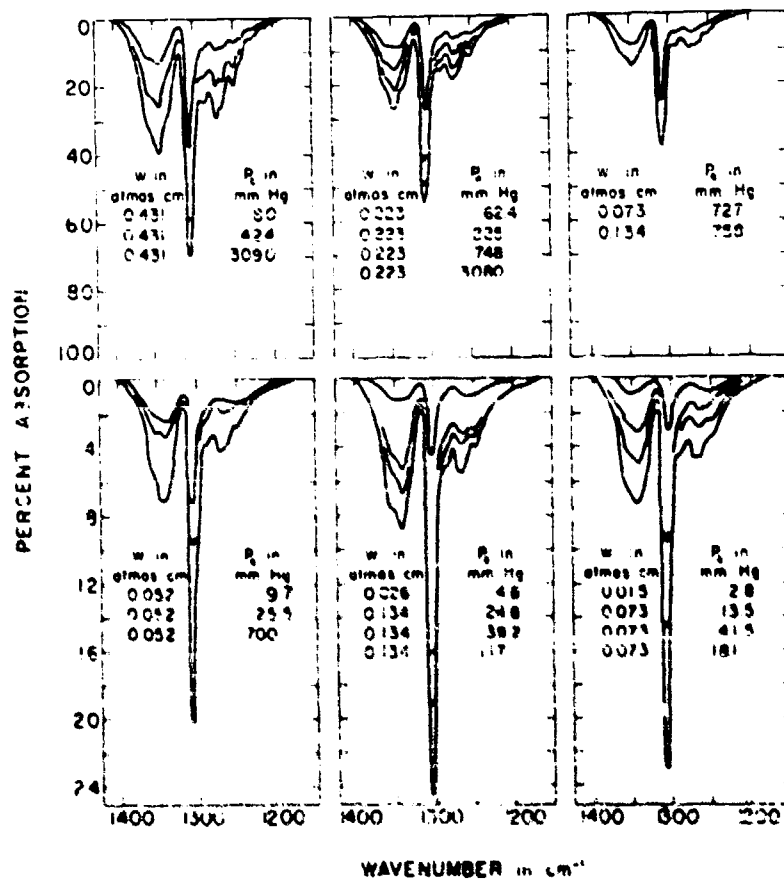


Fig. 47. Spectrum of the 100-cm Hg band

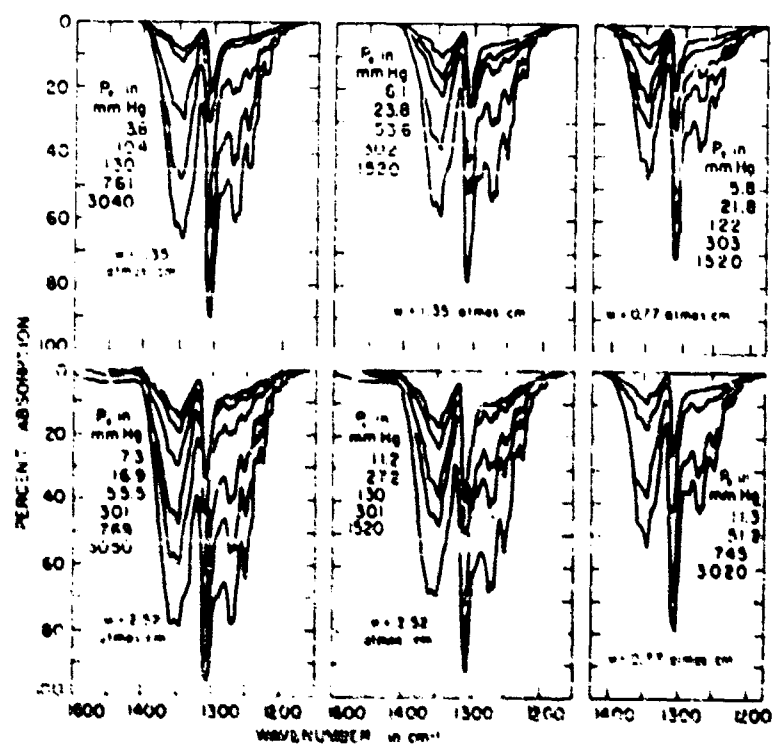


Fig. 53. Spectra of the 1305 cm⁻¹ CH₃ band

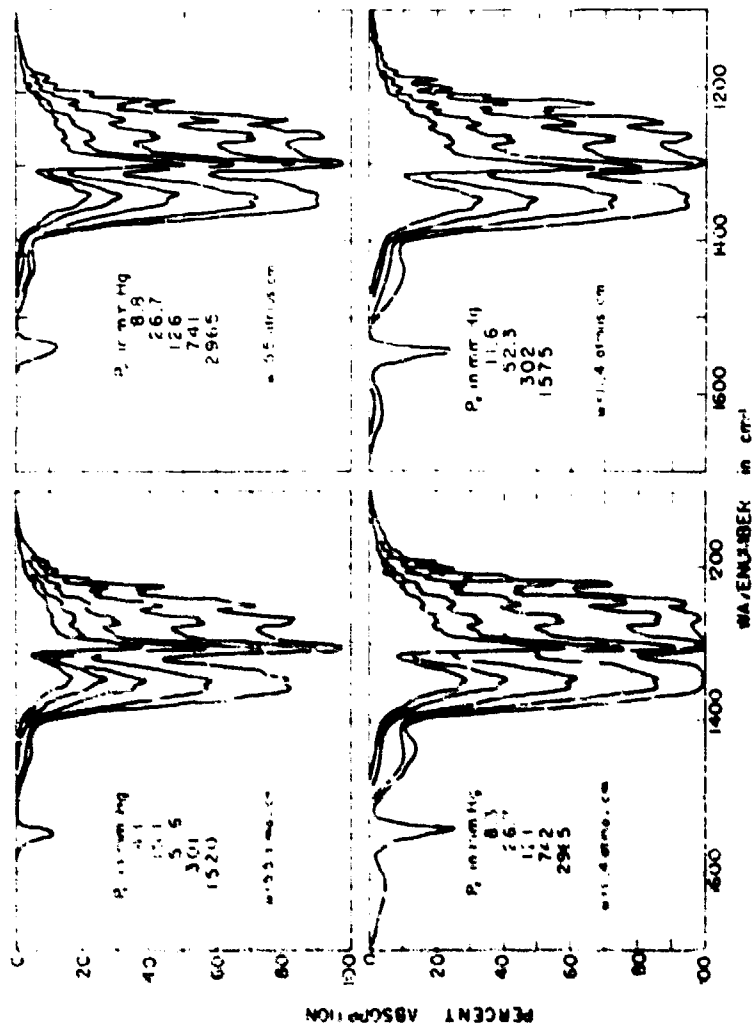


Fig. 10. Spectra of the 100 cm^{-1} and 1500 cm^{-1} IR bands

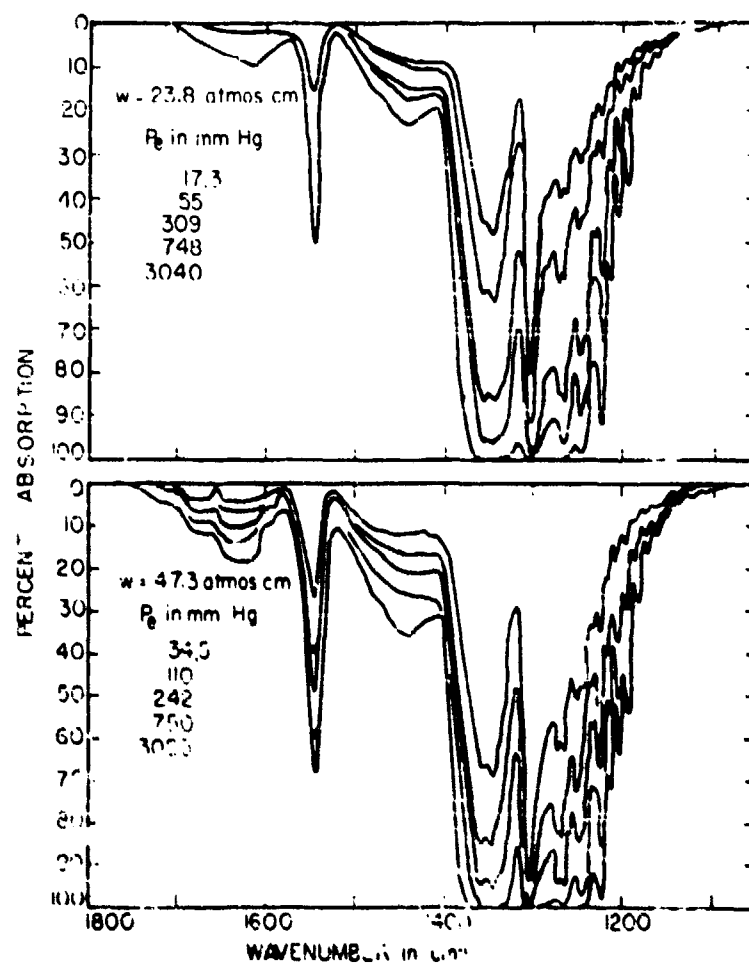


Fig. 40. Spectrum of the SiH_4 in the SiH_4 band.

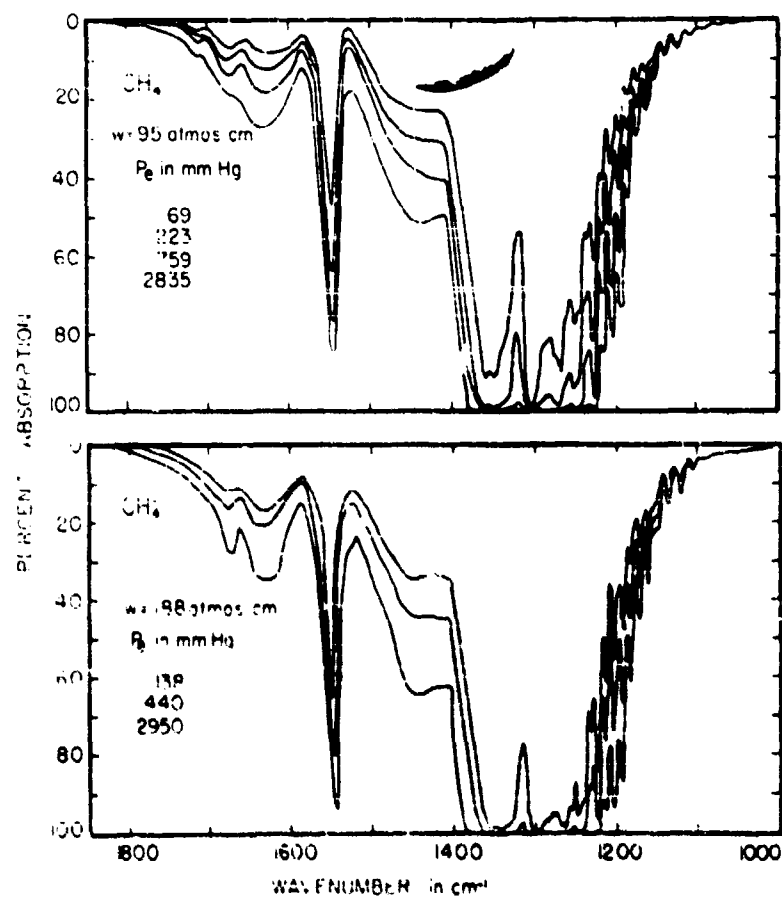


Fig. 1. Spectra of the 1300 and 1400 cm⁻¹ CH₄ bands.

band because of the over-lapping water vapor absorption; therefore, the same value of B , 1.36, was used for this band as for the 1306 cm^{-1} band. Since two different values of B were used in (14), two different values of P_e appear in Table 5 for each sample.

The data on the CH_4 absorption are presented in a manner similar to that in which the 2224 cm^{-1} H_2O and 2143 cm^{-1} CO data were presented in previous sections. Many of the 3020 cm^{-1} data are plotted in Fig. 52 with $\int A(\nu)d\nu$ versus P_e , where each curve corresponds to a constant value of ν . The features of the curves of Fig. 52 are similar to those of the corresponding curves for the 2224 cm^{-1} H_2O band in Fig. 12 and the 2143 cm^{-1} CO band in Fig. 30. However, two features of the curves of Fig. 52 should be noted. The maximum slope of any of the curves of Fig. 52 is approximately 0.23; this indicates that the maximum dependence on P_e is $P_e^{0.23}$, which is considerably less than for the H_2O and CO bands. It is also noted that the slopes of the curves corresponding to values of ν between 0.11 and 11.4 atm-cm increase with increasing values of equivalent pressure to approximately 75 mm Hg.

It is recalled that the slopes of some of the corresponding curves for H_2O and CO were found to increase with increasing equivalent pressure up to approximately 10 mm Hg. This phenomenon was attributed to the effect of the Doppler width of the absorption lines. However, it seems unlikely that an increase in the slope to pressures as high as 75 mm Hg could be a result of the Doppler width of the lines. It seems, therefore, that another explanation of the increasing slope of the curves of Fig. 52 is needed. A possible qualitative explanation which takes into account the rather unique structure of this band follows.

A high-resolution spectrum of the 3020 cm^{-1} CH_4 band shows that it is composed of several strong lines which occur in groups, each group being separated by approximately $10\text{--}12\text{ cm}^{-1}$. Also occurring in the spectrum are many weaker lines throughout the band. Except for samples with low pressure and very small values of absorber concentration, each group of strong lines could be treated as a single line for purposes of estimating the absorption. The band could then be approximated by a band model consisting of an Elsasser-type band of strong lines spaced $10\text{--}12\text{ cm}^{-1}$ apart, and superimposed on it another band consisting of much weaker lines spaced much closer together.

For relatively low pressures one might expect that there would be a rather wide range of values of ν over which the contribution to the absorption by the strong lines would have approximately a square-root dependence. The total absorption by these lines would therefore increase approximately as the square-root of the equivalent pressure. On the other hand, the contribution to the absorption by the weak lines would have little or no dependence on equivalent pressure. At low pressures a major portion of the absorption would arise from the weak lines; and the total absorption of the band would therefore have little dependence on pressure. However, as the pressure is increased, the relative

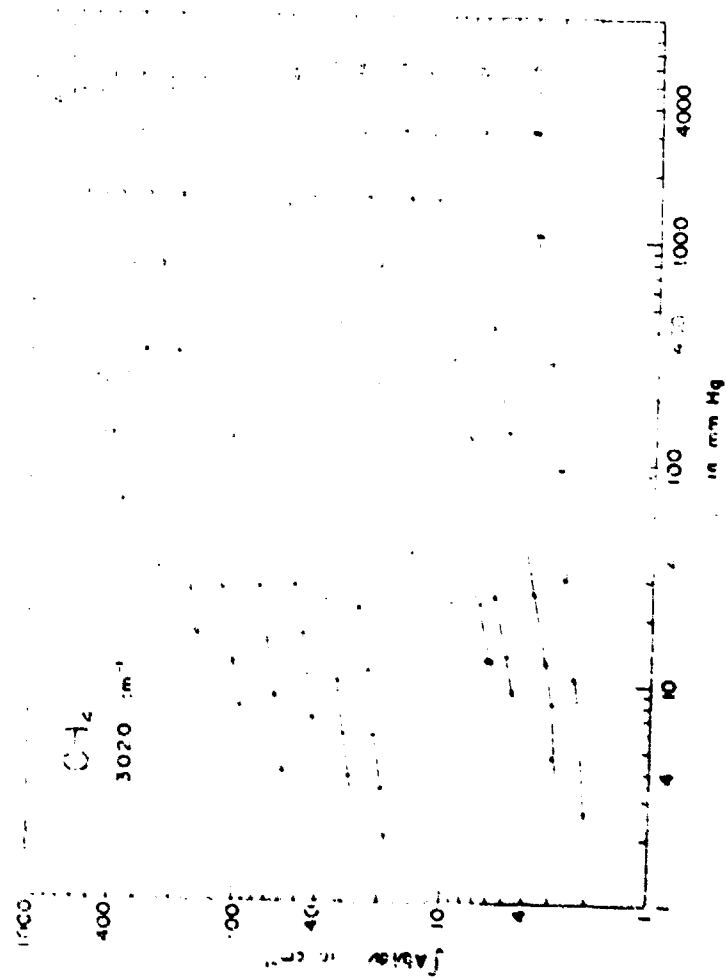


Fig. 20. The total absorption of CH_2 at 3020 cm^{-1} versus total pressure.

contribution of the pressure-dependent strong lines would become greater; the total absorption of the band would therefore exhibit the observed increasing dependence on pressure.

Without investigating the absorption in a highly resolved spectrum, it would be difficult to prove that the above explanation is valid. However, it can be said that it is a possible explanation of ν dependence on pressure not observed in most absorption bands studied, and is based on a band model which is similar to the actual band.

Values of $\int A(\nu) d\nu$ were taken from the curve of Fig. 52 and plotted in Fig. 53 against absorber concentration ν . Each curve corresponds to the constant value of P_0 as shown. By interpolation it is possible to determine the total absorption of a sample of CH_4 having values of ν and P_0 within the range included by the curves of Fig. 53. The features of the curves are similar to those of the corresponding figures for the H_2O and CO bands. The nearly linear portions of the curves were found to have slopes of approximately 0.55, indicating that the total absorption is proportional to $\nu^{0.55}$ for the ranges of values of ν and P_0 represented by the linear portions.

The band intensity $\int A(\nu) d\nu$ was estimated from the values of $\int A(\nu) d\nu$ determined. The accuracy of the value determined is probably less than in the case of the H_2O and CO bands. It is to be noted that the determination of the intensity from the absorption involves a number of assumptions which must be sufficiently high to make the band intensity determined sufficiently low so that the concentration is very small. Under these conditions the effect of pressure is very small. For the smallest values of ν and P_0 the band intensity is very small. For the largest values of ν and P_0 the band intensity is seen to increase. It is apparent that the band intensity could be determined directly by a direct reading from the 3000 mm Hg curve. The corresponding figures for the H_2O and CO bands are given by interpolating the curve to smaller values of ν , keeping in mind that the maximum slope of the extrapolated portion of the curve should be the value of the band intensity. The 3020 cm^{-1} CH_4 band was estimated to be given by

$$\int A(\nu) d\nu = 320 \text{ atm}^{-1} \text{ cm}^{-2} \text{ STP.} \quad (38)$$

This value, which is believed to be accurate to within 25%, is approximately 12% less than the value of 360 $\text{atm}^{-1} \text{ cm}^{-2}$ reported by Welsh, Fehler, and Dunn¹³.

Values of $\int A(\nu) d\nu$ for the 1306 cm^{-1} CH_4 band are plotted against P_0 in Fig. 54. Several of the curves of the figure contain portions having slopes of approximately 0.30, indicating a maximum dependence on P_0 , which is greater than the maximum dependence on ν for the 3020 cm^{-1} band but is still much less than a square-root dependence.

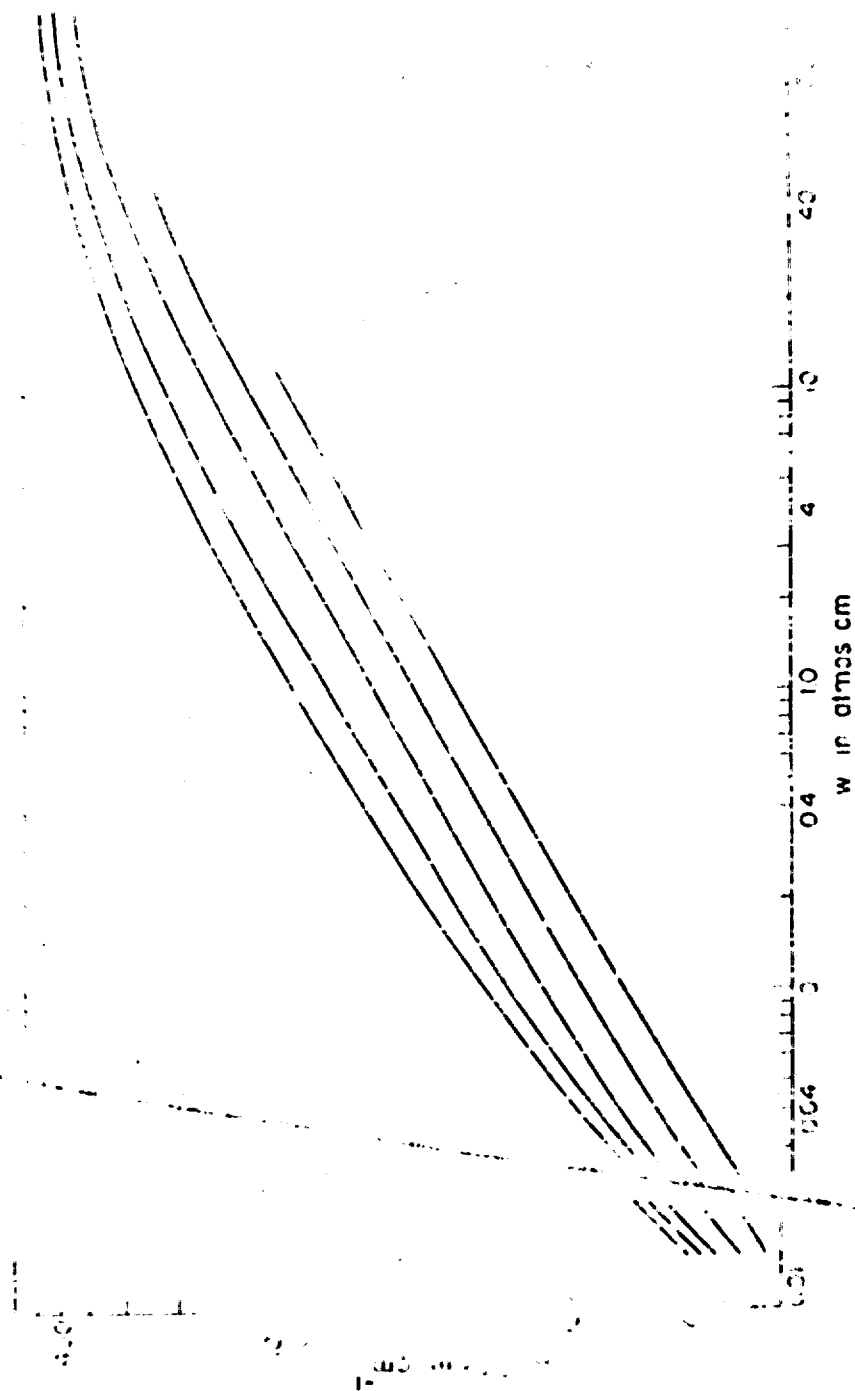
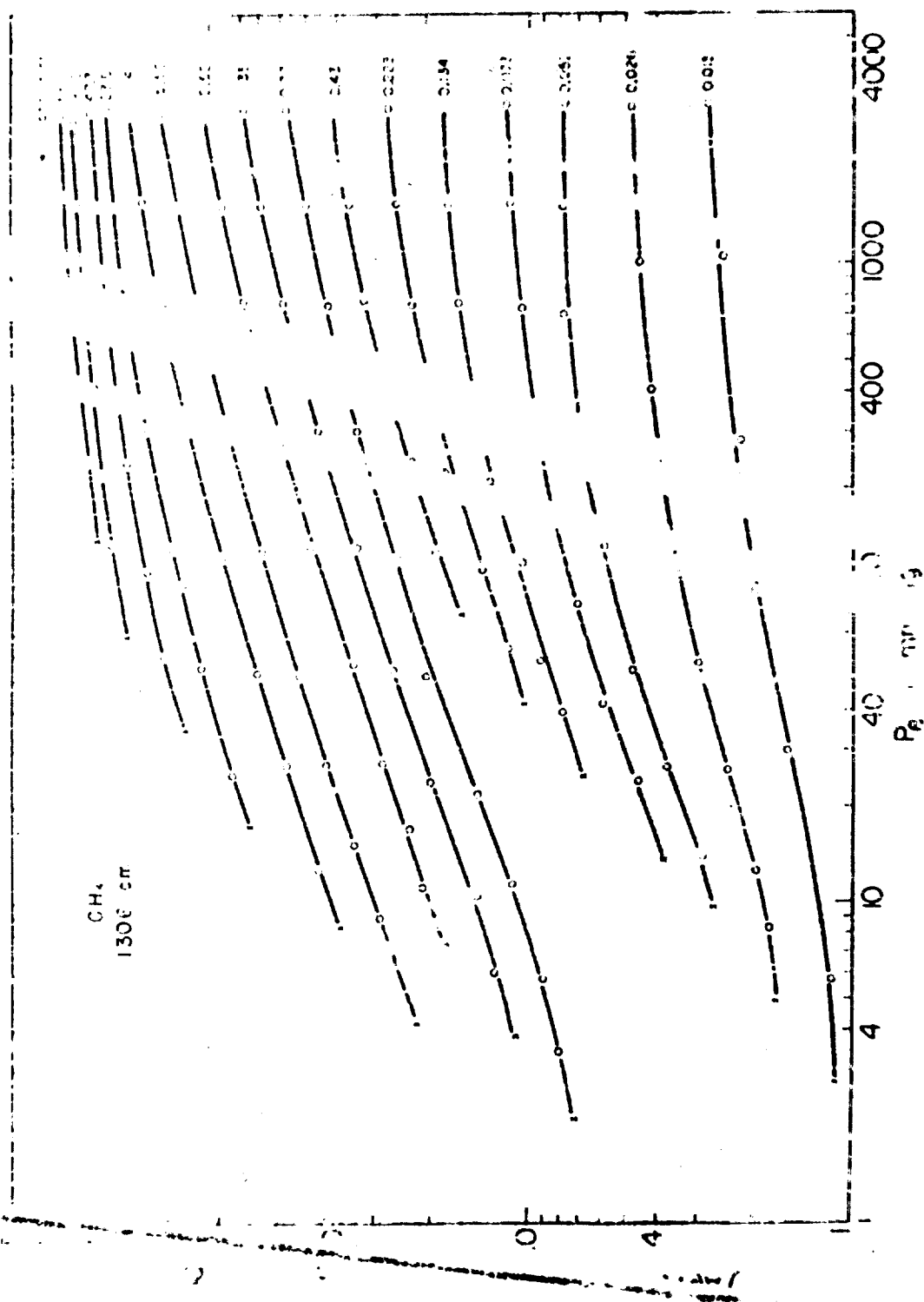
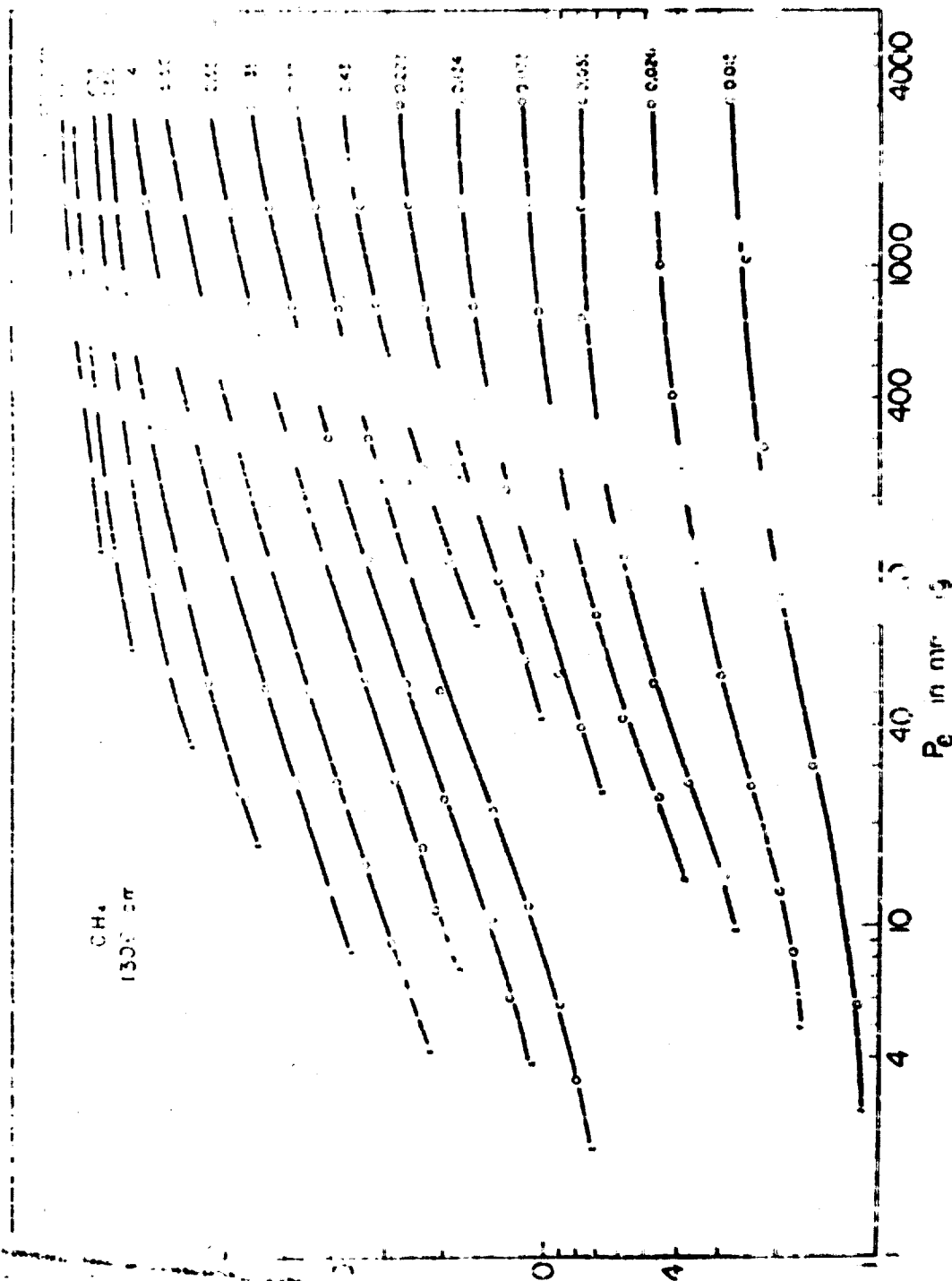


Fig. 55. The total absorption of the 3020 $\text{m}\mu$ line, band versus absorption concentration.

band versus absorption concentration



Best Available Copy



... for values of equivalent path length of 10 mm Hg. This result is, of course, in good agreement with that observed in Fig. 52 for the 1306 cm^{-1} band. Higher-order overtones of these two CH_2 bands show that their band structures are quite different from the simple band model which was used to describe the growth of the band would not be expected to be similar for the 1306 cm^{-1} band. would therefore not necessarily expect the two bands to grow with increasing pressure in the same manner.

Values of $\int A(\nu) d\nu$ were obtained from the curves of Fig. 54 and plotted against absorber concentration in Fig. 55 for the different values of P_0 indicated. Rather large portions of the curves were found to have a slope of approximately 0.48, indicating that the total absorption varies essentially as the square root of the absorber concentration for the values of ν and P_0 represented.

By extrapolating the curves of Fig. 55 to smaller values of ν , the band intensity of the 1306 cm^{-1} CH_2 band was found to be given by

$$k(\nu)d\nu = 187 \text{ atmos}^{-1} \text{ cm}^{-2} \quad (49)$$

This value, which is believed to be in error by less than 15%, is approximately 18% greater than the value of 157 $\text{atmos}^{-1} \text{ cm}^{-2}$ reported by Welsh and Sandiford²⁴.

The absorption by the 1306 cm^{-1} band overlaps the absorption by the 1345 cm^{-1} band for samples of large absorber concentration. The frequency 1345 cm^{-1} was chosen as the frequency dividing the two bands represents an intermediate value between the P- and Q-branches of the ν_2 band at 1345 cm^{-1} . The spectral region referred to in this report as the 1306 cm^{-1} band actually includes the 1345 cm^{-1} band. However, the value of the absolute band intensity determined from the curves is essentially unaffected by the absorption arising from the ν_2 band. This is believed to be true since the absorption by the 1345 cm^{-1} band in the region where the bands overlap is negligible for the samples and the small values of absorber concentration which are represented by the portions of the curves from which the band intensity was determined.

The data for the 1306 cm^{-1} CH_2 band are plotted in Fig. 56. The total absorption is plotted against P_0 in the left-hand portion for the values of ν indicated, and values were taken from these curves to obtain the curves in the right-hand portion of the figure. As stated previously, the data for this band were limited to samples having large absorber concentration, and the recording of the spectra was less accurate than for the other bands because of the overlapping absorption. The curves of Fig. 56 are probably accurate to about 10% for values of total absorption greater than 10-40 atmos^{-1} ; the error for the smaller samples might be as great as 15-20%.

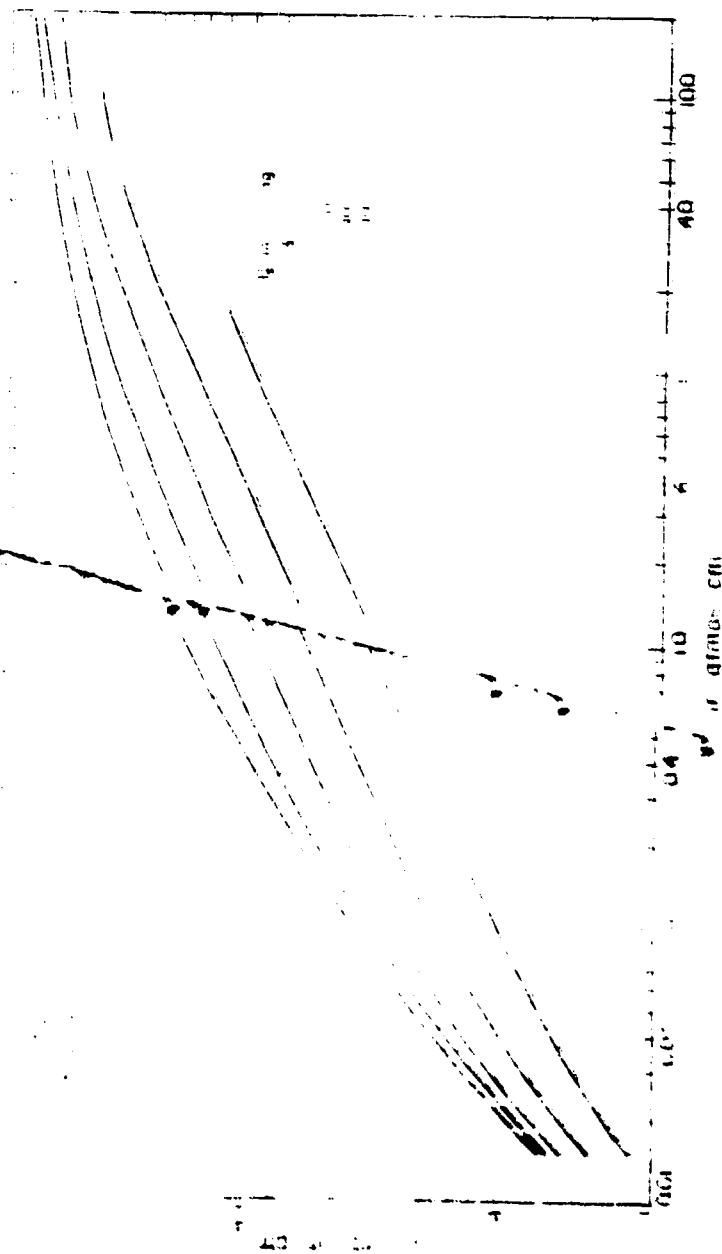


Fig. 1. Total absorption of the 1.06 μ m line of CO_2 vs. concentration of CO_2 in atmos cm.

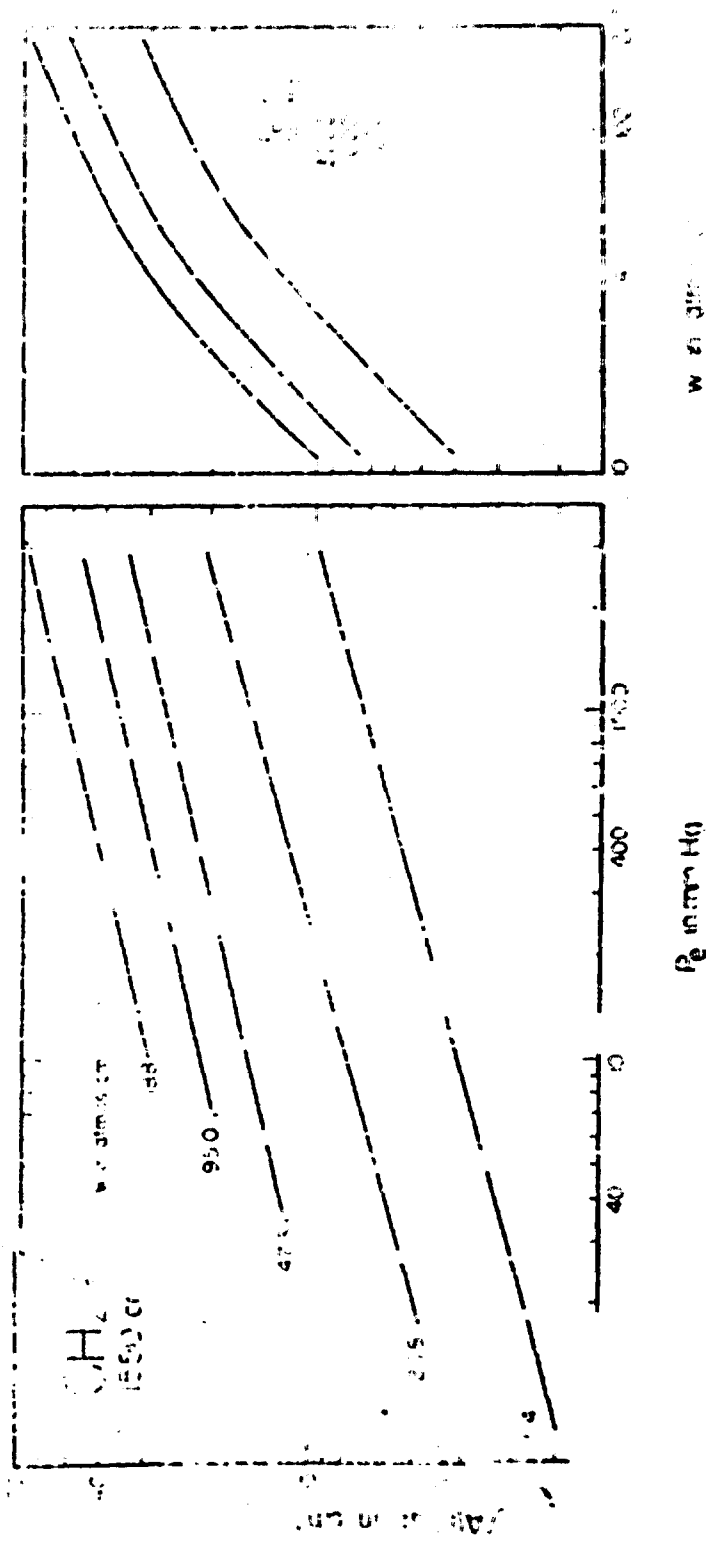


Fig. 12. The total absorption of CH_2Cl_2 vapor.

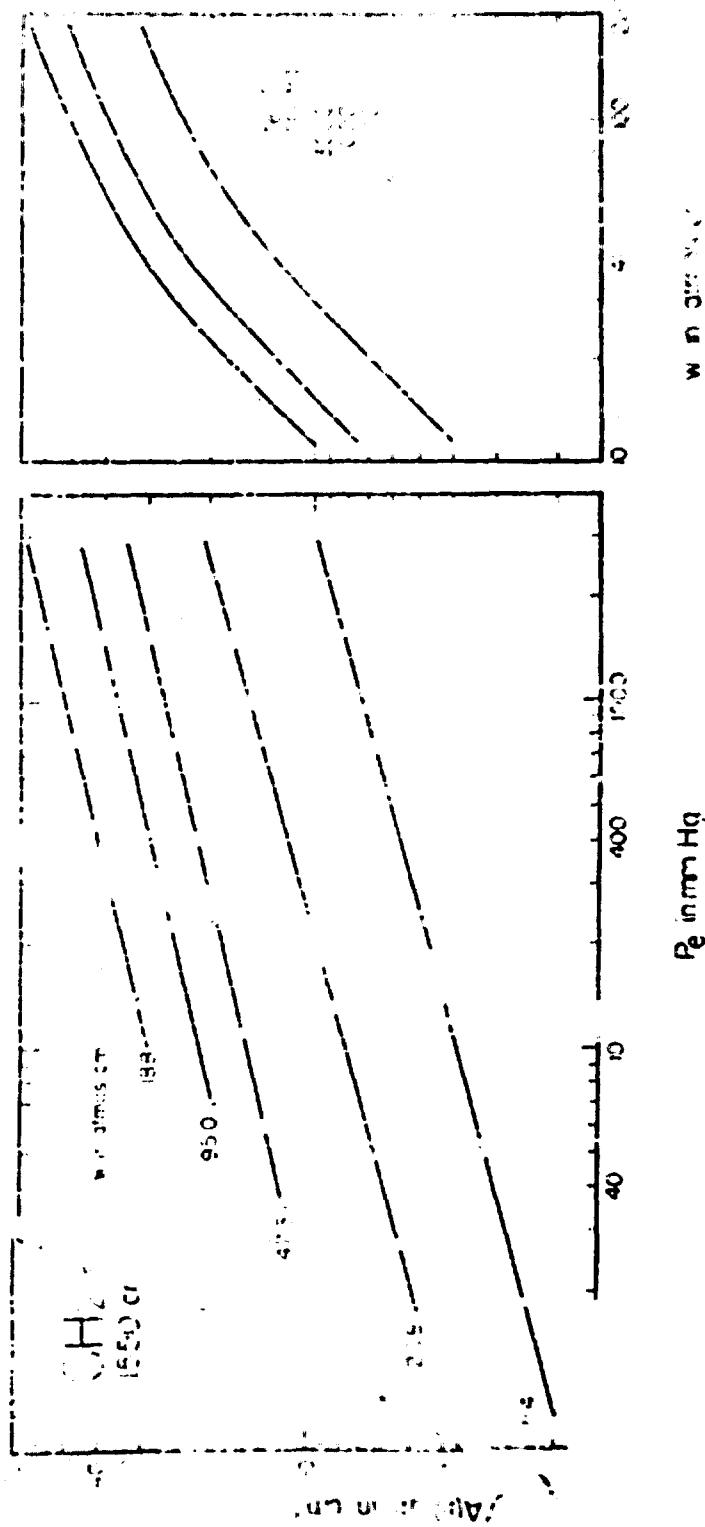


Fig. 55. The total absorption of the 15.50% CH_2Cl_2 band

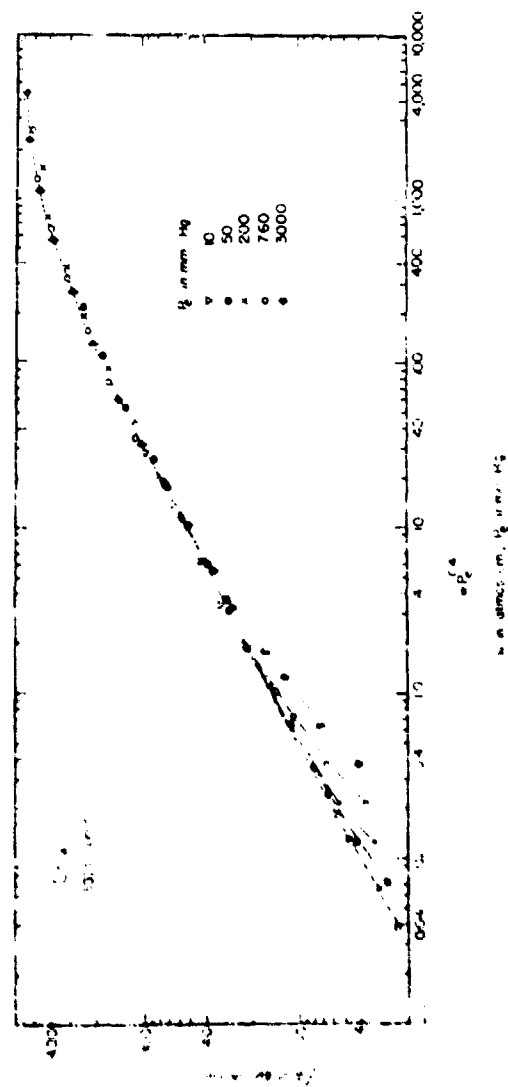
The slopes of the curves in the left-hand portion of Fig. 56 indicate a maximum dependence of approximately $P_0^{0.27}$ for the values of v and P_0 represented. This result is approximately the same as that observed for the other two CH_4 bands. The curves in the right-hand portion of the figure do not exhibit regions having slopes of approximately 0.5, as do the corresponding curves for the other bands, since the largest values of absorber concentration employed were not sufficiently great for the lines in this weak band to exhibit "strong-line" properties.

Because of the absorption by H_2O and the limited amount of data obtained for the 1550 cm^{-1} band, it was not possible to determine the band intensity with very high accuracy. The value of $\int A(v)dv$ indicated by the ordinate of Fig. 56 of course does not include absorption by the F-branch of the ν_2 band, since only the absorption at frequencies greater than 1555 cm^{-1} is included. Therefore, any value of absolute intensity determined by extrapolating the curves of Fig. 56 would be too low. However, by extrapolating these curves and by assuming that the contribution of the F-branch is approximately the same as the R-branch it can be estimated that the absolute intensity of the ν_2 band is between 2 and 3 $\text{atmos}^{-1}\text{ cm}^{-2}$. To the knowledge of the authors, the intensity of this weak band has not been measured previously.

In order to obtain more accurate values for the intensities of the CH_4 bands, higher values of equivalent pressure should be used and more data should be obtained for samples having small values of absorber concentration. In the case of the 1550 cm^{-1} band, the CH_4 gas should be dried and a spectrometer which could be evacuated or thoroughly dried should be used. This extra care was not taken since the determination of band intensities was only of secondary importance in the present study.

In order to obtain empirical equations to relate the total absorption of the 3020 cm^{-1} band to the parameters v and P_0 , the curves of Fig. 57 were drawn with the variable $vP_0^{0.4}$ as the abscissa. The value 0.4 was arrived at from the slopes of the linear portions of the curves of Figs. 52 and 53 in the same manner as was done for the 2224 cm^{-1} H_2O band. The points corresponding to the different values of pressure in Fig. 57 occur very close together over a large region of values of $\int A(v)dv$. Portions of several of the curves were omitted from the figure to avoid overcrowding, but the points corresponding to the different pressures were included. From Fig. 57 the following equations were derived for the 3020 cm^{-1} CH_4 band:

$$\begin{aligned} \text{for} \quad & \int A(v)dv > 15.0, \quad \left[vP_0^{0.4} \right]^{0.4} \\ \text{and} \quad & 15 < \int A(v)dv < 250\text{ cm}^{-1} \\ & 10 < P_0 < 160\text{ mm Hg.} \end{aligned} \quad (40)$$



57. The total absorption of the 3000 cm⁻¹ CH₃ band versus ν_{CH_3}

$$\begin{aligned}
&\int A(\nu) d\nu = -375 + 272 \log wP_e^{0.4} \\
\text{for} \quad &250 < \int A(\nu) d\nu < 500 \text{ cm}^{-1} \\
\text{and} \quad &10 < P_e < 3000 \text{ mm Hg} .
\end{aligned} \tag{41}$$

Values of $\int A(\nu) d\nu$ determined by use of the above equations are probably accurate to $\pm 10\%$, except for values of $\int A(\nu) d\nu < 40 \text{ cm}^{-1}$, below which the error might be as great as $\pm 15\%$.

Figure 58 shows the total absorption of the $1306 \text{ cm}^{-1} \text{ CH}_4$ band as ordinate and $wP_e^{0.6}$ as the abscissa. The curves are not as close as in portions of Fig. 57. It is possible that a somewhat different value of the exponent of P_e could be used to cause the curves more nearly to coincide; however, the various curves in Fig. 58 do not form the relatively simple pattern occurring in the corresponding figures discussed earlier; for example, a portion of the curve corresponding to 10 mm Hg lies between the curves corresponding to 50 mm Hg and 200 mm Hg . It is apparent that an increase in the value of the exponent of P_e would tend to cause the two curves corresponding to 760 and 50 mm Hg to occur closer together; but on the other hand, the curves corresponding to 10 mm Hg and 50 mm Hg would be further separated. The value 0.6 was used as a nominal value for the exponent.

Since the curves of Fig. 58 are not as close together as the corresponding curves for other bands, it is probable that any empirical equations derived from them would be less accurate than the equations derived for the other bands. The following equations which were obtained for the $1306 \text{ cm}^{-1} \text{ CH}_4$ band are believed to be capable of yielding correct values of total absorption to within $\pm 15\%$ for the conditions specified:

$$\begin{aligned}
&\int A(\nu) d\nu = 7.5 [wP_e^{0.6}]^{0.45} \\
\text{for} \quad &20 < \int A(\nu) d\nu < 130 \text{ cm}^{-1} \\
\text{and} \quad &10 < P_e < 760 \text{ mm Hg} .
\end{aligned} \tag{42}$$

$$\begin{aligned}
&\int A(\nu) d\nu = -190 + 115 \log wP_e^{0.6} \\
\text{for} \quad &130 < \int A(\nu) d\nu < 500 \text{ cm}^{-1} \\
\text{and} \quad &10 < P_e < 760 \text{ mm Hg} .
\end{aligned} \tag{43}$$

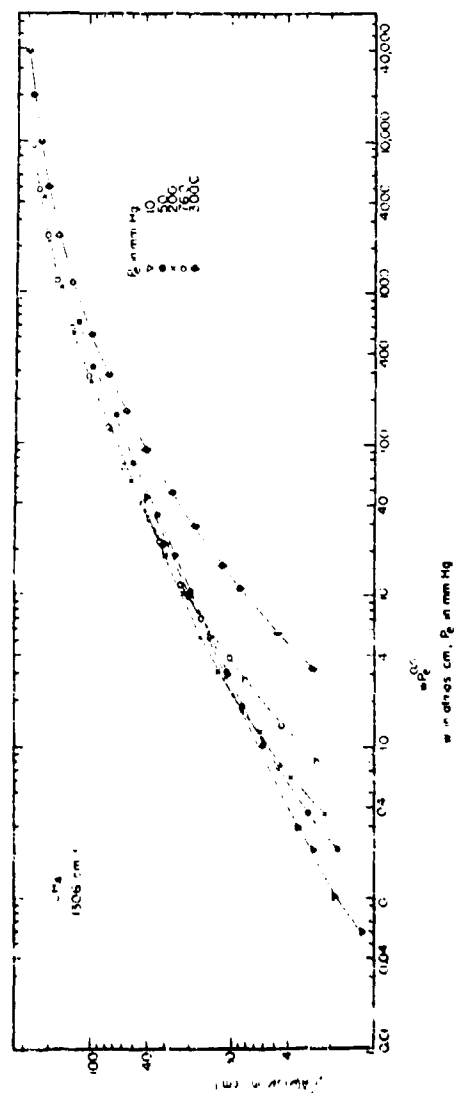


Fig. 56. The total absorption of the $1306 \text{ cm}^{-1} \text{ CH}_3$ band versus p_c .

VIII. SUMMARY

The work covered in the present report has dealt with the infrared absorption of the minor atmospheric gases nitrous oxide, carbon monoxide, and methane. Samples consisting of these gases alone and in binary mixtures with nitrogen have been investigated over wide ranges of absorber concentration ν and total pressure P . From the observed absorption for each band, it has been possible to present curves showing total absorption $\int A(\nu) d\nu$ for various values of absorber concentration as a function of equivalent pressure P_e , which is a parameter that includes the total pressure P and a small additional term proportional to the partial pressure of the absorbing gas; the magnitude of the additional term is also dependent on the value of a "self-broadening coefficient," defined in the report and measured experimentally for each absorption band. Another set of curves for each band shows the total absorption for various equivalent pressures as a function of absorber concentration. The curves provide a basis for the prediction of total absorption for any values of ν and P_e included in the wide range of these parameters covered in the study. Extensive tables included at the end of the report provide additional absorption data for use by other investigators who may be interested in atmospheric transmission or in more general problems of absorption.

The experimental results are compared with various theoretical predictions. For values of ν and P_e for which the "strong-line approximation" predicts the dependence $\int A(\nu) d\nu \sim \sqrt{\nu P_e}$, it has been found that $\int A(\nu) d\nu$ is indeed roughly proportional to $\sqrt{\nu}$ but not to $\sqrt{P_e}$. For sufficiently large values of P , overlapping of lines causes total band absorption to approach a "saturation value"; for very low values of P , the total absorption for a given absorber concentration also approaches a limiting value for which the Doppler broadening of lines, independent of pressure, predominates.

It has been possible to obtain empirical equations relating total absorption to ν and P_e for certain limited values of total absorption $\int A(\nu) d\nu$ and equivalent pressure P_e . The limits of validity for such equations are discussed. The empirical equations are summarized in Table 7.

By studying total absorption at small values of absorber concentration ν and sufficiently large values of equivalent pressure P_e , it has been possible to obtain values for the band intensity $\int A(\nu) d\nu$ for the various bands studied. Present results have been compared with the values reported by other investigators. The values obtained for band intensities are summarized in Table 8.

A second set of comparisons of the present results with existing theories has involved studies of the absorption $A(\nu)$ in spectral regions of maximum absorption in the P- and R-branches of various bands. In most cases it was found that $A(\nu) \sim \sqrt{\nu}$ over certain ranges of ν and P_e ; however, it was found that the proportionality $A(\nu) \sim \sqrt{P_e}$ was rarely

observed. The possible effect of weak lines adjacent to strong ones is discussed as one cause of the failure of the "strong line approximation": weak lines are always present in the wings of absorption bands, but sometimes are not present near the regions of maximum absorption in the P- and R-branches.

It is hoped that the present results can be used as a basis for the development of adequate general theories of absorption in the infrared spectra of gases as well as in more immediately "practical" studies of the atmosphere.

Table 1. Materials

Gas	Supplier and Grade	Purity, %	Impurities
H ₂ O	Mathieson	99	Chiefly H ₂ , traces of CO ₂
CO	Mathieson C. P.	97	Chiefly CO ₂
CH ₄	Mathieson C. P.	99.0	Traces of C ₂ H ₆ , N ₂ , CO ₂ and H ₂ O
H ₂	Linde High Purity Dry	99.99	Max. of 15 grains of H ₂ O per 1000 cu. ft.

Table 2. Self-Broadening Coefficients for
Minor Atmospheric Gases

Band	Self-Broadening Coefficient B^a
2224 cm^{-1} H_2O	1.12 ± 0.07
2143 cm^{-1} CO	1.02 ± 0.06
4260 cm^{-1} CO	1.08 ± 0.06
3020 cm^{-1} CH_4	1.50 ± 0.08
1306 cm^{-1} CH_4	1.58 ± 0.08
1550 cm^{-1} CH_4	1.58 ± 0.08

^aDefined in Eqs. (13) and (14),
where B_2 is the reference gas.

Table A. Data for the 2224 cm^{-1} H_2O Band

The Fig. No. corresponds to the figure in which the spectrum of each sample is shown. Absence of Fig. No. indicates spectrum is not shown. Uncertainties of values of $A(\nu)$ and $\int A(\nu)d\nu$ are discussed in text.

Sample No.	Fig. No.	ν (cm^{-1})	P_e (mm Hg)	$\int A(\nu)d\nu$ (cm^{-1})	$A(2240)$ %	$A(2213)$ %	Remarks
Path Length = 1.55 cm							
1	5	0.0016	1.0	1.00	1.5	1.4	Samples 1-21: H_2O alone in cell
2	5	0.0033	2.0	1.56	2.4	2.3	
3	5	0.0051	3.1	2.03	3.0	2.6	
4	5	0.0074	4.6	2.75	4.0	3.6	
5	5	0.0110	6.8	3.79	5.5	5.1	
6	5	0.0157	9.7	5.21	7.5	6.9	
7	5	0.0217	13.4	6.93	9.7	9.5	
8	5	0.0270	16.7	8.49	11.6	11.2	
9	5	0.0352	21.8	10.9	15.3	14.6	
10	5	0.0456	28.1	13.8	19.2	18.2	
11	8	0.057	35.3	16.1	23.3	21.3	10.5 mm Hg of H_2O
12	8	0.073	44.9	20.2	28.1	26.8	
13	8	0.091	56.2	24.7	34.0	33.0	
14		0.0947	53.8	15.3	21.3	20.6	
15	5	0.0724	44.6	19.6	27.5	25.8	
16	5	0.112	69.4	28.2	39.5	37.1	
17	5	0.172	106	40.2	55.0	52.1	
18	5	0.225	150	53.2	71.0	68.0	
19	5	0.389	241	69.3	69.1	65.0	
20	5	0.677	419	85.2	98.0	98.3	
21	5	1.36	841	96.8	99.0	100.0	Samples 22-30: H_2 added to samples 22
22	8	0.0186	11.5	5.93	8.3	7.7	
23	8	0.0186	21.6	7.21	10.2	9.6	
24	8	0.0186	42.4	9.31	13.0	12.3	
25	8	0.0186	91.2	12.2	15.2	16.6	
26	8	0.0186	186	15.8	24.2	21.6	
27	8	0.0186	360	18.7	30.0	26.2	
28	8	0.0186	749	22.0	36.0	31.8	
29		0.0186	1520	24.4	40.0	35.9	
30	6	0.0186	3035	24.9	41.1	36.8	
31	8	0.0101	6.2	3.62	5.1	4.4	5.5 mm Hg of H_2O
32	8	0.0101	10.9	4.21	6.0	5.1	
33	8	0.0101	26.6	5.60	8.0	7.3	
34	8	0.0101	50.0	6.86	10.1	9.3	
35	8	0.0101	114	9.11	14.0	12.5	
36	8	0.0101	259	11.6	19.5	16.5	
37	8	0.0101	746	14.4	23.3	20.6	
38	8	0.0101	1520	15.4	25.4	22.6	
39	8	0.0101	3035	15.7	25.6	22.9	

Table 5. Data for the 2224 cm^{-1} N_2O Band

The Fig. No. corresponds to the figure in which the spectrum of each sample is shown. Absence of Fig. No. indicates spectrum is not shown. Uncertainties of values of $A(\nu)$ and $\int A(\nu)d\nu$ are discussed in text.

Sample No.	Fig. No.	ν (atmos cm)	P_e (mm Hg)	$\int A(\nu)d\nu$ (cm^{-1})	$A(2240)$ %	$A(2213)$ %	Remarks
Path Length = 1.55 cm							
1	5	0.0016	1.0	1.00	1.5	1.4	Samples 1-21: N_2O alone in cell
2	5	0.0033	2.0	1.56	2.4	2.0	
3	5	0.0051	3.1	2.03	3.0	2.6	
4	5	0.0074	4.6	2.75	4.0	3.6	
5	5	0.0110	6.8	3.79	5.5	5.1	
6	5	0.0157	9.7	5.21	7.5	6.8	
7	5	0.0217	13.4	6.93	9.7	9.5	
8	5	0.0270	16.7	8.49	11.8	11.2	
9	5	0.0352	21.8	10.9	15.3	14.6	
10	5	0.0456	28.1	13.8	19.2	18.2	
11	8	0.057	35.3	16.1	23.3	21.3	
12	8	0.073	44.9	20.2	28.1	26.6	
13	8	0.091	55.2	24.7	34.0	33.0	
14		0.0747	33.8	15.3	21.3	20.6	
15	5	0.0724	44.6	19.6	27.5	25.8	
16	5	0.112	69.4	28.2	39.5	37.1	
17	5	0.172	106	40.2	55.0	52.1	
18	5	0.225	158	53.2	71.0	68.0	
19	5	0.389	241	69.3	69.1	85.0	
20	5	0.677	419	85.2	98.0	98.3	
21	5	1.36	841	96.8	99.0	100.0	
22	8	0.0186	11.5	5.73	8.3	7.7	10.5 mm Hg of N_2O Samples 23-30: N_2 added to samples 22
23	8	0.0186	21.6	7.21	10.2	9.6	
24	8	0.0186	42.4	9.31	13.7	12.3	
25	8	0.0186	91.0	12.2	15.2	16.4	
26	8	0.0186	186	15.8	24.2	21.6	
27	8	0.0186	460	18.7	30.0	26.2	
28	8	0.0186	749	22.0	36.0	31.8	
29		0.0186	1520	24.4	40.0	34.9	
30	6	0.0186	3035	24.9	41.1	36.0	
31	8	0.0101	6.2	3.62	5.1	4.4	5.6 mm Hg of N_2O Samples 31-39: N_2 added to sample 31
32	8	0.0101	10.9	4.21	6.0	5.1	
33	8	0.0101	26.6	5.60	8.0	7.3	
34	8	0.0101	50.0	6.86	10.1	9.3	
35	8	0.0101	114	9.11	14.0	12.5	
36	8	0.0101	239	11.6	15.6	16.5	
37	4	0.0101	746	14.4	23.3	20.6	
38	8	0.0101	1520	14.4	25.4	22.6	
39	8	0.0101	3035	15.7	25.6	22.9	

Table 3. (Continued)

Sample No.	Fig. No.	ν (atmos cm)	P_0 (mm Hg)	$\int A(\nu) d\nu$ (cm ⁻¹)	A(2240) %	A(2213) %	Remarks
40	7	0.0101	56.6	7.43	11.1	10.2	Sample 40:
41	7	0.0101	122	9.44	14.7	13.0	56 mm of mix-
42	7	0.0101	264	11.9	19.0	16.9	ture of 1/10
43	7	0.0101	759	14.4	24.1	20.8	H ₂ O and 9/10
44	7	0.0101	3035	15.5	25.8	23.0	H ₂ . Sam. 41- 44: H ₂ added to sample 40.
45		0.0054	3.4	2.32	3.3	3.2	Sample 45: 3.0
46		0.0054	6.6	2.59	3.6	3.5	mm Hg of H ₂ O
47		0.0054	12.1	3.14	4.6	4.2	alone. Samples
48		0.0054	30.4	4.24	6.3	5.9	46-48: H ₂ added to sample 45.
49	7	0.0054	30.4	4.18	6.2	5.7	Sample 49: 30
50	7	0.0054	72.0	5.40	8.5	7.8	mm Hg of 1/10
51	7	0.0054	189	7.02	11.0	10.0	H ₂ mixture.
52	7	0.0054	575	8.90	13.5	11.5	Samples 50-54:
53	7	0.0054	750	8.61	14.7	12.7	H ₂ added to
54	7	0.0054	3035	9.05	15.1	13.6	sample 49.
55		0.0032	2.0	1.44	2.1	1.9	Sample 55:
56		0.0032	4.2	1.73	2.6	2.3	1.75 mm Hg of
57		0.0032	9.9	2.09	3.2	2.9	H ₂ O. Samples
58		0.0032	17.7	2.61	4.0	3.7	56-58: H ₂
59		0.0032	35.0	3.21	5.2	4.6	added to sam- ple 55.
60	7	0.0032	17.7	2.53	3.8	3.5	Sample 60:
61	7	0.0032	40.4	3.21	5.1	4.5	17.5 mm Hg of
62	7	0.0032	105	4.20	6.8	6.2	1/10 H ₂ O mix-
63	7	0.0032	254	4.96	8.5	7.3	ture. Samples
64	7	0.0032	750	5.40	9.5	7.9	61-65: H ₂
65	7	0.0032	3035	5.57	9.7	8.3	added to sam- ple 60.
66	7	0.0020	11.1	1.59	2.3	2.2	Sample 66:
67	7	0.0020	25.1	2.07	3.2	2.8	11.1 mm Hg of
68	7	0.0020	40.0	2.44	3.8	3.5	1/10 H ₂ O mix-
69	7	0.0020	106	2.87	4.8	4.2	ture. Samples
70	7	0.0020	264	3.24	5.5	4.8	67-72: H ₂
71	7	0.0020	770	3.49	6.1	5.2	added to sam-
72	7	0.0020	3035	3.60	6.1	5.2	ple 66.

Table 3. (Continued)

Sample No.	Fig. No.	v (cm ⁻¹)	P_c (mm Hg)	$\int A(v)dv$ (cm ⁻¹)	$A(2240)$ %	$A(2213)$ %	Remarks
73	7	0.0011	6.1	0.98	1.5	1.3	Sample 73: 6.0
74	7	0.0011	15.6	1.22	1.9	1.6	mm Hg of 1/10
75		0.0011	39.9	1.54	2.4	2.1	N ₂ O mixture.
76	7	0.0011	110	1.75	3.0	2.5	Samples 74-79:
77		0.0011	259	1.90	3.3	2.8	N ₂ added to
78	7	0.0011	745	2.03	3.5	3.0	sample 73.
79		0.0011	3035	2.03	3.4	2.8	
80	6	0.0011	30.1	1.32	2.3	1.9	Sample 80:
81		0.0011	746	1.95	3.4	2.9	30.0 mm Hg of
82	6	0.0011	3035	2.00	3.5	3.0	1/50 N ₂ O mix- ture. Samples 81-82: N ₂ added to sam- ple 80
83	6	0.00072	20.1	1.03	1.6	1.4	Sample 83: 20.1
84	6	0.00072	98.0	1.21	2.1	1.7	mm Hg of 1/50
85		0.00072	250	1.30	2.2	1.9	N ₂ O mixture.
86	6	0.00072	746	1.30	2.3	1.9	Samples 84-87:
87		0.00072	3035	1.33	2.3	1.7	N ₂ added to sample 83.
88	6	0.00047	13.1	0.70	1.1	0.9	Sample 88: 13.1
89	6	0.00047	3035	0.86	1.5	1.3	mm Hg of 1/50 N ₂ O mixture. Sample 89: N ₂ added to sample 88.
90	6	0.00033	9.2	0.55	0.8	0.7	Sample 90: 9.2
91	6	0.00033	3035	0.62	0.9	0.8	mm Hg of 1/50 N ₂ O mixture. Sample 91: N ₂ added to sam- ple 90.
92	6	0.00024	6.5	0.37	0.7	0.5	Sample 92: 6.5
93	6	0.00024	3035	0.35	0.8	0.7	mm Hg of 1/50 N ₂ O mixture. Sample 93: N ₂ added to sam- ple 92.

Table 3. (Continued)

Sample No.	Fig. No.	ν (atmos cm)	P_0 (mm Hg)	$\int A(\nu) d\nu$ (cm ⁻¹)	$A(2240)$ %	$A(2213)$ %	Remarks
94	6	0.00016	4.5	0.27	0.5	0.4	Sample 94: 4.5 mm Hg of 1/50 H ₂ O mixture. Sample 95: H ₂ added to sample 94.
95	6	0.00016	3035	0.35	0.6	0.5	
96	7	0.00017	48.0	2.18	3.4	3.2	Samples 96-101: 1/50 H ₂ O mixture alone.
97	7	0.0033	90.0	3.93	6.4	5.7	
98	7	0.0060	165	6.96	11.2	9.9	
99	7	0.0098	270	11.33	18.3	16.1	
100	7	0.0136	375	15.4	25.0	22.0	
101		0.0223	618	23.7	37.5	33.5	
102	5	0.0016	9.1	1.50	2.1	1.8	Samples 102-112: 1/10 H ₂ O mixture alone.
103	5	0.0024	13.3	1.87	2.7	2.5	
104	5	0.0032	17.8	2.43	3.8	3.3	
105	5	0.0045	25.8	3.34	5.1	4.6	
106	5	0.0065	36.4	4.82	7.3	6.6	
107	5	0.0091	50.6	6.46	10.0	9.0	
108	5	0.0185	103	12.76	19.1	17.5	
109	5	0.0295	165	19.50	28.9	26.3	
110	5	0.0500	281	30.70	45.4	41.8	
111	5	0.0750	418	41.90	61.6	56.5	
112	5	0.1150	644	57.00	78.8	75.0	
Path Length = 6.35 cm							
113	10	0.0371	5.6	5.4	8.5	8.35	Sample 113: 5.0 mm Hg of H ₂ O. Samples 114-128: H ₂ added to sample 113.
114	10	0.0371	8.1	7.0	9.3	8.97	
115	10	0.0371	11.8	7.9	10.6	10.1	
116	10	0.0371	20.5	9.6	13.4	12.53	
117	10	0.0371	32.6	11.4	16.2	15.3	
118	10	0.0371	49.8	13.7	19.6	18.0	
119	10	0.0371	68.1	17.6	26.2	23.8	
120	10	0.0371	182	22.2	34.2	31.1	
121		0.0371	298	26.2	41.3	35.0	
122		0.0371	5.6	6.3	8.3	8.23	
123		0.0371	49.4	13.9	19.5	17.9	
124	10	0.0371	414	27.9	43.4	37.6	
125	10	0.0371	735	32.3	51.0	45.0	
126		0.0371	1550	35.9	58.0	52.4	
127		0.0371	2300	37.9	59.5	54.8	
128	10	0.0371	3070	37.9	59.5	54.9	

Table 3. (Continued)

Sample No.	Fig. No.	ν (cm ⁻¹)	P_r (mm Hg)	$\int A(\nu) d\nu$ (cm ⁻¹)	$A(2240)$ %	$A(2213)$ %	Remarks
129	10	0.074	11.2	11.5	15.7	15.3	Sample 129:
130	10	0.074	21.2	14.5	20.0	18.3	10.0 mm Hg of
131	10	0.074	51.2	19.8	28.7	25.7	H ₂ O. Samples
132	10	0.074	101	26.0	39.0	34.2	130-135: H ₂
133	10	0.074	200	33.2	49.7	43.5	added to sam-
134	10	0.074	400	42.7	65.5	55.5	ple 129.
135	10	0.074	740	49.7	75.2	66.5	
136		0.074	11.2	11.7	15.9	15.5	Sample 136:
137		0.074	101	25.8	38.7	34.0	10.0 mm Hg of
138		0.074	741	48.8	74.5	65.7	H ₂ O. Samples
139		0.074	1485	54.0	83.8	76.0	137-141: H ₂
140		0.074	2295	55.5	86.0	80.5	added to sam-
141	10	0.074	3075	56.3	85.7	81.2	ple 136
142	10	0.148	22.4	22.4	29.6	28.1	Sample 142:
143	10	0.148	44.2	24.5	34.0	32.0	20.0 mm Hg of
144	10	0.148	52.1	28.8	39.7	37.2	H ₂ O. Samples
145	10	0.148	105	37.2	53.3	48.0	143-151: H ₂
146	10	0.148	199	45.5	65.9	59.3	added to sam-
147	10	0.148	395	56.2	79.1	72.0	ple 142.
148	10	0.148	718	62.0	90.1	83.0	
149		0.148	1655	68.5	96.1	92.5	
150		0.148	2315	70.5	95.5	94.0	
151	10	0.148	3120	71.0	96.5	95.0	
152	9	0.37	56	46.9	60.1	59.3	Sample 152: 50
153	9	0.37	122	57.6	74.7	72.2	mm Hg of H ₂ O.
154	9	0.37	225	67.2	85.1	82.7	Samples 153-
155	9	0.37	368	75.2	93.8	91.9	160: H ₂ added
156	9	0.37	559	78.1	97.2	96.7	to sample 152.
157	9	0.37	789	80.2	97.4	97.4	
158		0.37	1210	82.8	97.9	98.1	
159		0.37	1985	85.5	98.0	98.5	
160	9	0.37	2975	84.5	98.2	98.9	
161	9	0.74	112	70.4	86.3	85.0	Sample 161:
162	9	0.74	131	77.6	93.1	91.9	100 mm Hg of
163	9	0.74	200	85.7	96.6	96.5	H ₂ O. Samples
164		0.74	479	90.8	98.4	98.5	162-167: H ₂
165	9	0.74	767	90.0	99.0	99.4	added to sam-
166		0.74	1530	92.2	99.5	99.6	ple 161.
167	9	0.74	3060	93.5	99.3	99.8	

Table 3. (Continued)

Sample No.	Fig. No.	w (atmos cm)	P (mm Hg)	$\int A(v)dv$ (cm^{-1})	$A(2240)$ %	$A(2213)$ %	Remarks
168	9	1.1	227	91.4	98.7	99.1	Sample 168:
169		1.51	365	94.8	99.5	99.8	201 mm Hg of
170	9	1.51	769	97.8	99.9	99.9	N_2O . Samples
171		1.51	1545	98.8	100	100	169-173: N_2
172		1.51	2360	98.9	100	100	added to sam-
173		1.51	3105	100	100	100	ple 168
174	9	3.02	456	102.1	100	100	Sample 174:
175		3.02	611	103.3	100	100	403 mm Hg of
176		3.02	877	104.5	100	100	N_2O . Samples
177		3.02	1570	105.6	100	100	175-178: N_2
178	9	3.02	2365	105.9	100	100	added to sam-
							ple 174.
179	6	0.0074	1.1	2.0	2.5	2.6	Samples 179-
180	6	0.0111	1.1	2.5	2.8	3.0	186: N_2O alone.
181	6	0.0148	2.2	2.8	3.9	3.8	
182	6	0.0192	3.5	3.5	4.5	4.4	
183	6	0.0223	3.4	3.8	5.1	4.7	
184	6	0.0270	4.2	4.9	6.6	6.5	
185	6	0.0740	11.2	11.7	16.0	15.8	
186	6	0.113	17.0	17.5	22.6	22.1	
Path Length = 400 cm							
187	11	1.4	3.2	31.7	36.4	38.4	Sample 187: 2.9
188	11	1.4	6.2	38.7	45.2	46.8	mm Hg of N_2O .
189	11	1.4	10.8	46.4	54.9	56.0	Samples 188-
190	11	1.4	30.0	61.7	74.5	74.5	194: N_2 added
191	11	1.4	74.0	80.0	91.5	91.5	to sample 187.
192	11	1.4	232	92.8	98.4	98.6	
193	11	1.4	736	98.8	99.5	100	
194	11	1.4	3055	100.2	100	100	
195	11	2.8	6.5	32.4	60.4	62.2	Sample 195:
196	11	2.8	13.7	64.1	73.9	75.0	5.8 mm Hg of
197	11	2.8	29.2	78.2	81.9	81.1	N_2O . Samples
198	11	2.8	75.7	92.2	97.3	97.8	196-201: N_2
199	11	2.8	226	101.4	99.8	100	added to sam-
200	11	2.8	745	106.3	100	100	ple 195.
201		2.8	3050	108.2	100	100	

Table 3. (Continued)

Sample No.	Fig. No.	ν (atmos cm)	P_n (mm Hg)	$\int A(\nu) d\nu$ (cm ⁻¹)	A(2240) %	A(2213) %	Remarks
202	11	5.8	13.9	79.9	87	90.0	Sample 202:
203	11	5.8	26.7	92.6	96.1	97.0	12.4 mm Hg of
204	11	5.8	64.5	100.0	99.0	99.6	N ₂ O. Samples
205	11	5.8	197	103.5	99.6	100	203-206: N ₂
206	11	5.8	750	113.4	100	100	added to sam- ple 202.
207	11	11.6	28.0	102.0	99.0	99.5	Sample 207:
208	11	11.6	61	108.8	100	100	25 mm Hg of
209	11	11.6	203	115.7	100	100	N ₂ O. Samples 208-209: N ₂ added to sam- ple 207.
210	10	23.7	56	115.6	100	100	Sample 210:
211	10	23.7	103	120.1	100	100	50.3 mm Hg of
212	10	23.7	217	125.3	100	100	N ₂ O. Samples 211-212: N ₂ added to sam- ple 210.
213	10	1.39	3.4	32.7	37.7	40.0	Samples 213-
214	10	2.32	5.6	45.8	52.7	54.5	216: H ₂ O
215	10	3.70	9.0	62.5	72.2	73.4	alone.
216	10	5.56	13.4	78.3	85.4	86.4	
<u>Path Length = 800 cm</u>							
217		18.8	22.4	103.2	100	100	Sample 217:
218		18.8	42.4	108.7	100	100	20.0 mm Hg of
219		18.8	101	115.2	100	100	N ₂ O. Samples
220		18.8	542	120.2	100	100	218-221: N ₂
221		18.8	742	121.8	100	100	added to sam- ple 217.
<u>Path Length = 1600 cm</u>							
222		16.4	44.8	125	100	100	Sample 222:
223		16.4	168	129	100	100	40.0 mm Hg of
224		16.4	211	129	100	100	N ₂ O. Samples 223-224: N ₂ added to sam- ple 222.

Table 4. Data for the 2145 cm^{-1} CO Band

The Fig. No. corresponds to the figure in which the spectrum of each sample is shown. Absence of Fig. No. indicates spectrum is not shown. Uncertainties of values of $A(\nu)$ and $\int A(\nu)d\nu$ are discussed in the text.

Sample No.	Fig. No.	ν (atmos cm)	P_0 (mm Hg)	$\int A(\nu)d\nu$ (cm $^{-1}$)	$A(2168)$ %	$A(2116)$ %	Remarks
Path Length = 1.55 cm							
1	23	0.00096	5.4	0.14	0.18	0.20	Sample 1: 5.4
2		0.00096	107	0.24	0.25	0.25	mm Hg of mix-
3		0.00096	670	0.26	0.30	0.30	ture of 1/10
4	23	0.00096	3020	0.27	0.32	0.32	CO and 9/10 N $_2$. Samples 2-4: N $_2$ added to sample 1.
5	23	0.00154	49.5	0.31	0.36	0.37	Samples 5-7:
6		0.00154	313	0.39	0.43	0.40	8.8 mm Hg of
7	23	0.00154	3040	0.39	0.43	0.40	mixture of 1/10 CO and 9/10 N $_2$ added.
8	23	0.00262	15	0.36	0.35	0.31	Sample 8: 15
9		0.00262	40.7	0.45	0.47	0.41	mm Hg of mix-
10	23	0.00262	106	0.56	0.65	0.56	ture of 1/10
11		0.00262	256	0.64	0.72	0.65	CO and 9/10 N $_2$.
12		0.00262	738	0.68	0.74	0.63	Samples 9-13:
13		0.00262	3020	0.69	0.76	0.70	N $_2$ added to sample 8.
14	23	0.00435	25	0.53	0.50	0.50	Sample 14: 25 mm
15		0.00435	68	0.68	0.70	0.68	Hg of mixture
16	23	0.00435	245	0.91	1.0	0.85	of 1/10 CO and
17		0.00435	619	0.99	1.1	0.95	9/10 N $_2$. Sam-
18		0.00435	1315	1.03	1.2	1.0	ples 15-19: N $_2$
19	23	0.00435	3020	1.09	1.3	1.1	added to sample 14.
20	23	0.00703	40	0.84	0.85	0.7	Sample 20: 40
21		0.00703	93	1.10	1.1	1.0	mm Hg of mix-
22	23	0.00703	220	1.40	1.5	1.2	ture of 1/10 CO
23		0.00703	410	1.60	1.7	1.4	and 9/10 N $_2$.
24		0.00703	1520	1.87	2.2	1.7	Samples 21-25:
25	23	0.00703	3020	1.91	2.2	1.7	N $_2$ added to sample 20.

Table 4. (Continued)

Sample No.	Fig. No.	ν (atmos cm)	T_e (mm Hg)	$\int A(\nu) d\nu$ (cm^{-1})	$A(2159)$ %	$A(2116)$ %	Remarks
26	23	0.0107	6.1	0.48	0.40	0.38	Sample 26: 6.0
27	23	0.0107	25.0	0.84	0.85	0.70	mm Hg of CO
28		0.0107	52.0	1.11	1.10	0.88	alone. Samples
29	23	0.0107	118	1.51	1.70	1.40	27-32: N_2 added
30	23	0.0107	314	2.14	2.45	1.90	to sample 26.
31	23	0.0107	720	2.50	2.95	2.35	
32	23	0.0107	3020	2.83	3.40	2.70	
33	23	0.0176	10.6	0.81	0.73	0.72	Sample 33: 10.0
34	23	0.0176	22.2	1.12	1.1	1.0	mm Hg of CO
35	23	0.0176	49.9	1.63	1.5	1.3	alone. Samples
36	23	0.0176	157	2.55	2.6	2.2	34-39: N_2 added
37	23	0.0176	412	3.48	3.7	3.2	to sample 33.
38	23	0.0176	1005	4.14	4.7	3.7	
39	23	0.0176	3020	4.67	5.6	4.3	
40	23	0.0362	20.9	1.57	1.4	1.2	Sample 40: 20.5
41	23	0.0362	45.6	2.32	2.2	1.9	mm Hg of CO
42	23	0.0362	131	3.79	3.5	3.1	alone. Samples
43	23	0.0362	254	5.10	4.9	4.2	41-46: N_2 added
44	23	0.0362	692	7.09	7.4	6.1	to sample 40.
45	23	0.0362	1520	8.43	9.3	7.4	
46	23	0.0362	3020	9.33	10.3	8.1	
47	23	0.0722	41.8	3.39	3.2	2.7	Sample 47: 41.0
48	23	0.0722	85	4.70	4.3	3.7	mm Hg of CO
49	23	0.0722	189	6.75	6.2	5.3	alone. Samples
50	23	0.0722	371	9.05	8.7	7.3	48-53: N_2 added
51	23	0.0722	788	11.97	11.9	9.9	to sample 47.
52	23	0.0722	1520	14.65	15.4	12.5	
53	23	0.0722	3020	16.76	18.4	14.6	
54	29	0.165	95.8	8.3	7.3	6.4	Samples 54-59:
55	29	0.349	203	17.6	15.2	13.8	CO alone.
56	29	0.709	412	34.4	29.3	26.1	
57	29	1.31	761	60.7	51.7	46.1	
58	29	2.67	1555	108	84.5	78.7	
59	29	5.52	3210	157	100	99.7	

Table 4. (Continued)

Sample No.	Fig. No.	P _e (atmos cm)	P _e (mm Hg)	$\int A(\nu) d\nu$ (cm ⁻¹)	A(2168) %	A(2116) %	Remarks
Path Length = 6.35 cm							
60	24	0.073	10.2	1.8	1.4	1.4	Sample 60: 10
61		0.073	16.0	2.3	1.8	1.7	mm Hg of CO
62	24	0.073	27.0	2.9	2.2	2.1	alone. Samples
63		0.073	45.0	3.7	3.1	2.7	61-70: N ₂ added
64	24	0.073	86.0	4.8	4.1	3.5	to sample 60.
65		0.073	170	6.2	5.7	4.8	
66	24	0.073	292	8.0	7.5	6.3	
67		0.073	492	10.0	9.5	8.1	
68	24	0.073	735	11.7	11.5	9.2	
69	24	0.073	1515	14.5	15.0	12.2	
70	24	0.073	2970	16.3	18.1	14.1	
71	24	0.145	20.4	3.8	3.1	2.8	Sample 71: 20
72		0.145	32.4	4.8	4.0	3.7	mm Hg of CO
73	24	0.145	49.8	5.6	4.7	4.2	alone. Samples
74	24	0.145	88.5	7.2	6.1	5.4	72-80: N ₂ added
75	24	0.145	152	9.1	8.0	6.7	to sample 71.
76		0.145	292	12.0	10.8	9.1	
77	24	0.145	545	15.9	14.6	12.3	
78		0.145	797	18.7	17.5	14.9	
79		0.145	1545	23.6	23.2	19.3	
80	25	0.145	3070	28.7	29.5	24.0	
81	24	0.298	42.0	7.6	6.3	5.8	Sample 81: 41
82	24	0.298	64.0	9.2	7.7	7.0	mm Hg of CO
83	24	0.298	95.0	11.0	9.4	8.3	alone. Samples
84	24	0.298	148	13.4	11.4	10.4	82-91: N ₂ added to
85	24	0.298	231	16.3	14.3	12.3	sample 81.
86	24	0.298	333	19.5	17.0	14.9	
87	24	0.298	450	22.2	19.8	17.1	
88	25	0.298	747	27.5	24.2	20.5	
89	25	0.298	1470	35.8	32.8	27.7	
90	25	0.298	2260	42.0	40.0	33.0	
91	25	0.298	2960	46.3	44.2	36.2	
92	24	0.440	59.0	10.9	8.6	8.2	Sample 92: 58
93	24	0.440	84.5	12.5	10.7	9.6	mm Hg of CO
94	24	0.440	153	16.5	14.0	12.7	alone. Samples
95	24	0.440	241	20.0	17.9	15.7	93-102: N ₂
96	26	0.440	341	24.5	20.8	18.3	added to sample
97	26	0.440	486	28.9	24.0	20.8	92.
98	26	0.440	727	34.0	29.0	24.7	
99		0.440	1240	42.4	37.4	31.7	
100	26	0.440	1660	48.7	42.8	36.2	
101		0.440	2160	52.9	47.6	40.3	
102	26	0.440	2955	58.8	53.3	45.3	

Table 4. (Continued)

Sample No.	Fig. No.	ν (atmos cm)	P_v (mm Hg)	$\int A(\nu) d\nu$ (cm^{-1})	A(2168) %	A(2116) %	Remarks
103	26	0.800	112	19.9	16.2	14.3	Sample 103: 110 mm Hg of CO alone. Samples 104-112: N_2 added to sample 103.
104	26	0.800	169	24.0	19.8	18.0	
105	26	0.800	247	27.9	23.2	20.9	
106	26	0.800	388	35.1	29.5	26.2	
107	26	0.800	513	39.5	33.0	29.3	
108	26	0.800	748	47.1	40.0	34.8	
109	26	0.800	1260	58.1	49.6	43.0	
110	26	0.800	1615	64.6	55.6	48.2	
111	26	0.800	2215	73.9	62.0	54.4	
112	26	0.800	2940	81.3	68.5	60.5	
113	26	1.48	207	37.5	30.0	27.5	Sample 113: 203 mm Hg of CO alone. Samples 114-120: N_2 added to sample 113.
114	26	1.48	304	45.2	36.0	32.2	
115	26	1.48	461	54.5	43.2	39.0	
116	26	1.48	752	66.5	52.8	47.2	
117	26	1.48	1240	81.3	64.0	57.0	
118	26	1.48	1960	95.0	74.3	66.2	
119	26	1.48	2310	100	78.5	70.5	
120	26	1.48	3060	110	82.0	76.8	
121	25	2.94	412	70.2	56.0	51.0	Sample 121: 404 mm Hg of CO alone. Samples 122-127: N_2 added to sample 121.
122	25	2.94	591	80.2	63.5	58.5	
123	25	2.94	853	93.1	76.0	66.0	
124	25	2.94	1275	106	80.8	74.5	
125	25	2.94	1770	119	81.8	81.5	
126	25	2.94	2295	127	82.8	88.8	
127	25	2.94	2940	135	86.8	91.2	
128	25	5.55	711	115	84.1	79.2	Sample 128: 762 mm Hg of CO alone. Samples 129-133: N_2 added to sample 128.
129	25	5.55	1180	129	92.8	89.2	
130	25	5.55	1465	138	96.0	91.5	
131	25	5.55	1815	145	95.2	95.0	
132	25	5.55	2295	152	98.8	97.0	
133	25	5.55	2975	158	99.2	98.4	
134	25	10.9	1330	163	99.7	98.8	Sample 134: 1500 mm Hg of CO alone. Samples 135-137: N_2 added to sample 134.
135	25	10.9	1840	169	100	99.3	
136	25	10.9	2295	172	99.7	99.5	
137	25	10.9	3085	178	100	99.5	

Table 4. (Continued)

Sample No.	Fig. No.	ν (atmos cm)	P_e (mm Hg)	$\int A(\nu) d\nu$ (cm^{-1})	$A(2168)$ %	$A(2116)$ %	Remarks
138	25	16.6	2325	182	99.6	99.6	Sample 138: 2280 mm Hg of CO alone. Sam- ple 139: H_2 added to sam- ple 138.
139	25	16.6	3140	187	99.7	99.7	
140	25	22.2	3115	194	99.6	99.6	Sample 140: 3050 mm Hg of CO alone.
Path Length = 400 cm							
141	27	1.32	3.0	6.0	4.4	4.3	Sample 141: 2.9 mm Hg of CO alone. Samples 142-149: H_2 added to sample 141.
142	27	1.32	5.5	6.9	5.2	4.9	
143	27	1.32	10.0	9.4	5.8	6.6	
144	27	1.32	26.2	14.2	10.9	10.0	
145	27	1.32	61.1	19.7	15.6	14.7	
146	27	1.32	170	33.6	26.1	24.2	
147	27	1.32	503	51.8	42.2	38.3	
148	27	1.32	1520	81.9	66.8	60.0	
149	27	1.32	2970	102.6	81.8	74.0	
150	28	2.62	5.8	10.0	6.8	6.6	Sample 150: 5.7 mm Hg of CO alone. Samples 151-157: H_2 added to sample 150.
151	28	2.62	10.4	13.6	9.0	8.3	
152	28	2.62	29.2	20.9	13.0	11.9	
153	28	2.62	59.1	29.0	21.1	19.4	
154	28	2.62	186	46.7	36.1	33.3	
155	28	2.62	503	73.2	56.7	52.2	
156	28	2.62	1520	109	82.0	75.6	
157	28	2.62	2970	131.5	95.0	90.0	
158	28	4.82	10.9	17.8	13.6	12.9	Sample 158: 10.7 mm Hg of CO alone. Samples 159-164: H_2 added to sample 158.
159	28	4.82	24.4	26.0	20.2	19.0	
160	28	4.82	65.5	38.6	30.8	28.6	
161	28	4.82	174	60.2	47.9	44.2	
162	28	4.82	510	83.6	71.7	66.8	
163	28	4.82	1520	131.5	94.3	88.0	
164	28	4.82	2970	151.0	95.8	91.3	

Table 4. (Continued)

Sample No.	Fig. No.	ν (atmos. cm)	P_r (mm Hg)	$\int A(\nu) d\nu$ (cm ⁻¹)	$A(2168)$ %	$A(2116)$ %	Remarks
165	26	14.4	32.6	50.7	39.4	36.4	Sample 165: 32
166	26	14.4	83.6	73.8	56.9	53.1	mm Hg of CO
167	26	14.4	237	110.0	81.9	75.7	alone. Samples
168	26	14.4	756	150.9	98.1	96.6	166-170: H ₂
169	26	14.4	1520	170.1	100	99.9	added to sam-
170	26	14.4	2970	183.4	100	100	ple 165.
171	26	45.6	101	123.3	89.0	82.3	Sample 171: 100
172	26	45.6	257	156.8	98.8	97.4	mm Hg of CO
173	26	45.6	771	184.6	100	100	alone. Samples
							172-173: H ₂
							added to sample
							171.
174	27	0.46	1.0	2.47	1.8	1.8	Samples 174-179:
175	27	0.91	2.0	4.35	3.1	2.9	CO alone:
176	27	1.37	3.1	5.76	4.8	4.7	
177	27	2.28	5.1	8.70	6.7	6.2	
178	27	9.10	20.4	31.90	25.6	23.3	
179	27	22.8	51.0	73.90	57.6	53.2	

Table 5. Data for the $^{12}\text{C}^{18}\text{O}$ Band

The Fig. No. corresponds to the figure in which the spectrum of each sample is shown. Absence of Fig. No. indicates spectrum is not shown. Uncertainties of the values of $\int A(\nu) d\nu$ are discussed in the text.

Sample No.	Fig. No.	ν (atmos. cm)	P_{CO} (mm Hg)	Path (cm)	$\int A(\nu) d\nu$ (cm ⁻¹)	Remarks
1	40	36.6	54	625	8.2	49.9 mm Hg of coin cell alone.
2	39	72.0	54	1232	10.3	
3	40	143	54	2445	15.5	
4	39	285	54	4875	22.1	
5	40	36.6	217	625	16.2	H ₂ added to above sample to total pressure of 213 mm Hg.
6	39	72.0	217	1232	22.2	
7	40	143	217	2445	30.1	
8	39	285	217	4875	43.0	
9	40	36.6	404	625	21.0	H ₂ added to above sample to total pressure of 400 mm Hg.
10	39	72.0	404	1232	28.2	
11	40	143	404	2445	35.7	
12	39	285	404	4875	56.7	
13	40	36.6	744	625	25.8	H ₂ added to above sample to total pressure of 740 mm Hg.
14	39	72.0	744	1232	38.0	
15	40	143	744	2445	52.6	
16	39	285	744	4875	72.2	
17		285	744	4875	71.0	Sam. 17 is rerun of sam. 16.
18		72.4	108	1232	16.0	100 mm Hg of CO in cell alone.
19		143	108	2445	29.9	
20		285	108	4875	30.6	
21	40	564	108	4875	42.9	
22		72.4	208	625	19.9	H ₂ added to above sample to total pressure of 200 mm Hg.
23		143	208	1232	29.5	
24		285	208	2445	40.8	
25	40	564	208	4875	56.6	
26		72.4	408	625	28.0	H ₂ added to above sample to total pressure of 400 mm Hg.
27		143	408	1232	40.4	
28		285	408	2445	54.1	
29	40	564	408	4875	77.0	
30		72.4	748	625	36.9	H ₂ added to above sample to total pressure of 740 mm Hg.
31		143	748	1232	51.5	
32		285	748	2445	70.1	
33	40	564	748	4875	94.0	

Table 5. (Continued)

Sample No.	Fig. No.	ν (atmos. cm)	P_0 (mm Hg)	Path (cm)	$\int A(\nu)d\nu$ (cm ⁻¹)	Remarks
34	39	146	216	625	30.3	200 mm Hg of CO in cell alone.
35		288	216	1232	43.4	
36		572	216	2445	58.5	
37		1140	216	4875	81.0	
38	39	146	420	625	41.7	N ₂ added to above sample to total pressure of 404 mm Hg.
39		288	420	1232	58.0	
40		572	420	2445	77.8	
41		1140	420	4875	105	
42	39	146	756	625	53.5	N ₂ added to above sample to total pressure of 740 mm Hg.
43		288	756	1232	70.6	
44		572	756	2445	94.6	
45		1140	756	4875	125	

Table 6. Data for the OH₂ Bands

The Fig. No. corresponds to the figure in which the spectrum of each sample is shown. Absence of Fig. No. indicates spectrum is not shown. Uncertainties of the values of $\int A(\nu) d\nu$ are discussed in the text. Absence of a calculated value of $\int A(\nu) d\nu$ for the 1550 cm⁻¹ band indicates it was too weak to measure.

Sample No.	ν (cm ⁻¹)	1550 cm ⁻¹ band		1500 cm ⁻¹ band		$\int A(\nu) d\nu$ (cm ⁻¹)	Remarks
		ν (cm ⁻¹)	Fig. No.	ν (cm ⁻¹)	Fig. No.		
Path length = 6.35 cm							
1	1.15	2.6	4	1.65	2.8	4.7	Sam. 1, 2.0 mm H ₂ O, alone; sam. 2-6, H ₂ added to Sam. 1.
2	0.15	5.2		3.05	5.8		
3	0.15	10.7		2.10	10.8	1.22	
4	0.15	20.6		2.15	30.2	1.16	
5	0.15	57.6	43	2.60	93.8	2.30	
6	0.15	101		3.20	281	2.20	
7	0.15	1055		3.70	1055	2.50	
8	0.15	3465	43	4.10	3465	2.78	
9	0.026	4.6	43	2.95	4.8	1.70	Sam. 9, 3.5 mm H ₂ O, alone;
10	0.026	8.1		3.00	8.3	1.80	Sam. 10-17, H ₂ added to Sam. 9.
11	0.026	12.4		3.25	18.6	2.00	
12	0.026	25.7	43	3.75	25.9	2.45	
13	0.026	56.0		4.40	56.3	3.00	
14	0.026	137		5.1	137	3.6	
15	0.026	106		6.1	406	4.2	

Table 6. (Continued)

Sample No.	ν (cm ⁻¹)	ν (cm ⁻¹)	ν (cm ⁻¹)	ν (cm ⁻¹)	ν (cm ⁻¹)	ν (cm ⁻¹)	ν (cm ⁻¹)	ν (cm ⁻¹)	Remarks
16	0.026	1005	6.9	1005	4.6				
17	0.026	5075	7.1	5075	4.8				
18	0.052	9.1	4.7	9.7	47	2.7			Sam. 18, 7.0 mm Hg CH ₄ alone;
19	0.052	13.4	4.9	14.0		2.9			
20	0.052	20.7	5.5	25.5	47	3.8			Sam. 19-26, H ₂ added to Sam. 18.
21	0.052	51.0	6.8	50.0		4.8			
22	0.052	129	7.8	130		5.9			
23	0.052	292	9.6	293		7.0			
24	0.052	699	11.0	700	47	7.9			
25	0.052	1515	11.6	1520		7.8			
26	0.052	5075	12.4	5080		7.8			
27	0.073	12.7	5.9	13.5	47	3.8			Sam. 27, 9.8 mm Hg CH ₄ alone;
28	0.073	23.2	6.8	24.0		4.6			
29	0.073	42.7	7.8	41.5	47	5.9			Sam. 28-35, H ₂ added to Sam. 27.
30	0.073	85	9.5	85.7		7.1			
31	0.073	160	11.1	161	47	8.6			
32	0.073	362	13.0	363		9.6			
33	0.073	726	13.8	727	47	10.5			

Table 6. (Continued)

Sample No.	ν (cm ⁻¹)	1500 cm ⁻¹ band		1550 & 1306 cm ⁻¹ band		$\int A(\nu) d\nu$ (cm ⁻¹)		Remarks
		P_0 (mm Hg)	Fig. No.	P_0 (mm Hg)	Fig. No.	1306 cm ⁻¹ band	$\int A(\nu) d\nu$ (cm ⁻¹)	
34	0.075	1530	43	1530	47		11.5	
35	0.075	5075		5075			11.8	
36	0.134	35.4	44	9.3	47	24.8	6.8	Sam. 36, 18 mm Hg CH ₄ alone;
37	0.134	57.8						
38	0.134	56.0	44	10.5	47	39.2	7.9	Sam. 37-43, N ₂ added to Sam. 36.
39	0.134	115	44	13.6	47	117	10.5	
40	0.134	239		15.5		211	13.2	
41	0.134	325	44	19.1	47	400	15.6	
42	0.134	736		22.9		798	16.6	
43	0.134	1525	44	24.8		1530	18.0	
44	0.223	99	44	14.6		41.4	10.4	Sam. 44, 30 mm Hg CH ₄ alone;
45	0.223	60		16.0	47	52.4	11.6	Sam. 45-51, N ₂ added to Sam. 44.
46	0.223	138	44	18.5		110	14.0	
47	0.223	225	44	22.1	47	225	18.4	
48	0.223	438	44	25.0		408	20.4	
49	0.223	746		26.5	47	748	23.1	
50	0.223	1530		32.3		1530	26.0	
51	0.223	3650		36.0	47	3090	27.7	

Table 6. (Continued)

Sample No.	ν (cm ⁻¹)	3420 cm ⁻¹ band		1550 & 1506 cm ⁻¹ band		1306 cm ⁻¹ band		Remarks
		ν (cm ⁻¹)	Fig. No.	ν (cm ⁻¹)	Fig. No.	ν (cm ⁻¹)	Fig. No.	
52	0.431	75.5		22.9		80	47	Sam. 52, 58 mm Hg CH ₄ alone;
53	0.431	121	44	25.5		126		Sam. 53-58, H ₂ added to Sam. 52.
54	0.431	258	44	70.0		243		
55	0.431	419	44	33.4		424	47	28.0 32.8
56	0.431	765	44	59.0		775		
57	0.431	535	44	46.0		1540		36.5 40.6
58	0.431	1085	44	54.2		3090	47	
59	0.728	127	44	34.3				Sam. 59, 98 mm Hg CH ₄ alone;
60	0.728	602	44	49.5				Sam. 60-62, H ₂ added to Sam. 59.
61	0.728	355	44	59.3				
62	0.728	3390	44	73.0				
$\text{Path Length} = 400 \text{ cm}$								
63	0.77	2.0	44	18.9		2.1		Sam. 63, 1.52 mm Hg CH ₄ alone;
64	0.77	3.5	44	19.8		3.4		Sam. 64-73, H ₂ added to Sam. 63.
65	0.77	5.7	44	21.5		5.8	48	
66	0.77	11.2	44	23.2		11.3	48	9.0 11.5

Table 6. (Continued)

Sample No.	ν (cm ⁻¹)	1200 cm ⁻¹ band		1550 & 1506 cm ⁻¹ band		λ (v) μ (cm ⁻¹)		Remarks
		ν (cm ⁻¹)	Fig. No.	ν (cm ⁻¹)	Fig. No.	ν (cm ⁻¹)	Fig. No.	
67	C.F.	21.7	44	25.9		21.5	48	14.4
68	C.F.	51.6		50.5		51.2	48	20.9
69	C.F.	121		36.5		122	48	25.8
70	C.F.					135	48	34.6
71	C.F.	744		54.5		745	48	42.3
72	C.F.	1520		64.5		1520	48	49.4
73	C.F.	3020		76.0		3020	48	57.4
74	1.55	3.7	41	28.4		3.8	46	10.9
75	1.55	5.8	44	50.0		6.1	48	12.8
76	1.55	10.1	45	32.5		10.4	48	14.5
77	1.55	23.5		50.0		23.8	48	20.2
78	1.55	53.5	45	44.0		53.6	48	26.4
79	1.55	130		51.5		130	48	34.5
80	1.55	301	45	64.0		302	48	45.5
81	1.55	761	45	79.0		761	48	58.2
82	1.55	1520	45	92.9		1520	48	68.4
83	1.55	3040	45	109		3040	48	77.5

Soln. 74, 2.75 mm Hg
 CH₄ 21/1000;
 Soln. 75-83, H₂ added
 Soln. 74.

Table 6. (Continued)

Sample No.	ν (cm ⁻¹)	2120 cm ⁻¹ band		1506 cm ⁻¹ band		1306 cm ⁻¹ band		Remarks
		ν (cm ⁻¹)	Fig. No.	ν (cm ⁻¹)	Fig. No.	ν (cm ⁻¹)	Fig. No.	
84	2152	6.9	45	42.4	7.3	48	17.6	Sam. 84, 5.3 mm Hg CH ₄ alone; Sam. 85-94, N ₂ added to Sam. 84.
85	2152	10.4	45	45.2	11.2	48	21.5	
86	2152	16.5	45	47.6	16.9	48	25.5	
87	2152	27.5	45	52.2	27.2	48	28.5	
88	2152	55.0	45	67.5	55.5	48	35.0	
89	2152	59	45	73.2	59	48	47.9	
90	2152	300	45	90.0	301	48	59.9	
91	2152				301	48	61.7	
92	2152	768	45	109	769	48	78.0	
93	2152	1520	45	126	1520	48	90.0	
94	2152	3050	45	155	3050	48	108.0	
Path Length = 1600 cm								
95	5.5	9.9	45	59.0	4.1	49	22.0	Sam. 95, 3 mm Hg CH ₄ alone;
96	5.5	8.6	45	65.5	8.8	49	29.0	Sam. 96-134, N ₂ added to Sam. 95.
97	5.5	14.9	45	71.0	15.1	49	35.0	
98	5.5	26.5	45	77.0	26.7	49	42.5	
99	5.5	51.5	45	87.8	51.6	49	51.7	
100	5.5	126	45	108	126	49	67.3	

Table 6. (Continued)

Sample No.	ν (atmos. cm)	1020 cm^{-1} band		1550 cm^{-1} band		1306 cm^{-1} band		$\int A(\nu) d\nu$ (cm $^{-1}$)		$\int A(\nu) d\nu$ (cm $^{-1}$)		Remarks
		ν_p (mm Hg)	Fig. No.	ν_p (mm Hg)	Fig. No.	ν_p (mm Hg)	Fig. No.	1020 cm^{-1} band	1306 cm^{-1} band	1550 cm^{-1} band	1306 cm^{-1} band	
101	5.5	301	132	132	49	301	49	85.9				
102	5.5	741	164	164	49	741	49	107				
103	5.5	1520	193	193	49	1520	49	126				
104	5.5	2965	220	220	49	2965	49	141				
105	11.4	7.8	45	95	49	8.3	49	38.4				Sam. 105, 6mm Hg CH ₄ alone;
106	11.4	12.1	45	103	49	11.6	49	45.0				Sam. 106-113, H ₂ added to Sam. 105.
107	11.4	26.2	45	117	49	26.7	49	55.9				
108	11.4	51.8	45	136	49	52.3	49	69.4				
109	11.4	121	45	161	49	121	49	90.2				
110	11.4	302	45	197	49	302	49	115				
111	11.4	742	45	250	45	742	45	141				
112	11.4	1525	45	269	49	1575	49	160				
113	11.4	2965	45	307	49	2965	49	176				
114	23.8	16.3	46	155	50	17.3	50	73				Sam. 111, 12.5 mm Hg CH ₄ alone;
115	23.8	25.9		167		26.9		83				Sam. 115-121, H ₂ added to Sam. 114.
116	23.8	53.8	46	196		55.0	50	104				

Table 6. (Continued)

Sample No.	ν (a-zos. cm)	3020 cm^{-1} band		1550 cm^{-1} band		1306 cm^{-1} band		$\int A(\nu) d\nu$ (cm $^{-1}$) 1306 cm^{-1} band	$\int A(\nu) d\nu$ (cm $^{-1}$) 1550 cm^{-1} band	Remarks
		P_e (mm Hg)	Fig. No.	P_e (mm Hg)	Fig. No.	P_e (mm Hg)	Fig. No.			
117	23.8	130	46	213	131		130		9.0	
118	23.8	304	46	263	309	50	154			
119	23.8	747	46	310	748	50	180		14.7	
120	23.8	1525	46	374	1525		195		17.0	
121	23.8	3040	46	114	3040	50	208		21.0	
122	47.3	32.5	45	237	34.5	50	115		12.0	Sam. 122, 25 mm Hg CH_4 alone;
123	47.3	57.5	45	263	59.5		135		14.4	Sam. 123-125, Y_2 added to Sam. 122.
124	47.3	108	46	257	110	50	154		16.7	
125	47.3	240	46	317	242	50	179		19.4	
126	47.3	409	46	381	410	50	193		21.3	
127	47.3	748	46	413	750		209		25.6	
128	47.3	1530	46	450	1530	50	222		30.2	
129	47.3	3030	46	479	3025	50	234		34.9	
130	95.0	65	46	360	69	51	175		19.5	Sam. 130, 50 mm Hg CH_4 alone;
131	95.0	129	46	401	133		199		24.7	Sam. 131-136, Y_2 added to Sam. 130.
132	95.0	219	46	440	223	51	214		25.3	

Table 1. (Continued)

Sample No.	ν (cm ⁻¹)	3000 cm ⁻¹ band		1550 & 1306 cm ⁻¹ band		1305 cm ⁻¹ band		1550 cm ⁻¹ band		Remarks
		P_e (mm Hg)	Fig. No.	$\int A(\nu) d\nu$ (cm ⁻¹)	P_e (mm Hg)	Fig. No.	$\int A(\nu) d\nu$ (cm ⁻¹)	$\int A(\nu) d\nu$ (cm ⁻¹)	$\int A(\nu) d\nu$ (cm ⁻¹)	
133	95.0	413	46	480	417	51	227	31.4		
134	95.0	755	46	516	759	51	242	35.7		
135	95.0	1540	46	560	1545	51	257	41.0		
136	95.0	2830	46	583	2835	51	267	48.0		
137	184	130	46	442	138	51	220	32.8		Sam. 137, 100 mm Hg CH ₄ alone;
138	188	235	46	485	243	51	238	39.0		Sam. 138-142
139	188	432	46	522	440	51	253	44.2		N ₂ added to Sam. 137.
140	188	776	46	550	784		265	48.0		
141	188	1540	46	597	1550		280	60.0		
142	188	2950	46	628	2950	51	290	67.5		

Table 1. Summary of Empirical Constants

I. $\int A(\nu) d\nu = c \left[\nu P_e^a \right]^b$

II. $\int A(\nu) d\nu = C + D \log_{10} \left[\nu P_e^a \right]$

$\int A(\nu) d\nu$ can be calculated by use of tabulated empirical constants in I and II above for values of P_e and $\int A(\nu) d\nu$ within specified limits

Band (cm^{-1})	Band limits (cm^{-1})	c	b	a	C	D	P_e limits (mm Hg)	$\int A(\nu) d\nu$ limits (cm^{-1})
2224 N ₂ O	2100 - 2300	18.0	0.53	0.7			10 - 25	10 - 45
				0.7	15	40	10 - 760	45 - 120
2143	1975 - 2275	2.75	0.55	0.8			20 - 250	4 - 40
		2.75	0.55	0.8			20 - 760	10 - 40
		3.20	0.43	1			20 - 760	40 - 120
3020 CH ₄	2400 - 3400	15.5	0.55	0.4	-106	61	20 - 3000	120 - 200
				0.4	-375	272	10 - 3000	250 - 500
1306 CH ₄		7.3	0.45	0.6			10 - 760	20 - 130
	1050 - 1355*			0.6	-190	115	10 - 760	130 - 500
1550 cm^{-1} CH ₄	1535 - 1600	No empirical equations derived.						

*1535 cm^{-1} is boundary between 1306 cm^{-1} and 1550 cm^{-1} CH₄ bands; other band limits represent frequencies beyond which there is negligible absorption for samples used in the present study.

Table 5. Summary of Band Intensities

Band	Band Assignment	$\int \kappa(\nu) d\nu$ atmos ⁻¹ cm ⁻²
2224 cm ⁻¹ H ₂ O	ν_3	1450 ± 105
2145 cm ⁻¹ CO	ν_1	260 ± 26
4260 cm ⁻¹ CO	$2\nu_1$	Not measured
3020 cm ⁻¹ CH ₄	ν_3	320 ± 48
1306 cm ⁻¹ CH ₄	ν_4	185 ± 28
1550 cm ⁻¹ CH ₄	ν_2	2.5 ± 0.5

BIBLIOGRAPHY

1. R. M. Chapman and J. N. Howard, Contract W44-099-eng-400 Ohio State Univ. Res. Rpt. Reports 18, 20, 21 (1949); Also Contract DA-44-099-eng-12, Report 1 (1950), and J. Opt. Soc. Am. 42, 423, 856 (1952).
2. J. N. Howard, D. E. Burch, and D. Williams, Geophysical Research Paper No. 40, GRD, Air Force Cambridge Research Center (1955). See also J. Opt. Soc. Am., 46, 186, 237, 242, 334, 452 (1956).
3. "Infrared Absorption Laws for Some Minor Atmospheric Constituents", D. E. Burch, Ph.D. dissertation, Ohio State University (1959).
4. R. Ladenberg and F. Peiche, Ann. Physik 42, 181 (1913).
5. W. M. Elsasser, "Harvard Meteorological Studies No. 6", Harvard University, 1942.
6. R. M. Goody, Quart. J. Roy. Met. Soc., 18, 105 (1952).
7. H. Mayer, Methods of Opacity Calculations, Los Alamos. LA-647, Oct. 1947.
8. G. H. Plass, J. Opt. Soc. Am. 45, 690 (1958).
9. G. H. Plass, J. Opt. Soc. Am. 50, 868 (1960).
10. J. U. Valte, J. Opt. Soc. Am., 32, 205 (1942).
11. "Effects of Foreign Gases on the Total Absorption of Entire Bands in the Infrared," E. B. Singleton, Ph.D. dissertation, Ohio State University, (1944).
12. H. W. Thompson and R. L. Williams, Proc. Roy. Soc. A. 208, 376 (1951).
13. J. W. Birksland and J. N. Shaw, J. Opt. Soc. Am. 49, 637 (1959).
14. D. M. Macleod and T. W. Morrell, Proc. Roy. Soc. A. 202, 174 (1951).
15. W. Benedict, R. Berman, G. Moore, and J. P. Foltz, Canad. J. Phys., 31, 630, 639 (1953).
16. J. M. Thornton, A. J. Miller, and A. E. Wilton, J. Res. Phys., 18, 101 (1947).
17. H. J. Oelchans, D. C. McKeen, and H. W. Thompson, Proc. Roy. Soc. A. 208, 382 (1951).
18. D. F. Eggers and P. J. Crawford, J. Res. Phys., 18, 154 (1947).

19. M. V. Migeotte, Phys. Rev., 75 1108 (1949).
20. J. E. Shav, Sci., Report 6, Contract AF 19(604)-1003, The Ohio State Univ. Res. Pn. (1957).
21. S. S. Penner and D. Weber, J. Chem. Phys. 19, 807 (1951).
22. M. V. Migeotte, Phys. Rev. 72, 519 (1948).
23. E. L. Welsh, P. Z. Pashler, and A. F. Lusa, J. Chem. Phys. 19, 340 (1951).
24. E. L. Welsh and P. J. Sandiford, J. Chem. Phys. 20, 1646 (1952).

APPENDIX I

ADSORPTION EFFECTS

It is a well-known phenomenon that gases are adsorbed on the surfaces of containers. Because of the sampling procedure used in the present study it was necessary to investigate the possibility of sampling errors which might arise as a result of such adsorption.

The absorber concentration v for a given sample was determined by measuring the partial pressure of the absorbing gas. If one could assume that a negligible amount of gas was adsorbed by the cell windows, the amount of absorbing gas traversed by infrared radiation would be given by the product of the cell length and the partial pressure of the gas, regardless of any adsorption on the cell walls. However, when nitrogen is added to a sample of absorbing gas as was done in the present investigation, the question arises as to how much absorbing gas remains in the optical path. It seems possible that the nitrogen might displace some of the absorbing gas from the cell walls; this effect would result in a greater amount of absorbing gas in the optical path.

Penner and Weber²¹, in a study of infrared absorption by CO at high pressures, found that the CO concentration did increase as nitrogen was added to produce high total pressures. They attributed the increase to an "adsorption-desorption" process in which CO was adsorbed on the cell walls and then was displaced by N_2 which was added later. The CO concentration in portions of the sample taken from the cell was determined by Penner and Weber with a mass spectrometer.

In the present study no mass spectrometer was available to use to monitor the absorber concentration. However, several experiments, which involved the three gases CO, H_2O , and CH_4 in the three different absorption cells, were performed in order to gain a better understanding of such an adsorption-desorption process and to determine which sampling procedures could be expected to yield minimum sampling error. As a result of these experiments, along with what is generally known about adsorption, the following conclusions were made and the corresponding sampling procedures were decided upon:

- (1) It was found that the adsorption was essentially complete within a period of a few seconds after the absorbing gas had been added to an evacuated cell. This phenomenon was checked by adding a sample of absorbing gas (H_2O , CO and CH_4) to a cell while monitoring the infrared absorption by the sample. The infrared absorption was never found to decrease significantly after the sample had been added, thus indicating that no absorber was disappearing from the optical path as a result of slow adsorption by the cell walls. This experiment, of course, did not prove that there had been any adsorption at all; but initial adsorption was confirmed by the next experiment.

(ii) In the second experiment, some absorbing gas was added to an initially evacuated cell; H_2 was then added and an absorption spectrum was obtained immediately. The sample was allowed to remain in the cell and spectra were recorded periodically for several hours or even days. In most cases the infrared absorption was found to increase, indicating that the amount of absorber in the optical path was increasing. This increase was found to take place rather slowly; within a few minutes only a slight increase in absorption was observed, but after a few hours the increase in absorption might correspond to as much as a 10 to 20% increase in absorber concentration in extreme cases. Because of the slowness with which the "desorption" took place, the sampling error was minimized by making a set of runs within as short a time interval as was practical. In no case were data used which were obtained from samples left in the absorption cell over night. In most cases samples were not in the absorption cell more than two - three hours.

(iii) It is to be expected that the relative amount of gas adsorbed and displaced by H_2 decreases with increasing partial pressure of the absorbing gas. It is known that the amount of gas adsorbed is approximately proportional to p^a , where p is the pressure of the gas and a has a value that may not be constant but is always less than unity; thus, it is to be expected that the fraction of the gas that is adsorbed decreases with increasing pressure. This result was also confirmed experimentally in the present study: a negligible increase in infrared absorption, if any at all, was observed after adding H_2 to samples having partial pressures of the absorbing gas in excess of 200-300 mm Hg. The greatest relative increase was observed in the case of samples in which the partial pressure of the absorber was between 1 and 10 mm Hg. For this reason very few results are included which involve samples formed by adding H_2 to samples of absorbing gas having a partial pressure less than 1 or 5 mm Hg. Short absorption cells (1.55 cm and 6.55 cm) were used in order to obtain samples of low absorber concentration without using excessively low partial pressures of the absorbing gas.

(iv) Considerable time is required to remove the adsorbed gas from the cell walls by pumping, a phenomenon well-known by anyone who has dealt with high-vacuum systems. However, some of the results of the experimental checks of this phenomenon seem worthy of discussion. A typical experiment might go as follows: A sample with a pressure of approximately 100 mm Hg of H_2O was put in the cell and allowed to remain for a few minutes. The cell was then opened to the vacuum pump and pumped for approximately one minute after the pressure had been reduced to 0.1 mm Hg. The valve to the cell was then closed and a spectrum of the 2200 cm^{-1} region was immediately scanned with the cell in the optical path. No absorption of

the infrared radiation could be detected; but if the cell were allowed to remain for several minutes, or even hours, it would be found that some radiation was being absorbed, and the amount of absorption increased with time. This result indicates that some of the absorbed H_2 was leaving the walls of the cell and entering the optical path.

A second, but similar experiment, might typically go as follows: The cell was filled with H_2 and pumped as before, but instead of allowing the cell to remain evacuated, H_2 was added to a pressure of 100 mm Hg and a spectrum was recorded immediately. The first spectrum could show very little, if any, absorption of the infrared radiation, indicating that H_2 was in the optical path. However, spectra obtained periodically afterward would show increasing absorption as in the previous experiment. In the latter case the increase in absorption was much more rapid, indicating that the H_2 was being removed more rapidly by being displaced by H_2 .

One might expect that adding H_2 to the cell in the manner described above would cause increased absorption by the different processes. The first aspect of the fact that a very small H_2 molecule from the walls of the cell. The second aspect of the fact that absorption by any gas is increased by increasing the pressure because of pressure broadening. It is apparent that the increase in absorption associated with adding H_2 in the experiment described above was not a result of pressure broadening alone since the absorption was still negligible immediately after the H_2 was added.

One could expect that any H_2 which might be adsorbed on the surfaces of the cell windows would absorb part of the radiation, especially when the pressure was increased by adding H_2 . However, since no absorption was observed immediately after the H_2 was added, it seems reasonable to conclude that very little H_2 was adsorbed on the windows.

As the amount of gas introduced into the cell varies, the displacement by H_2 depends on the "size" of the cell and the order in which the different gases are introduced. It was shown in the experiments described above that the amount of gas introduced into the cell was controlled by pumping. Therefore, care was taken to insure that the cell was flushed with H_2 and pumped repeatedly after samples which were of large amounts of reacting gas had been studied.

It was found that the amount of absorption as well as the displacement by H_2 was small and varied with the samples.

which were formed by first introducing some N_2 (say 20-30 mm Hg), then adding the absorbing gas, and finally more N_2 to the desired pressure. It is presumed that the first N_2 introduced was sufficient to form a layer of N_2 on the cell walls before the absorbing gas was introduced. The amount of absorbing gas which was adsorbed on the walls was apparently reduced because of the presence of the N_2 layer on the cell walls.

This result suggests that the samples should be formed by adding N_2 before the absorbing gas, then by adding more N_2 to the desired pressure. Although it would still be difficult to be sure, one might expect that some absorbing gas would displace some N_2 from the walls, and the amount of absorbing gas in the optical path would decrease. This method of forming the samples has the disadvantage that the partial pressure of the absorbing gas cannot be measured as accurately when it is being added to N_2 as when the cell is evacuated. For example, if N_2 were added to a cell to a pressure of 100 mm Hg and H_2O added to this until the pressure was 105 mm Hg, the partial pressure of H_2O (5 mm Hg) could not be determined as accurately as if the H_2O were added to a evacuated cell and the pressure measured with the absolute pressure gauge.

The method of adding N_2 , then the absorbing gas, and finally more N_2 , has the further disadvantage that no spectra of the sample can be obtained for values of pressure less than the pressure of the N_2 initially added plus the partial pressure of the absorbing gas. The total absorptions of several samples formed by this method were compared with those of samples believed to have the same values of absorber concentration and pressure but which were formed by introducing the absorbing gas in the cell before the N_2 was added. If the latter sample was formed by adding an absorbing gas to the cell after it had been flushed with N_2 and pumped only sufficiently long to reduce the pressure to approximately 0.02-0.1 mm Hg, it was found that the agreement was good. This result suggests that a layer of N_2 still remained on the cell walls after the short pumping period and served to reduce the adsorption of the absorbing gas.

Another method used to estimate the amount of sampling error arising from adsorption-desorption effects was to compare spectra of samples in two different cells but with values of absorber concentration and equivalent pressure believed to be equal. (Equivalent pressure is defined above in the section on self-broadening.) For example, H_2O might be added to the 1.55-cm cell to a pressure of 10 mm Hg; H_2O was then added to the 6.55-cm cell to a pressure of $20 \times 1.55/6.55 = 4.0$ mm Hg. N_2 was then added to the 6.55-cm cell until the equivalent pressure was the same in both cells. Both cells then had the same absorber concentration except for changes in the 6.55-cm cell due to adsorption or desorption. Since the shorter cell contained only H_2O , no error in the determination of its absorber concentration should arise from adsorption or desorption. Comparison of the absorption spectra of the two samples served to give an indication of the amount of adsorption-desorption which took place in the cell containing both H_2O and N_2 .

Samples of very small absorber concentration for CO and N₂O were formed by adding to the cell mixtures containing a known fraction of absorbing gas (1/10 or 1/50) in N₂. The mixtures were made in a separate tank by adding N₂ first, and then the proper amount of absorber (CO or N₂O) in order to reduce the adsorption of the absorber on the walls of the tank. The mixture was formed at pressures sufficiently high so that the relative error in measuring the partial pressure of the absorbing gas was small. An electrically driven fan in the tank was used to insure uniform mixing.

A portion of the mixture was then admitted to the absorption cell after it had been flushed with N₂ and evacuated. By this method it was possible to use samples having a partial pressure of the absorbing gas equal to a fraction of a mm of Hg, without having to measure pressures less than 5-10 mm Hg. This procedure should increase the accuracy of sampling. Higher pressures were then obtained by adding more N₂ to the mixture.

Since the N₂ was added to the mixing tank first, and the cell was flushed with N₂ before being evacuated, one would expect on the basis of the previous discussion that these containers would have a layer of N₂ on the walls which would tend to reduce the adsorption of the absorbing gas. One would further expect that what adsorption did take place would occur slowly after the sample was admitted to the cell, and that any change in the absorber concentration would be a decrease. This is in contrast to the expected increase in absorber concentration caused by the displacement of the absorbing gas by N₂ when the absorbing gas was admitted first in the usual way. Several samples formed by mixtures were compared with samples which were believed to have the same values of absorber concentration and pressure but were formed by adding N₂ to the cell after the absorbing gas was admitted. This comparison served as another indication of the amount of error caused by adsorption or desorption.

It should be noted that the experiments performed were insufficient to prove that the processes described above, such as the adsorption, the displacement of one gas on the cell walls by another, the forming of a layer of one gas, etc., actually occur in the manner suggested. It can only be said that these proposed processes seem reasonable in view of what is to be found in the literature concerning adsorption, and that they would account for the results of the many sampling experiments which were performed.

As a result of these experiments it can be concluded that, in studies such as the present one, care must be taken to prevent excessive sampling error from adsorption effects. It is believed that, by following the sampling procedures just described, errors in the determination of total absorptions arising from adsorption effects were held to less than two or three percent for samples having the partial pressure of the absorbing gas greater than 50 mm Hg, and to less than five percent for even the smallest samples used.

PART B

ABSORPTION BY CARBON DIOXIDE

by

Darrell F. Burch, David Gryvnak
and Dudley Williams

CONTENTS-PART B

	<u>Page</u>
List of Figures	iii
I. INTRODUCTION	1
A. Units, Symbols, and Definition of Quantities	2
II. EXPERIMENTAL PROCEDURE AND ANALYSIS OF DATA	2
A. Self-Broadening Coefficient and Equivalent Pressure	4
B. Deficiencies of Double-Beaming Techniques in the Study of Strong Atmospheric Bands	5
C. Errors and Accuracy	8
III. EXPERIMENTAL RESULTS FOR THE 3716 AND 3609 cm^{-1} CO_2 BANDS	10
IV. EXPERIMENTAL RESULTS FOR THE 2530 cm^{-1} CO BAND	22
V. EXPERIMENTAL RESULTS FOR THE 1064 AND 961 cm^{-1} BANDS	27
A. Effect of Temperature on Total Absorption	37
B. Comparison of Present Results with Those of Edwards	41
VI. EXPERIMENTAL RESULTS FOR THE 475-495 cm^{-1} SPECTRAL REGION	41
A. Effect of Temperature on Mean Fractional Absorption	63
B. Comparison of Results with Previous Work	65
VII. BAND INTENSITIES	68
VIII. SUMMARY	69
REFERENCES	84

LIST OF FIGURES-PART B

<u>Figure No.</u>		<u>Page</u>
1	Absorption curves for the 2350 cm^{-1} CO_2 band illustrating the error arising from air in the optical path of the spectrometer.	9
2	Absorption curves of the 3716 and 3609 cm^{-1} CO_2 bands.	11
3	Absorption curves of the 3716 and 3609 cm^{-1} CO_2 bands.	12
4	The total absorption of the 3716 cm^{-1} CO_2 band versus equivalent pressure.	13
5	The total absorption of the 3716 cm^{-1} CO_2 band versus absorber concentration.	14
6	The total absorption of the 3609 cm^{-1} CO_2 band versus equivalent pressure.	15
7	The total absorption of the 3609 cm^{-1} CO_2 band versus absorber concentration.	16
8	The total absorption of the 3716 and 3609 cm^{-1} CO_2 bands versus equivalent pressure.	17
9	The total absorption of the 3716 and 3609 cm^{-1} CO_2 bands versus absorber concentration.	19
10	The total absorption of the 3716 and 3609 cm^{-1} CO_2 bands versus w_0 .	20
11	Absorption curves of the 2350 cm^{-1} CO_2 band.	23
12	Absorption curves of the 2350 cm^{-1} CO_2 band.	24
13	The total absorption of the 2350 cm^{-1} CO_2 band versus equivalent pressure.	25
14	The total absorption of the 2350 cm^{-1} CO_2 band versus absorber concentration.	26
15	The total absorption of the 2350 cm^{-1} CO_2 band versus w_0 .	28
16	Absorption curves of the 1064 and 961 cm^{-1} CO_2 bands.	29

LIST OF FIGURES (CONT'D)-PART B

<u>Figure No.</u>		<u>Page</u>
17	Absorption curves of the 1064 and 961 cm^{-1} CO_2 bands and the 720-875 cm^{-1} sub-region.	30
18	Absorption curves of the 1064 and 961 cm^{-1} CO_2 bands for a given sample at various temperatures above ambient.	31
19	The total absorption of the 1064 cm^{-1} CO_2 band versus equivalent pressure.	33
20	The total absorption of the 1064 cm^{-1} CO_2 band versus \underline{v} in part A; and versus $\text{wP}_e^{0.30}$ in part B.	34
21	The total absorption of the 961 cm^{-1} CO_2 band versus equivalent pressure.	35
22	The total absorption of the 961 cm^{-1} CO_2 band versus \underline{v} in part A; and versus $\text{wP}_e^{0.25}$ in part B.	36
23	Temperature dependence of the total absorption of the 1064 and 961 cm^{-1} CO_2 bands.	38
24	Absorption curves of the 875-495 cm^{-1} CO_2 region.	42
25	Absorption curves of the 875-495 cm^{-1} CO_2 region.	43
26	Absorption curves of the 875-495 cm^{-1} CO_2 region.	44
27	Absorption curves of the 875-495 cm^{-1} CO_2 region.	45
28	Absorption curves of the 875-495 cm^{-1} CO_2 region.	46
29	Absorption curves of the 875-495 cm^{-1} CO_2 region.	47
30	Absorption curves of the 875-495 cm^{-1} CO_2 region.	48
31	Absorption curves of the 875-495 cm^{-1} CO_2 region.	49
32	Absorption curves of CO_2 samples at elevated temperatures in the 875-495 cm^{-1} region.	50
33	$\bar{A}(720-875 \text{ cm}^{-1})$ versus P_e for samples of CH_2 alone.	52
34	$\bar{A}(720-875 \text{ cm}^{-1})$ versus P_e for various values of \underline{v} .	53
35	$\bar{A}(720-875 \text{ cm}^{-1})$ versus \underline{v} for various values of P_e .	54

LIST OF FIGURES (CONT'D)-PART B

<u>Figure No.</u>		<u>Page</u>
36	$\bar{A}(667-720 \text{ cm}^{-1})$ versus P_0 for samples of CO_2 alone.	55
37	$\bar{A}(667-720 \text{ cm}^{-1})$ versus P_0 for various values of \underline{v} .	56
38	$\bar{A}(667-720 \text{ cm}^{-1})$ versus \underline{v} for various values of P_0 .	57
39	$\bar{A}(617-667 \text{ cm}^{-1})$ versus P_0 for samples of CO_2 alone.	58
40	$\bar{A}(616-667 \text{ cm}^{-1})$ versus P_0 for various values of \underline{v} .	59
41	$\bar{A}(617-667 \text{ cm}^{-1})$ versus \underline{v} for various values of P_0 .	60
42	$\bar{A}(545-617 \text{ cm}^{-1})$ versus P_0 for samples of CO_2 alone.	61
43	$\bar{A}(545-617 \text{ cm}^{-1})$ versus P_0 for various values of \underline{v} .	62
44	$\bar{A}(545-617 \text{ cm}^{-1})$ versus \underline{v} for various values of P_0 .	63
45	$\bar{A}(495-545 \text{ cm}^{-1})$ versus P_0 for various values of \underline{v} in the left-hand portion; $\bar{A}(495-545 \text{ cm}^{-1})$ versus \underline{v} for three values of P_0 in the right-hand portion.	64
46	$\bar{A}(667-720 \text{ cm}^{-1})$, $\bar{A}(617-667 \text{ cm}^{-1})$, $\bar{A}(720-875 \text{ cm}^{-1})$, and $\bar{A}(545-617 \text{ cm}^{-1})$ versus temperature for four different samples.	66

ABSORPTION BY CARBON DIOXIDE

I. INTRODUCTION

This report is the second of three to be published in the present research program, which involves the investigation of the infrared absorption by gases occurring in the atmosphere. Included in this report are the results of the investigation of the absorption by CO_2 bands at 3761 and 3609 cm^{-1} , at 2350 cm^{-1} , at 1064 and 961 cm^{-1} , and in the spectral range from 875 - 495 cm^{-1} . The first report¹ (hereafter referred to as Report 1) in the present program contains results of absorption measurements of the following bands: 2224 cm^{-1} H_2O , 2143 cm^{-1} and 4260 cm^{-1} CO ; and 3020 cm^{-1} , 1306 cm^{-1} and 1550 cm^{-1} CH_4 . The third report², which will be called the Final Report, will include results of the measurements of other H_2O bands and some strong H_2O bands as well as a section dealing with the "relative broadening abilities" of different gases. The contents of these three reports are intended to supplement earlier work reported by Foward, Burch, and Williams³ (hereafter referred to as FBW) which included measurements of CO_2 and H_2O absorption.

The work by FBW was limited to frequencies greater than approximately 670 cm^{-1} because of the limitations of the spectrometer. Since a large portion of the absorption by CO_2 in the 875 - 495 cm^{-1} region occurs at frequencies below 670 cm^{-1} , it seemed desirable to study the absorption in the entire spectral region, 875 - 495 cm^{-1} , by the use of apparatus developed since the FBW work was completed. Besides extending the spectral region covered, it has been possible with the new apparatus to obtain absorption measurements which are somewhat more accurate and include samples corresponding to shorter paths.

Samples containing smaller amounts of CO_2 and, therefore, corresponding to shorter paths than those employed by FBW were used in the investigation of the absorption by the bands at 3761, 3609, and 2350 cm^{-1} . The two bands at 1064 and 961 cm^{-1} are so weak as to be of only minor importance in the study of the earth's atmosphere; however, a knowledge of the absorption by these bands is essential for other reasons, such as in the study of the atmospheres of other planets containing large quantities of CO_2 . For this reason an investigation of these bands was included in the present research program.

Several experiments which have been proposed recently involve the measurement of the absorption and the estimation of atmospheric CO_2 . These measurements will be made by the use of instruments in airplanes, balloons, earth satellites, and even planetary probes. In order to interpret data obtained in these experiments it is necessary to understand CO_2 absorption and emission and its dependence on such parameters as path length, temperature, absorber partial pressure, and total pressure. It is hoped that the present data will further the knowledge of CO_2 absorption and its relationship to these parameters. The data will, as in earlier reports, be presented by the use of absorption curves, tables, graphs, and empirical equations.

A. UNITS, SYMBOLS, AND DEFINITION OF QUANTITIES

Spectral regions and frequencies are expressed in terms of frequency with units of cm^{-1} throughout the present study, except in reference to other work. All tabulated values of partial pressure, p , total pressure, P , and equivalent pressure, P_e , are expressed in mm Hg ; and absorber path lengths are in cm . Values of absorber concentration w are in units of atmos cm , and are determined by multiplying the absorber path length by the partial pressure of the absorbing gas in atmospheres, corrected to standard temperature. The temperatures, T , of the gas samples are given in degrees centigrade, except in instances where it is advantageous to use degrees Kelvin, for which the symbol θ is used.

$A'(v)$ is the true fractional absorption at frequency v , which would be observed with an instrument of infinite resolving power. $A(v)$, the observed fractional absorption at v , depends on the spectral slit width and is expressed as a fraction or as a percentage. The total absorption of an absorption band $\int A(v)dv$ is equal to $\int A'(v)dv$ and is independent of the spectral slit width provided the limits of integration include the entire band.

In section VI a quantity called the mean fractional absorption is used; this quantity is given by

$$A(v_1 - v_2) = \left(\frac{1}{v_2 - v_1} \right) \int_{v_1}^{v_2} A(v)dv, \quad (1)$$

and represents the mean fractional absorption in the spectral region $v_1 - v_2$.

II. EXPERIMENTAL PROCEDURES AND ANALYSIS OF DATA

Two different spectrometers were used to obtain the absorption curves for the present investigation. A Perkin-Elmer Model 21 equipped with dual multiple-pass absorption cells was used for absorption paths between 400 and 1200 cm^{-1} . Shorter absorption cells of lengths 1.55 and 11.6 cm were employed with a Perkin-Elmer Model 99 spectrometer which was enclosed in a vacuum tank. All samples were composed of either CO_2 alone or of mixtures of CO_2 and S_2 . The techniques used in sampling, as well as the construction of the absorption cells, and the method of determining the total absorption from the absorption curves were discussed in Report 1.

The CO_2 data reported in the present study can conveniently be divided in the four spectral regions which are referred to as follows:

(i) the 3716 and 3609 cm^{-1} bands, (ii) the 1660 cm^{-1} band, (iii) the 1464 and 961 cm^{-1} bands, and (iv) the 875 - 495 cm^{-1} region. The data for each of these spectral regions were obtained separately and the results are presented in sections III, IV, V, and VI, respectively.

Each of these four spectral regions covers a rather wide spectral region. It therefore seemed advantageous to divide each region into smaller sub-regions and to determine either the total absorption or the mean fractional absorption of each sub-region. It is desirable to divide the larger spectral regions into small sub-regions in such a way that the total absorption determined for each sub-region is virtually independent of the spectral slit-width and equal to the value which would be determined with infinite resolving power. As mentioned earlier, the total absorption $\int A(\nu) d\nu$ of an entire band has been shown to be independent of the spectral slit-width, provided there is no absorption beyond the limits of integration. It follows that the total absorption of the sub-regions could be independent of spectral slit-width if they were divided at frequencies where there was zero absorption. However, it will be seen in sections III - VI that there are no frequencies within the larger spectral regions at which the absorption is zero for samples having large values of ν . It was therefore necessary to choose optimum frequencies, at which there was absorption, as boundaries between the sub-regions such that the dependence of total absorption of each sub-region was least dependent on the spectral slit-width.

If ν_1 is the frequency at which two sub-regions are divided, the observed $A(\nu)$ just to one side of ν_1 is partially due to absorption at frequencies slightly to the other side of ν_1 , as a result of the finite spectral slit width $\Delta\nu$. The boundary frequencies were chosen so that the fractional absorption was virtually symmetrical about ν_1 for approximately $\pm \nu$ wave numbers on each side of ν_1 , i.e., the fractional absorption was nearly equal at a given distance on either side of ν_1 . If the fractional absorption is symmetrical about ν_1 and the spectral slit function is also symmetrical, one would expect the total absorption of sub-regions divided at ν_1 to have very little dependence on spectral slit-width.

The absorption curves for the 3716 and 3609 cm^{-1} bands were divided into two regions with the division at 3660 cm^{-1} , which corresponds to a minimum in absorption. It will be seen in section III that the absorption curves are nearly symmetrical about 3660 cm^{-1} for a few cm^{-1} on each side, thus making it a suitable frequency at which to divide the bands. The total absorption measured from the portions of the absorption curves at frequencies greater than 3660 cm^{-1} is referred to as the 3716 cm^{-1} band; and that on the low-frequency side of the interval is referred to as the 3609 cm^{-1} band.

The 1464 and 961 cm^{-1} bands are similarly divided at 1000 cm^{-1} , the frequency corresponding to an absorption minimum between the bands. For the larger samples studied, the fractional absorption did not decrease to zero on the low-frequency side of the 961 cm^{-1} band, but

reached a minimum at approximately 875 cm^{-1} , below which the fractional absorption increases. The limits of the 961 cm^{-1} band were therefore chosen to be 1000 cm^{-1} and 875 cm^{-1} .

The 2350 cm^{-1} band was divided at the band center and the total absorption on each side of this boundary was determined. The total absorption of the entire band was found by adding the values of total absorption of the two portions.

There are several strong and medium bands in the spectral region between 875 and 495 cm^{-1} , the strongest band having its center at 667 cm^{-1} . The frequencies corresponding to the absorption minima are not the same for all samples; and these frequencies are therefore not suitable for boundaries between the sub-regions. The major portion of the absorption arises from bands having prominent Q branches. The frequency of maximum absorption in each of these Q branches is essentially the same for all samples; and the absorption curves are nearly symmetric, about the frequency of maximum absorption for a few cm^{-1} on each side. On the basis of the above discussion, it was decided that the centers of the Q branches at 720 , 667 , 617 , and 545 cm^{-1} would be used as boundaries between the spectral sub-regions. For even the largest samples used, the absorption was essentially zero at frequencies below 495 cm^{-1} , and absorption at frequencies greater than 875 cm^{-1} was treated as a part of the 961 cm^{-1} band. The 875 - 495 cm^{-1} region was therefore divided into the following sub-regions for the purpose of analysis: 720 - 875 cm^{-1} , 667 - 720 cm^{-1} , 617 - 667 cm^{-1} , 545 - 617 cm^{-1} , and 495 - 545 cm^{-1} .

The mean fractional absorption, which is related to the total absorption by Eq. (1) for each of these sub-regions, is related to the parameters y and P_0 by curves given in Section VI. The quantity "mean fractional absorption" rather than "total absorption" was found for each of the sub-regions in the 875 - 495 cm^{-1} region. This was done since the term "total absorption" usually refers to an entire band; and since the mean fractional absorption for the interval $\nu_1 - \nu_2$ is equal to the fraction of the radiation power in that interval which is absorbed, provided the incident radiation is the same for all frequencies.

A. SELF-BROADENING COEFFICIENT AND EQUIVALENT PRESSURE

The absorption of a binary mixture of H_2 and an absorbing gas having a given absorber concentration y is known to depend on the partial pressure p of the absorber as well as upon the total pressure P . This phenomenon is a result of the different broadening abilities of the two gases involved. However, it was found that the broadening effects of two gases can be expressed in terms of a single variable called the equivalent pressure P_0 , which is defined by

$$P_0 = P + (B-1)p = P_{H_2} + np \quad (2)$$

where B, the self-broadening coefficient, can be determined experimentally.

The value of B was determined by the method described in Report 1 to be approximately 1.30 for the CO₂ bands included in the present study. It was shown in Report 1 that the value of B may be somewhat different for different bands of the same gas; it may even be slightly different for different frequencies within a given band. Although there may be small differences in the value of B for different frequencies, the value of 1.30 is believed to be correct to within ± 6 to $\pm 8\%$ for virtually all portions of the bands studied*.

By substituting the value $B = 1.30$ into Eq. (2), one obtains the following expression for the equivalent pressure of the CO₂ - N₂ samples:

$$P_e = P + 0.30p = P_{N_2} + 1.30p. \quad (3)$$

It is noted that no quantity defined to be equivalent pressure was used by HEW. However, the quantity $(P+p)$, which was called a "weighted pressure", was used as a single parameter in the same manner that P_e is used in the present study. Using $(P+p)$ as an equivalent pressure is, of course, the same as using a value of $B = 2$, which is to be compared with the value of 1.30. The latter value is based on rather careful measurements made recently and is in good agreement with theoretical predictions by two well-known theorists, Levin Kaplan⁴ and William Benedict⁵. Edwards⁶ in a recent study of the total absorption of CO₂ bands used an expression for P_e which is equivalent to the following:

$$P_e = (P + p + 0.5 p^2). \text{ (pressure in atmospheres)}$$

This expression for P_e is equivalent to using $B = (2 + 0.5p)$, a value which is greater than that used in the present study or by HEW.

B. DEFICIENCIES OF DOUBLE-BEAMING TECHNIQUES IN THE STUDY OF STRONG ATMOSPHERIC BANDS

It is well known that, when a conventional single-beam spectrometer is employed with the optical path open to the atmosphere, there are spectral regions over which the radiant power incident on the detector is reduced as a result of absorption by atmospheric gases. It will be shown

*The Final Report will contain more detailed information concerning the determination of B in a section devoted to the relative broadening abilities of various gases.

that care must be taken in order to determine the correct value of the fractional absorption $A(\nu)$ of a sample at frequencies in a region of atmospheric absorption. It will also be demonstrated that atmospheric absorption within a double-beam spectrometer can give rise to error in the measurement of the fractional absorption of some samples, notably atmospheric gases. In order to demonstrate these phenomena the following quantities are defined: $R_0(\nu)$ is the radiant power incident on the detector with the spectrometer set at frequency ν if there is no absorption by the atmospheric gases in the optical path. The power $R_0(\nu)$ includes radiation within the frequency interval $\Delta\nu$ passed by the spectrometer slit. The spectral intensity distribution of the power $R_0(\nu)$ over the interval $\Delta\nu$ depends, of course, on the spectral intensity distribution of the source as well as upon the "slit function" of the spectrometer. In spectrometers such as the ones used in the present study the intensity of the source is nearly constant over $\Delta\nu$ and the spectrometer slit function is such that the intensity of $R_0(\nu)$ changes gradually over $\Delta\nu$ with its maximum at frequency ν .

If a sample is placed in the beam and the radiant power incident on the detector is reduced to $R(\nu)$, the fractional absorption $A(\nu)$ of the sample is defined to be

$$A(\nu) = \frac{R_0(\nu) - R(\nu)}{R_0(\nu)} . \quad (4)$$

In the case of a sample for which $A'(\nu)$, the true fractional absorption as viewed with infinite resolving power, changes rapidly, it is apparent that $A(\nu)$ will depend on the value of $\Delta\nu$ and on the slit function.

If frequency ν occurs within an absorption band of one of the atmospheric gases present in the optical path, the radiant power incident upon the detector is reduced to $Rg(\nu)$. If the sample having fractional absorption $A(\nu)$ is placed in the beam, the power reaching the detector is reduced to $R^*(\nu)$. The apparent fractional absorption of the sample $A^*(\nu)$ is then given by

$$A^*(\nu) = \frac{Rg(\nu) - R^*(\nu)}{Rg(\nu)} . \quad (5)$$

Care must be taken not to assume that $A^*(\nu) = A(\nu)$. This equality is approximately valid in many cases; however, it has been shown by GHW that $A^*(\nu) < A(\nu)$ if the sample being studied is the same gas as the atmospheric gas causing the absorption. The inequality immediately above can be explained in an elementary way if one thinks of the radiation as having passed through the atmospheric path before being incident on the sample gas. (Actually it does not matter whether the radiation passes through the sample first or last, but for the purpose of discussion it will be considered as having passed through the sample last.) The intensity of the radiation incident on the sample will not be constant as in the case of no atmospheric absorption, but it will have minima at frequencies corresponding to absorption lines and maxima at frequencies between the lines. Since the sample being studied is the same gas as the atmospheric component giving rise to the absorption, the radiation incident on the sample is greatest at frequencies for which it absorbs least and is least at frequencies for which it absorbs most. The net result is that the fraction $A^*(\nu)$ of the radiation absorbed by the sample is less than $A(\nu)$, the fractional absorption observed with no atmospheric interference.

It is apparent that if the sample being measured is different from the atmospheric gas giving rise to the absorption, $A^*(\nu)$ might be greater or less than $A(\nu)$, depending on the relative positions of the absorption lines of the sample and the atmospheric gas. If the absorption lines of the sample happen to occur at frequencies between the lines of the atmospheric gas, $A^*(\nu)$ would be greater than $A(\nu)$.

In a double-beam type of instrument such as the Perkin-Elmer Model 21 used in the present investigation, error is also introduced by the atmospheric gases in the optical path when the absorption of CO_2 or H_2O samples is being studied. Such an instrument records directly the ratio of the transmission of the sample beam to the transmission of the reference beam. If $R_0(\nu)$ is the radiation power incident on the detector from the reference beam, $[1-A^*(\nu)] R_0(\nu)$ is the power incident on the detector from the sample beam which has passed through a sample having fractional transmission $A(\nu)$. The apparent fractional absorption recorded by the double-beam instrument is

$$1 - \left\{ \frac{[1-A^*(\nu)] R_0(\nu)}{R_0(\nu)} \right\} = A^*(\nu).$$

Thus, the double-beam instrument yields the same "zero reading" as a single-beam instrument having the same spectral slit function and the same compensating gas length.

The fact that a double-beam instrument which is open to the atmosphere indicates two small values of fractional absorption for a H_2 sample is illustrated in Fig. 1. Curve 1 was obtained with the sample instrument and with the instrument open to the atmosphere. The apparent fractional absorption is seen to be considerably less throughout the band than in curve 2, which was obtained with the same H_2 sample with the spectrometer closed and H_2 to remove the amount of H_2 present.

The method of reducing the errors arising from atmospheric absorption is to close the spectrometer with H_2 as was done to obtain curve 2 in Fig. 1. However, it is not a constant amount of atmospheric absorption, which removes H_2 or O_2 or water vapor. If the absorption compensation of the sample source studied is much greater than that of the atmospheric gas, the error due to atmospheric absorption is negligible. It was found that it was difficult to close the double-beam spectrometer sufficiently well to avoid error in measuring samples of small ϵ for the 17.1, 18.9, and 23.9 μm bands and for the region near $15\text{--}16\text{ }\mu\text{m}$.

Errors due to atmospheric absorption which, of course, is eliminated by evacuating the spectrometer. This source is negligible, if not negligible. In the case of the Model 21, however, a vacuum tank was built to enclose the Model 22 which was used with the 17.1- and 18.9- μm bands to obtain absorption curves for the 17.1, 18.9, and 23.9 μm bands and for regions of relatively small ϵ for the region near $15\text{--}16\text{ }\mu\text{m}$. The Model 21 was used to obtain absorption curves of samples of larger ϵ for the 17.1- μm region and all of the curves for the 18.9 and 23.9 μm bands. A sketch of description of the design of the vacuum tank which enclosed the Model 22 spectrometer will appear in the Final Report.

RESULTS AND SUMMARY

A detailed comparison of the various sources of error inherent in a study such as the present one was given in Report 1. It is concluded that the overall error in the measured values of total absorption is less than 1% of the total absorption is greater than 10^{-2} , and that the errors are still less for values of total absorption between 10^{-2} and 10^{-3} . For the very small values of total absorption, less than 10^{-3} , the estimated error may be as high as 1% to 2%. In the case of the 17.1- μm region the most fractional absorption, rather than the total absorption, was determined. The estimated error in the tabulated values of total fractional absorption is less than 1% for values of total fractional absorption greater than 1.0. For smaller values of total fractional absorption the error increases to approximately 1% to 2% for the 17.1- μm region.

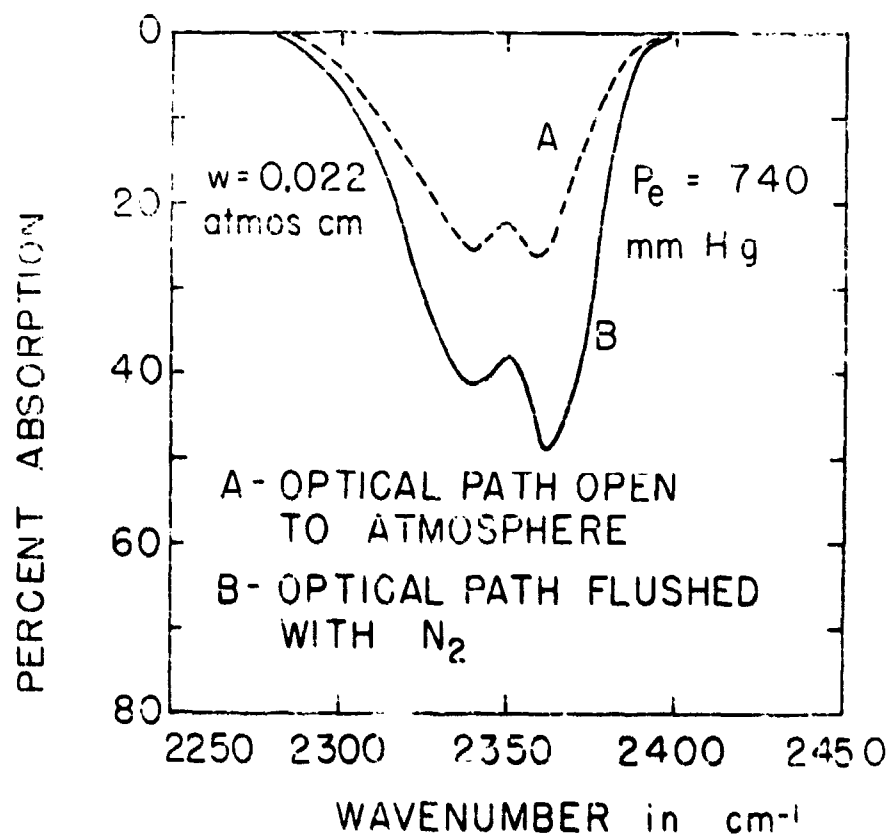


Fig. 1. Absorption curve for the 2350 cm^{-1} CO_2 band illustrating the error arising from air in the optical path of the spectrometer. The absorber concentration of the sample is approximately one-third as great as the absorber concentration of the CO_2 in the atmospheric path of the sample beam.

III. EXPERIMENTAL RESULTS FOR THE 3716 AND 3609 cm^{-1} CO_2 BANDS

Tracings of many of the absorption curves for the 3716 and 3609 cm^{-1} bands of CO_2 are shown in Figs. 2 and 3 with the spectral slit-width indicated in the lower left-hand portion of Fig. 3. The vertical dashed line at 3660 cm^{-1} represents the boundary between the "bands".

The data are tabulated in Table 1, which includes the values of absorber concentration y and equivalent pressure P_e for each sample as well as numbers of the figures in which many of the absorption curves appear. Also included are remarks concerning composition of the sample and the values of total absorption of each of the two bands along with their sum. The value of the sum of the total absorptions of two bands is included for comparison with data reported by HSW and for the convenience of other workers who treat these two separate bands as one. The temperatures of the samples, which were near room temperature and varied by approximately ± 4 degrees C, were not included since the total absorption of these two bands varies only slightly with temperatures.

Representative data for the 3716 cm^{-1} band are plotted in Fig. 4, where the different curves corresponding to various values of y relate the total absorption to P_e . A qualitative explanation of the features of curves such as those in Fig. 4, as well as of other figures in this report, was given in Report 1 and will not be repeated.

In order to show the dependence of total absorption on absorber concentration, values of absorber concentration were taken from the curves of Fig. 4 and used to obtain the "smoothed" curves of Fig. 5, where each curve corresponds to a given value of P_e . The results of measurements of the 3609 cm^{-1} band are presented in a similar manner in Figs. 6 and 7.

In Fig. 8 is shown the sum of the total absorptions of the two bands plotted against P_e for various values of y . The solid curves are based on data obtained in the present investigation, while the dashed curves are based on HSW data which are shown for comparison. This figure permits a direct comparison of the present results with the earlier work for values of $y = 4.74$ and 9.48 atmos cm. If one were to interpolate between the two curves corresponding to 3.02 and 6.08 atmos cm for values of P_e between approximately 500 and 1000 mm Hg to determine values of total absorption corresponding to $y = 4.74$ atmos cm, one would find that these values differed by approximately 5 to 10% from values taken from the curve corresponding to 4.74 atmos cm from the HSW data. Similarly the 9.48 atmos cm curve is seen to occur close to where one would expect it to be relative to those for 6.08 and 12.7. It should be noted that the HSW data used in the comparison represent the smallest samples investigated, for which one would expect the experimental error to be the greatest. The estimated error in the HSW results, as well as the present results, is approximately $\pm 5\%$; thus, one concludes that there is fairly

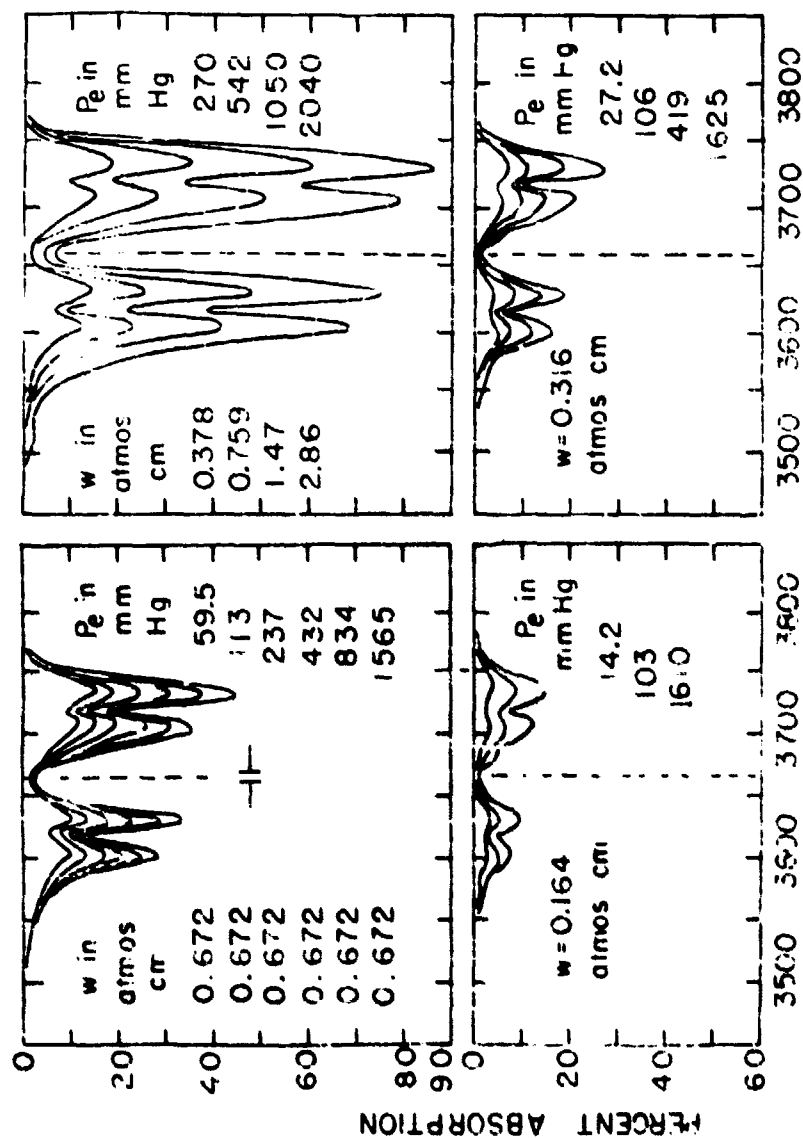


Fig. 2. Absorption curves of the 3716 and 3709 cm⁻¹ CO₂ bands. The spectral slit-width indicated in the upper-left portion of the figure applies to the curves in Figs. 2 and 3.

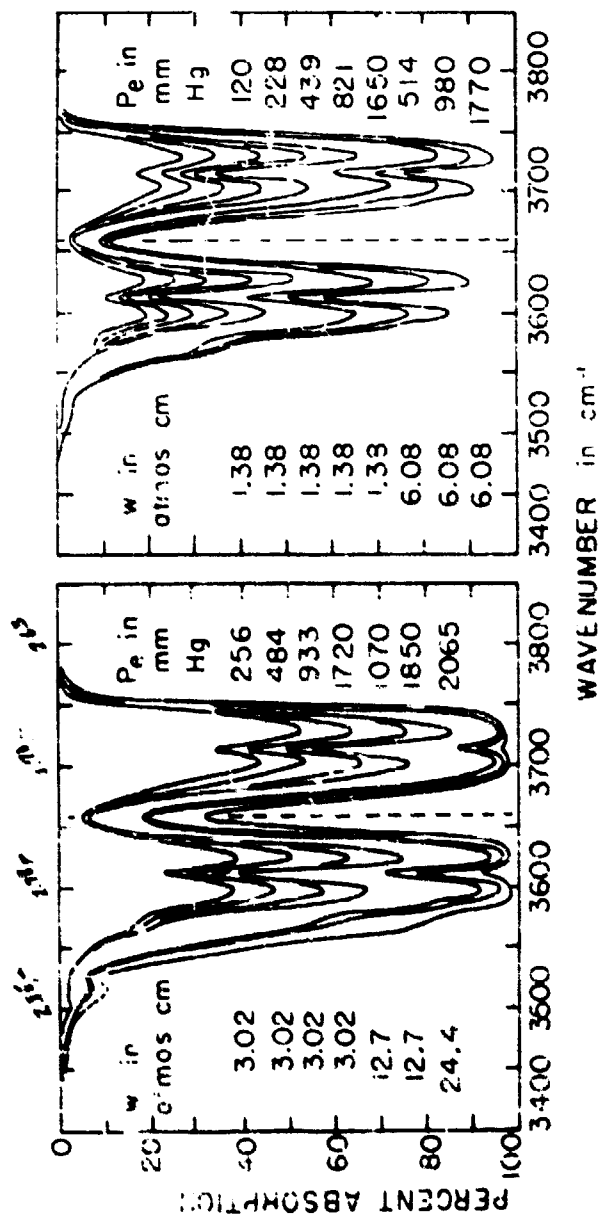


Fig. 5. Absorption curves of the 3716 and 3509 cm^{-1} CO_2 bands.

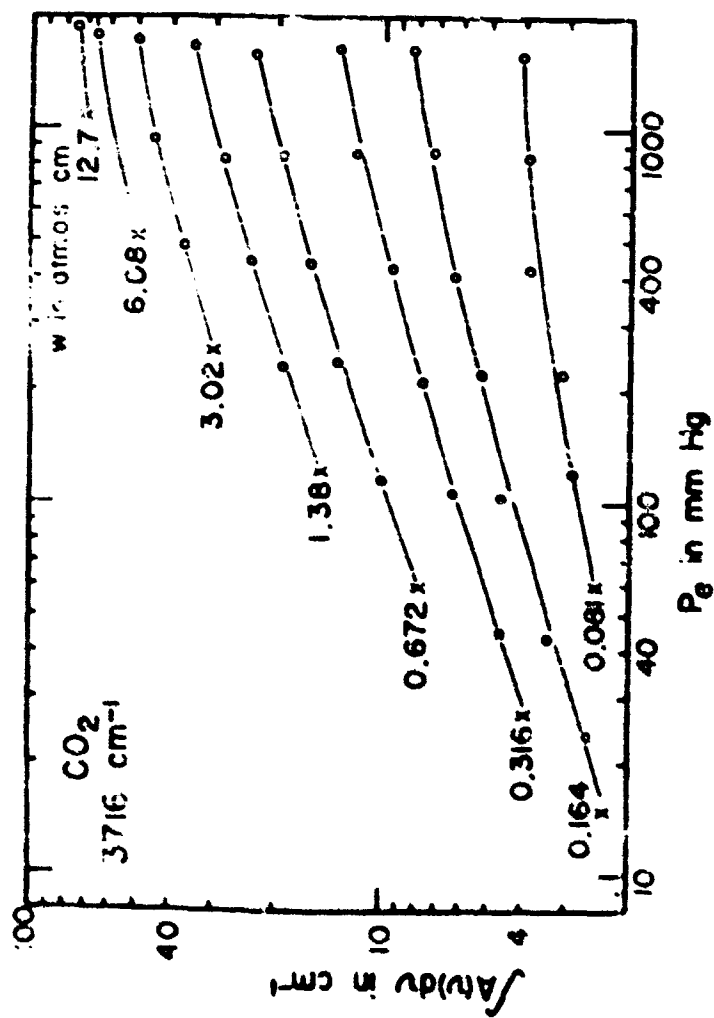


Fig. 4. The total absorption of the 5.15 cm^{-1} CO_2 band versus equivalent pressure. It's correspond to an O_2 of CO_2 0.164 and 0.6 to mixtures of CO_2 and N_2 .

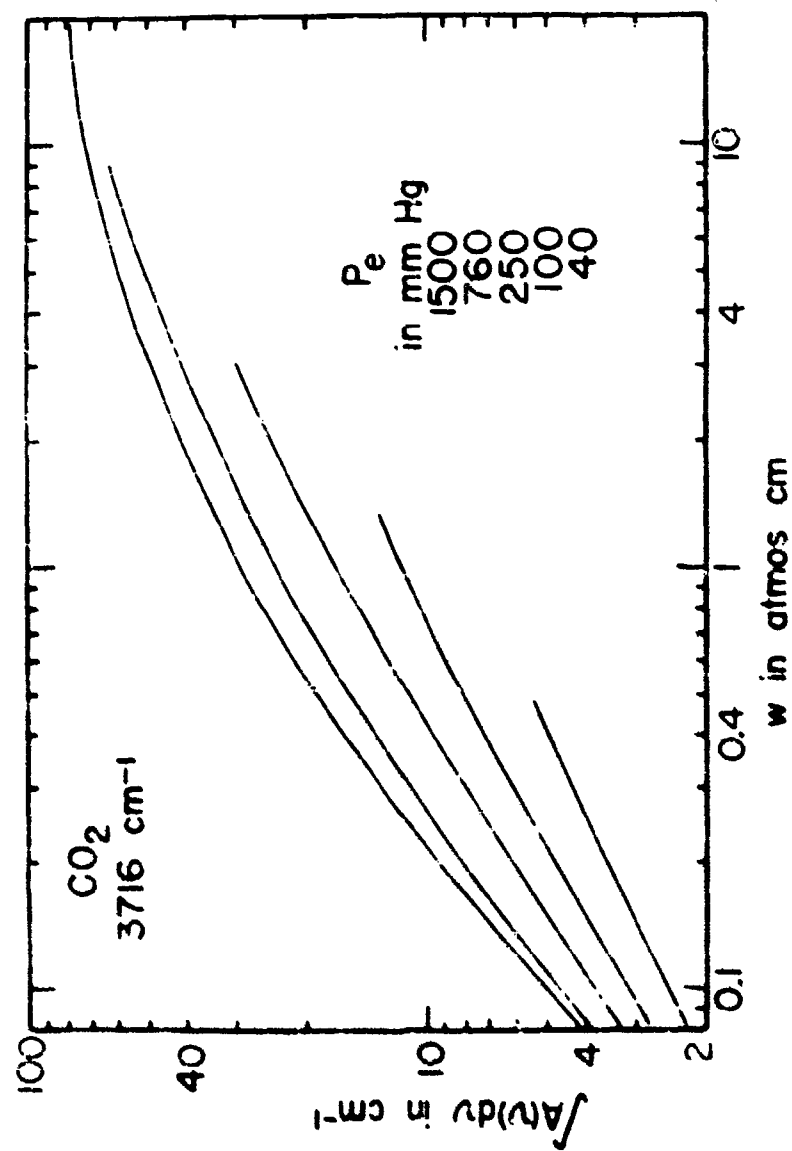


Fig. 5. The total absorption of the 3716 cm⁻¹ CO₂ band versus absorber concentration.

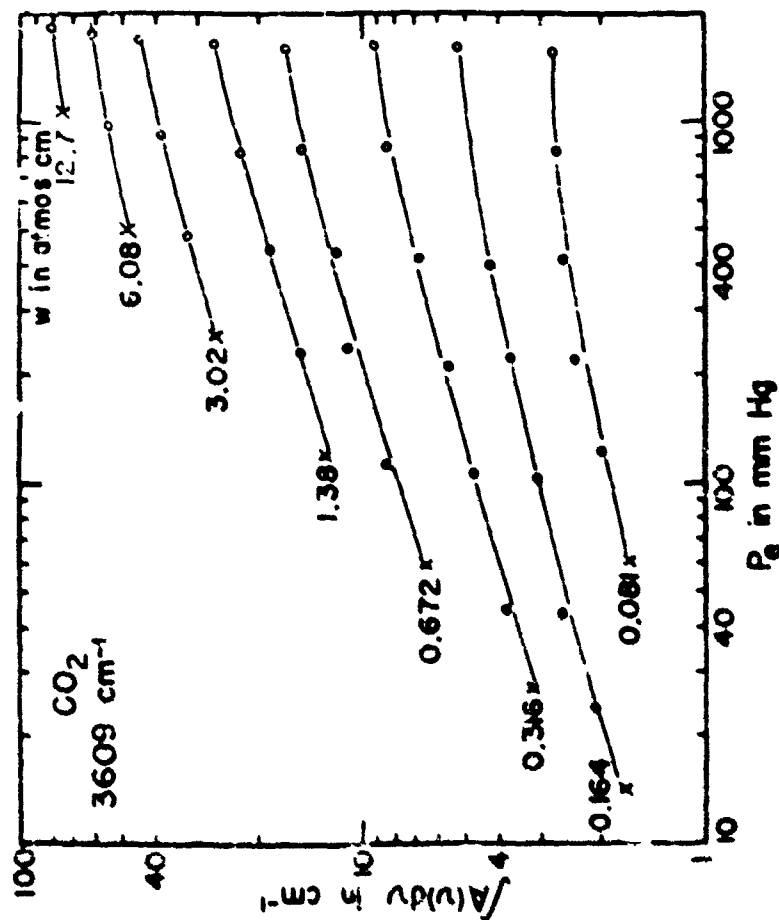


Fig. 6. The total absorption of the 3609 cm⁻¹ CO₂ band versus equivalent pressure. X's correspond to samples of CO₂ alone, and O's to mixtures of CO₂ and H₂.

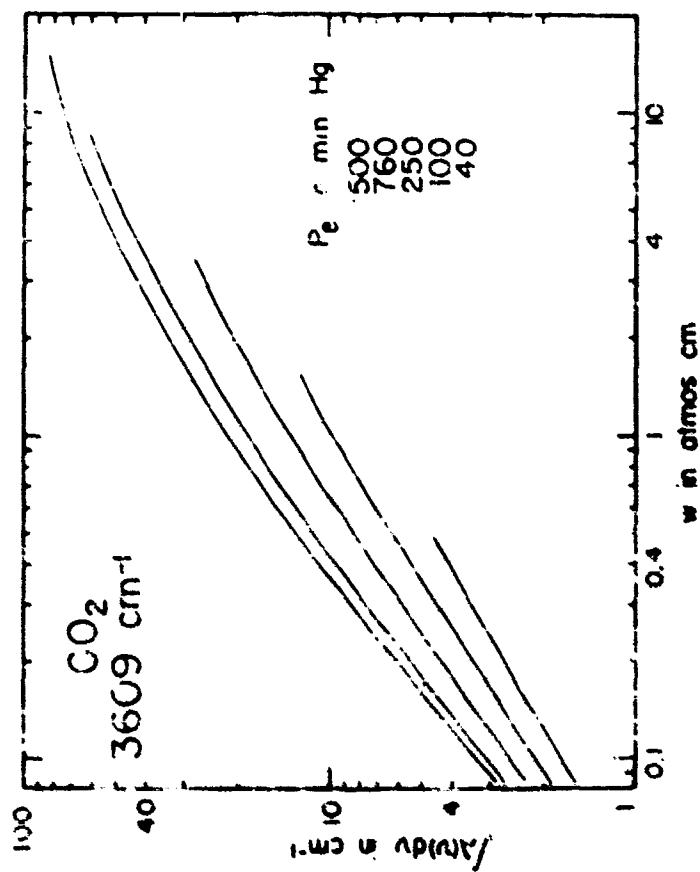


Fig. 1. The total absorption of the 3609 cm⁻¹ CO₂ band versus absorber concentration.

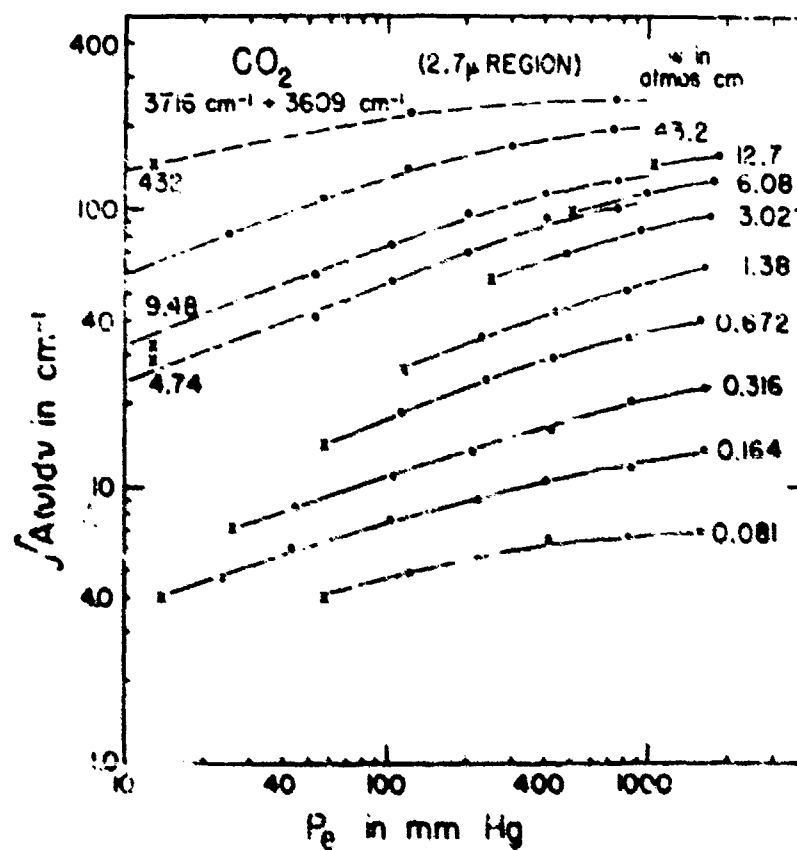


Fig. 9. Integrated absorption in the 2.7 μ and 2.6 μ CO₂ bands versus equivalent pressure. The solid curves are based on data obtained in the present investigation; the dashed curves are based on data from the NBS report and are shown for comparison. w corresponds to samples of CO₂ alone; for the 9:1 mixture of CO₂ and N₂.

satisfactory agreement between the present and the earlier work for values of \bar{v} and P_e covered by both.

Values of total absorption from Fig. 8, as well as from HSW data which are not shown in Fig. 8, were used to obtain the curves of Fig. 9 where total absorption is plotted against \bar{v} for the various values of equivalent pressure indicated. By interpolating between the curves of Fig. 9 it is possible to determine the total absorption of the 3710 and 3609 cm^{-1} bands for samples for which the values of \bar{v} and P_e are included by the curves.

It is sometimes desirable to have empirical equations which relate the total absorption to the parameters \bar{v} and P_e , although the values can usually be determined more accurately from curves such as those in Fig. 9. Two different empirical equations of this sort were reported by HSW for this band: one for values of total absorption greater than 50 cm^{-1} , and another for smaller values. The equation intended for small values of total absorption was based on the results of only approximately 10-12 samples, the maximum pressure of which was less than 50 mm Hg. Many of the samples used in the present investigation yielded values of total absorption less than 50 cm^{-1} , and the equivalent pressure of these samples varied from a few mm Hg to approximately 1300 mm Hg. Since the present data represent greater ranges of \bar{v} and P_e , and since the equivalent pressure used in the present study is believed to be more reliable than the "weighted pressure" used by HSW, it seemed desirable to revise the empirical equation to be used for values of total absorption less than 50 cm^{-1} .

It was demonstrated in Report 1 that an equation of the form

$$\int A'(\bar{v}) d\bar{v} = a (vP_e)^b \quad (1)$$

was useful for small values of $A(\bar{v})/\bar{v}$, and that the values of the constants a and b could be easily determined graphically. In order to determine the value of the empirical constant a , values of total absorption were taken from the curves of Fig. 8 for different values of P_e and plotted against vP_e^b . Different values of b were tried, and the set of curves produced by using $b = 0.65$ are shown in Fig. 10. The value of 0.65 was selected since in Fig. 10 the five curves corresponding to $P_e < 760$ mm Hg are nearly coincident for values of total absorption between 30 and 50 cm^{-1} . Since these portions of the curves are nearly coincident it is apparent that the total absorption can be expressed as a function of the single variable $vP_e^{0.65}$ for the values of \bar{v} and total absorption represented. Portions of some of the curves of Fig. 10 were omitted to prevent overcrowding; however, points are included to indicate positions of the curves.

The four sets of points in Fig. 10 corresponding to $P_e = 1300, 1000, 760$ and 500 mm Hg are for values of total absorption between 3 and 10 cm^{-1} .

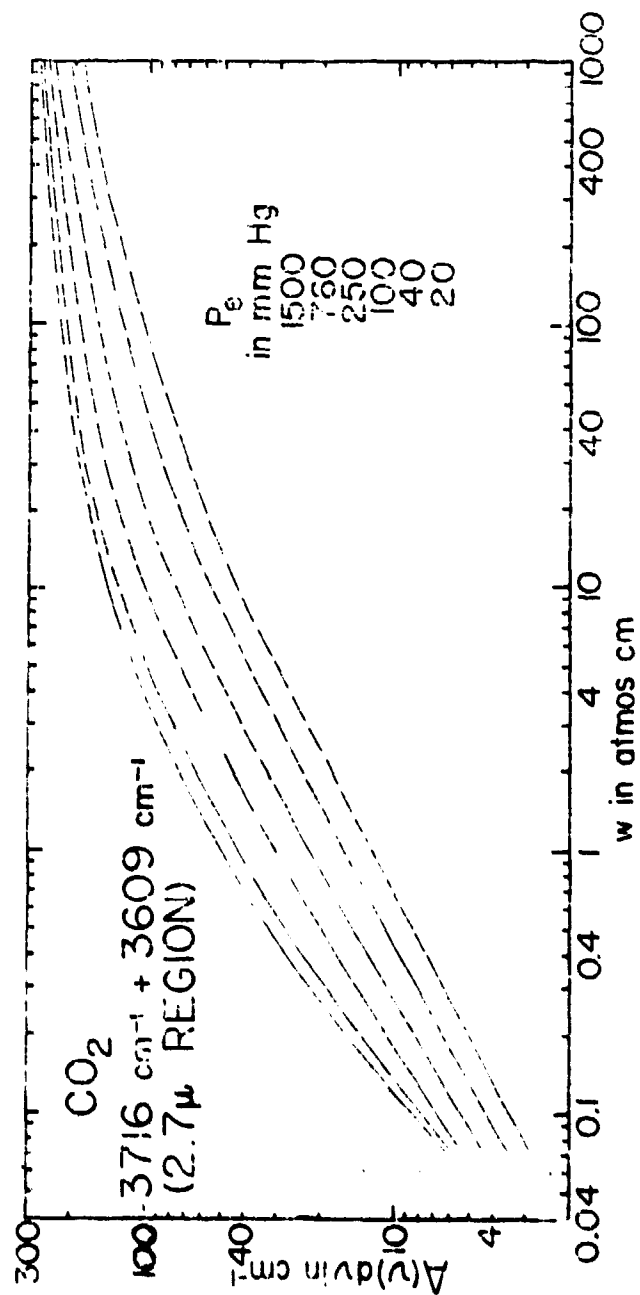


Fig. 9. The total absorption of the 3716 and 3609 cm⁻¹ CO₂ bands versus absorber concentration. The solid portions of the curves are based on data obtained in the present investigation, while the dashed portions are based on data from the BB4 report.

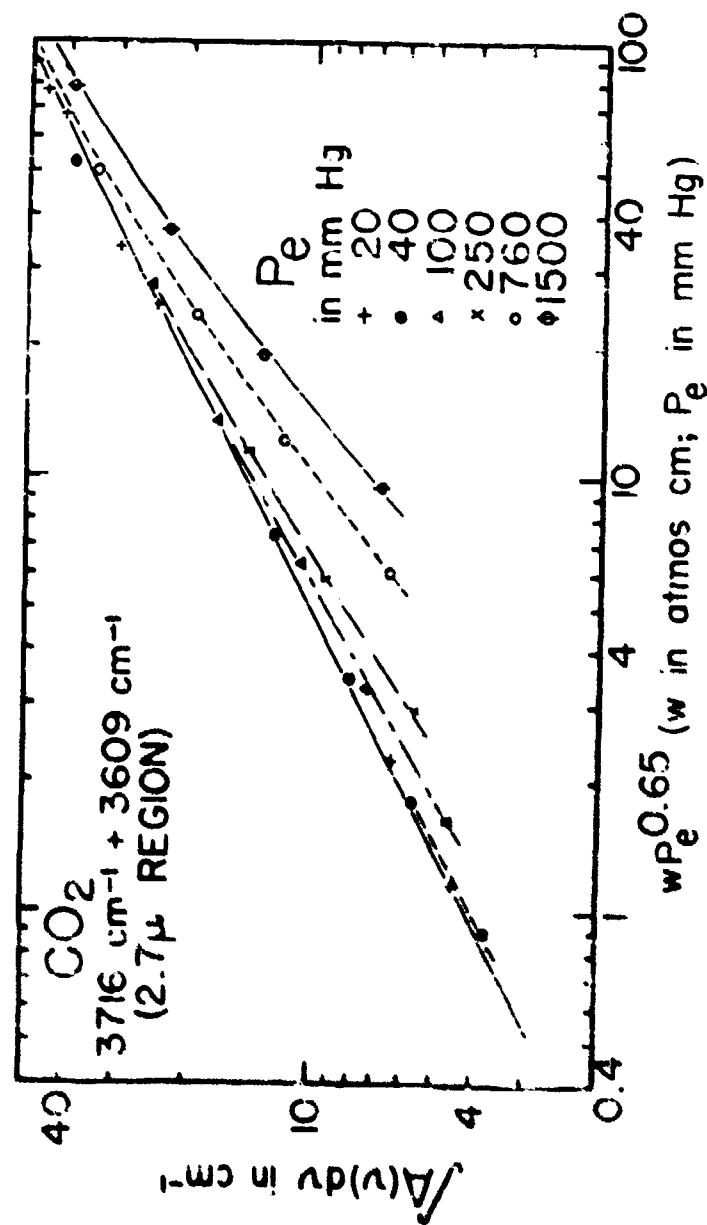


Fig. 10 Net total absorption of the 3716 and 3609 cm^{-1} CO_2 bands versus $wP_e^{0.65}$.

Thus, if P_0 is limited to less than 250 mm Hg, values of total absorption between 10 and 50 cm^{-1} can be expressed as a function of $vP_0^{0.65}$. Since both the ordinate and the abscissa of Fig. 10 are logarithmic, the value of b for Eq. (6) was determined from the slope of the single straight line which best fitted the points corresponding to the values of total absorption and equivalent pressure specified. The value of b was found to be 0.58.

On the basis of the above discussion the following empirical equation and its region of validity were derived for the 3716 and 3609 cm^{-1} CO_2 bands.

$$\int A(v)dv = 3.5 (vP_0^{0.65})^{0.58} \quad (7)$$

for

$$20 < P_0 < 250 \text{ mm Hg},$$

and

$$10 < \int A(v)dv < 50 \text{ cm}^{-1}.$$

It can be used for $20 < P_0 < 160$ mm Hg if $30 < \int A(v)dv < 50 \text{ cm}^{-1}$.

This empirical equation can be compared with the corresponding equation from FHM, which it is intended to replace:

$$\int A(v)dv = 3.15 v^{0.5} (P_0 P)^{0.43}.$$

The curves of Fig. 10 which correspond to higher equivalent pressure could be shifted to the left, and made to occur closer to the curves corresponding to lower pressures, by using an exponent a for P_0 smaller than the value of 0.65 which was used. However, if the same exponent were used, the curves corresponding to the high pressures would occur to the left of and above the curves of lower pressure for larger values of total absorption. Thus one concludes that the total absorption cannot be described by a function of vP_0^a for large values of P_0 and small values of v . This result was discussed in some detail in report 1 and is confirmed in the present investigation. It is probably true that by limiting the range of values of $\int A(v)dv$ and P_0 for each equation and by using different values of a , one could find a series of equations which would satisfactorily relate $\int A(v)dv$ to v and P_0 for all the data reported. It is apparent that several such equations would be necessary, and that each would be valid only over very limited ranges of values of $\int A(v)dv$ and P_0 . It did not seem worthwhile to derive an

many equations as would be necessary; and it is recommended that the curves of Fig. 9 be used for values of $A(\nu)d < 50 \text{ cm}^{-1}$ for which Eq. (7) is not suited.

IV. EXPERIMENTAL RESULTS FOR THE $2350 \text{ cm}^{-1} \text{ CO}_2$ BAND

Tracings of many of the absorption curves of the $2350 \text{ cm}^{-1} \text{ CO}_2$ band are shown in Figs. 11 and 12. The data are listed in Table 2 in a manner similar to that used in Table 1. Before measuring the total absorption of each spectrum, it was divided into two portions at 2350 cm^{-1} , and the total absorption of each portion was then determined. Values of total absorption of each portion are given in Table 2 along with the sum of these values, which represents the total absorption of the entire band. Although the results for the two portions are not analyzed separately in the present study, they are tabulated for possible future use by others.

Representative data are presented in Fig. 13 where the total absorption of the entire band for various values of absorber concentration is plotted against equivalent pressure. The solid curves are based on data obtained in the present investigation. The dashed curve representing KMW data corresponding to 4.7 atmos cm is seen to occur slightly above the solid curve corresponding to 4.99 atmos cm for values of P_0 between approximately 400 and 800 mm Hg. The values of total absorption indicated by the 4.7 atmos cm curve are approximately 6 to 8% greater than one would predict on the basis of the solid curves. Other KMW results, which are not shown, were compared and found to be less than 8% different from corresponding results in the present study. The estimated error in the KMW results as well as the present results is approximately 1%. Thus, one concludes that the agreement between the earlier work and the present work is within the indicated experimental uncertainties for values of y and P_0 covered in both investigations. As in the case of the 3716 cm^{-1} and 3609 cm^{-1} bands, the KMW results which were compared with the present results represented the samples of least absorber concentration, for which the uncertainty would be the greatest.

Values of total absorption were taken from Fig. 13 and from KMW data to produce the curves of Fig. 14, where the total absorption is plotted against absorber concentration. By interpolating between the curves it is possible to determine the total absorption of a known sample for which the values of y and P_0 occur within the range covered by Fig. 14.

In the KMW report an empirical equation was derived to relate values of total absorption less than 50 cm^{-1} to y and P_0 . In order to derive an empirical relationship for the smaller samples for which the values

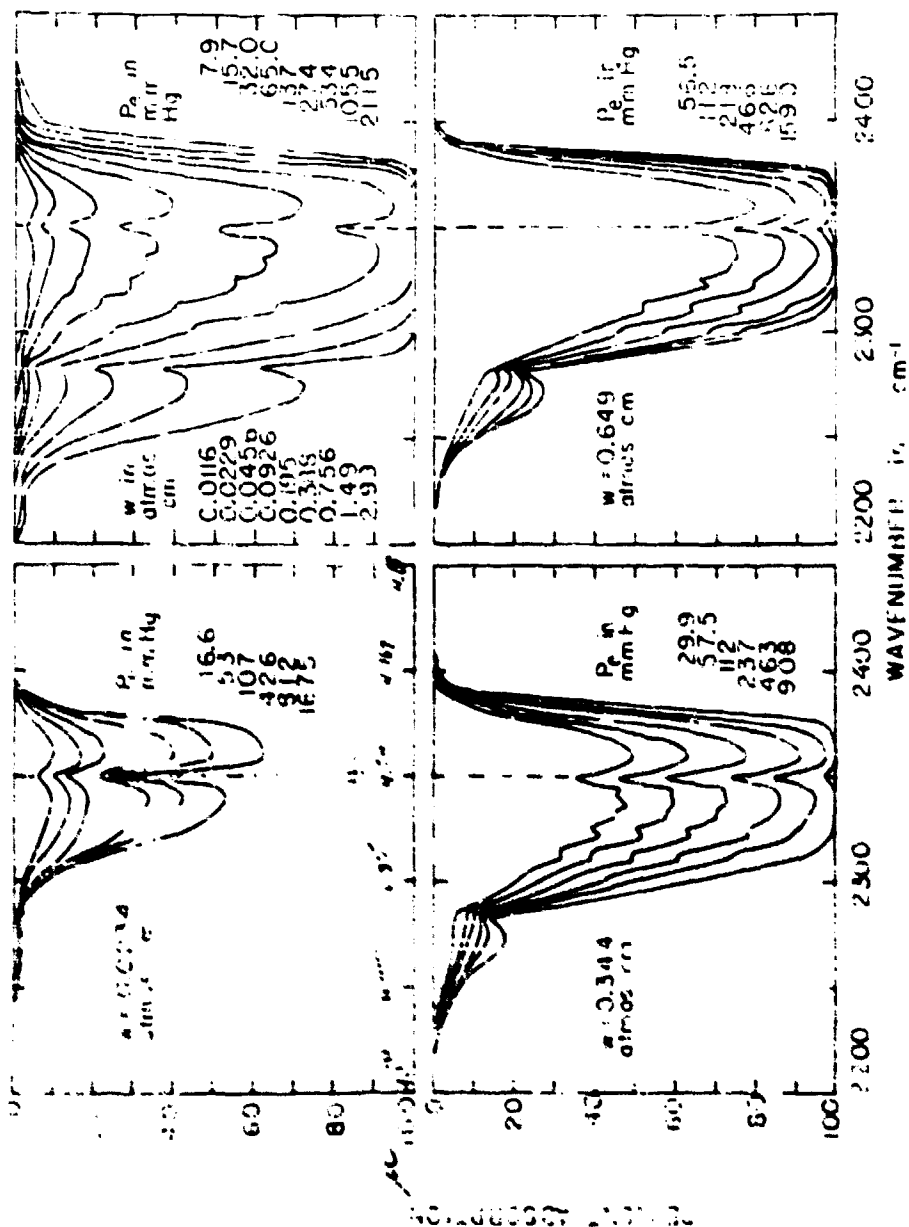


Fig. 11. Absorption curves of the 2550 cm^{-1} CO_2 band. The spectral slit-width indicated in the upper-left portion of the figure applies to the curves in Figs. 1, and 12.

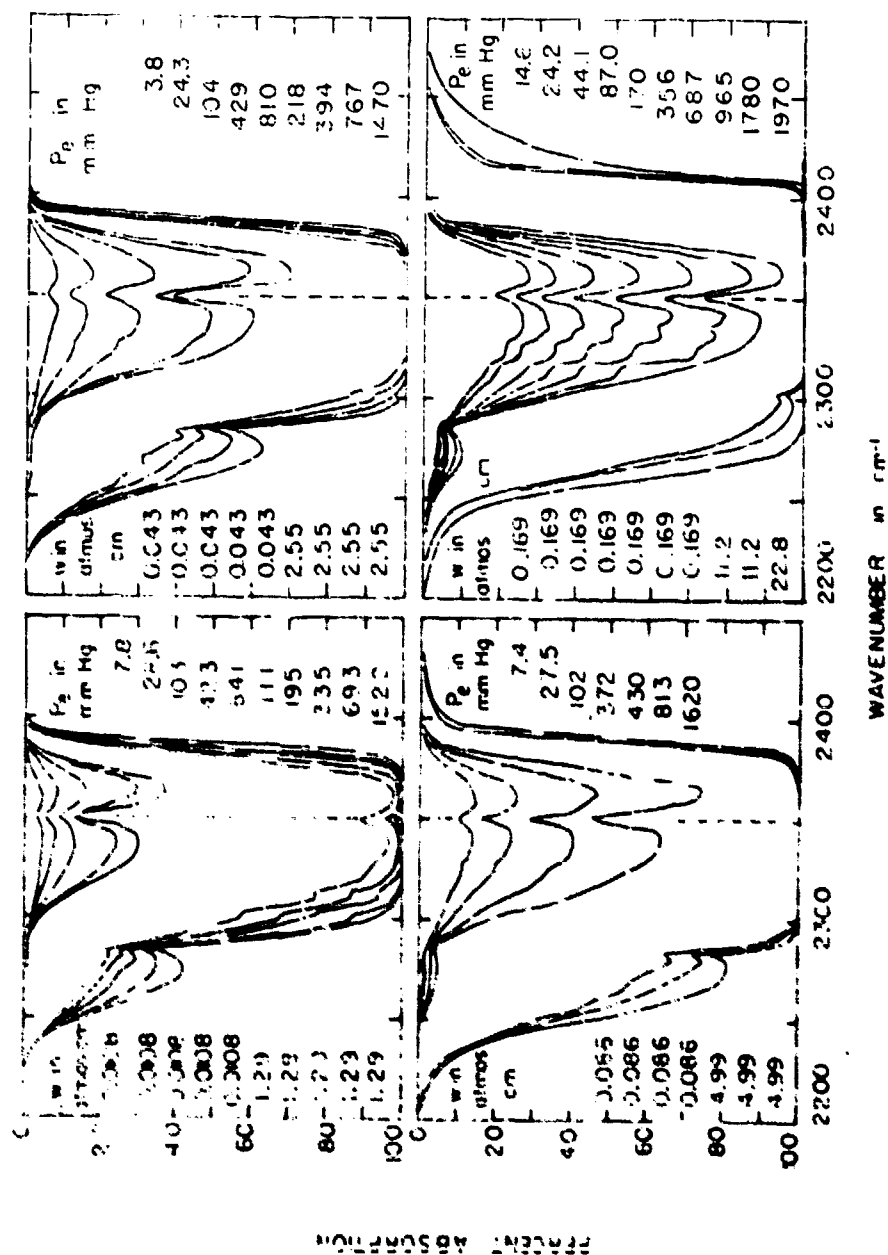


Fig. 12. Absorption curves of the 2350 cm⁻¹ band.

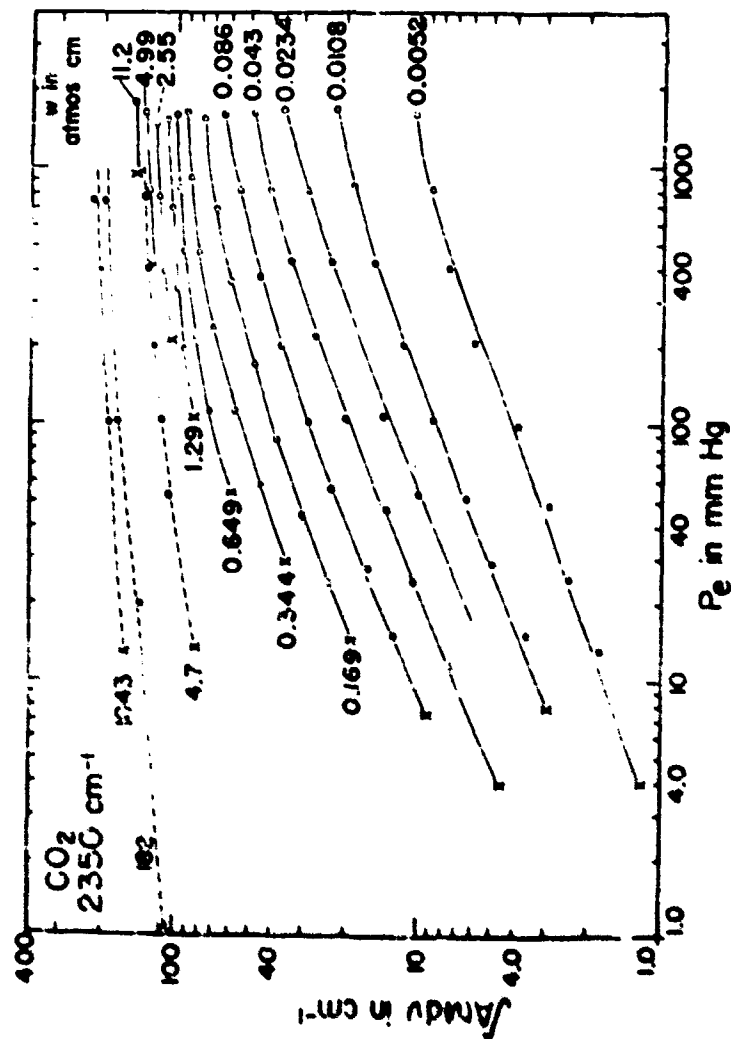


Fig. 15. The total absorption of the 2350 cm⁻¹ CO₂ band versus equivalent pressure. The solid curves are based on data obtained in the present investigation; the dashed curves are based on data from the NBS report and are shown for comparison. "x", "y", "z" correspond to mixtures of CO₂ alone; "O's" and "C's" to mixtures of CO₂ and N₂.

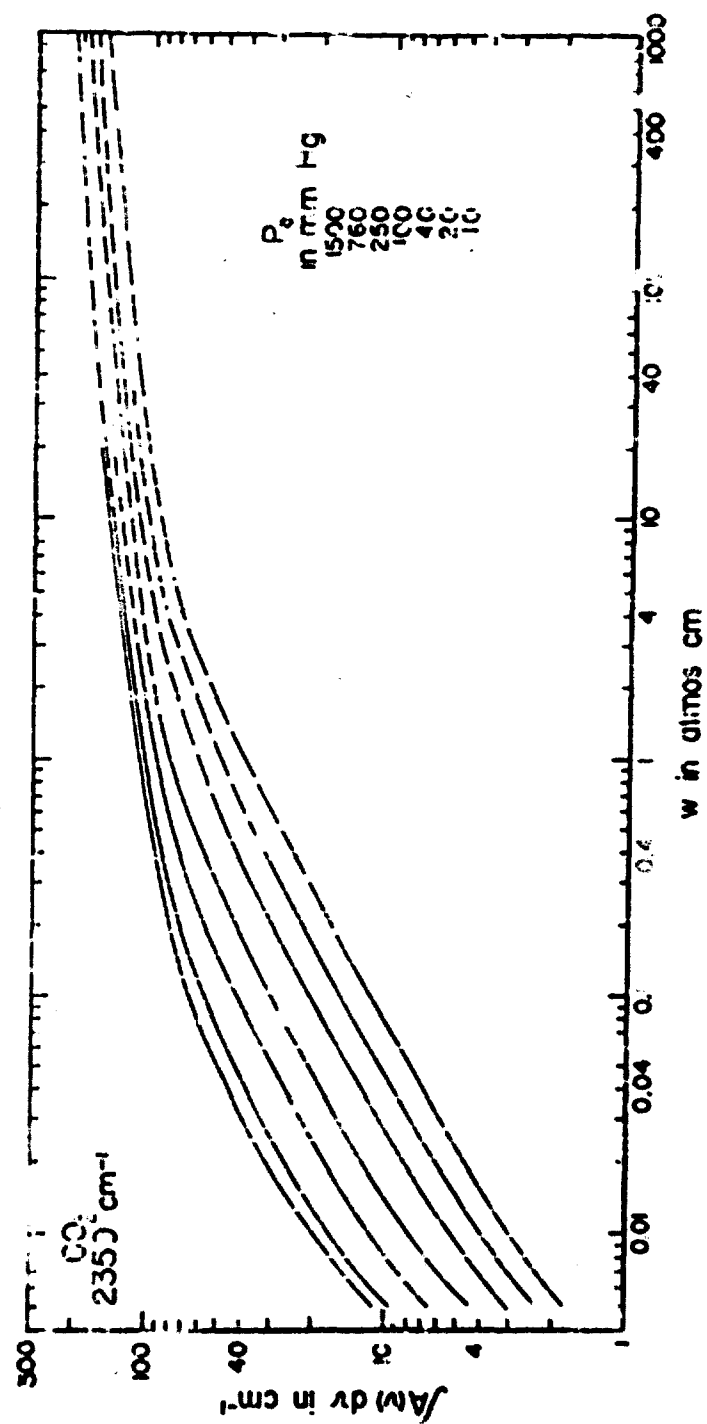


Fig. 11. The total absorption of $2350 \text{ cm}^{-1} \text{ CO}_2$ and various P_2 for concentration. The solid portion of the curves are based on the values obtained in the present investigation. The dashed portions are based on the values of the authors.

of total absorption are less than 50 cm^{-1} , values are taken from the curves of Fig. 15 and replotted in Fig. 15 again. The value of the empirical constant 0.75 was determined in the case of Fig. 10. From this figure the following equation was derived:

$$\int A(\nu) d\nu = 15.0 [\nu_p(0.75)] \nu_p^{0.54} \quad (8)$$

$$\epsilon < \int A(\nu) d\nu < 50 \text{ cm}^{-1}$$

$$10 < P_0 < 250 \text{ mm Hg.}$$

Equation (8) is also valid for

$$10 < P_0 < 760 \text{ mm Hg}$$

and

$$15 < \int A(\nu) d\nu < 50 \text{ cm}^{-1}.$$

V. EXPERIMENTAL RESULTS FOR THE 1064 AND 961 cm^{-1} BANDS

Tracings of several absorption curves of the 1064 and 961 cm^{-1} bands are shown in Figs. 16, 17, 18; those in Figs. 16 and 18 correspond to samples consisting of CO_2 alone, while the curves in Fig. 17 correspond to samples consisting of CO_2 and N_2 . The absorption curves of Fig. 17 were extended to approximately 700 cm^{-1} , and the results of the portions of these curves between 875 and 720 cm^{-1} are discussed in the next section. The absorption curves in Fig. 18 represent a given sample of CO_2 alone at various temperatures above ambient; the results of these curves, as well as others obtained from samples at elevated temperatures, will be discussed near the end of this section.

It is seen from Figs. 16 and 17 that the absorption is essentially zero at approximately 1125 cm^{-1} for even the largest samples, and that the bands overlap with an absorption minimum near 1000 cm^{-1} . On the low frequency side of the bands another absorption minimum occurs at 875 cm^{-1} ; the vertical dashed lines at 1000 cm^{-1} and 875 cm^{-1} in Figs. 16-18 represent the boundaries between the bands which were discussed in section II.

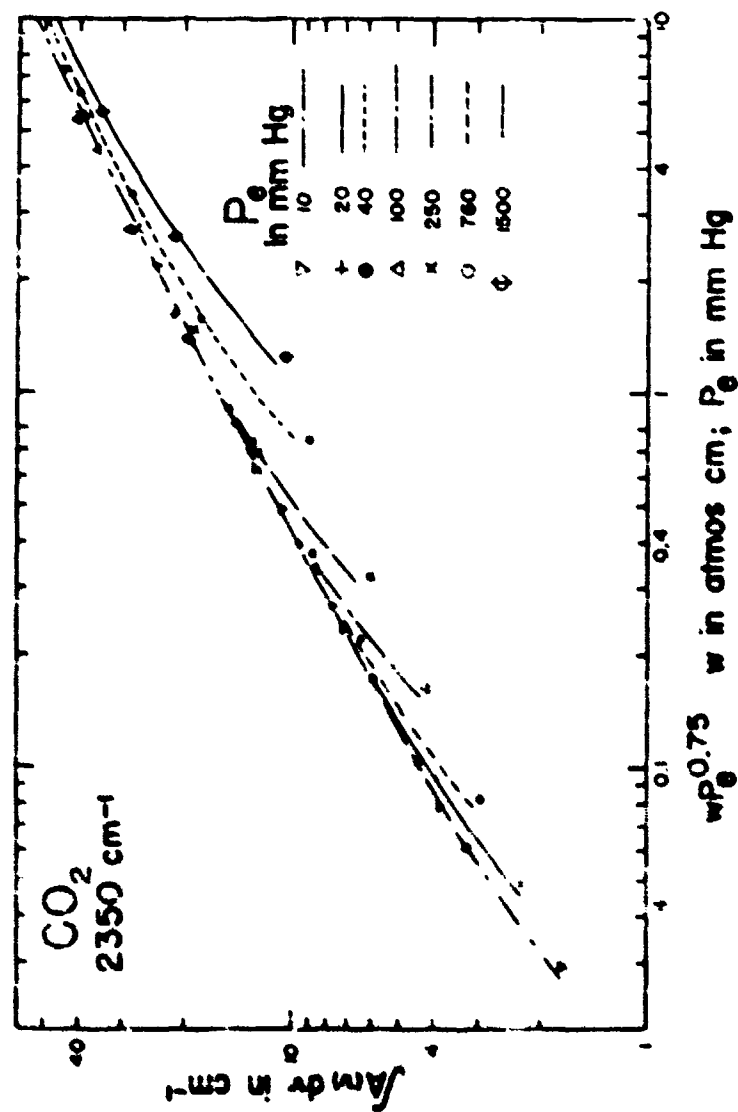


Fig. 1. The total absorption of the CO₂ and CO₂ band versus $wP_{0.75}$.

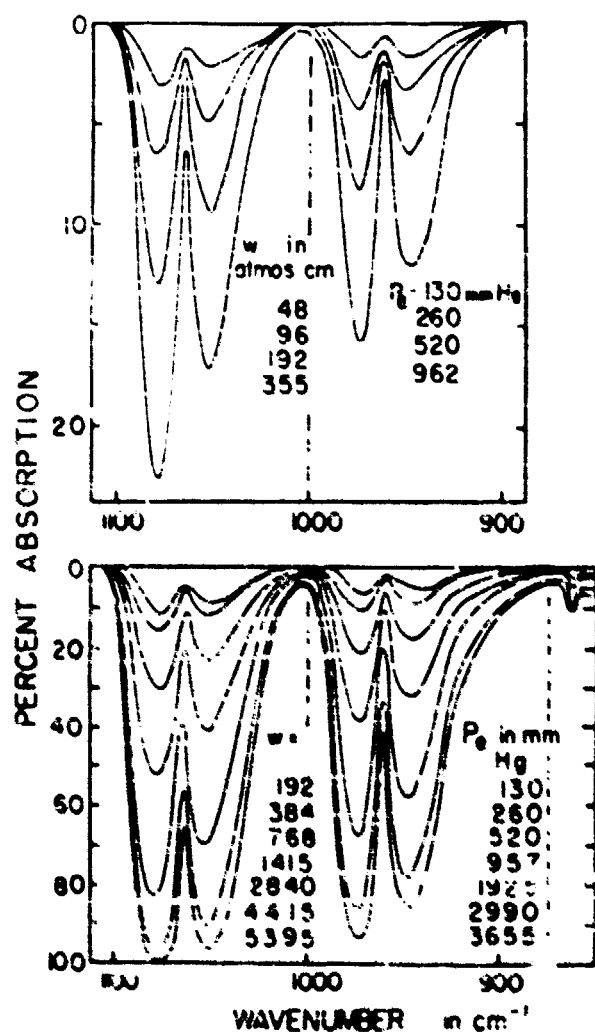


Fig. 16. Absorption curves of the 10 μ and 9.6 μ CO₂ bands. The ordinate scale of the spectrometer was extended by a factor of 5 while obtaining spectra shown in the upper portion of the figure.

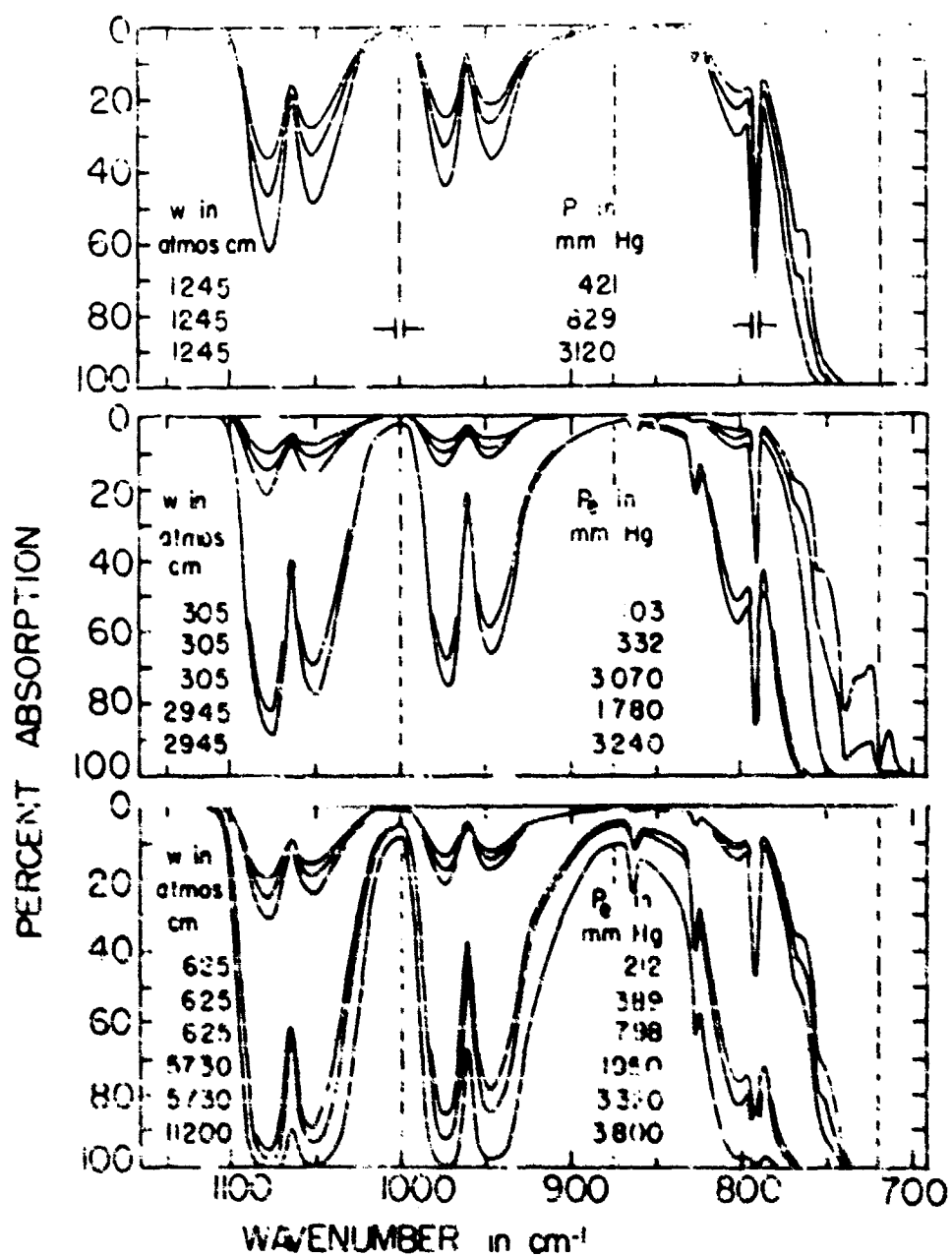


Fig. 1. Absorption curves of the 1004 and 951 cm^{-1} CO bands and the 1004 cm^{-1} sub-region. Results of the 1004 cm^{-1} sub-region are discussed in Section VI. The spectral calibrations indicated in the upper portion of the figure apply to the curves in Figs. 1a-c.

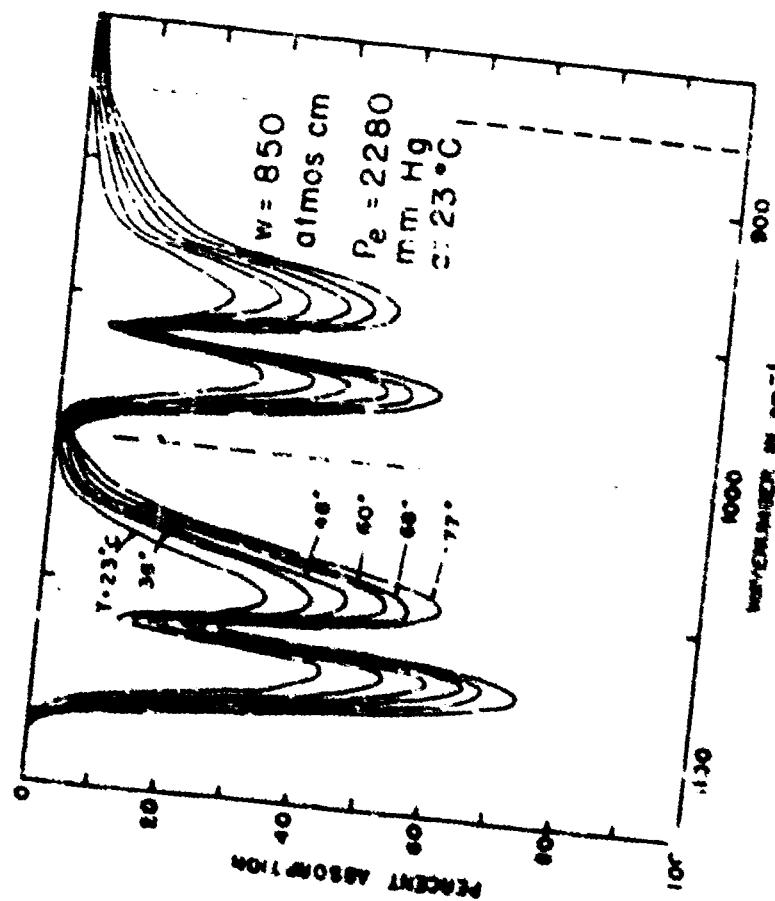


FIG. 18 Absorption curves of the 1024 and 816 μm^{-1} bands for a diene sample at various temperatures above ambient.

The data for the 1064 and 961 cm^{-1} bands are shown in Table 3, which includes the sample temperature, to the nearest 0.5 degrees C. as well as the parameters listed in Tables 1 and 2. Samples consisting of $\text{CO}_2 - \text{N}_2$ mixtures are limited to those having an absorber path length of 3200 cm .

It is recalled that the total absorption of the 1064 and 961 cm^{-1} bands is strongly dependent on temperature; it was therefore necessary to correct the values of total absorption to the same temperature. The values of total absorption of all the samples studied near room temperature were corrected to 26°C , which was approximately the average temperature. The necessary corrections were determined from the information given near the end of this section concerning the growth of the bands with increasing temperature. All figures which relate the total absorption of these bands to y and P_0 therefore correspond to 26°C .

In part A of Fig. 19, the values of total absorption of the samples of CO_2 alone are plotted against P_0 for the 1064 cm^{-1} band. Each curve corresponds to a given path length and y is therefore proportional to P_0 . In part B of Fig. 19 total absorption is also plotted against P_0 , but each curve corresponds to a given value of y as indicated.

Values were taken from the curves of Fig. 19 to obtain the curves of Fig. 20. In part A the total absorption was plotted against y for the different values of P_0 indicated. Part B was included to demonstrate the relationship between total absorption and the variable $yP_0^{0.30}$ where the value of the empirical constant was determined in the same manner as for Fig. 10. All of the points shown in part B of Fig. 20 were obtained from the curves of Fig. 19; and it is seen that a single curve fits pretty well all of the points corresponding to the different values of P_0 . From this curve the following equation was derived and the limits of validity were determined for the 1064 cm^{-1} band:

$$\int \Delta(\nu) d\nu = 0.123 (yP_0^{0.30})^{0.75} \quad (9)$$

for

$$0 < \int \Delta(\nu) d\nu < 100\text{ cm}^{-1}$$

and

$$100 < P_0 < 760\text{ mm Hg}.$$

Curves similar to those in Figs. 19 and 20 were drawn for the 961 cm^{-1} CO_2 band in Figs. 21 and 22. It is seen in part B of Fig. 22 that the total absorption can be represented by a function of the variable $yP_0^{0.25}$; from this portion of the figure the following equation

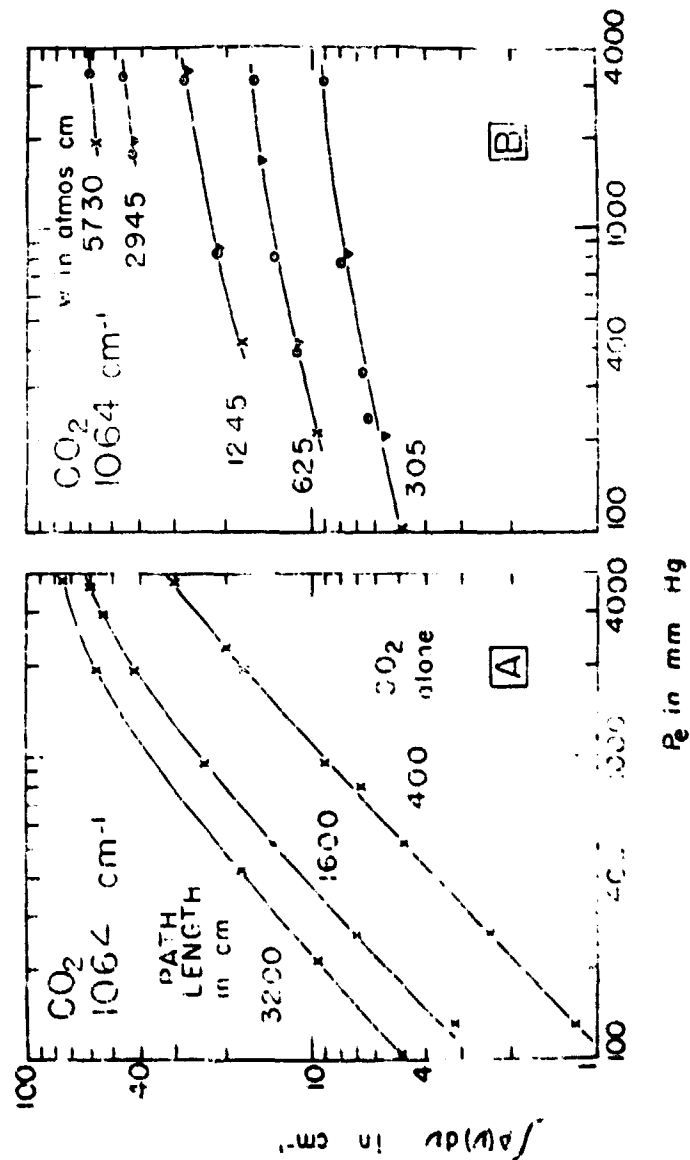


Fig. 19. The total absorption of the 1064 cm⁻¹ CO₂ band versus equivalent pressure. In part A each curve corresponds to a given absorber path length and w is therefore proportional to P_e . In part B each curve corresponds to a given value of w . K 's represent samples of CO₂ alone; Δ 's represent samples of CO₂ and H₂O's in part B represent values taken from curves of part A.

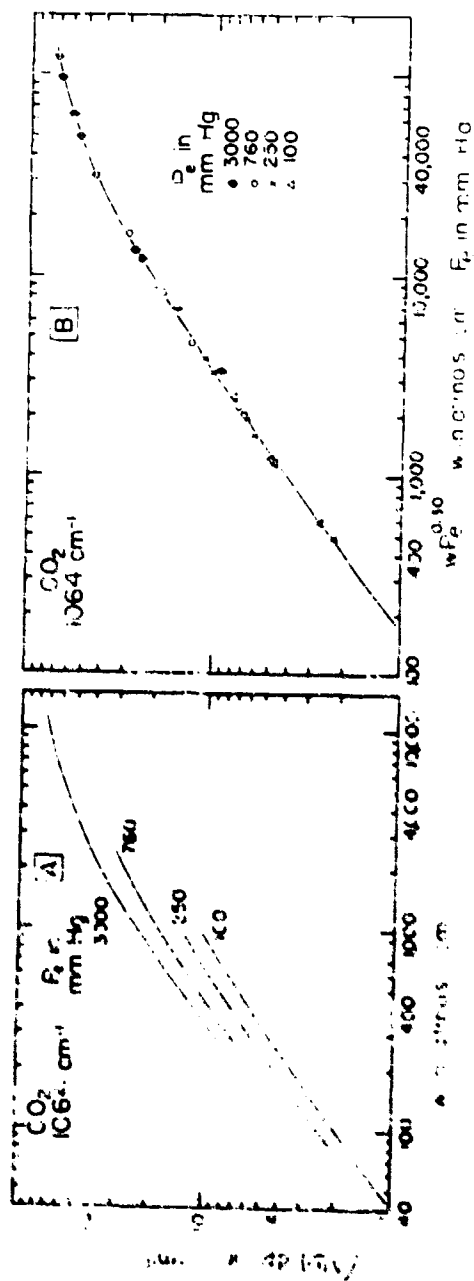


Fig. 20. The total absorption of the 1064 cm⁻¹ CO₂ band versus ν in part A; and versus ν/ν_0 in part B.

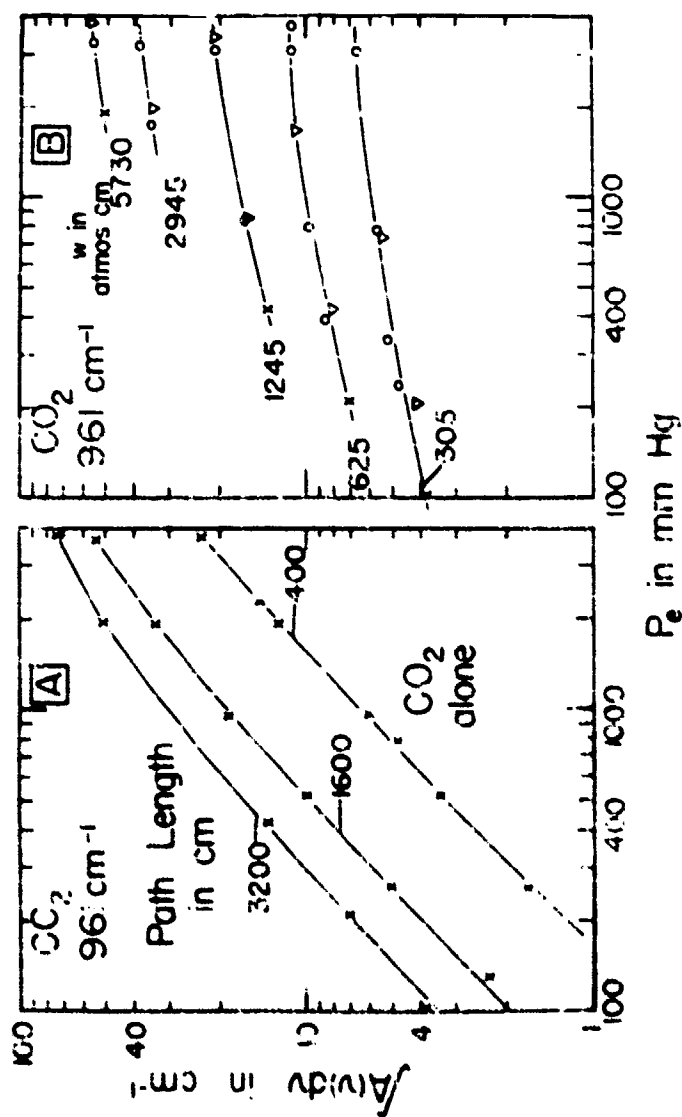


Fig. 2. The total absorption of the 961 cm^{-1} CO_2 band versus equivalent pressure. In part A each curve corresponds to a given absorption path length and w is therefore proportional to P_e . In part B each curve corresponds to a given value of w . X's represent samples of CO_2 alone; C's represent samples of CO_2 and H_2O . V's in part B represent values taken from curves in part A.

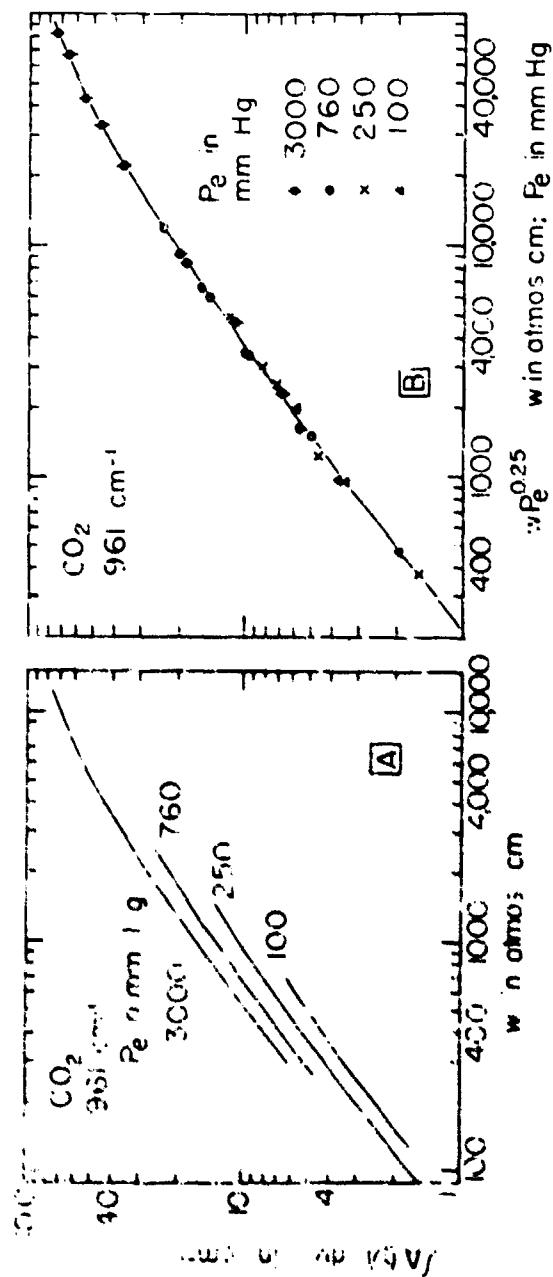


Fig. 22. The total absorption of the 961 cm^{-1} CO_2 band versus w in part A, and versus $w P_e^{0.25}$ in part B.

was derived and its limits of validity were determined for the 961 cm^{-1} CO_2 band:

$$\int A(\nu) d\nu = 0.016 [\nu P_0]^{0.25} 0.78 \quad (10)$$

for

$$1 < \int A(\nu) d\nu < 35 \text{ cm}^{-1}$$

and

$$100 < P_0 < 760 \text{ mm Hg}.$$

A. EFFECT OF TEMPERATURE ON TOTAL ABSORPTION

In order to obtain information on the temperature dependence of the total absorption, absorption curves were recorded for three different sets of samples at temperatures above ambient. A thermometer was placed in each end of the cell and a temperature difference between the ends was found to exist. This difference was approximately 1°C for temperatures near ambient and increased to approximately 4°C for temperatures near 75°C . The temperature tabulated in Table 3 is an average of the two to the nearest 0.5°C . It was not possible to cool the absorption cell.

Absorption curves corresponding to one of the sets of samples investigated at different temperatures are shown in Fig. 18; and the fractional absorption is seen to increase with temperature at all frequencies. Values of total absorption for both bands are plotted against temperature in parts A and B of Fig. 25. The curves of parts A and B as well as parts C and D are discussed below in determining a quantitative relationship between total absorption and temperature.

There are several factors which might contribute to the change in total absorption with temperature. One of these factors involves the collision frequency of the absorbing molecules, which is proportional to the line half width α . The change in α with temperature is believed to contribute only a minor part of the increase in total absorption with temperature of the two bands under consideration. This belief is based on the fact that the total absorption of the 2350 cm^{-1} CO_2 band, as well as other fundamental bands, increases only slightly with temperature, and one would not expect the half-width of the lines of one CO_2 band to increase more rapidly with temperature than the lines of another CO_2 band.

Undoubtedly, the most important factor contributing to the increase in total absorption with temperature is increase in the population of

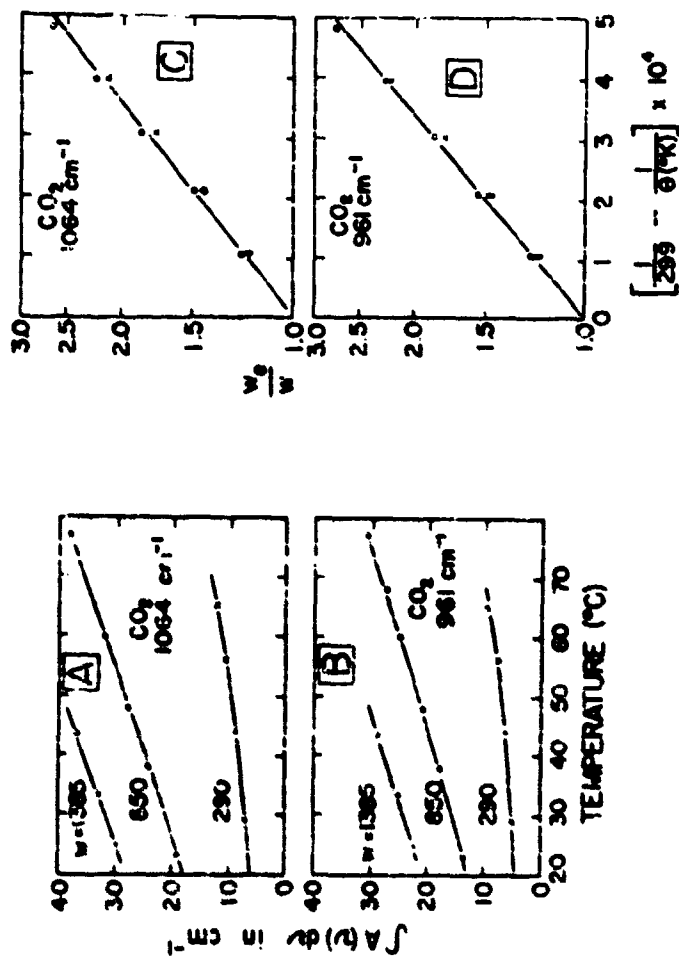


Fig. 25. Temperature dependence of the total absorption of the 1064 and 961 cm^{-1} CO_2 bands. Parts A and B relate the total absorption to temperature for three different samples. Parts C and D relate the effective concentration ratio to a quantity based on the calculated change in population of the lower vibrational energy level. The $\pm 2.0^\circ\text{C}$ and $\pm 1^\circ\text{C}$ in C and D each correspond to the same sample as in A and B.

the lower vibrational energy state giving rise to the absorption. Another less important factor is the redistribution of the population of the rotational energy levels associated with the lower vibrational state. One would expect that the latter factor would result in a change in the shape of the band, but its effect on the total absorption would be small in comparison with the effect of the change in population of the lower vibrational energy state.

The lower vibrational states of the 1064 cm^{-1} band and the 961 cm^{-1} band are designated by (0200) and (1000), respectively. Their energy levels are 1286 cm^{-1} and 1388 cm^{-1} above the zero-point energy level (0000).

The quantity $r(\theta)$ is defined as the fraction of the molecules of a Boltzmann gas in the energy state E_i at temperature θ (in $^{\circ}\text{K}$). If E_i is the energy above the zero-point energy level of one of the lower vibrational states involved in the present investigation, and θ_1 and θ_2 are two temperatures near room temperature, it can be shown that the following expression is approximately true:

$$\frac{r(\theta_2)}{r(\theta_1)} = \exp \left[\frac{E_i}{k} \left(\frac{1}{\theta_1} - \frac{1}{\theta_2} \right) \right] \quad (11)$$

If one assumes that an increase in the population of the lower energy state by increased temperature produces the same effect on the total absorption as the same relative increase in absorber concentration v at constant temperature, it follows from Eq. (11) that an effective concentration v_e can be found by

$$v_e = v \exp \left[\frac{E_i}{k} \left(\frac{1}{\theta_1} - \frac{1}{\theta_2} \right) \right], \quad (12)$$

where $v_e = v$ at temperature θ_1 . On the basis of Eq. (12) we would expect that experimentally determined values of $\log (v_e/v)$ would yield a straight line if plotted against $(1/\theta_1 - 1/\theta_2)$. Values of v_e/v were determined from the data and the suggested curves plotted in the following manner.

From the curve in part A of Fig. 23 corresponding to $v = 850$ atmos cm, one sees that a total absorption of 20.0 cm^{-1} for the 1064 cm^{-1} band corresponds to a temperature of 26°C , and a total absorption of 23.4 cm^{-1}

corresponds to a temperature of 36°C. From the curve in Fig. 20 one sees that total absorptions of 20.0 cm⁻¹ and 23.4 cm⁻¹ correspond to values of w_e equal to 8800 and 10,900, respectively. The actual value of w_e is not important, but the apparent effective concentration is increased by 10,900/8800 = 1.24. Similar calculations were made for 46, 56, 66, and 76°C and for the curves corresponding to $v = 1385$ and 290 atmos cm. The ratio w_e/w is based on $w_e = w$ at 26°C for all curves. The calculated values of w_e/w for the three different sets of samples were plotted in part C of Fig. 23 in the manner suggested above.

One sees that the points in part C of Fig. 23 form a straight line, within expected experimental error; and it was found that an effective absorber concentration can be calculated by the following equation:

$$w_e = w \exp[1950 (1/299 - 1/\theta)] \quad (13)$$

where the factor (1950) was determined from the slope of the line in part C of Fig. 23.

Similar calculations were made for the 961 cm⁻¹ band; calculated values of w_e/w are plotted in part D of Fig. 23. From the slope of the line, it was found that the effective absorber concentration for the 961 cm⁻¹ band is given by

$$w_e = w \exp[2040 (1/299 - 1/\theta)] \quad (14)$$

The experimentally determined constants, 1950 and 2040, in Eqs. (13) and (14) can be compared with E_1/k from Eq. (11). If the energy value 1286 cm⁻¹, which corresponds to the 1064 cm⁻¹ band, is substituted for E_1 in Eq. (11), one obtains 1850 in comparison with the experimentally determined value of 1950. Similarly, if 1388 cm⁻¹ is substituted in Eq. (11), one obtains 2000 in comparison with the experimentally determined value of 2040 for the 961 cm⁻¹ band. In view of the assumption made and the possible experimental errors, this agreement is quite good. One then concludes that the dependence of total absorption of these "hot bands" on temperature can be approximately explained on the basis of an increase in effective absorber concentration which is proportional to the increase in the population of the lower vibrational states.

On the basis of this conclusion, one would expect that Eqs. (9) and (10) could be used to predict the total absorption of sample at temperatures between 20°C and 70°C by substituting for w the value of w_e from Eqs. (13) or (14) respectively.

B. COMPARISON OF PRESENT RESULTS WITH THOSE OF EDWARDS

Edwards⁶ has recently published results of measurements of total absorption of several CO₂ bands at temperatures from ambient up to 1390°K. The samples for which Edwards measured the total absorption of the 1064 and 961 cm⁻¹ bands contained relatively small values of \bar{w} ; the total absorption for the samples at room temperature was therefore small and the uncertainty was rather large. The equivalent pressures of many of the samples investigated by Edwards were considerably higher than the maximum value of 3000 mm Hg used in the present study; therefore, there are only a few of his results which can be compared directly with those of the present study. The total absorptions of the samples which could be compared were in most cases approximately 30 to 40% less than the values predicted for these samples on the basis of the curves in Figs. 20 and 22. Even this large difference was within the experimental uncertainty since the total absorptions being measured were small.

The ranges of temperatures covered by the two investigations of the 1064 and 961 cm⁻¹ band were so different that the results could not be compared.

Edwards also investigated the total absorption by the other CO₂ bands covered in the present study. His results for the 875-495 cm⁻¹ region will be compared to the present results in the next section. The results of the 3716 + 3609 cm⁻¹ bands and the 2350 cm⁻¹ band could not be compared since the total absorption of the smallest sample studied by Edwards was approximately equal to that of the largest sample used in the present study.

VI. EXPERIMENTAL RESULTS FOR THE 875 - 495 cm⁻¹ SPECTRAL REGION

The 875 - 495 cm⁻¹ spectral region was divided into five sub-regions for the purpose of analysis. Tracings of many of the absorption curves are shown in Figs. 24 - 32; the curves of Fig. 32 correspond to samples of CO₂ alone at various temperatures above ambient, while absorption curves in the other figures correspond to samples near ambient temperature. The spectral slit-width indicated at various frequencies: in Fig. 24 applies to the absorption curves in Figs. 24, 25, and 26, which were obtained with the Model 99 spectrometer; while the spectral slit-width indicated in Fig. 31 applied to the absorption curve in Figs. 27-32 which were obtained with the Model 21 spectrometer.

The data are presented in Table 4, which includes the values of the mean fractional absorption $\bar{A}(v_1-v_2)$ for each spectral sub-region as well as the total absorption $\int A(v)dv$ for the entire spectral region 495 - 875 cm⁻¹, which was included for possible future by other workers.

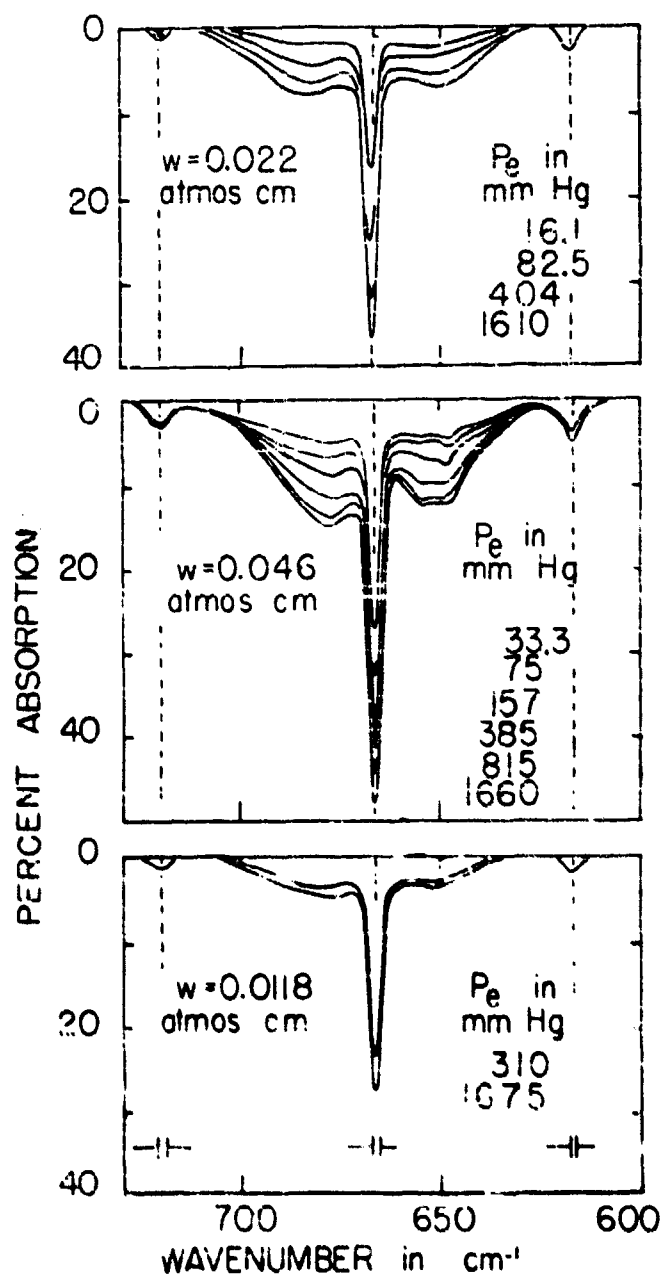


Fig. 24 Absorption curves of the $675-695 \text{ cm}^{-1}$ CO₂ region. The spectral slit-widths indicated in the lower portion of the figure apply to the curves in Figs. 24-26.

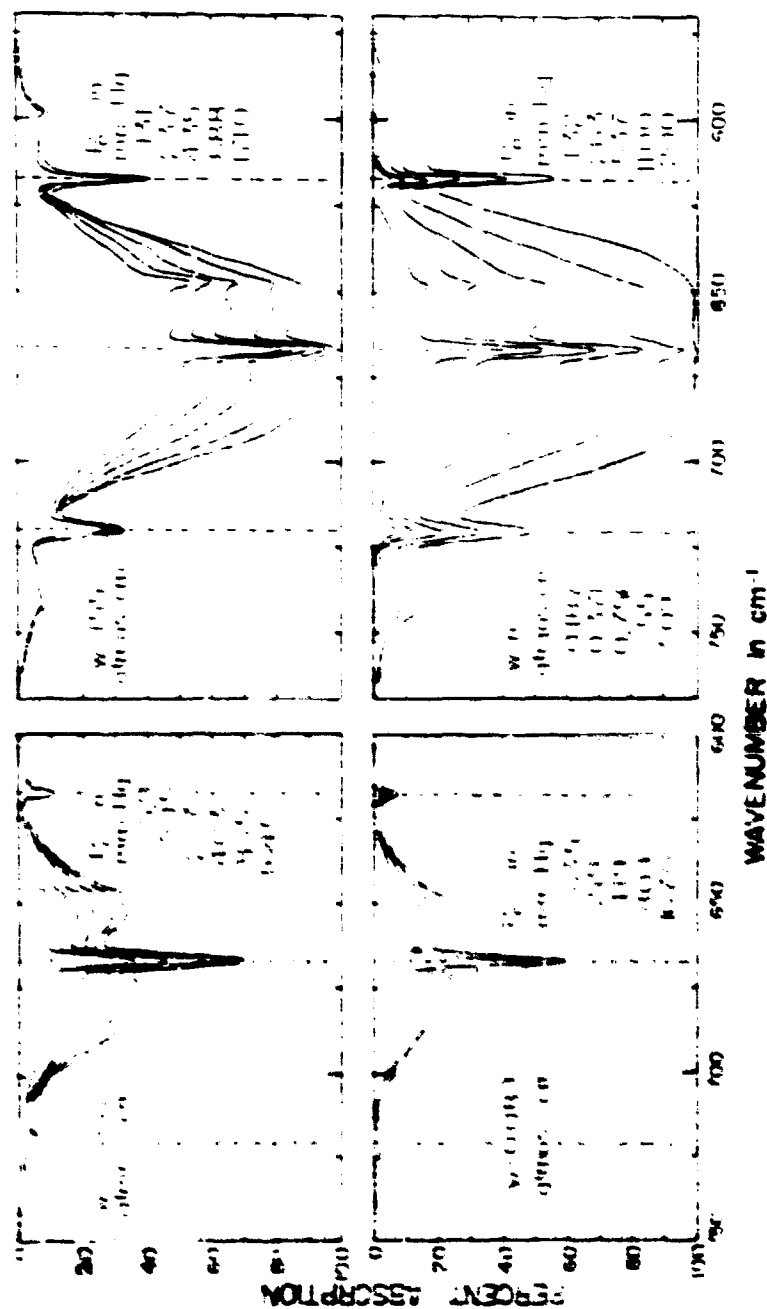


Fig. 1. Infrared spectra of the γ -irradiated samples.

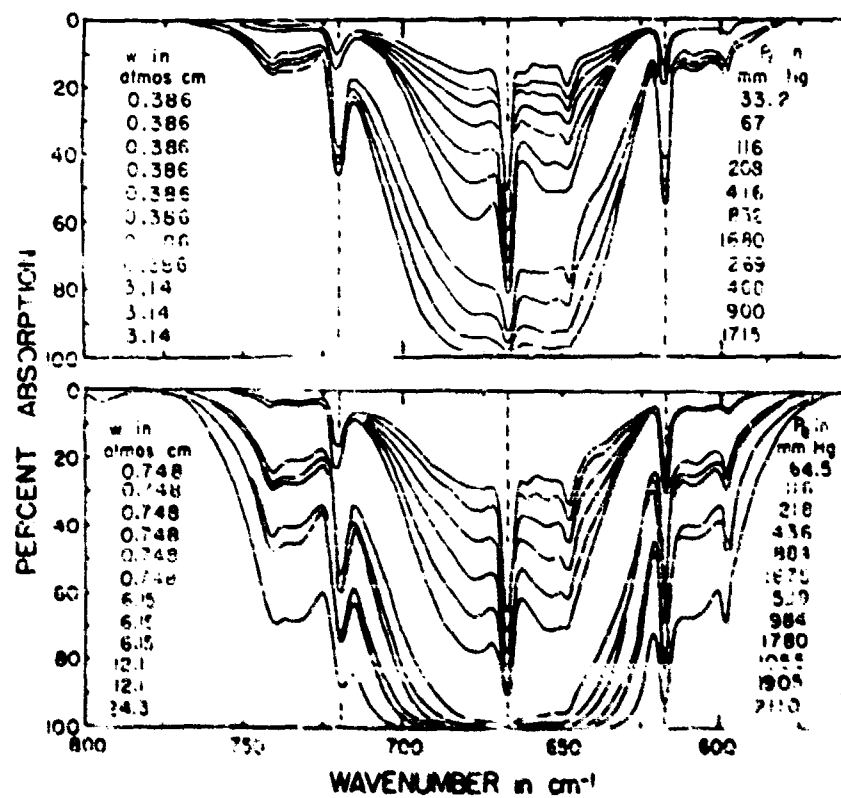


Fig. 26. Absorption curves of the H₂O₂ cell, Fig. 1, ion.

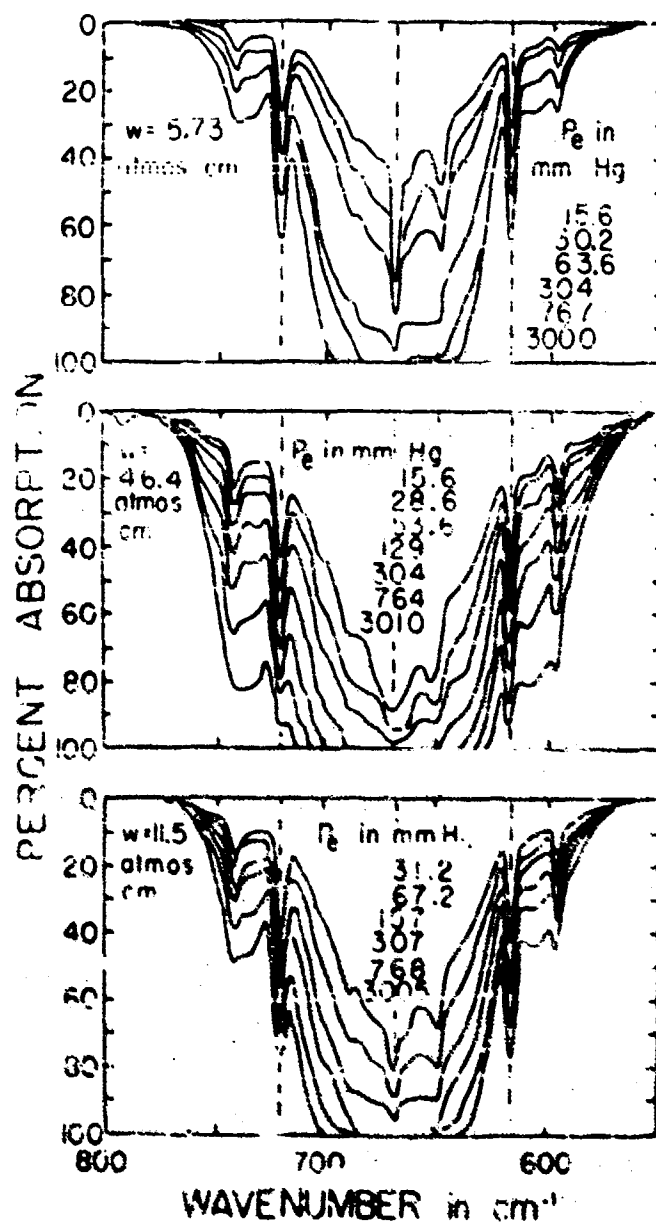
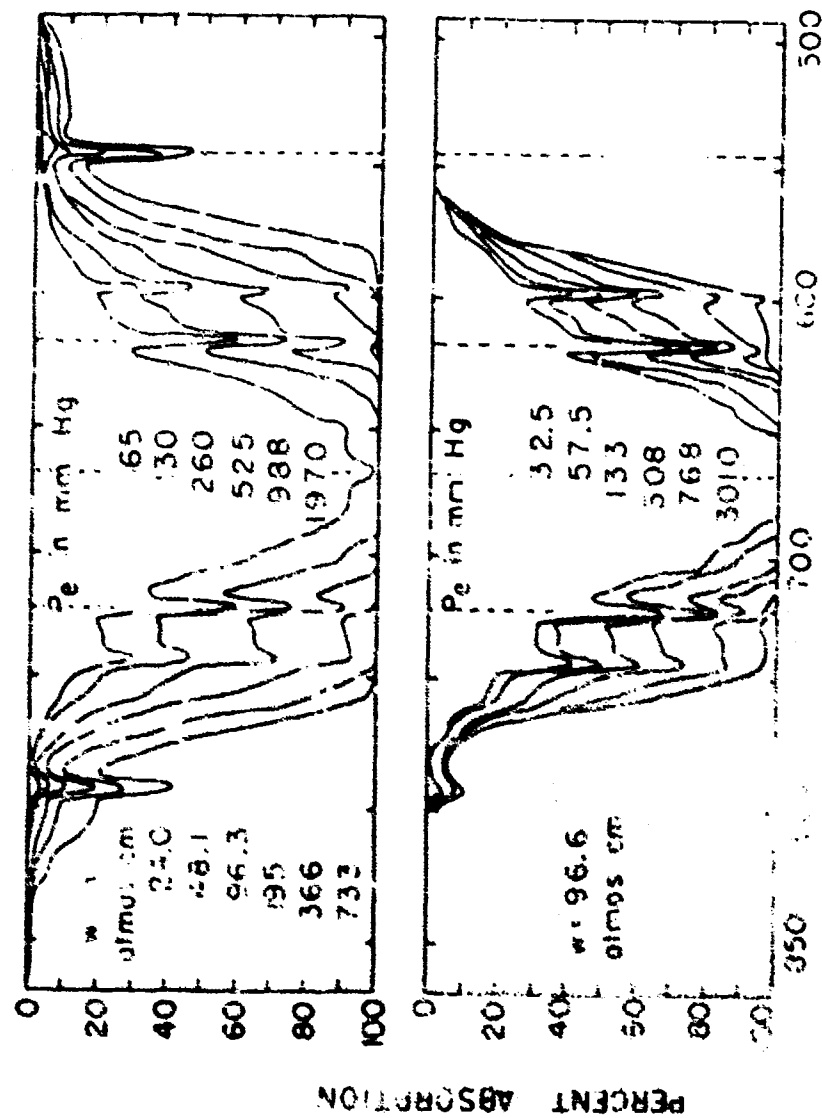


Fig. 87 Absorption curves of the 600-800 cm^{-1} region.



WAVENUMBER in cm^{-1}

Fig. 22. Infrared curves of the H_2O and H_2O region.

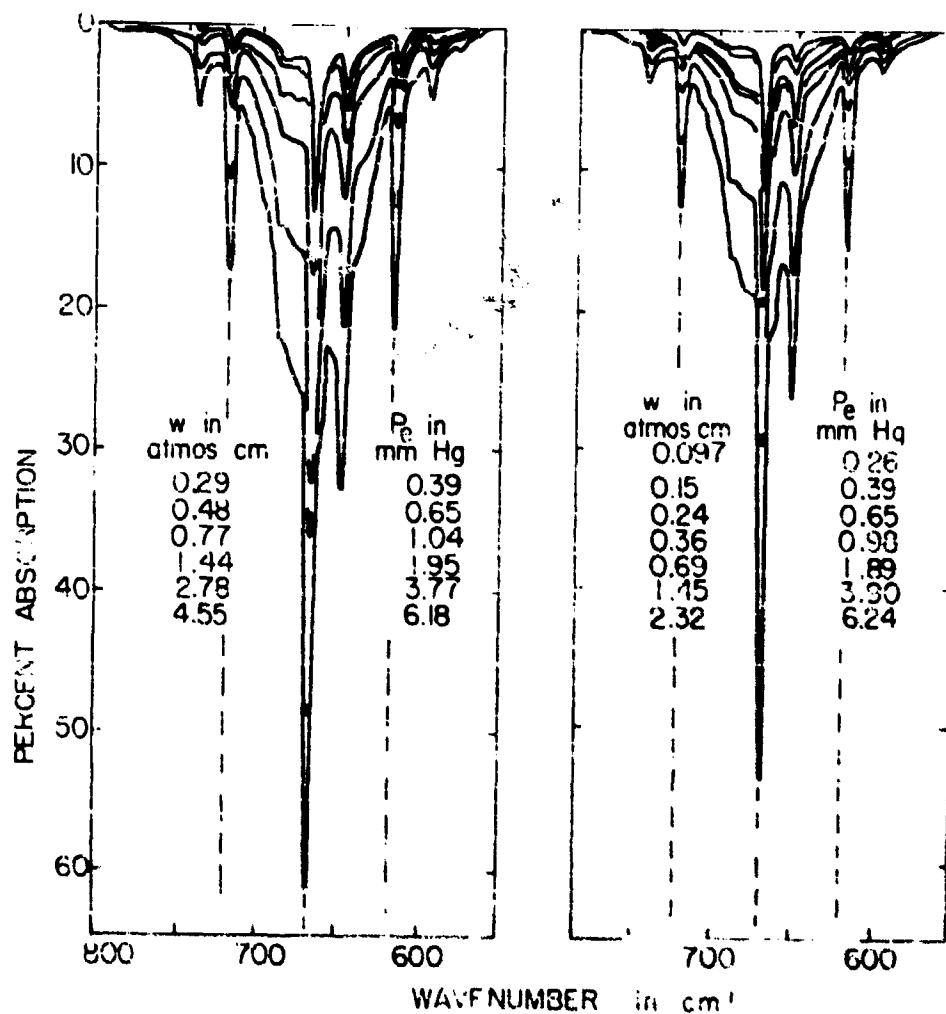


Fig. 29. Absorption curves of the $617-667 \text{ cm}^{-1}$ CO_2 region.

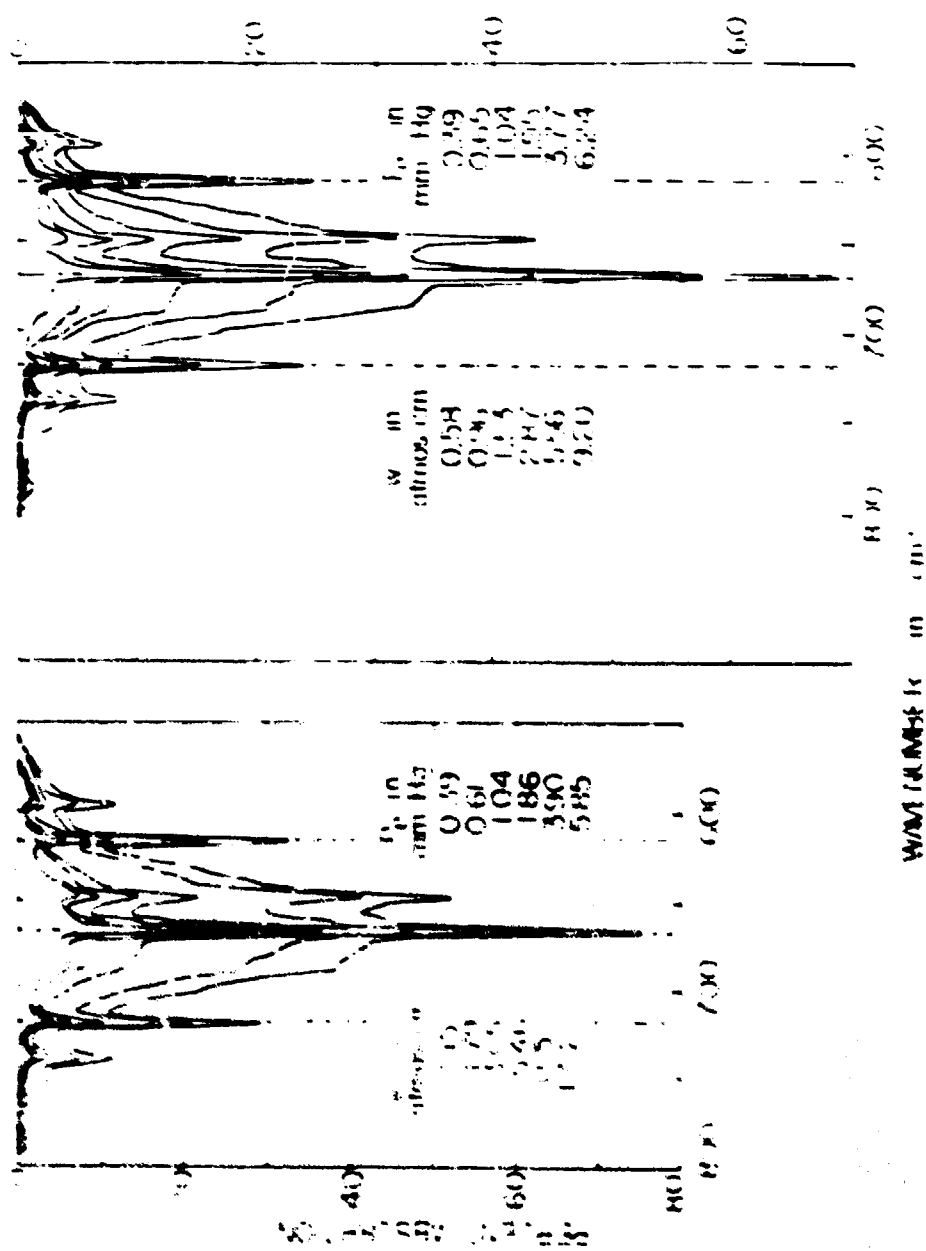


Fig. 20. Absorption curves in the 10-100 cm⁻¹ region.

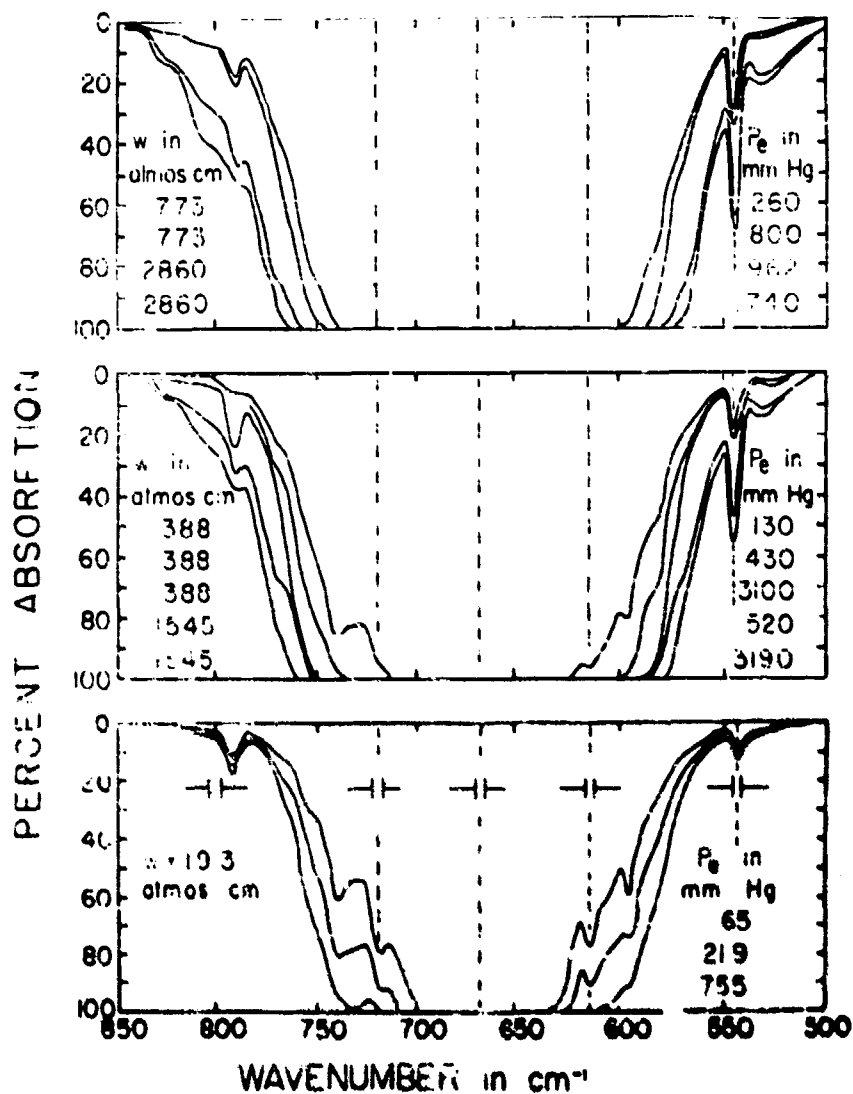


Fig. 31. Absorption curves of the 674-495 cm^{-1} CO_2 region. The spectral slit-widths indicated in the lower portion of the figure apply to the curves in Figs. 27-30.

In the case of samples having small value of y , the major portion of the absorption occurs near the strong fundamental band at 667 cm^{-1} .

In Fig. 33 are plotted six curves, each corresponding to a different absorber path length, which relate $\bar{A}(720-875\text{ cm}^{-1})$ to P_0 for samples of CO_2 alone. It is noted that the values of $\bar{A}(v_1-v_2)$ which are plotted in Figs. 33-45 have been corrected to a temperature of 26°C by use of the curves of Fig. 46, which relate the increase in $\bar{A}(v_1-v_2)$ to temperature.

$\bar{A}(720-875\text{ cm}^{-1})$ was plotted against P_0 in Fig. 34, where each curve corresponds to a given value of y as indicated. The x 's correspond to samples of CO_2 alone and the \circ 's to samples formed by adding N_2 to the CO_2 sample. The triangles on each curve correspond to values taken from the curves of Fig. 33; these values were obtained by first calculating for each cell path length the value of P_0 which corresponded to the values of y listed on the curves of Fig. 34. The values of $\bar{A}(720-875\text{ cm}^{-1})$ corresponding to the calculated values of P_0 were then determined from Fig. 33 and plotted in Fig. 34. By using the values represented by the triangles in Fig. 34 it was possible to extend many of the curves over considerably wider ranges of values of P_0 . The sets of samples with y less than 11.5 atmos cm could have been formed by starting with small amounts of CO_2 in the 3200-cm cell and adding N_2 to obtain the required value of P_0 . This procedure was not followed since the initial partial pressure of CO_2 for each sample would have been too low for accurate measurement. Further error might also arise from adsorption of CO_2 on the cell walls; a phenomenon which is more serious at low pressures and which was discussed in some detail in Appendix I of Report 1.

The two curves in Fig. 34 corresponding to $y = 5750$ and 2945 atmos cm represent samples C38-C41, which were investigated by use of the Model 21 with a NaCl prism. The other curves represent samples investigated by use of a KBr prism, with which it was necessary to use larger spectral slit-widths.

The values of $\bar{A}(720-875\text{ cm}^{-1})$ for the NaCl data, most of which is not represented in Fig. 34 since it would result in overcrowding of the curves, were compared with values predicted on the basis of the KBr data. In most cases the difference was less than 5% with only a few values differing by as much as 8%. The differences are believed to be due chiefly to experimental errors, not to differences arising from differing spectral slit-widths.

Values of $\bar{A}(720-875\text{ cm}^{-1})$ were obtained from the curves of Fig. 34 and were plotted in Fig. 35 against y for the different y 's of P_0 indicated. The "smoothed" curves of Fig. 35 are believed to best represent the data, and the points which were used to determine these curves were marked in order that values could be read from the curves more readily. It is recommended that Fig. 35 and the corresponding figures for the other spectral sub-regions be used to determine values of $\bar{A}(v_1-v_2)$ for known samples.

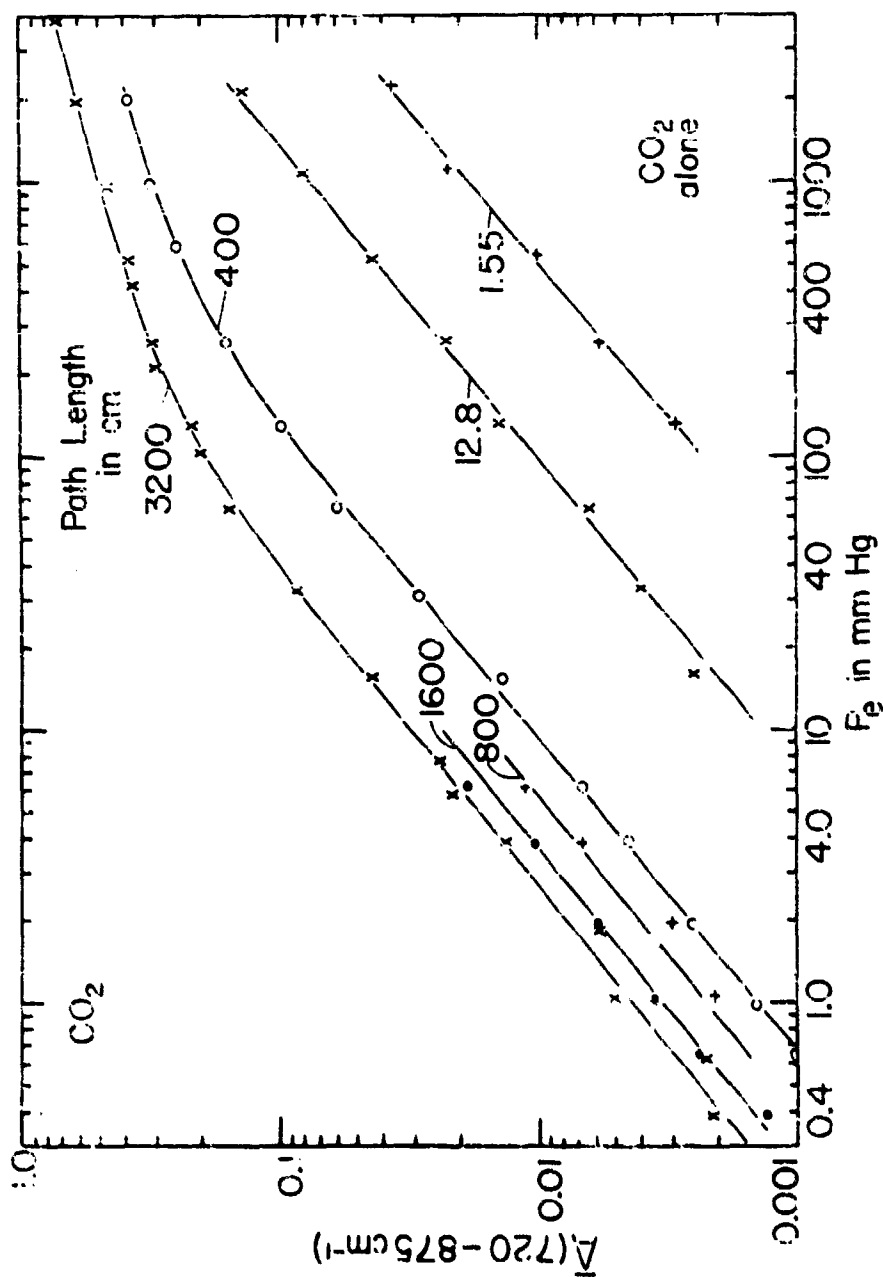


Fig. 13. $\bar{A}_{(720-875 \text{ cm}^{-1})}$ versus P_e for samples of CO₂ alone.

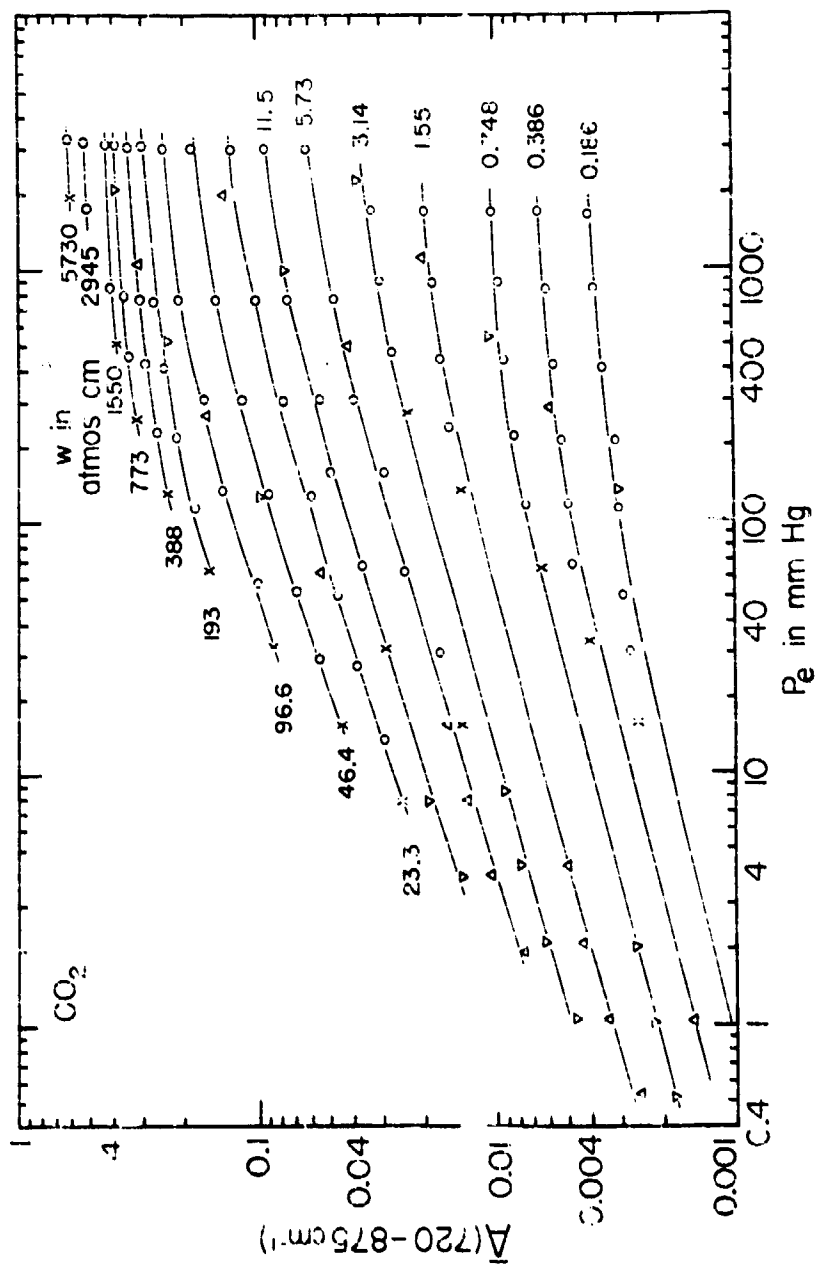


Fig. 34. $A(720-875 \text{ cm}^{-1})$ versus P_e for various values of w . X's represent samples of CO₂ alone, O's represent samples of CO₂ and N₂. Triangles represent values taken from curves of Fig. 33.

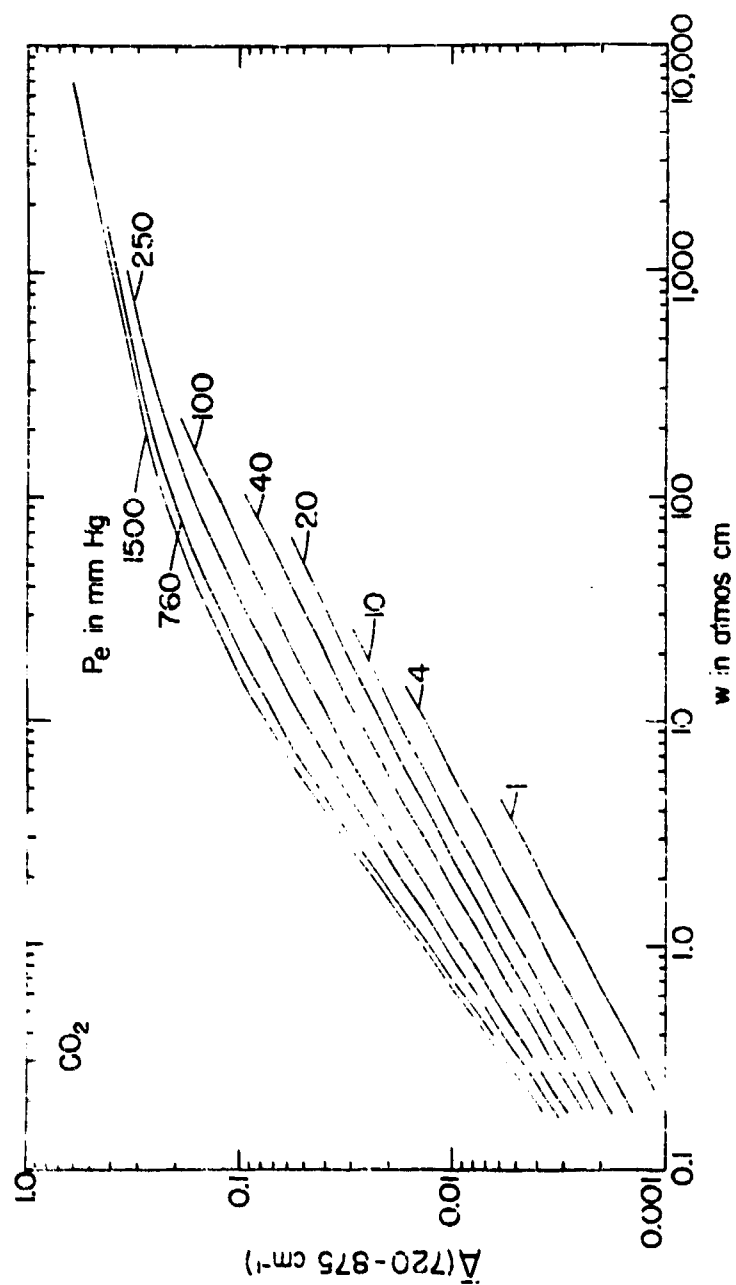


Fig. 35. $\bar{A}(720-875 \text{ cm}^{-1})$ versus w for various values of P_e .

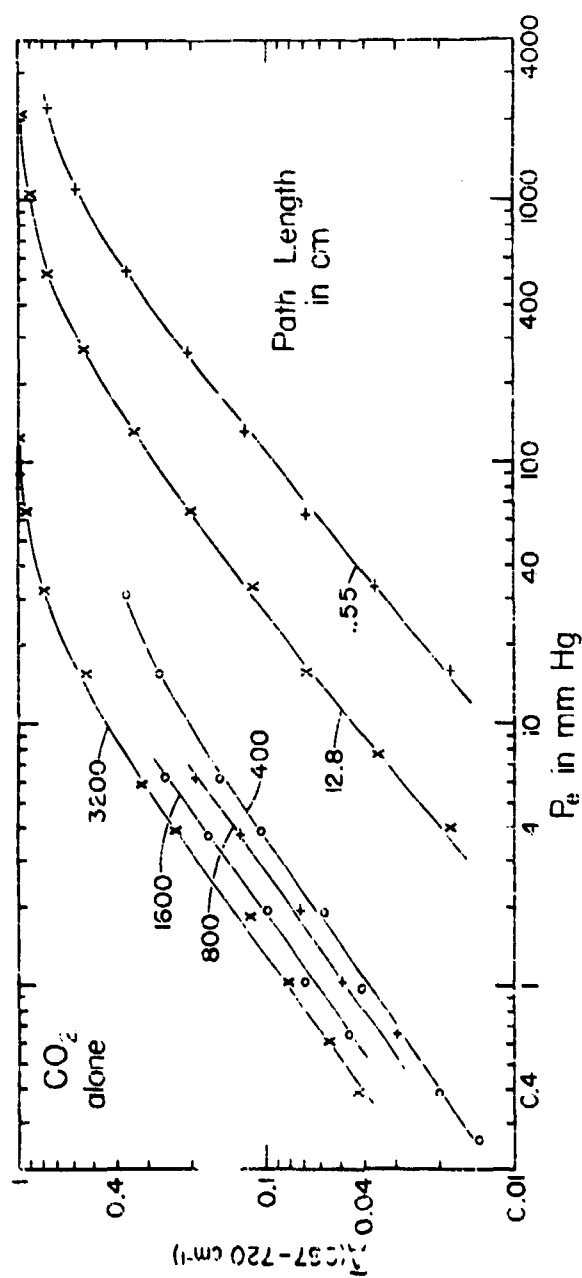


Fig. 36. $\bar{\lambda}$ (667-720 cm^{-1}) versus P_e for samples of CO₂ alone.

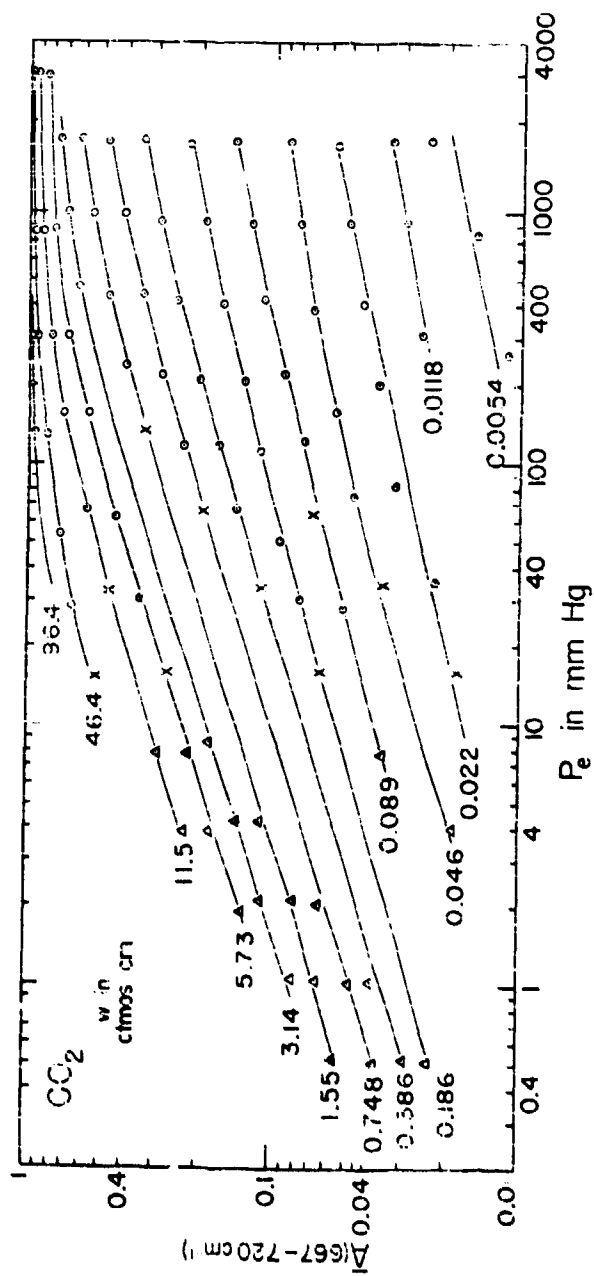


Fig. 57. $T(667-720 \text{ cm}^{-1})$ versus P_e for various values of γ .

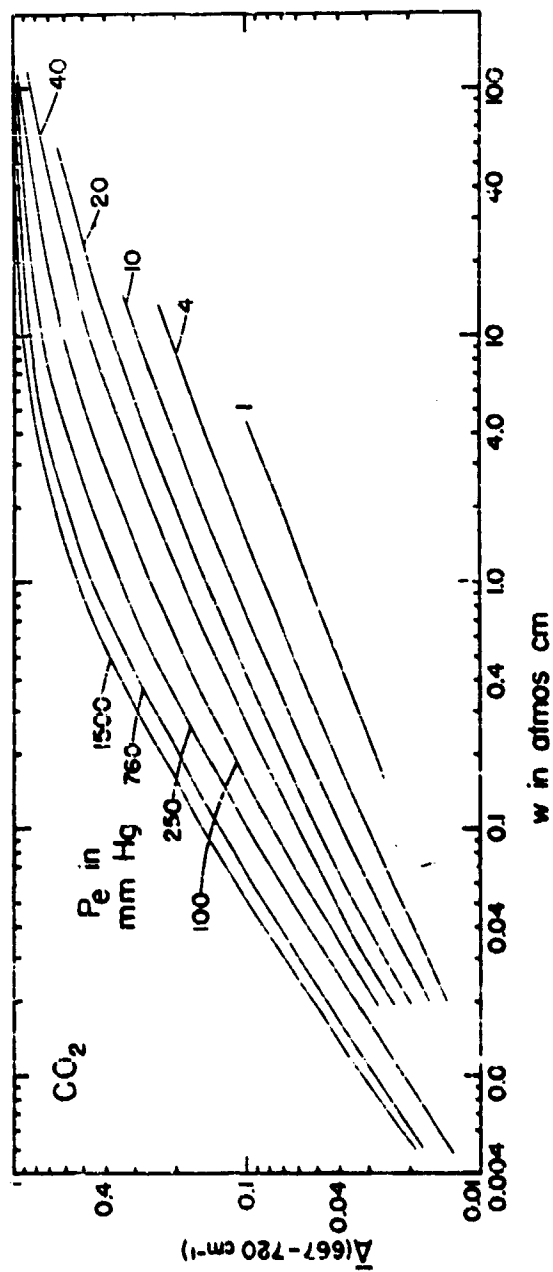


Fig. 38. $\bar{\Delta}(667-720 \text{ cm}^{-1})$ versus w for various values of P_e .

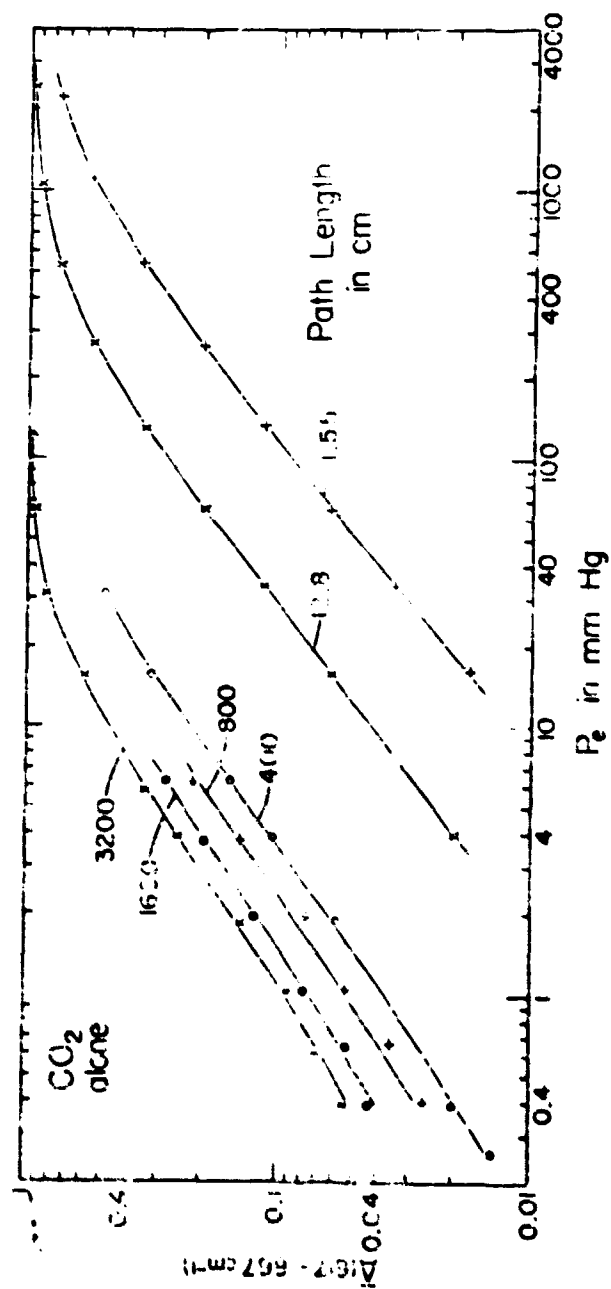


Fig. 39. Δ (517-567 cm⁻¹) versus P_2 for samples of CO₂ alone.

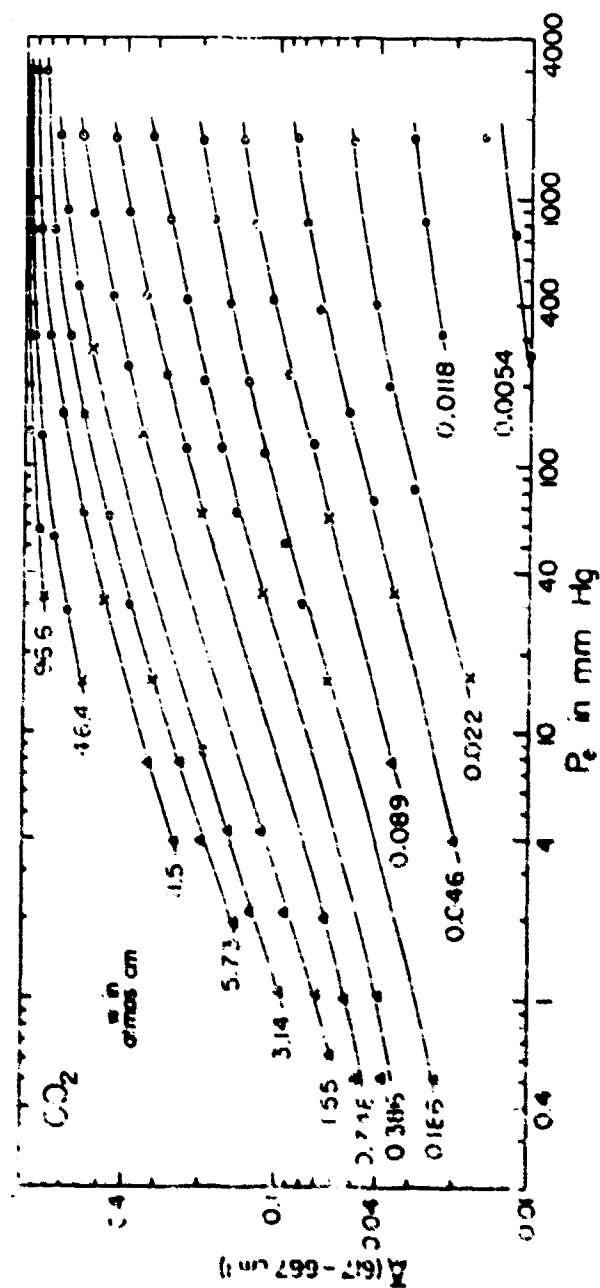


Fig. 60. $\bar{K}'(617-657 \text{ cm}^{-1})$ versus P_0 for various values of \bar{v} .

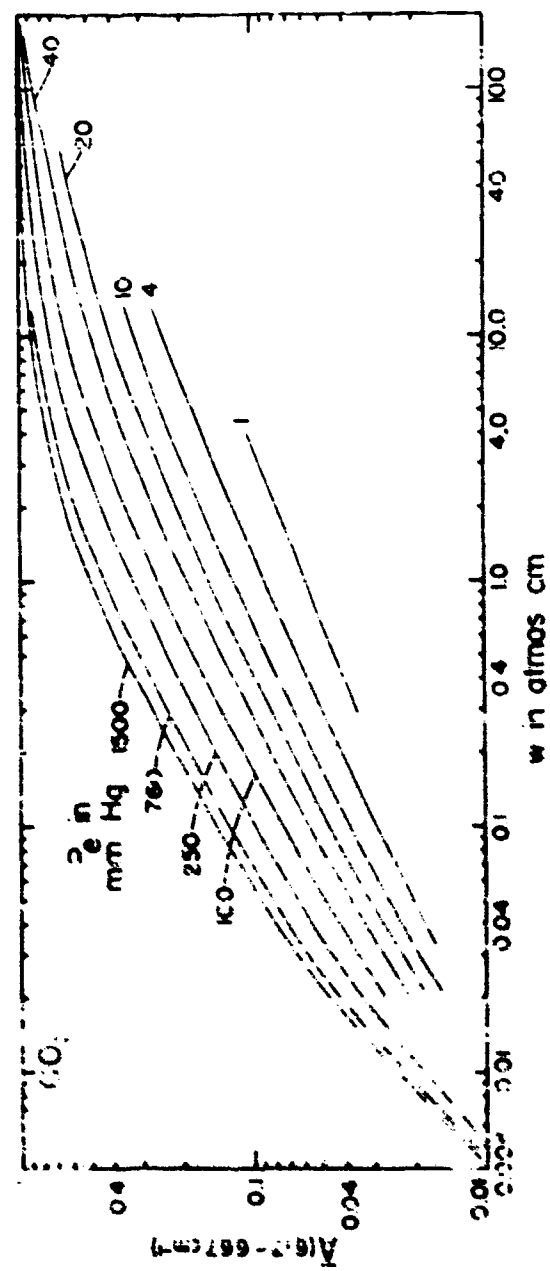


Fig. 6. $A(637-667 \text{ cm}^{-1})$ versus w for various values of p_e .

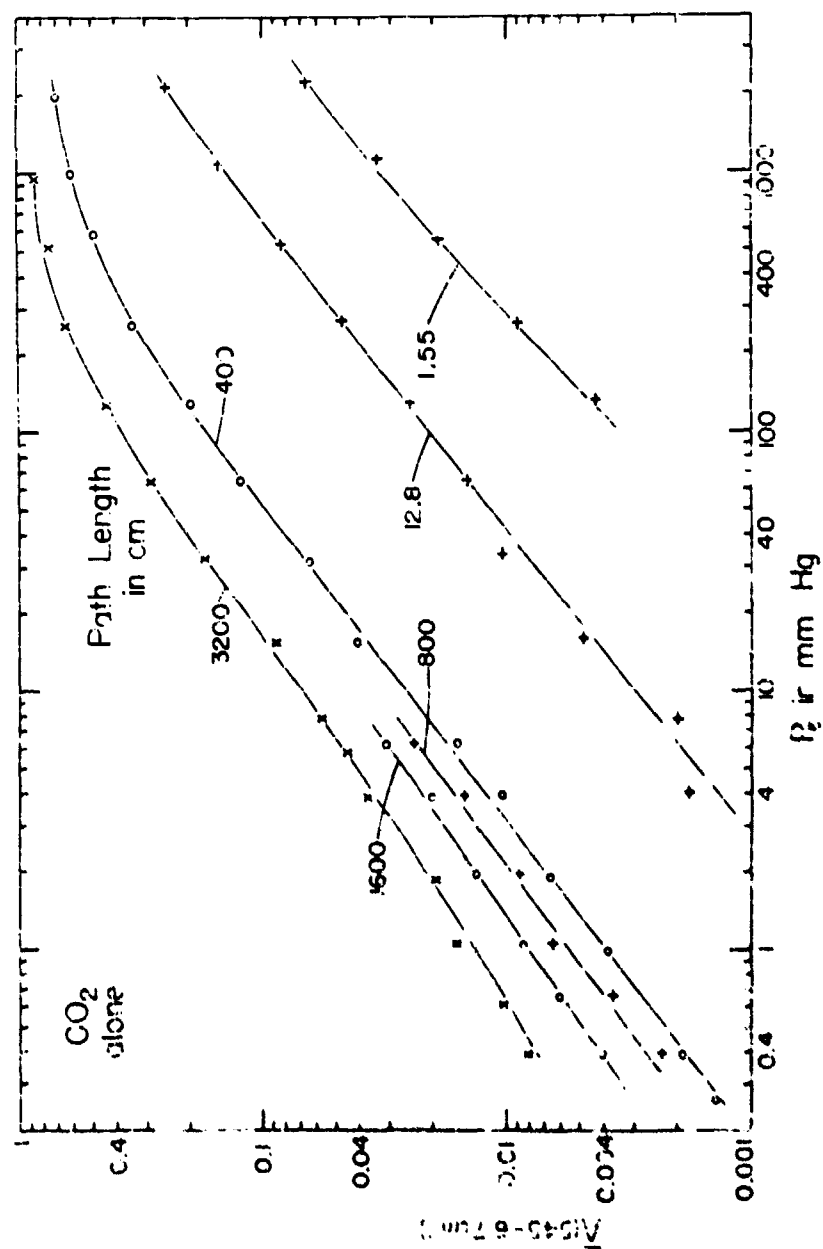


Fig. 42. $T(545-617 \text{ cm}^{-1})$ versus P_{O_2} for samples of O_2 alone.

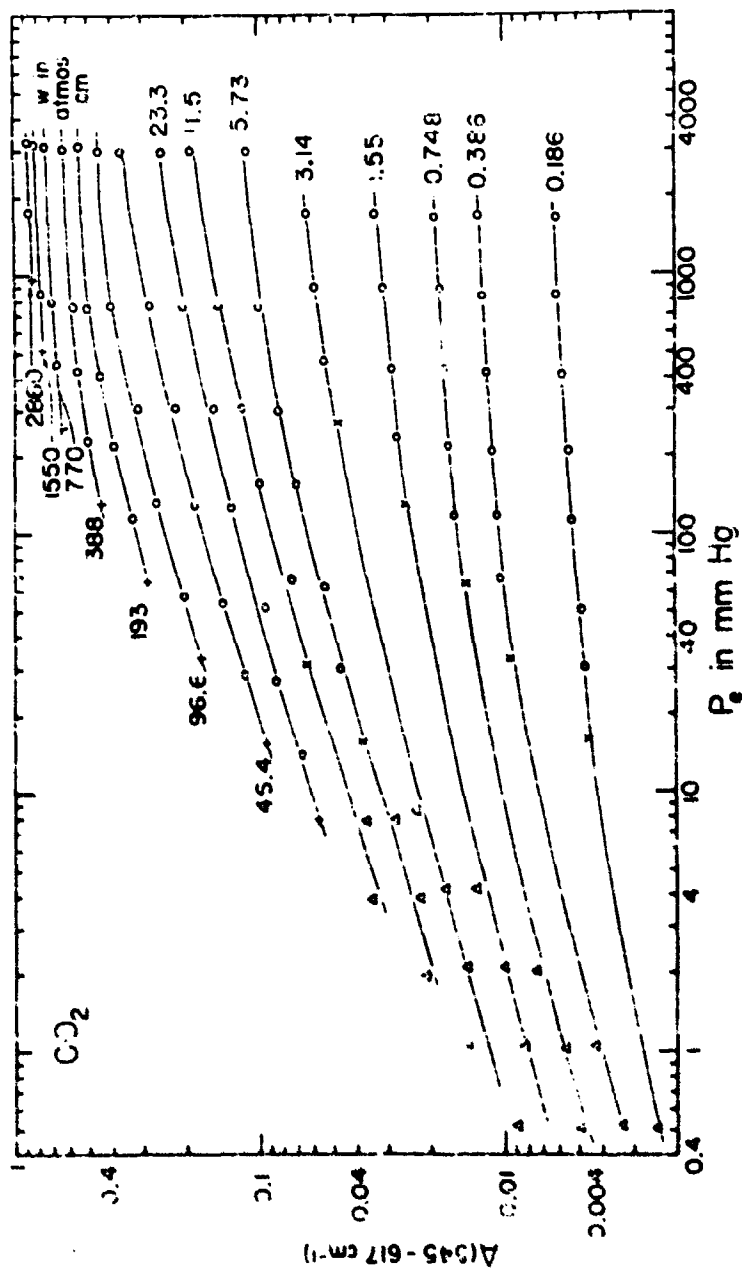


Fig. 3. $K(545-617 \text{ cm}^{-1})$ versus P_e for various values of w .

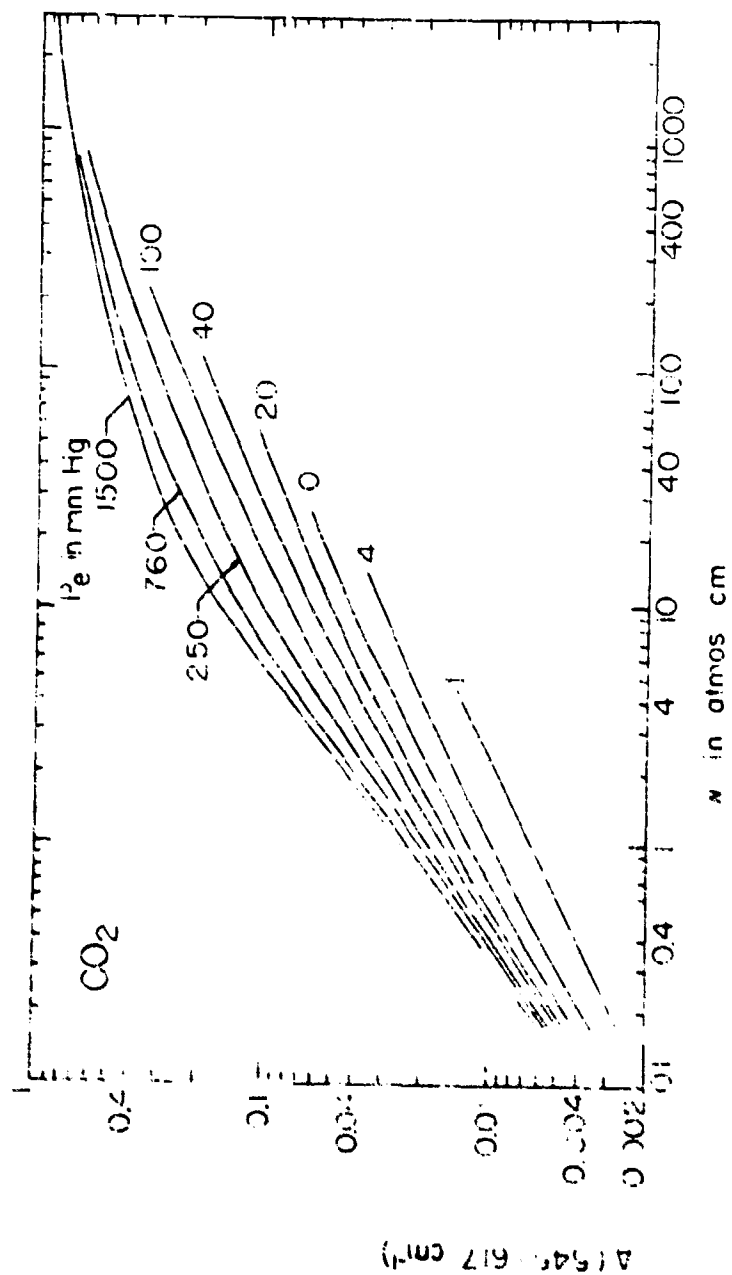


Fig. 44. $\Delta(545-617 \text{ cm}^{-1})$ versus w for various values of P_e .

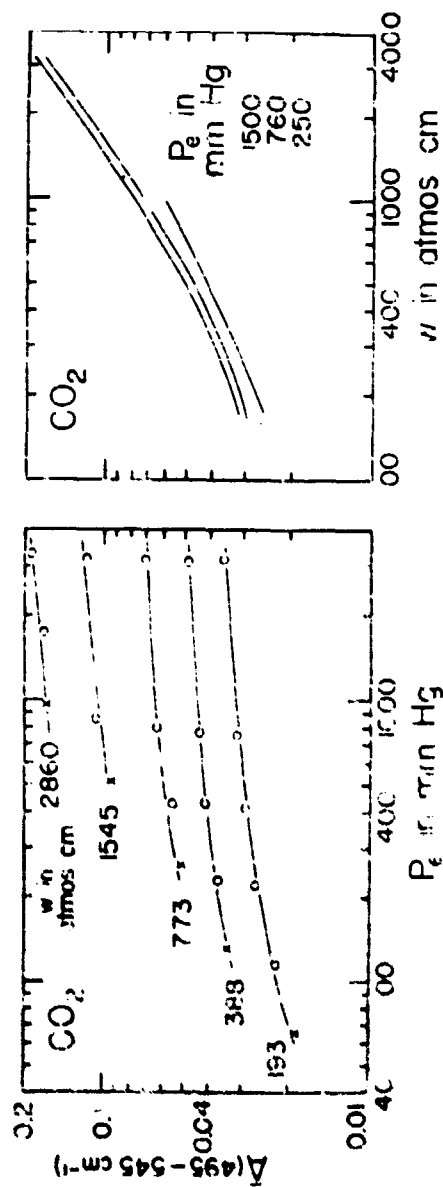


Fig. 45. λ (495-545 cm^{-1}) versus P_e for various values of w in the left-hand portion; w (495-545 cm^{-1}) versus P_e for three values of P_e in the right-hand portion.

Curves corresponding to those in Figs. 33, 34, and 35 were drawn for the other spectral sub-regions and are shown in Figs. 36 - 45. No figure was drawn for the $495 - 545 \text{ cm}^{-1}$ interval which related $\bar{A}(495 - 545 \text{ cm}^{-1})$ to P_0 for samples of CO_2 alone, since only the samples of large v produced a measurable amount of absorption.

A. EFFECT OF TEMPERATURE ON MEAN FRACTIONAL ABSORPTION

Several of the absorption curves obtained for samples at elevated temperatures are shown in Fig. 32; and the results for these samples ($100^\circ\text{C} - 240^\circ\text{C}$), are given in Table 4. Only samples of CO_2 alone were investigated; the pressures of the samples were checked at the various temperatures and were found to increase essentially as for a perfect gas. The absorption curves for the samples at elevated temperatures were found to be erratic in the vicinity of the $495 - 545 \text{ cm}^{-1}$ sub-region; and these portions of the curves were therefore omitted from Fig. 32. The excessive scatter in the data may have been caused by the water vapor in the spectrometer, whose temperature increased as the absorption cell was heated, or by temperature gradients within the spectrometer. It is also possible that the amplifier gain was not sufficiently high for the recorder pen to respond properly. Regardless of the cause, the results for this spectral sub-region were much less consistent than those for the remainder of the absorption curves, and were omitted in making analyses.

The mean fractional absorption of each of the other four intervals is plotted against temperature in Fig. 46. The mean fractional absorptions of all four intervals increase with temperature. No attempts were made to compare the observed increase in absorption to predictions based on the changes in population of certain energy levels. Two or more bands contribute to the absorption in any of the spectral sub-regions, and a simple calculation such as that made in connection with the 1064 and 961 cm^{-1} bands could not be made. Detailed theoretical calculations of the effect of temperature variation on the absorption by CO_2 in the $875 - 495 \text{ cm}^{-1}$ region have been made by several investigators including Sasamori¹.

B. COMPARISON OF RESULTS WITH PREVIOUS WORK

The IBM report contains the results of measurement of total absorption of all samples of CO_2 and $\text{CO}_2\text{-N}_2$ mixtures in the $875 - 495 \text{ cm}^{-1}$ spectral region. These samples include absorber concentrations in the range from approximately 1 to 900 atmos cm, and the results can be compared with the results of the present investigation. It is not possible to compare the total absorption or mean fractional absorption of each sub-region since only the total absorption of the entire region is listed

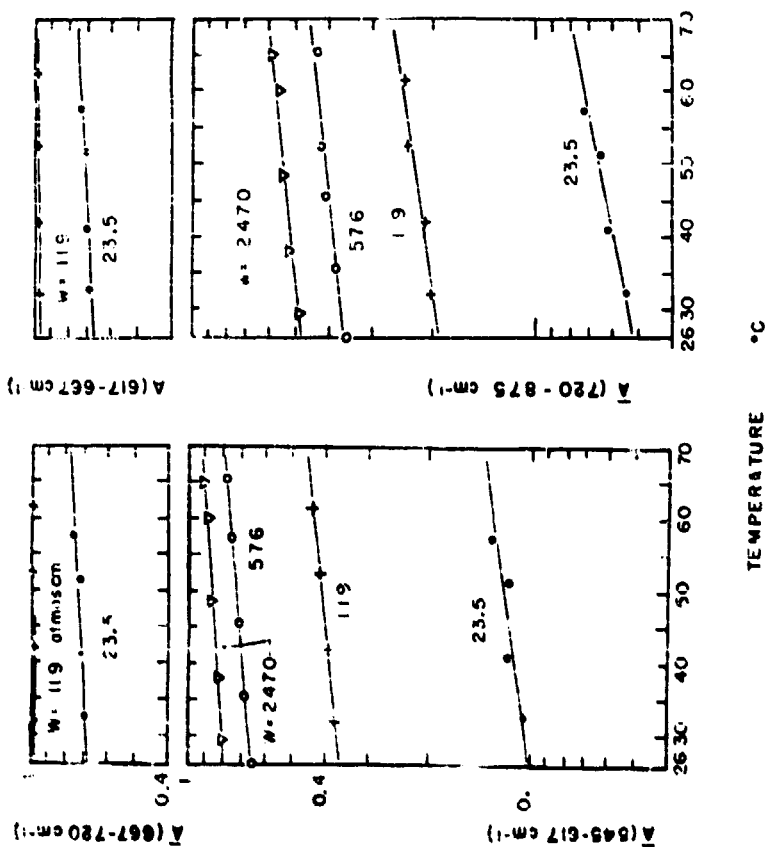


Fig. 1-6. $A(667-720 \text{ cm}^{-1})$, $A(617-667 \text{ cm}^{-1})$, $A(720-875 \text{ cm}^{-1})$, and $A(545-617 \text{ cm}^{-1})$ versus temperature for four different samples.

in the HEW report. Values of total pressure P and CO_2 partial pressure p from the HEW data were used to calculate the value of equivalent pressure P_e for each sample by use of Eq. (3). This value of P_e along with the value of y was used with the curves of Figs. 35, 38, 41, 44, and 45 to predict the mean fractional absorption produced by each sample in each of the five sub-regions. The total absorption of each sub-region was then calculated from the mean fractional absorption by use of Eq. (1); the total absorption of the entire region was then found by adding up the results for each of the five sub-regions. This value of total absorption, which was predicted for each sample on the basis of the present work, was compared with the value obtained by HEW.

The samples having the smallest absorber concentration showed the greatest deviation between predicted value of total absorption and that observed by HEW. This is a result which one might expect since the CO_2 partial pressure, which is proportional to y , was too low to be measured accurately in the HEW study. Errors in the determination of y as a result of adsorption of CO_2 on the cell walls also contribute greater relative error in the predicted values of total absorption for samples containing a low CO_2 partial pressure (see Appendix I, Report 1). Uncertainty in the position of the zero absorption curve also contributes greater relative error in the measurement of total absorption of samples of small y whose total absorption is small.

Other than the fact that the largest deviations were associated with samples producing low total absorption, there was no apparent correlation between the deviation and either of the parameters y or P_e . The predicted values of total absorption averaged approximately 2.8% less than the observed values; this phenomenon could arise from a number of things, such as systematic errors in sampling, errors in calibrations of the spectrometers, errors in the positioning of the zero-absorption curve, etc.

The root-mean-square deviation was found to be approximately 9%, a result which indicates the experimental error in the HEW work was somewhat larger for the $875 - 405 \text{ cm}^{-1}$ band (15-micron) than for the other bands.

The data reported by Edwards⁶ for the 15-micron CO_2 absorption include 16 samples at ambient temperature, whose values of y and P_e overlap those covered in the present study. The values of y , P_e , and p for Edwards' samples were used with the curves presented in this section of this report, in the same manner as was done for the HEW data, to predict the total absorption of each sample. With the exception of the sample producing the least total absorption, for which the predicted total absorption was 9.7% greater than the observed value, the deviation between predicted and observed values was less than 5%. The predicted value averaged approximately 3% greater than the observed value; this result could be partially explained by the fact that the Edwards results were obtained with samples at 294°K while the present data were obtained

at 299°K. If the predicted values had been corrected to 294°K, the deviation would have been even less; with the exception of the one sample the maximum deviation would have been approximately 5 or 4%, and the average deviation would have been very small. Thus, one concludes that the agreement is extremely good and is well within the estimated experimental error.

The Edwards data and the HBW data provided checks for the samples of the present study which have intermediate values of \bar{w} ; but no data were available to compare with the smallest and largest values. It should also be noted that the minimum value of equivalent pressure, as determined by Eq. (3) for the Edwards data, was 385 mm Hg.

VII. BAND INTENSITIES

It was demonstrated in Report 1 that under certain conditions the band intensity $\int k(\nu)d\nu$ of an absorption band, where $k(\nu)$ is the absorber coefficient, can be determined from curves relating the total absorption to absorber concentration. The total absorption for samples for which $k(\nu)/\bar{w} < 1$ for all frequencies, is related to the band intensity by

$$A(\nu)d\nu = \bar{w} \int k(\nu)d\nu \quad (15)$$

The conditions for the validity of Eq. (15) correspond to high pressures and small values of \bar{w} . For sufficiently high pressures and small values of \bar{w} , it follows from Eq. (15) that curves such as those in Fig. 5, for which the log of $\int A(\nu)d\nu$ is plotted against the log of \bar{w} , should be linear with a slope of unity. The value of $\int k(\nu)d\nu$ can then be determined directly from the linear portion of the curves.

In the present study, few, if any, of the samples had pressures sufficiently high and values of \bar{w} sufficiently small so that the simple linear relationship given by Eq. (15) was completely valid. However, it was possible to extrapolate to smaller values of \bar{w} the curves corresponding to the largest value of P_0 in Fig. 5 and in the corresponding figures for the other bands. From the extrapolated portions of the curves it was then possible to estimate the values of band intensity $\int k(\nu)d\nu$. The extrapolated curves were based on the fact that the slopes of the curves increase with decreasing \bar{w} to a maximum value of unity, and that all of the curves representing different values of P_0 tend to converge.

It is recalled that values of mean fractional absorption $A(\nu_1-\nu_2)$, rather than total absorption $\int A(\nu)d\nu$, were determined for the sub-region in the 875-495 cm^{-1} region. Therefore, in order to determine the intensity of the 675 cm^{-1} CO_2 band, it was necessary to determine values

of $\int A(\nu) d\nu$ from readings of $\bar{A}(\nu_1 - \nu_2)$ for the 617 - 667 cm^{-1} and 667 - 720 cm^{-1} sub-regions from Figs. 41 and 38 respectively. The absorption by the 667 cm^{-1} band is limited to these two sub-regions for values of ν and P_e represented by portions of the curves used to determine the band intensity. Kaplan and Eggers⁸ have found that a small portion of the absorption in the two sub-regions given above arises from weak bands other than the fundamental band whose center occurs at 667 cm^{-1} . The value of band intensity for the 667 cm^{-1} band therefore includes a small contribution not due to the fundamental.

The intensities of the other bands in the 875 - 495 cm^{-1} region, whose prominent Q-branches are seen in Figs. 25 - 32, were not determined because of overlapping of the different bands. The intensities of two of these bands have been determined from high-resolution spectra by Kostkowski and Kaplan⁹.

Because of the extrapolation which was involved in determining the values of band intensities, the uncertainty is approximately 20 to 25%, and is somewhat greater than for the results given in Report 1. If the determination of band intensities had been the primary rather than a secondary purpose of the present investigation, higher pressures would have been used and more emphasis would have been put on samples of small ν .

The values of band intensity which were determined in the present investigation are listed in Table 5, along with the results of other workers for comparison.

VIII. SUMMARY

The work covered in the present report has dealt with the infrared absorption of carbon dioxide, and is intended as a supplement to earlier work. Samples consisting of carbon dioxide alone, and in binary mixtures with nitrogen, have been investigated over wide ranges of absorber concentration ν and total pressure P . From the absorption by each band or spectral interval, it was possible to determine either the total absorption $\int A(\nu) d\nu$ or the mean fractional absorption $\bar{A}(\nu_1 - \nu_2)$ for each sample. Curves are presented which show the total absorption of the CO_2 bands at 3716, 3609, 2350, 1064, and 961 cm^{-1} for various values of absorber concentration as a function of equivalent pressure P_e , which is a parameter that includes the total pressure P and a small additional term proportional to the partial pressure of the absorbing gas. Similar sets of curves for the sub-regions in the 875-495 cm^{-1} region were drawn to show the mean fractional absorption as a function of P_e .

Another set of curves shows the total absorption of each band and the mean fractional absorption of each spectral sub-region for various

equivalent pressures as a function of absorber concentration. These curves provide a means of predicting total absorption or mean fractional absorption for any values of w and P_0 included in the wide range of these parameters covered in the study. It was also possible to obtain empirical equations which relate total absorption to w and P_0 for certain limited values of total absorption $\int A(v)dv$ and equivalent pressure P_0 .

Absorption curves for the 1064 and 961 cm^{-1} bands as well as for the 870 - 490 cm^{-1} region, were obtained for different samples of CO_2 at temperatures from ambient to approximately 70°C. The effects of temperature on the absorption were illustrated by the use of graphs. It was found that for the temperature range covered it is possible to predict the increase in total absorption of the 1064 and 961 cm^{-1} bands by use of an elementary function which is based on the calculated increase in population of the lower energy level giving rise to the absorption.

Extensive tables which include all the CO_2 absorption data are presented at the end of the report for the use of other investigators who may be interested in an analysis different from that given in the present report.

It is hoped that the present results will be useful to investigators who are interested in the many types of atmospheric studies involving the absorption and emission of infrared radiation by carbon dioxide.

Table 1. Data for the 3716 and 3609 cm^{-1} CO_2 bands

The figure number corresponds to the figure in which the spectrum of each sample is shown. Absence of figure number indicates spectrum is not shown.

sample No.	Fig. No.	ν in cm^{-1}	P_0 in Hg	$\int A(\nu) d\nu \text{ cm}^{-1}$		Remarks
				3609 cm^{-1} band	3716 cm^{-1} band	
<u>1.55 cm Path Length</u>						
A 1		0.61	58	1.5	2.5	Sample 1; 44.6 mm Hg of CO_2 . Sample 2 - 6; H_2 added to Sample 1.
A 2		0.61	121	2.0	2.9	
A 3		0.61	221	2.4	3.1	
A 4		0.61	417	2.6	3.9	
A 5		0.61	850	2.7	3.9	Sample 7; 89.6 mm Hg of CO_2 . Samples 8 - 11 H_2 added to Sample 7.
A 6		0.61	1555	2.8	4.1	
A 7		0.65	117	3.5	4.2	
A 8		0.165	201	4.2	4.9	
A 9		0.165	420	4.6	6.2	Sample 12; 375 mm Hg. of CO_2 . Sample 13-14; H_2 added to Sample 12.
A 10		0.165	825	5.0	7.4	
A 11		0.165	1620	6.0	7.7	
A 12		0.687	388	13.6	17.1	
A 13		0.687	324	15.1	20.2	Sample 15; 208 mm Hg. of CO_2 . Sample 16; 417 mm Hg. of CO_2 . Sample 17; 808 mm Hg. of CO_2 . Sample 18; 1570 mm Hg. of CO_2 .
A 14		0.687	1665	17.6	22.5	
A 15		0.718	270	7.1	9.5	
A 16	2	0.799	542	13.0	17.9	
A 17	2	1.17	1350	24.3	32.2	
A 18	2	2.66	2342	43.8	51.1	

Table 1. (Cont'd)

Sample	No.	Date	Time	F ₀ mm Hg	$\int A(\nu) d\nu$ cm ⁻¹		Remarks
					3604 cm ⁻¹ band	3716 + 3609 cm ⁻¹	
<u>12.8 cm Path Length</u>							
A 15	1			14.2	1.7	2.3	Sample 15; 10.9 mm Hg of CO ₂ . Sample 20-26; H ₂ added to Sample 19.
A 16	1			23.6	2.1	2.6	
A 17	2			43.2	2.5	3.4	
A 18	2			101	3.1	4.6	
A 19	2			222	3.7	5.3	
A 20	2			403	4.2	6.3	
A 21	2			847	1.6	7.3	
A 22	2			1612	3.3	8.3	
A 23	2			27.2	3.2	3.9	Sample 23; 20.9 mm Hg of CO ₂ . Sample 28-33; H ₂ added to Sample 27.
A 24	2			44.8	3.8	4.6	
A 25	2			106	4.7	6.3	
A 26	2			213	5.6	7.7	
A 27	2			419	6.8	9.5	
A 28	2			844	8.4	12.0	
A 29	2			1623	9.2	13.4	
A 30	2			39.2	6.4	7.6	Sample 34; 45.7 mm Hg of CO ₂ . Sample 35-39; H ₂ added to Sample 34.
A 31	2			115	8.5	0.1	
A 32	2			237	11.0	3.4	
A 33	2			432	11.8	6.1	
A 34	2			854	14.7	9.1	
A 35	2			1565	15.7	13.2	

Table 1. (Cont'd)

Sample No.	Pig. No.	ν , cm ⁻¹	P_0 , cm Hg	$\frac{A(\nu)}{A(\nu_0)}$, cm ⁻¹	$\frac{A(\nu)}{A(\nu_0)}$, cm ⁻¹	Remarks
				band	band	
12.6 cm Path Length (Cont'd)						
A 40	5	1.35	120	12.3	14.6	Sample 40; 32.5 mm Hg of CO ₂ . Sample 41-44; H ₂ added to Sample 40.
A 41	5	1.35	220	15.1	19.4	
A 42	5	1.35	499	18.6	24.0	
A 43	5	1.35	921	22.5	28.4	
A 44	5	1.35	1450	27.0	34.5	
A 45	5	3.02	295	26.8	30.4	Sample 45; 197 mm Hg of CO ₂ . Sample 46-48; H ₂ added to Sample 45.
A 46	5	3.02	434	32.3	36.8	
A 47	5	3.02	935	38.8	45.1	
A 48	5	3.02	1720	44.8	50.5	
A 49	5	5.08	514	48.1	50.2	Sample 49; 395 mm Hg of CO ₂ . Sample 50-51; H ₂ added to Sample 49.
A 50	5	5.08	980	55.1	59.3	
A 51	5	5.08	1770	61.8	65.6	
A 52	5	13.7	1070	75.0	70.3	Sample 52; 824 mm Hg of CO ₂ . Sample 53; 1605 mm Hg of CO ₂ .
A 53	5	13.7	1840	81.1	76.7	
A 54		20.4	2055	97.4	81.6	Sample 54; 1500 mm Hg of CO ₂ .
					179	

Table 2. Data for the 2550 cm⁻¹ CO₂ Band

Each absorption curve was divided at the band center, 2550 cm⁻¹. The value of total absorption of each portion was determined and are tabulated below along with the total absorption of the entire band. The figure number corresponds to the figure in which the spectrum of each sample is shown. Absorption figure number indicated spectrum is not shown.

Sample No.	Fig. No.	ν , cm ⁻¹	P_0 , cm ⁻¹	$\frac{\Delta A(\nu)}{A(\nu)}$		Entire Band	Remarks
				< 2550 cm ⁻¹	> 2550 cm ⁻¹		
<u>1.55 cm Path Length</u>							
8 1		0.0022	3.6	0.80	3.95	1.55	Sample 1; 2.5 mm Hg of CO ₂ .
8 2		0.0032	13.1	1.05	0.75	1.80	Sample 2-9; H ₂ added to Sample 1.
8 3		0.0032	25.3	1.40	1.00	2.40	
8 4		0.0032	48.6	1.75	1.15	2.9	
8 5		0.0032	59	2.3	1.4	4.1	
8 6		0.0032	206	3.5	2.5	6.0	
8 7		0.0032	408	4.2	3.4	7.6	
8 8		0.0032	822	6.7	4.9	9.0	
8 9		0.0032	1615	3.5	5.0	10.5	
8 10		0.0038	7.8	2.05	0.95	3.0	Sample 10; 6 mm Hg of CO ₂ .
8 11		0.0038	15.2	2.4	1.2	3.6	Sample 11-18; H ₂ added to Sample 10.
8 12		0.0038	28.6	3.0	1.0	5.0	
8 13		0.0038	51.1	3.4	1.0	6.2	
8 14		0.0038	105	5.0	1.65	8.65	
8 15		0.0038	205	6.5	3.2	11.7	
8 16		0.0038	425	9.6	5.75	15.35	
8 17		0.0038	841	10.4	6.45	16.85	
8 18		0.0038	1675	12.2	10.15	22.35	
8 19		0.0034	16.5	5.7	2.0	5.7	Sample 19; 12.8 mm Hg of CO ₂ . Sample 20-25; H ₂ added to Sample 19.
8 20		0.0034	27.7	4.75	2.85	7.6	
8 21		0.0034	55	5.75	4.2	9.95	
8 22		0.0034	107	8.35	5.65	14.2	
8 23		0.0034	426	13.0	10.1	23.1	
8 24		0.0034	832	15.2	13.2	29.1	
8 25		0.0034	1675	19.65	16.9	36.75	

Table 2. (Cont'd.)

Sample No.	Fig. No.	v atmos cm	P mm Hg	$\frac{A(v)Mv}{\lambda}$		Remarks
				< 2350 cm ⁻¹	> 2350 cm ⁻¹	
1.55 cm Path Length (Cont'd.)						
B 25		0.17C	120	56.3	16.9	Sample 26; 92.5 mm Hg of CO ₂ . Samples 27-30; H ₂ added to Sample 26.
B 27		0.17C	226	32.8	21.0	
B 28		0.17C	443	43.0	25.5	
B 29		0.17C	655	43.7	28.9	
B 30		0.17C	1700	47.4	30.9	73.3
B 31		0.0059	4.2	0.85	0.50	1.35
B 32	11	0.0116	7.9	1.00	1.25	3.05
B 33	11	0.0229	15.7	5.95	2.20	6.15
B 34	11	0.0455	32	7.85	5.00	12.3
B 35	11	0.0925	55	15.4	9.5	25.3
B 36	11	0.195	137	29.5	18.5	48.3
B 37	11	0.398	274	56.2	27.6	73.8
B 38	11	0.756	534	62.1	32.9	95.0
B 39	11	1.49	1055	74.5	36.2	130.7
B 40	11	2.99	2115	67.8	40.0	127.3
12.8 cm Path Length						
B 41	12	0.043	3.8	3.1	1.75	4.85
B 42	12	0.043	11.4	4.5	2.9	7.40
B 43	12	0.043	24.3	6.5	4.05	13.6
B 44	12	0.043	46.6	8.2	5.45	15.7
B 45	12	0.043	104	22.0	8.25	26.2
B 46	12	0.043	218	15.4	11.5	26.9
B 47	12	0.043	429	19.6	14.5	34.1
B 48	12	0.043	810	23.5	17.75	41.2
B 49	12	0.043	1615	26	20.7	43.7

Table 2. (Cont'd)

Sample No.	C	v	P ₀ cm Hg	$\frac{f(\lambda)_{H_2}}{\lambda}$		Remarks
				< 22.0 cm ⁻¹	> 22.0 cm ⁻¹	
12.6 cm Path Length (Cont'd)						
50	1	0.206	7.4	5.05	5.55	Sample 50; 5.7 mm Hg of D ₂
51	1	0.206	14.4	9.1	4.65	Sample 51-58; H ₂ added to sample 50.
52	1	0.206	27.5	10.0	6.25	
53	1	0.206	55	14.1	8.95	
54	1	0.206	102	17.2	11.8	
55	1	0.205	202	22.1	15.5	
56	1	0.205	372	27.1	18.8	
57	1	0.205	510	31.8	23.6	
58	1	0.205	1595	57.2	27.5	
59	1	0.165	14.6	1.7	6.85	Sample 59; 11.2 mm Hg of D ₂
60	1	0.169	24.2	14.5	0.8	Co Sample 60-66, N ₂ added to Sample 59.
61	1	0.169	44.1	19.0	11.6	
62	1	0.169	97.0	25.7	15.1	
63	1	0.169	170	29.2	18.9	
64	1	0.169	346	36.5	23.9	
65	1	0.169	637	41.4	27.5	
66	1	0.169	1555	47.2	30.8	
67	1	0.34	24.9	22.4	17.9	Sample 67; 25 mm Hg of D ₂
68	1	0.34	57.5	28.9	14.4	Sample 68-73; H ₂ added to Sample 67.
69	1	0.34	112	35.9	21.7	
70	1	0.34	237	44.5	26.9	
71	1	0.34	465	50.5	29.9	
72	1	0.34	908	55.8	32.8	
73	1	0.34	1650	57.8	35.1	

Table 2. (Cont'd)

Sample No.	Flt. No.	ν atoms cm ⁻¹	P_0 mm Hg	$\int A(\nu) d\nu$		Remarks
				< 2350 cm ⁻¹	> 2350 cm ⁻¹	
<u>22.8 cm Path Length (Cont'd.)</u>						
874	11	0.649	56.5	36.6	22.2	Sample 74; 43.5 mm Hg of CO ₂ . Sample 75-79; H ₂ added to Sample 74.
875	11	0.649	112	46.6	26.1	
876	11	0.649	218	53.8	30.7	
877	11	0.649	426	60.1	34.2	
878	11	0.649	826	62.9	35.5	
879	11	0.649	1590	65.4	36.7	
880	12	1.29	111	55.1	30.4	Sample 80; 85 mm Hg of CO ₂ . Sample 81-84; H ₂ added to Sample 80.
881	12	1.29	195	61.1	33.5	
882	12	1.29	335	65.1	34.5	
883	12	1.29	695	70.5	35.4	
884	12	1.29	1520	73.7	37.2	
885	12	2.55	218	71.5	35.5	Sample 85; 168 mm Hg of CO ₂ . Sample 86-88; H ₂ added to Sample 85.
886	12	2.55	394	75.4	37.8	
887	12	2.55	757	79.5	38.8	
888	12	2.55	1470	85.8	40.2	
889	12	4.99	450	86.1	40.3	Sample 89; 331 mm Hg of CO ₂ . Sample 90, 91; H ₂ added to Sample 89.
890	12	4.99	815	90.5	41.5	
891	12	4.99	1620	94.8	42.8	
892	12	11.2	965	105	45.6	Sample 92; 743 mm Hg of CO ₂ . Sample 93; H ₂ added to Sample 92.
893	12	11.2	1760	106	45.7	
894	12	22.5	1970	115	52.2	Sample 94; 1515 mm Hg of CO ₂ .

Table 3. Data for the 1064 and 961 cm^{-1} CO_2 Bands

The figure number corresponds to the figure in which the spectrum of each sample is shown. Absence of figure number indicates spectrum is not shown.

If figure number indicates spectrum is not shown.						
Sample No.	Fig. No.	Temp. $^{\circ}$ deg	ν (cmos cm)	P_0 (mm Hg)	$\frac{\int A(\nu)d\nu \text{ (cm}^{-1}\text{)}}{1064 \text{ cm}^{-1} \quad 961 \text{ cm}^{-1}}$	Remarks
<u>Path Length = 1600 cm</u>						
C 1	16	26.0	192	190	3.2	Samples 1-7; CO_2 alone. Pressure of CO_2 equals $P_0/1.3$ for all samples of CO_2 alone.
C 2	16	26.0	584	250	7.0	
C 3	16	26.0	766	520	13.7	
C 4	16	26.0	1515	957	24.1	
C 5	16	26.0	2340	1925	41.6	
C 6	16	26.0	4415	3990	54.4	
C 7	16	26.0	5995	4655	60.6	
<u>Path Length = 400 cm</u>						
C 8	16	24.0	148	140	1.2	Samples 8-12; CO_2 alone.
C 9	16	26.0	96	250	2.4	
C 10	16	26.0	192	520	4.8	
C 11	16	26.0	755	552	9.0	
C 12	16	26.0	715	1935	17.5	
C 13	16	29.0	190	795	7.5	Sample 13; 610 mm Hg of CO_2 . Samples 14-16; Sample 15 heated to indicated temp.
C 14	16	44.0	190		9.1	
C 15	16	56.0	190		10.8	
C 16	16	65.0	190		12.4	Sample 17; 2875 mm Hg of CO_2 . Samples 18-19; Sample 17 heated.
C 17	16	25.0	1485	5755	29.8	
C 18	16	35.5	1485		33.0	
C 19	16	45.5	1485		36.9	

Table 5. (Cont'd)

[illegible]

Table 3. (Cont'd)

Sample No.	Fig. No.	Temp. C. deg	ν (cmos cm)	P_g (mm Hg)	$\int A(\nu)dv$ (cm ⁻¹)		Remarks
					10 ⁴ cm ⁻¹	361 cm ⁻¹	
Path Length = 3203 cm (Cont'd)							
C 38	17	25.0	2945	1780	42.4	34.5	Samples 38-39, N ₂ added to 768 mm Hg of CO ₂ .
C 39	17	25.0	2945	2240	46.5	36.1	
C 40	17	25.0	3730	2550	57.2	50.9	Sample 40; 1495 cm Hg of CO ₂ . Sample 41; H ₂ added to Sample 40.
C 41	17	25.0	3730	2320	61.1	55.1	
C 42	17	25.0	11,200	2600	75.3	72.9	Sample 42; 2920 mm Hg of CO ₂ .

samples were investigated by use of the evacuated Model 99 spectrometer; all others were studied with the Model 21. The figure number corresponds to the figure in which the spectrum of each sample is shown. Absence of figure number indicates spectrum is not shown. Absence of a value in parentheses indicates that this quantity was too small to measure accurately or that the result was deleted because of some other cause. The values of λ_{max} correspond to the entire spectral region 0.5-100 μ .

Date	Time	T _g °C	V (cc)	P _g (mm Hg)	λ (μ)		Path Length = 1.55 cm	J ₉₅	Remarks
					720-775 cm ⁻¹	617-667 cm ⁻¹			
1-1	11	20.1	3.0034	20.1	1.1 × 10 ⁻²	1 × 10 ⁻²	1.08	Same. 1-3; 5.1 mm Hg of CO ₂ plus H ₂ added.	
1-2	31	17.6	3.0034	17.6	1.2	1.40	1.40		
1-3	31	17.6	3.0034	17.6	1.5	2.02	2.02		
2-1	21.5	31.0	0.0118	31.0	2.5	2.53	2.53	Same. 4-6; 6.1 mm Hg of CO ₂ plus H ₂ added.	
2-2	21.5	31.0	0.0118	31.0	3.0	2.94	2.94		
2-3	21.5	31.0	0.0118	31.0	3.4	3.35	3.35		
3-1	2	16.1	0.022	16.1	1.6	1.7	1.65	Same. 7; 12.4 mm Hg of CO ₂ . Same. 9-11; H ₂ added to Sam. 7.	
3-2	2	16.1	0.022	16.1	2.0	2.4	2.41		
3-3	2	16.1	0.022	16.1	2.4	2.9	3.20		
4-1	2	16.1	0.022	16.1	3.3	3.6	3.85		
4-2	2	16.1	0.022	16.1	4.0	4.1	4.45		
4-3	2	16.1	0.022	16.1	5.0	4.5	4.95		
5-1	2	16.1	0.022	16.1	5.5	5.2	5.65		
6-1	2	16.1	0.046	16.1	1.6 × 10 ⁻²	3.5 × 10 ⁻²	3.85	Same. 14; 25.6 mm Hg of CO ₂ . Same. 15-17; H ₂ added to Sam. 14.	
6-2	2	16.1	0.046	16.1	4.5	4.4	4.4		
6-3	2	16.1	0.046	16.1	5.7	5.2	5.82		
7-1	2	16.1	0.046	16.1	6.0	7.0	7.0		
7-2	2	16.1	0.046	16.1	6.5	6.5	8.35		
8-1	2	16.1	0.089	16.1	6.9	6.5	7.11	Same. 20; 42.6 mm Hg of CO ₂ . Same. 21-23; H ₂ added to Sam. 20.	
8-2	2	16.1	0.089	16.1	7.5	7.5	8.01		
8-3	2	16.1	0.089	16.1	8.2	8.2	9.88		
9-1	2	16.1	0.089	16.1	11.1	10.6	11.6		
9-2	2	16.1	0.089	16.1	12.1	12.3	13.4		
9-3	2	16.1	0.089	16.1	14.7	15.8	15.3		
10-1	2	16.1	0.171	16.1	12.1	1.5	12.9	Same. 26-30; CO ₂ alone.	
10-2	2	16.1	0.171	16.1	15.6	0.0	22.4		
10-3	2	16.1	0.171	16.1	16.7	0.50	22.4		
11-1	2	16.1	0.171	16.1	16.7	2.1	40.3		
11-2	2	16.1	0.171	16.1	16.7	4.2	56.1		
11-3	2	16.1	0.171	16.1	16.7	7.0	89.1		
12-1	2	16.1	0.171	16.1	16.7	15.8	15.3		
13-1	2	16.1	0.171	16.1	16.7	15.8	15.3		
14-1	2	16.1	0.171	16.1	16.7	15.8	15.3		
15-1	2	16.1	0.171	16.1	16.7	15.8	15.3		
16-1	2	16.1	0.171	16.1	16.7	15.8	15.3		
17-1	2	16.1	0.171	16.1	16.7	15.8	15.3		
18-1	2	16.1	0.171	16.1	16.7	15.8	15.3		
19-1	2	16.1	0.171	16.1	16.7	15.8	15.3		
20-1	2	16.1	0.171	16.1	16.7	15.8	15.3		
21-1	2	16.1	0.171	16.1	16.7	15.8	15.3		
22-1	2	16.1	0.171	16.1	16.7	15.8	15.3		
23-1	2	16.1	0.171	16.1	16.7	15.8	15.3		
24-1	2	16.1	0.171	16.1	16.7	15.8	15.3		
25-1	2	16.1	0.171	16.1	16.7	15.8	15.3		
26-1	2	16.1	0.171	16.1	16.7	15.8	15.3		
27-1	2	16.1	0.171	16.1	16.7	15.8	15.3		
28-1	2	16.1	0.171	16.1	16.7	15.8	15.3		
29-1	2	16.1	0.171	16.1	16.7	15.8	15.3		
30-1	2	16.1	0.171	16.1	16.7	15.8	15.3		
31-1	2	16.1	0.171	16.1	16.7	15.8	15.3		
32-1	2	16.1	0.171	16.1	16.7	15.8	15.3		
33-1	2	16.1	0.171	16.1	16.7	15.8	15.3		
34-1	2	16.1	0.171	16.1	16.7	15.8	15.3		
35-1	2	16.1	0.171	16.1	16.7	15.8	15.3		
36-1	2	16.1	0.171	16.1	16.7	15.8	15.3		
37-1	2	16.1	0.171	16.1	16.7	15.8	15.3		
38-1	2	16.1	0.171	16.1	16.7	15.8	15.3		
39-1	2	16.1	0.171	16.1	16.7	15.8	15.3		
40-1	2	16.1	0.171	16.1	16.7	15.8	15.3		
41-1	2	16.1	0.171	16.1	16.7	15.8	15.3		
42-1	2	16.1	0.171	16.1	16.7	15.8	15.3		
43-1	2	16.1	0.171	16.1	16.7	15.8	15.3		
44-1	2	16.1	0.171	16.1	16.7	15.8	15.3		
45-1	2	16.1	0.171	16.1	16.7	15.8	15.3		
46-1	2	16.1	0.171	16.1	16.7	15.8	15.3		
47-1	2	16.1	0.171	16.1	16.7	15.8	15.3		
48-1	2	16.1	0.171	16.1	16.7	15.8	15.3		
49-1	2	16.1	0.171	16.1	16.7	15.8	15.3		
50-1	2	16.1	0.171	16.1	16.7	15.8	15.3		
51-1	2	16.1	0.171	16.1	16.7	15.8	15.3		
52-1	2	16.1	0.171	16.1	16.7	15.8	15.3		
53-1	2	16.1	0.171	16.1	16.7	15.8	15.3		
54-1	2	16.1	0.171	16.1	16.7	15.8	15.3		
55-1	2	16.1	0.171	16.1	16.7	15.8	15.3		
56-1	2	16.1	0.171	16.1	16.7	15.8	15.3		
57-1	2	16.1	0.171	16.1	16.7	15.8	15.3		
58-1	2	16.1	0.171	16.1	16.7	15.8	15.3		
59-1	2	16.1	0.171	16.1	16.7	15.8	15.3		
60-1	2	16.1	0.171	16.1	16.7	15.8	15.3		
61-1	2	16.1	0.171	16.1	16.7	15.8	15.3		
62-1	2	16.1	0.171	16.1	16.7	15.8	15.3		
63-1	2	16.1	0.171	16.1	16.7	15.8	15.3		
64-1	2	16.1	0.171	16.1	16.7	15.8	15.3		
65-1	2	16.1	0.171	16.1	16.7	15.8	15.3		
66-1	2	16.1	0.171	16.1	16.7	15.8	15.3		
67-1	2	16.1	0.171	16.1	16.7	15.8	15.3		
68-1	2	16.1	0.171	16.1	16.7	15.8	15.3		
69-1	2	16.1	0.171	16.1	16.7	15.8	15.3		
70-1	2	16.1	0.171	16.1	16.7	15.8	15.3		
71-1	2	16.1	0.171	16.1	16.7	15.8	15.3		
72-1	2	16.1	0.171	16.1	16.7	15.8	15.3		
73-1	2	16.1	0.171	16.1	16.7	15.8	15.3		
74-1	2	16.1	0.171	16.1	16.7	15.8	15.3		
75-1	2	16.1	0.171	16.1	16.7	15.8	15.3		
76-1	2	16.1	0.171	16.1	16.7	15.8	15.3		
77-1	2	16.1	0.171	16.1	16.7	15.8	15.3		
78-1	2	16.1	0.171	16.1	16.7	15.8	15.3		
79-1	2	16.1	0.171	16.1	16.7	15.8	15.3		
80-1	2	16.1	0.171	16.1	16.7	15.8	15.3		
81-1	2	16.1	0.171	16.1	16.7	15.8	15.3		
82-1	2	16.1	0.171	16.1	16.7	15.8	15.3		
83-1	2	16.1	0.171	16.1	16.7	15.8	15.3		
84-1	2	16.1	0.171	16.1	16.7	15.8	15.3		
85-1	2	16.1	0.171	16.1	16.7	15.8	15.3		
86-1	2	16.1	0.171	16.1	16.7	15.8	15.3		
87-1	2	16.1	0.171	16.1	16.7	15.8	15.3		
88-1	2	16.1	0.171	16.1	16.7	15.8	15.3		
89-1	2	16.1	0.171	16.1	16.7	15.8	15.3		
90-1	2	16.1	0.171	16.1	16.7	15.8	15.3		
91-1	2	16.1	0.171	16.1	16.7	15.8	15.3		
92-1	2	16.1	0.171	16.1	16.7	15.8	15.3		
93-1	2	16.1	0.171	16.1	16.7	15.8	15.3		
94-1	2	16.1	0.171	16.1	16.7	15.8	15.3		
95-1	2	16.1	0.171	16.1	16.7	15.8	15.3		
96-1	2	16.1	0.171	16.1	16.7	15.8	15.3		
97-1	2	16.1	0.171	16.1	16.7	15.8	15.3		
98-1	2	16.1	0.171	16.1	16.7	15.8	15.3		
99-1	2	16.1	0.171	16.1	16.7	15.8	15.3		
100-1	2	16.1	0.171	16.1	16.7	15.8	15.3		

Table 4. (Cont.)

Sample No.	Lat. N	Long. W	Depth (m)	P_0 (mm Hg)	$750-875 \text{ cm}^{-1}$	$667-720 \text{ cm}^{-1}$	$517-667 \text{ cm}^{-1}$	$345-617 \text{ cm}^{-1}$	$1495-945 \text{ cm}^{-1}$	Remarks
Path Length = 12.8 (Cont'd)										
25	27	27	27	53.2	2.4×10^{-2}	11.2×10^{-2}	11.2×10^{-2}	1.1×10^{-2}	13.0	Sam. 39; 25.5 mm Hg of CO_2 . Same. 43-45; H_2 added to Sam. 39.
26	27	27	27	67	0.6	14.5	14.5	1.1	16.4	
27	27	27	27	116	0.2	16.9	16.7	1.2	19.0	
28	27	27	27	203	0.45	20.5	19.9	1.2	22.4	
29	27	27	27	315	0.8	24.9	23.1	1.2	26.6	
30	27	27	27	332	0.63	29.1	27.1	1.2	30.9	
31	27	27	27	1580	0.68	34.5	30.8	1.5	35.6	
32	27	27	27	64.5	0.66×10^{-2}	19.9×10^{-2}	19.9×10^{-2}	1.5×10^{-2}	22.6	Sam. 46; 49.6 mm Hg of CO_2 . Same. 51-53; H_2 added to Sam. 46.
33	27	27	27	116	0.9	23.1	23.1	1.7	26.4	
34	27	27	27	218	0.6	28.7	24.9	1.8	30.4	
35	27	27	27	456	0.7	34.4	33.2	1.8	37.2	
36	27	27	27	528	1.1	41.2	39.1	1.9	44.5	
37	27	27	27	1674	1.1	43.5	44.6	2.0	51.1	
38	27	27	27	131	1.5×10^{-2}	24.2×10^{-2}	24.2×10^{-2}	2.5×10^{-2}	39.2	Sam. 52; 101 mm Hg of CO_2 . Same. 53-55; H_2 added to Sam. 52.
39	27	27	27	237	1.4	39.4	39.4	2.8	45.6	
40	27	27	27	435	1.7	47.2	45.7	2.9	52.6	
41	27	27	27	601	2.0	54.1	54.1	3.2	62.0	
42	27	27	27	1710	2.0	62.4	60.1	3.4	68.2	
43	27	27	27	269	2.4×10^{-2}	55.1×10^{-2}	55.1×10^{-2}	4.9×10^{-2}	64.1	Sam. 57; 207 mm Hg of CO_2 . Same. 58-60; H_2 added to Sam. 57.
44	27	27	27	310	2.6	62.9	62.1	5.6	72.8	
45	27	27	27	700	3.1	69.3	69.9	6.0	80.6	
46	27	27	27	1715	3.5	75.5	74.0	6.5	87.0	
47	27	27	27	529	4.7×10^{-2}	76.4×10^{-2}	75.9×10^{-2}	8.7×10^{-2}	92.1	Sam. 61; 407 mm Hg of CO_2 . Same. 62-63; H_2 added to Sam. 61.
48	27	27	27	904	5.4	81.8	80.5	9.6	99.0	
49	27	27	27	1780	5.6	81.3	81.1	10.9	103	
50	27	27	27	1555	8.4×10^{-2}	93.6×10^{-2}	93.1×10^{-2}	16.5×10^{-2}	118	Sam. 64; 811 mm Hg of CO_2 . Same. 65; H_2 added to Sam. 64.
51	27	27	27	1905	9.7	94.4	94.5	19.9	124	
52	27	27	27	4.0	1.8×10^{-2}	2.0×10^{-2}	2.0×10^{-2}		1.95	Same. 66-68; CO_2 alone.
53	27	27	27	7.7	3.5	3.5	3.5		3.66	
54	27	27	27	2110	17.7	17.6	30.6	26.6×10^{-2}	142	
Path Length = 400 cm										
55	27	27	27	154.6	1.1×10^{-2}	26.6×10^{-2}	31.1×10^{-2}	9.8×10^{-2}	14.5	Sam. 69; 121.0 mm Hg of $\text{$

Table 4. (Cont'd.)

Sample No.	Pig. No.	Temp. C.	Temp. deg.	V (mm cm)	P (mm Hg)	N (m ² sec ⁻¹)				A (v) \int_{495}^{875}	Remarks	
						730-875 cm ⁻¹	667-720 cm ⁻¹	617-667 cm ⁻¹	545-617 cm ⁻¹			495-545 cm ⁻¹
Path Length = 400 cm (Cont'd.)												
875	29	26.5	11.5	31.2	3.0 x 10 ⁻²	46.4 x 10 ⁻²	43.4 x 10 ⁻²	43.4 x 10 ⁻²	6.4 x 10 ⁻²	58.3	Sam. 76; 24.0 mm Hg of CO ₂ . Same 77-81; H ₂ added to Sam. 76.	
876	29	26.5	11.5	67.2	3.7	57.5	53.4	53.4	7.2	70.7		
877	29	26.5	11.5	157	4.8	71.1	71.4	71.4	9.8	87.9		
878	29	26.5	11.5	347	5.6	85.9	82.4	82.4	11.7	100		
879	29	26.5	11.5	759	7.6	88.3	87.3	87.3	14.7	113		
880	29	26.5	11.5	535	9.5	93.6	91.0	91.0	18.4	123		
881	29	26.5	11.5	0.197	0.26	1.2 x 10 ⁻²	1.4 x 10 ⁻²	1.4 x 10 ⁻²	0.1 x 10 ⁻²	1.44	Same. 82-94; CO ₂ alone.	
882	29	26.5	11.5	0.39	0.39	2.0	2.0	2.0	0.2	1.88		
883	29	26.5	11.5	0.59	0.59	3.4	3.6	3.6	0.4	4.04		
884	29	26.5	11.5	0.79	0.79	4.1	4.1	4.1	0.4	4.15		
885	29	26.5	11.5	0.99	0.99	5.0	5.8	5.8	0.7	6.32		
886	29	26.5	11.5	1.19	1.19	9.2	10.3	10.3	1.1	11.5		
887	29	26.5	11.5	2.32	2.24	15.5	15.2	15.2	1.6	16.9		
888	29	26.5	11.5	24.0	65	71.1 x 10 ⁻²	71.4 x 10 ⁻²	71.4 x 10 ⁻²	12.3	91.6	Same. 95-105; CO ₂ alone.	
889	29	26.5	11.5	43.0	150	88.8	88.8	88.8	19.7	121		
890	29	26.5	11.5	86.0	260	97.3	96.6	96.6	31.0	151		
891	29	26.5	11.5	98.5	34.5	100	99.6	99.6	49.0	176		
892	29	26.5	11.5	195	58.5	100	100	100	61.3	193		
893	29	26.5	11.5	364	988	100	100	100	70.1	216		
894	29	26.5	11.5	735	1970	100	100	100	70.1	216		
Path Length = 800 cm												
895	29	26.5	11.5	0.59	0.39	2.1 x 10 ⁻²	2.6	2.6	0.26 x 10 ⁻²	2.66		Same. 95-105; CO ₂ alone.
896	29	26.5	11.5	0.18	0.65	3.0	3.5	3.5	0.36	3.72		
897	29	26.5	11.5	0.77	1.04	4.9	5.3	5.3	0.64	5.02		
898	29	26.5	11.5	1.44	1.55	7.2	7.6	7.6	0.78	8.59		
899	29	26.5	11.5	2.15	2.77	12.6	15.9	1.5	1.5	15.6		
900	29	26.5	11.5	4.55	6.15	19.2	21.4	2.4	2.4	24.5		
Path Length = 1600 cm												
901	29	26.5	11.5	0.18	0.39	2.3 x 10 ⁻²	3.5 x 10 ⁻²	3.5 x 10 ⁻²	0.41 x 10 ⁻²	3.37		Same. 107; 9.0 mm Hg of H ₂ added to cell, then CO ₂ added to total pressure of 12.0 mm Hg; H ₂ was added to reduce absorptivity of cell. Same 110-113; H ₂ added to Sam. 107.
902	29	26.5	11.5	0.36	0.65	4.6	7.2	7.2	0.61	6.85		
903	29	26.5	11.5	1.25	1.04	6.3	7.7	7.7	0.85	8.06		
904	29	26.5	11.5	2.47	2.77	12.2	15.2	1.7	1.7	15.1		
905	29	26.5	11.5	3.56	2.77	17.0	19.1	3.0	3.0	21.7		
906	29	26.5	11.5	5.40	6.24	25.5	27.5	3.1	3.1	32.6		
Path Length = 3200 cm												
907	29	26.5	11.5	12.9	12.9	2.4 x 10 ⁻²	3.1	3.1	4.5 x 10 ⁻²	4.5		Same. 107; 9.0 mm Hg of H ₂ added to cell, then CO ₂ added to total pressure of 12.0 mm Hg; H ₂ was added to reduce absorptivity of cell. Same 110-113; H ₂ added to Sam. 107.
908	29	26.5	11.5	24.9	24.9	3.0	3.0	3.0	7.2	7.2		
909	29	26.5	11.5	51	51	5.1	5.1	5.1	9.2	9.2		
910	29	26.5	11.5	86.1	86.1	81.3 x 10 ⁻²	82.9 x 10 ⁻²	82.9 x 10 ⁻²	12.4	12.4		
911	29	26.5	11.5	161	161	85.8	86.1	86.1	14.9	14.9		
912	29	26.5	11.5	300	300	91.5	90.8	90.8	17.8	17.8		

Table 4. (Cont'd)

Sample No.	Flt. No.	Wavelength (Å)	$\lambda(\nu_1-\nu_2)$	657-720 cm^{-1}	617-667 cm^{-1}	545-617 cm^{-1}	495-545 cm^{-1}	$\int_{495}^{875} A(\nu) d\nu$	Remarks
Path length = 3000 cm (cont'd)									
B 101	27	23.5	7.8	1.5×10^{-2}			5.7×10^{-2}		Sam. 114; 6.0 mm Hg of CO_2 . Sam. 115-121; H_2 added to Sam. 114.
B 102	27	23.5	13.0				3.6		
B 103	27	23.5	22.7				9.5		
B 104	27	23.5	31.5				12.9		
B 105	27	23.5	42.7				15.3		
B 106	27	23.5	52				20.5		
B 107	27	23.5	62				24.7		
B 108	27	23.5	70					95.9	
B 109	27	23.5	80					110	
B 110	27	23.5	90					125	
B 111	27	23.5	100					135	
B 112	27	23.5	110						Sam. 122; 12.0 mm Hg of CO_2 . Sam. 123-126; H_2 added to Sam. 122.
B 113	27	23.5	120					71.5	
B 114	27	23.5	130					85.6	
B 115	27	23.5	140					97.7	
B 116	27	23.5	150					114	
B 117	27	23.5	160					128	
B 118	27	23.5	170					141	
B 119	27	23.5	180					156	
B 120	27	23.5	190						
B 121	27	23.5	200						
B 122	27	23.5	210						
B 123	27	23.5	220						
B 124	27	23.5	230						
B 125	27	23.5	240						
B 126	27	23.5	250						
B 127	27	23.5	260						
B 128	27	23.5	270						
B 129	27	23.5	280						
B 130	27	23.5	290						
B 131	27	23.5	300						
B 132	27	23.5	310						
B 133	27	23.5	320						
B 134	27	23.5	330						
B 135	27	23.5	340						
B 136	27	23.5	350						
B 137	27	23.5	360						
B 138	27	23.5	370						
B 139	27	23.5	380						
B 140	27	23.5	390						
B 141	27	23.5	400						
B 142	27	23.5	410						
B 143	27	23.5	420						
B 144	27	23.5	430						
B 145	27	23.5	440						
B 146	27	23.5	450						
B 147	27	23.5	460						
B 148	27	23.5	470						
B 149	27	23.5	480						
B 150	27	23.5	490						
B 151	27	23.5	500						
B 152	27	23.5	510						
B 153	27	23.5	520						
B 154	27	23.5	530						
B 155	27	23.5	540						
B 156	27	23.5	550						
B 157	27	23.5	560						
B 158	27	23.5	570						
B 159	27	23.5	580						
B 160	27	23.5	590						
B 161	27	23.5	600						
B 162	27	23.5	610						
B 163	27	23.5	620						
B 164	27	23.5	630						
B 165	27	23.5	640						
B 166	27	23.5	650						
B 167	27	23.5	660						
B 168	27	23.5	670						
B 169	27	23.5	680						
B 170	27	23.5	690						
B 171	27	23.5	700						
B 172	27	23.5	710						
B 173	27	23.5	720						
B 174	27	23.5	730						
B 175	27	23.5	740						
B 176	27	23.5	750						
B 177	27	23.5	760						
B 178	27	23.5	770						
B 179	27	23.5	780						
B 180	27	23.5	790						
B 181	27	23.5	800						
B 182	27	23.5	810						
B 183	27	23.5	820						
B 184	27	23.5	830						
B 185	27	23.5	840						
B 186	27	23.5	850						
B 187	27	23.5	860						
B 188	27	23.5	870						
B 189	27	23.5	880						
B 190	27	23.5	890						
B 191	27	23.5	900						
B 192	27	23.5	910						
B 193	27	23.5	920						
B 194	27	23.5	930						
B 195	27	23.5	940						
B 196	27	23.5	950						
B 197	27	23.5	960						
B 198	27	23.5	970						
B 199	27	23.5	980						
B 200	27	23.5	990						
B 201	27	23.5	1000						
B 202	27	23.5	1010						
B 203	27	23.5	1020						
B 204	27	23.5	1030						
B 205	27	23.5	1040						
B 206	27	23.5	1050						
B 207	27	23.5	1060						
B 208	27	23.5	1070						
B 209	27	23.5	1080						
B 210	27	23.5	1090						
B 211	27	23.5	1100						
B 212	27	23.5	1110						
B 213	27	23.5	1120						
B 214	27	23.5	1130						
B 215	27	23.5	1140						
B 216	27	23.5	1150						
B 217	27	23.5	1160						
B 218	27	23.5	1170						
B 219	27	23.5	1180						
B 220	27	23.5	1190						
B 221	27	23.5	1200						
B 222	27	23.5	1210						
B 223	27	23.5	1220						
B 224	27	23.5	1230						
B 225	27	23.5	1240						
B 226	27	23.5	1250						
B 227	27	23.5	1260						
B 228	27	23.5	1270						
B 229	27	23.5	1280						
B 230	27	23.5	1290						
B 231	27	23.5	1300						
B 232	27	23.5	1310						
B 233	27	23.5	1320						
B 234	27	23.5	1330						
B 235	27	23.5	1340						
B 236	27	23.5	1350						
B 237	27	23.5	1360						
B 238	27	23.5	1370						
B 239	27	23.5	1380						
B 240	27	23.5	1390						
B 241	27	23.5	1400						
B 242	27	23.5	1410						
B 243	27	23.5	1420						
B 244	27	23.5	1430						
B 245	27	23.5	1440						
B 246	27	23.5	1450						
B 247	27	23.5	1460						
B 248	27	23.5	1470						
B 249	27	23.5	1480						
B 250	27	23.5	1490						
B 251	27	23.5	1500						
B 252	27	23.5	1510						
B 253	27	23.5	1520						
B 254	27	23.5	1530						
B 255	27	23.5	1540						
B 256	27	23.5	1550						
B 257	27	23.5	1560						
B 258	27	23.5	1570						
B 259	27	23.5	1580						
B 260	27	23.5	1590						
B 261	27	23.5	1600						
B 262	27	23.5	1610						
B 263	27	23.5	1620						
B 264	27	23.5	1630						
B 265	27	23.5	1640						
B 266	27	23.5	1650						
B 267	27	23.5	1660						
B 268	27	23.5	1670						
B 269	27	23.5	1680						
B 270	27	23.5	1690						
B 271	27	23.5	1700						
B 272	27	23.5	1710						
B 273	27	23.5	1720						
B 274	27	23.5	1730						
B 275	27	23.5	1740						
B 276	27	23.5	1750						
B 277	27	23.5	1760						
B 278	27	23.5	1770						
B 279	27	23.5	1780						
B 280	27	23.5	1790						
B 281	27	23.5	1800						
B 282	27	23.5	1810						
B 283	27	23.5	1820						
B 284	27	23.5	1830						
B 285	27	23.5	1840						
B 286	27	23.5	1850						
B 287									

2010

Sample No.	Age (yr.)	Depth (cm)	^{14}C (p.p.m.)	^{13}C (p.p.m.)	$\delta^{13}\text{C}$ (‰)	Notes
1	0	0	100	100	0	
2	1	1	95	95	-5	
3	2	2	90	90	-10	
4	3	3	85	85	-15	
5	4	4	80	80	-20	
6	5	5	75	75	-25	
7	6	6	70	70	-30	
8	7	7	65	65	-35	
9	8	8	60	60	-40	
10	9	9	55	55	-45	
11	10	10	50	50	-50	
12	11	11	45	45	-55	
13	12	12	40	40	-60	
14	13	13	35	35	-65	
15	14	14	30	30	-70	
16	15	15	25	25	-75	
17	16	16	20	20	-80	
18	17	17	15	15	-85	
19	18	18	10	10	-90	
20	19	19	5	5	-95	
21	20	20	0	0	-100	

Table 4. (Cont'd)

Sample No.	Fig. No.	Temp. C. deg.	ν (cmos cm)	(mm Hg)	$\bar{\nu}$ (720-875 cm ⁻¹)	Remarks
Path Length = 3200 cm						
C 26	17	25.0	305	103	20.2 x 10 ⁻²	Spectra of same. C 26 - C 42 were obtained in connection with the investigation of the 1064 and 961 cm ⁻¹ CO ₂ bands. A NaCl prism was used and frequencies less than 670 cm ⁻¹ could not be investigated.
C 27		25.0	305	236	24.4	
C 28	17	25.0	305	332	26.0	
C 29		25.0	305	767	29.1	
C 30	17	25.0	305	3070	33.5	
C 31	17	25.0	685	212	30.0	Sampling procedures for same. C 26 - C 42 are given in Table 3.
C 32	17	25.0	685	389	32.4	
C 33	17	25.0	685	798	34.8	
C 34		25.0	685	3075	36.6	
C 35	17	25.0	1245	481	37.1	
C 36	17	25.0	1245	889	40.0	
C 37	17	25.0	1245	3120	43.7	
C 38	17	25.0	2945	1780	51.3	
C 39	17	25.0	2945	3240	53.0	
C 40	17	25.0	5730	1990	61.0	
C 41	17	25.0	5730	3380	62.7	
C 42	17	25.0	11800	1800	71.3	

Table 5. Band Intensities

The values of $\int k(\nu) d\nu$ are in units of $\text{atmos}^{-1} \text{cm}^{-2}$ S.T.P.. Values given for the present study correspond to a temperature of 25°C , and the estimated uncertainties are indicated.

Wavenumber	$\int k(\nu) d\nu$
<u>3716 cm^{-1} Band</u>	
Present Study	54 ± 10
Eggers and Crawford ¹⁰	39
<u>1609 cm^{-1} Band</u>	
Present Study	37 ± 8
<u>2122 cm^{-1} Band</u>	
Present Study	2500 ± 400
Eggers and Crawford ¹⁰	2100
<u>1024 cm^{-1} Band</u>	
Present Study	0.045 ± 0.010
<u>751 cm^{-1} Band</u>	
Present Study	0.023 ± 0.006
<u>567 cm^{-1} Band</u>	
Present Study	130 ± 90
Eggers and Crawford ¹⁰	161
Kaplan and Eggers ¹¹	240
Thorndike ¹¹	187
Weber et al. ¹²	170
Yamamoto and Sanoori	212

REFERENCES

1. D. E. Burch and D. Williams, Scientific Report 1, Contract No. AF 19(604)-2633, Geophysics Research Directorate, Air Research and Development Command, Hanscom Field, Bedford, Massachusetts.
2. D. E. Burch, E. B. Singleton, et al., Final Report, Contract No. AF 19(604)-2633, Geophysics Research Directorate, Air Research and Development Command, Hanscom Field, Bedford, Massachusetts.
3. J. R. Howard, D. E. Burch, and D. Williams, Geophysical Research Paper No. 40, GRC, Air Force Cambridge Research Center (1955). See also J. Opt. Soc. Am., 46, 136, 237, 242, 334, 452 (1946).
4. Lewis Kaplan, Department of Meteorology, Mass. Inst. of Tech. (Private Communication).
5. William Penzance, Laboratory of Astrophysics and Physical Meteorology, The Johns Hopkins University (Private Communication).
6. J. A. Edwards, J. Opt. Soc. Am. 50, 617 (1960).
7. The Infrared, The Department of Physics at the University of Chicago
Carbon Monoxide Band, The Science Reports of the Johns University,
Series in Geophysics, Vol. 11, No. 1.
8. L. D. Kaplan and D. F. Eggers, J. Chem. Phys. 31, 576 (1959).
9. F. J. Rothman and L. D. Kaplan, J. Chem. Phys. 35, 1242 (1961).
10. D. F. Eggers and F. J. Rothman, J. Chem. Phys. 30, 1554 (1951).
11. L. H. Thomas, J. Chem. Phys. 11, 565 (1943).
12. J. Weber, Kuhn, and E. S. Pomeroy, J. Chem. Phys. 20, 1680 (1952).
13. G. Yoshida and T. Goshima, "Calculation of the Absorption of the
The Carbon Monoxide Band," The Science Reports of the Johns University,
Series in Geophysics, Vol. 11, No. 1, July 1960.

PART C

ABSORPTION BY WATER VAPOR
AND NITROUS OXIDE

by

Darrell E. Burch, Edgar B. Singleton
Wilbur L. France, and Dudley Williams

CONTENTS-PART C

<u>Section</u>		<u>Page</u>
I	INTRODUCTION	1
	Symbols and Units	2
II	RELATIVE BROADENING ABILITIES	3
	Foreign-Gas Broadening	14
	Experimental Results for the H_2O Bands at 2563, 2461, 1265, 1167, 629 and 569 cm^{-1}	20
	Band Intensities	38
	The H_2O Bands at 5332, 3700, and 1595 cm^{-1}	39
	Absorption Effects and the Determination of Absorber Concentration	39
	Experimental Results	42
	SUMMARY	60
	REFERENCES	61
APPENDIX I	A VACUUM TUBE FOR A PERCUT-FLAME SINGLE-BEAM MONOCHROMATOR	62

List of Tables

Table No.

1	Self-Broadening Coefficients	13
2	Foreign-Broadening Coefficients and Relative Molecular Cross Sections	17
3	Comparison of Ratios of Collision Cross Sections with Results of Cross and Danials	18
4	Comparison of Broadening Abilities and Collision Cross Sections with Results of Hensch and Elder	19
5	Data for the 2563 and 2461 cm^{-1} H_2O Bands	22
6	Data for the 1265 and 1167 cm^{-1} H_2O Bands	26

List of Tables (Cont'd)-PART C

Table No.		Page
7	Data for the 589 and 692 cm^{-1} H_2O Bands	34
8	H_2O Band Intensities	36
9	Data for the 5332 cm^{-1} H_2O Band	44
10	Data for the 3700 cm^{-1} H_2O Band	50
11	Data for the 1595 cm^{-1} H_2O Band	58

List of Figures

Figure No.		
1	The self-broadening coefficient B for the 2224 cm^{-1} H_2O band	6
2	The self-broadening coefficient B for the 3020 cm^{-1} CH_4 band	8
3	The self-broadening coefficient B for the 1306 cm^{-1} CH_4 band	9
4	The self-broadening coefficient B for CO_2 in the 667 cm^{-1} region	10
5	Total absorption versus total pressure for 2145 cm^{-1} CO band	15
6	Absorption curves for the 2565 cm^{-1} and 2461 cm^{-1} H_2O bands	21
7	The total absorption of the 2565 cm^{-1} H_2O band versus P_0 and y	23
8	The total absorption of the 2461 cm^{-1} H_2O band versus P_0 and y	24
9	Absorption curves for the 1205 cm^{-1} and 1167 cm^{-1} H_2O bands	25
10	The total absorption of the 1205 cm^{-1} H_2O band versus P_0	26
11	The total absorption of the 1167 cm^{-1} H_2O band versus y	29

List of Figures (Cont'd)-PART C

<u>Figure No.</u>		<u>Page</u>
12	The total absorption of the 1167 cm^{-1} H_2O band versus P_0	30
13	The total absorption of the 1167 cm^{-1} H_2O band versus y	31
14	Absorption curves for the 589 cm^{-1} and 629 cm^{-1} H_2O bands	33
15	The total absorption of the 589 cm^{-1} H_2O band versus P_0	36
16	The total absorption of the 589 cm^{-1} H_2O band versus y	37
17	Representative absorption curves of the 5332 cm^{-1} H_2O band	43
18	The total absorption of the 5332 H_2O cm^{-1} band versus P_0	46
19	The total absorption of the 5332 cm^{-1} H_2O band versus y	48
20	Representative absorption curves for the 3700 cm^{-1} H_2O band	49
21	The total absorption of the 3700 cm^{-1} H_2O band versus P_0	52
22	The total absorption of the 3700 cm^{-1} H_2O band versus y	53
23	Representative absorption curves of the 1595 cm^{-1} H_2O band	54
24	Representative absorption curves of the 1595 cm^{-1} H_2O band	55
25	The total absorption of the 1595 cm^{-1} H_2O band versus P_0	56
26	The total absorption of the 1595 cm^{-1} H_2O band versus y	57
27	Drawing of vacuum tank containing a Perkin-Elmer Model 99 spectrometer	60

ABSORPTION BY WATER VAPOR AND NITROUS OXIDE

I. INTRODUCTION

This is the third and final report dealing with the results of a research program concerned with the absorption of infrared radiation by various atmospheric gases. The contents of the three reports are as follows:

REPORT 1¹: Absorption by nitrous oxide in the 2224 cm^{-1} region; absorption by carbon monoxide in the region of its fundamental (2143 cm^{-1}) band and its first overtone (4260 cm^{-1}) band; absorption of methane bands at 3000 cm^{-1} , 1550 cm^{-1} , and 1306 cm^{-1} .

REPORT 2²: Absorption by carbon dioxide bands at 2350 cm^{-1} , at 3609 cm^{-1} , at 3716 cm^{-1} , at 961 cm^{-1} , at 1054 cm^{-1} , and in the range 875-895 cm^{-1} .

FINAL REPORT (herewith): A study of the relative pressure "broadening abilities" of all of the absorbing gases studied in the research program, and of various inactive gases. Absorption by water vapor in the region of its vibration-rotation bands at 1595 cm^{-1} , at 5332 cm^{-1} , and near 3700 cm^{-1} ; absorption by nitrous oxide bands at 2563 cm^{-1} , 2461 cm^{-1} , 1265 cm^{-1} , 1167 cm^{-1} , 692 cm^{-1} , and at 589 cm^{-1} .

A portion of the data on the relative broadening abilities of inactive gases, and on the H_2O , CO , and CO_2 bands, was reported previously in Ph.D. dissertations by two of us.^{3,4} However, additional data included in the three reports outlined above were not included in these dissertations.

The present research program is a continuation of two earlier studies made in this department, in 1946 by Chapman and Howard,⁵ and in 1953 by Howard, Burch, and Williams⁶ (hereafter referred to as HW⁶).

The experimental methods used in gas sampling, in obtaining the absorption curves, and in analyzing the data were described in Report 1 and will not be repeated, with the exception of the method of sampling water vapor which is described below in Section IV.

The original plans included a study of water vapor absorption in the 480-1000 cm^{-1} region; however, this portion of the study was postponed and will probably be done as a part of another future program in this laboratory.

Symbols and Units

Values of absorber partial pressure p , total pressure P , and equivalent pressure P_e (defined by equation (5)) are expressed in units of mm Hg absolute. Absorber path lengths are in cm. Values of absorber concentration w of water vapor are in units of precipitable centimeters (abbreviated pr. cm) which represents the depth in centimeters of the water that would be obtained if all the water vapor in a column containing the beam were condensed out. The values of absorber concentration of other gas samples are expressed in units of atmos cm, and are found by multiplying the absorber path length in cm times the absorber partial pressure in atmospheres corrected to standard temperature.

Frequencies and values of total absorption $\int A(\nu)d\nu$, where $A(\nu)$ is the observed fractional absorption at frequency ν , are in units of cm^{-1} ; and band intensities $\int k(\nu)d\nu$, where $k(\nu)$ is the absorption coefficient at frequency ν , are in units of $\text{atmos}^{-1} \text{cm}^{-2} \text{ S.T.P.}$

II. RELATIVE BROADENING ABILITIES

A method of measuring the "self-broadening ability" of an absorbing gas relative to the "broadening ability" of the non-absorbing gas H_2 has been given in Report 1. It was shown that the analysis of total absorption data obtained from samples containing H_2 along with an absorbing gas was simplified by use of an experimentally determined ratio of the broadening abilities of the gases. The broadening effect of both gases can then be expressed in terms of a single variable, which is called the equivalent pressure and is defined below in Eq. (5); and the total absorption can be expressed as a function of two variables: absorber concentration, and equivalent pressure. In this section all the results of self-broadening measurements carried out in the present research investigations are summarized, and these results are discussed in some detail and compared with those of other workers.

Aside from its importance in the analysis of infrared absorption data, a knowledge of the relative broadening abilities of gases provides information concerning the collision cross sections of the molecules, which are determined by various forces of interaction between the molecules. For the same reason that a knowledge of self-broadening is important, so is a knowledge of the broadening abilities of nonabsorbing gases other than H_2 , such as O_2 , N_2 , Ar , H_2 . The latter portion of this section deals with the relative broadening abilities of these nonabsorbing gases, as well as with some other gases such as CO , CH_4 , and C_2H_6 which were used as "foreign" broadening gases in the study of absorption bands occurring at frequencies where these gases do not absorb.

The half-width α of a collision-broadened spectral line is proportional to the collision frequency F of each absorbing molecule. From kinetic theory it can be shown that the half-width α of a collision-broadened line is given by the relation

$$\alpha = \frac{F}{2\pi} = \frac{1}{2\pi} \sum_i N_i (\bar{u}_{c,i})^2 \left[\sum_j \left(\frac{1}{u_j} + \frac{1}{u_i} \right) \right]^{1/2}, \quad (1)$$

where N_i is the number of molecules of the i -th type per unit volume, $\bar{u}_{c,i}$ is the sum of the optical collision diameters of the absorbing molecule and a molecule of the i -th type, k is Boltzmann's constant, T is the absolute temperature, m_i is the mass of the absorbing molecule, and m_j is the mass of a molecule of the j -th type.

The appearance of $\bar{u}_{c,i}$ and m_j in (1) indicates that different gases have different "broadening" effects on spectral lines. Since most of the gas samples employed in the experimental work consisted of binary mixtures of absorbing gases and nitrogen, which was used as a nonbroadening "broadening gas," it is desirable to consider (1) for the

special case of a binary mixture of an absorbing gas a and a broadening gas b. The summation in (1) will in this case have two terms: a self-broadening term in which $i = a$, and a second term for the effects of broadening by the inert gas: $i = b$. Equation (1) then assumes the form,

$$\alpha = \frac{1}{4\pi} \left[\frac{2\pi}{kT} \right]^{1/2} \left\{ N_a (D_{a,a})^2 \left[\frac{2}{M_a} \right]^{1/2} + N_b (D_{a,b})^2 \left[\frac{M_a + M_b}{M_a M_b} \right]^{1/2} \right\} \quad (2)$$

By recalling that the partial pressure p_i of gas of the i -th type is given by $p_i = N_i kT$ and by assuming that collision diameters are independent of temperature and pressure, one can write (2) in the form

$$\alpha = \frac{1}{4\pi} \left[\frac{2\pi}{kT} \right]^{1/2} C_{a,a} p_a + C_{a,b} p_b \quad (3)$$

where $C_{a,a}$ and $C_{a,b}$ are constants involving the optical collision diameters and masses of the absorbing and broadening gases. Since the total pressure $P = p_a + p_b$, one may obtain an expression for α in terms of P and p_a by rewriting (3) in the form

$$\alpha = \frac{1}{4\pi} \left[\frac{2\pi}{kT} \right]^{1/2} C_{a,b} \left\{ P + (B-1)p_a \right\} \quad (4)$$

where $B = C_{a,a}/C_{a,b}$ is called the self-broadening coefficient of the absorbing gas and represents the ratio of the "self-broadening ability" of the absorbing gas to the "broadening ability" of the nonabsorbing gas. Methods for determining B for various absorbing gases relative to N_2 will be described below. The term in brackets in (4) is called the equivalent pressure P_e of the gas sample.

$$P_e = P + (B-1)p = p_{pp} + Bp \quad (5)$$

where p is the partial pressure of the absorbing gas and P is the measured total pressure of the sample due to the absorbing gas and N_2 . It is seen that P_e reduces to P in the case of $p \ll P$.

From (4) one sees that for a given temperature α is proportional to P_e , and once the value of P has been determined it is possible to describe the "broadening effect" of the two gases in terms of the parameter B . It was shown in Report 1 that the fractional absorption $A(\nu)$ and the total absorption $A(\nu)_{\text{av}}$ are functions of only two parameters, P_e and absorber concentration y .

The experimental determination of B involves a study of the transmission of radiation through cells of different length l in which the absorber concentration y is the same. The sample in the short cell, called the "reference cell," consists of a pure sample of the

absorbing gas at pressure p ; for this cell $p^{\text{ref}} = p^{\text{ref}}$ and the equivalent pressure is given by

$$P_0 = B p^{\text{ref}} \quad (\text{Reference cell}). \quad (6)$$

The sample in the longer cell, called the "sample cell," initially consists of a sample of the pure absorber at the partial pressure p required to produce an absorber concentration w equal to that in the reference cell. Initially, the absorption of radiation in the sample cell is considerably less than that in the reference cell, since the partial pressure and total pressure are less than those in the shorter reference cell. Various amounts of M_2 are then added to the reference cell corresponding to equivalent pressures

$$P_0 = p_{M_2} + B p \quad (\text{Sample Cell}), \quad (7)$$

where p_{M_2} is the partial pressure of the broadening gas. For the situation in which the absorptions in the sample and reference cells are most nearly equal, it is assumed that the values of P_0 in (6) and (7) are equal. The value of the self-broadening coefficient can then be determined from the relation

$$B = \frac{p_{M_2}}{p^{\text{ref}} - p} \quad (8)$$

where p_{M_2} is the partial pressure of M_2 in the longer sample cell when the absorptions in the two cells are equal. If the reference cell also contains M_2 at a partial pressure $p_{M_2}^{\text{ref}}$, it can easily be shown that

$$p = \frac{p_{M_2}^{\text{ref}} - p_{M_2}}{p^{\text{ref}} - p} \quad (9)$$

The value of B was determined for several of the absorption bands included in the present research program by making use of the double-beam Perkin-Elmer or the Perkin-Elmer Model 21 spectrometer. In some cases a 6.44-cm absorption cell was used in the sample beam with a 1.55-cm cell in the reference beam; in other cases a 440-cm reference cell was used with either an 800-cm or 1600-cm sample cell to investigate samples having large values of w .

Typical spectral comparisons which were obtained in this manner for the 2224 cm^{-1} M_2O band are shown in Part I of Fig. 1 for various values of total pressure in the sample cell. The spectrometer recorded the ratio of the transmission of the sample cell $T(\text{sam})$ to the transmission of the reference cell $T(\text{ref})$; the dashed line at

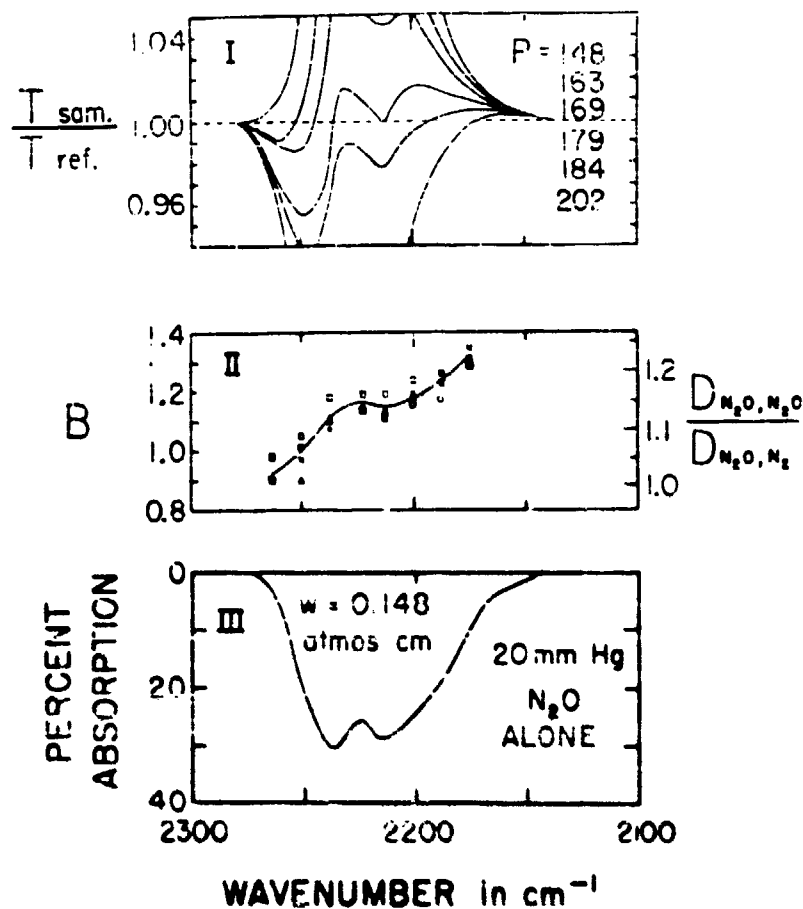


Fig. 1. The self-broadening coefficient B for the 2284 cm^{-1} N_2O band.
Part I: Spectra obtained with $w = 0.50 \text{ atmos cm}$ of N_2O in both reference and sample cells; total pressure in reference cell = 164 mm Hg . Total pressure in sample cell for each spectrum is indicated.
Part II: Plot of B and collision cross section ratio. The four different geometrical points correspond to the results of the set of spectra shown in Part I as well as to three other sets of samples having different values of w .
Part III: A typical absorption curve which is shown for comparison.

$T(\text{sam.})/T(\text{ref.}) = 1.00$ represents the recorder pen position when the two beams were "balanced," i.e., the transmissions of both samples were the same. It is seen that the ratio of the transmissions decreased with increasing pressure in the sample cell as would be expected, and that some of the curves representing the ratios occur above the balance line for some frequencies and below the line for others. Therefore, the total pressure corresponding to balance was not the same for all frequencies; the pressure corresponding to balance for any given frequency was determined by interpolating between the two successive curves which occur on opposite sides of the balance line.

Since the value of p_{B_2} corresponding to equal transmission of the cells was found to vary with frequency, it is apparent that the value of B varies throughout the band. Points corresponding to the experimentally determined value B were plotted against frequency in Part II of Fig. 1. The collision cross section ratio which is shown by the right-hand scale in Part II of Fig. 1 can be shown by use of (2), (3), and (4) to be related to B by

$$B = \left[\frac{2M_b}{M_a + M_b} \right]^{1/2} \left[\frac{D_{a,b}}{D_{b,b}} \right]^2 \quad (10)$$

where M_b is the mass of the B_2 molecule M_{B_2} .

A typical absorption curve of an H_2O sample is shown in Part III of Fig. 1 in order that the "structure" of the absorption curve can be correlated with the structure of the curve relating B to wavenumber.

In Figures 2, 3, and 4 are shown curves of B vs. wavenumber, and the related collision cross section ratio, for the 3080 cm^{-1} and 1306 cm^{-1} CH_4 bands and for CO_2 in the 667 cm^{-1} region, respectively; a typical absorption curve is shown in each figure for comparison. The curves of B for these bands were chosen as illustrations since the value of B changes very definitely throughout the bands. The value of B was found to be more nearly constant for other bands investigated by the method described above.

It should be emphasized that the accuracy of the value of B determined by this method depends strongly upon the accuracy to which the absorber concentration y is made the same in both the reference and sample cells. If y were not the same in both cells, a false value of B would be determined; the shape of the curve relating B to wavenumber would also be modified.

In the process of measuring B for each band, cells of samples having different values of y and Y were used; samples of $y \approx 1\%$ were used primarily to determine B at frequencies of strong absorption, while samples of larger y were necessary in investigating the wings of

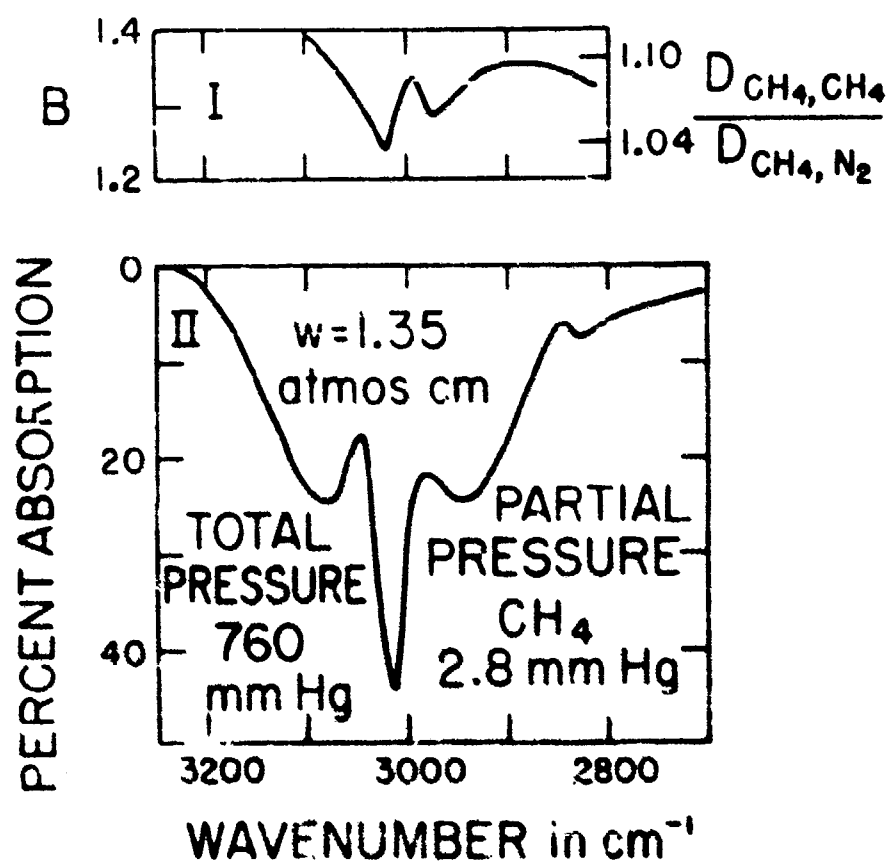


Fig. 2. The self-broadening coefficient B for the 3000 cm^{-1} CH_4 band.
 Part I: Plot of B and the collision cross section ratio.
 Part II: A typical absorption curve which is shown for comparison.

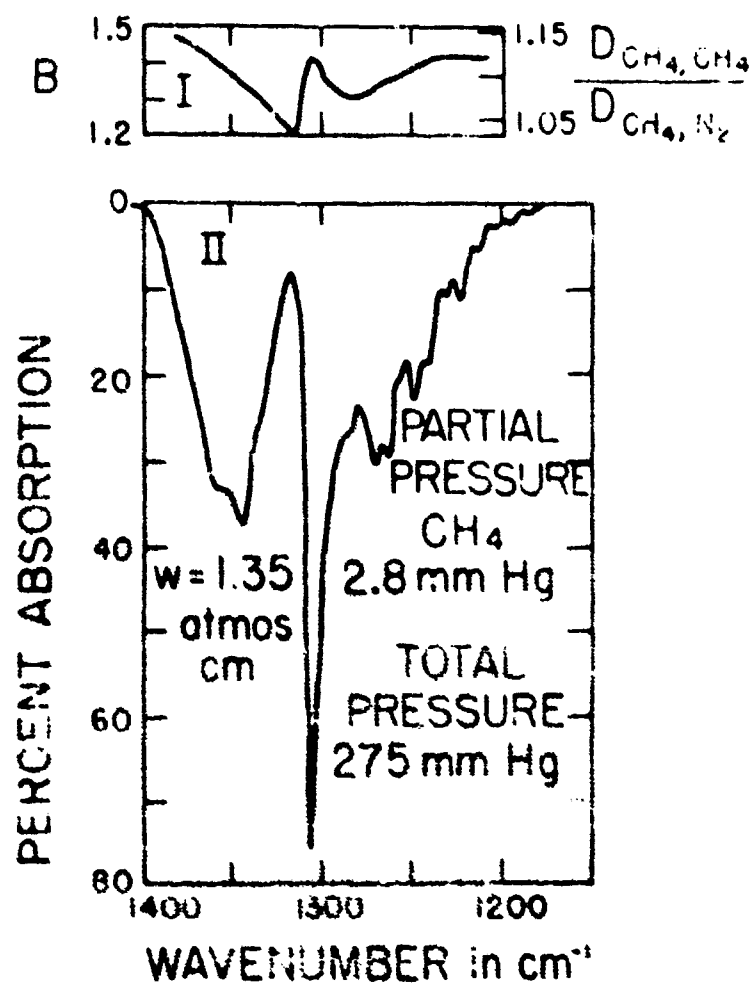


Fig. 2. The self-broadening coefficient b for the 1306 cm^{-1} CH_4 band.
 Part I: Plot of b and the collision cross section σ .
 Part II: A typical absorption curve which is shown for comparison.

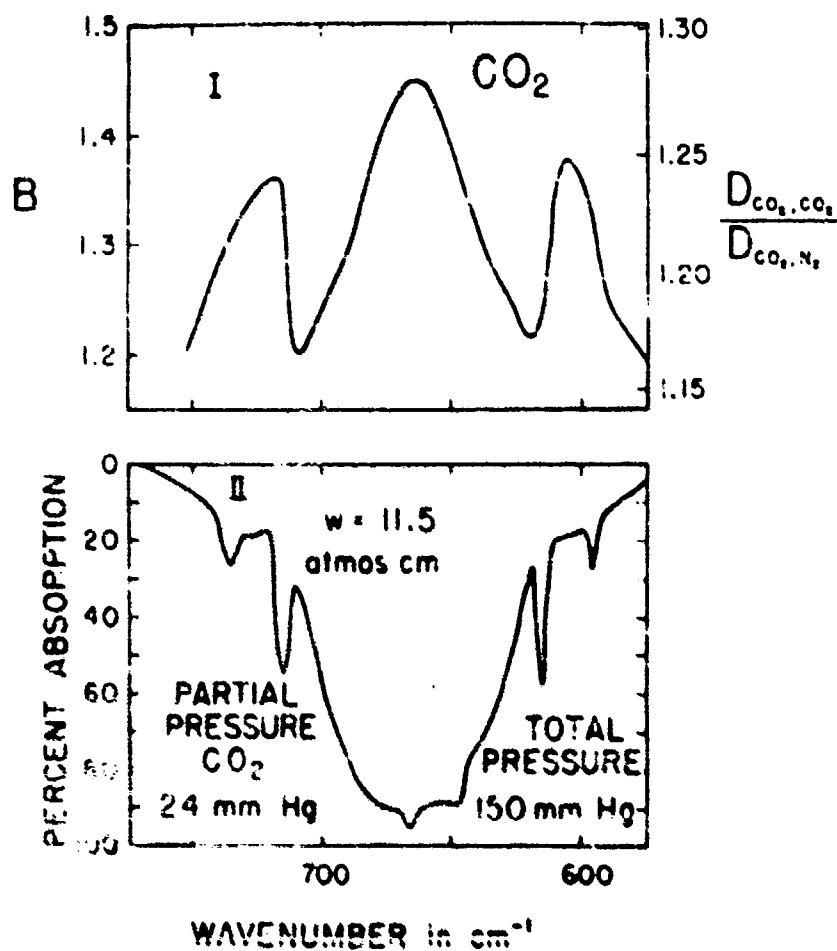


Fig. 1. The self-broadening coefficient B for CO₂ in the 657 cm^{-1} region.
 Part I: Plot of B and the collision cross section ratio.
 Part II: A typical absorption curve which is shown for comparison.

the bands. The samples were formed so that the fractional absorption of the samples being compared was usually between 0.3 and 0.9 in the spectral interval being investigated. For smaller fractional absorption the spectrometer was less sensitive to small changes in pressure, and thus, the total pressure corresponding to equal absorption in the two cells could not be determined as accurately. For values of fractional absorption greater than approximately 0.9, the power generated by the detector was too low to properly drive the servomechanism which controls the comb in the reference beam; a false reading might then be obtained unless extra care was taken. This difficulty could be overcome to some extent by increasing the amplifier gain and increasing the scanning time; however, as the fractional absorption approaches unity, the effect of scattered light of frequencies other than that being studied might become important and give rise to false readings. If the scattered light were equally intense in both the reference and the sample beams it would have no effect on the reading of the spectrometer, but it is possible that the intensities of the scattered light in the two beams were not equal; and values of B were not calculated for samples at frequencies at which the fractional absorption was greater than approximately 0.9.

Total pressures were also restricted to values less than approximately 1000 mm Hg, since for larger pressures the spectral lines become smeared and the dependence of absorption on pressure becomes less.

For the ranges of pressures and fractional absorption of the samples investigated, no dependence of the measured value of B at a given frequency on either of these parameters was found.

Some of the data were obtained by use of a single-beam Perkin-Elmer Model 99 spectrometer which was mounted in a vacuum tank*. This spectrometer was used to determine B for the 4260 cm^{-1} CO band, since this band could not be studied by use of the Model 21, which was limited to frequencies below 4000 cm^{-1} because of the prism used. The Model 99 was also used to investigate the total absorption and to measure B for some strong Cl_2 and H_2O bands.

Since the Model 99 is a single-beam instrument it was not possible to compare simultaneously the fractional absorption of two samples in different cells by the method described in connection with Fig. 1. Instead, "curves of growth" of total absorption were obtained for various samples with two or more different cell lengths. The "effective" value of B for the entire band was determined from the curves by finding the total pressure required for a sample in the longer cell to produce the same total absorption as a sample in the shorter cell which had the same absorber concentration. A sample calculation for this method of determining B was given in Report 1 in connection with the 4260 cm^{-1} CO band.

*This apparatus is described in some detail in Appendix I of this report.

The present research program deals primarily with total absorption rather than with fractional absorption at certain frequencies. It was therefore desirable to obtain a nominal value of B which could be used for an entire band. The method of determining B by use of the single-beam instrument, of course, yielded such an effective value of B since it was determined on the basis of total absorption. In the case of bands studied with the double-beam spectrometer, a nominal value of B for the entire band was determined by taking a "weighted average" value of B from curves such as those in Figs. 1-4, with extra weight given to the frequency ranges which contribute most of the absorption.

The values of B determined for each band included in Reports 1 and 2, as well as in this report, are listed in Table 1, and wherever possible they are compared to the results of other workers. Except for the case of H_2O , the tabulated values are believed to be accurate to $\pm 6\%$ as an effective value for the entire bands.

It is somewhat more difficult to determine B for H_2O bands than for the other bands for two reasons: (1) the value of absorber concentration y of an H_2O sample cannot be found as accurately because of the adsorption of the H_2O on the walls of the absorption cell. The method of determining y for H_2O samples, which involves finding the dew point, is discussed below in Section IV; (2) the range of available partial pressures of H_2O is limited to values less than the vapor pressure.

In the investigation of H_2O , a multiple-traversal cell whose path length could be adjusted by external controls, was used; different path lengths corresponding to 4, 18, 16, and 32 traversals were therefore easily obtained. From curves of growth of total absorption for different samples investigated at different path lengths it was possible to determine B for the H_2O bands. Because of the limitations stated above with regard to the accuracy of determining B for the H_2O bands, the value may be in error by as much as 25 to 30%.

It is apparent from the curves of Figs. 1-4 that a nominal value of B does not change slightly with total absorption, since for large total absorption the major portion of the growth occurs at different frequencies than for small total absorption. Since the nominal value was obtained by "weighting" the value of B at different frequencies according to the contribution to the growth, the best effective value for the entire band would therefore change with total absorption. However, it is seen from the curves of Figs. 1-4 that B varies by only a few percent for the different frequencies, and any change in the nominal value of B for the entire band would be negligible.

It was stated above that the measured value of B at any frequency did not apparently change with pressure or with fractional absorption for the limits over which these parameters were varied. Benedict and Palmer¹⁰, in an article on the absorption by H_2O in the 20 micron region,

Table 1. Self-Broadening Coefficients

Band	Investigator	Self-broadening Coefficient B
H_2O^a 2224 cm^{-1} , 1285 cm^{-1} and 167 cm^{-1} 1285 cm^{-1} 1167 cm^{-1} 2224 cm^{-1}	Present Study Goody and Mermell ⁷ Goody and Mermell ⁷ Cross and Daniels ⁸	1.12 \pm 0.07 1.27 \pm 0.34 1.55 \pm 0.07 1.2 ^b
CO 2.45 cm^{-1} 4.50 cm^{-1}	Present Study Present Study	1.02 \pm 0.06 1.03 \pm 0.06
CH_4 ⁺ 1020 cm^{-1} 1306 cm^{-1}	Present Study Present Study	1.30 \pm 0.08 1.30 \pm 0.08
CO_2 5716 cm^{-1} , 1609 cm^{-1} , 2350 cm^{-1} , 1064 cm^{-1} , 961 cm^{-1} bands and the 875-895 cm^{-1} region Same CO_2 bands	Present Study Rivaris ⁹	1.30 \pm 0.08 2 \pm 0.5p (where p = CO_2 partial pressure).
H_2O 5592 cm^{-1} , 3756 cm^{-1} , and 1595 cm^{-1} 20 micron region 4325 \pm cm^{-1} H_2O line 4 lines in 500-600 cm^{-1} region	Present Study Palmer ¹⁰ Vasilovsky and Reporant ¹¹ Itatli ¹²	5 \pm 1.5 6-11, increasing linearly with fractional absorption 6 5.6-5.5

^a5 was not measured for 2563 cm^{-1} , 2161 cm^{-1} and 589 cm^{-1} bands; but 1.12 was used in the analysis of these bands.

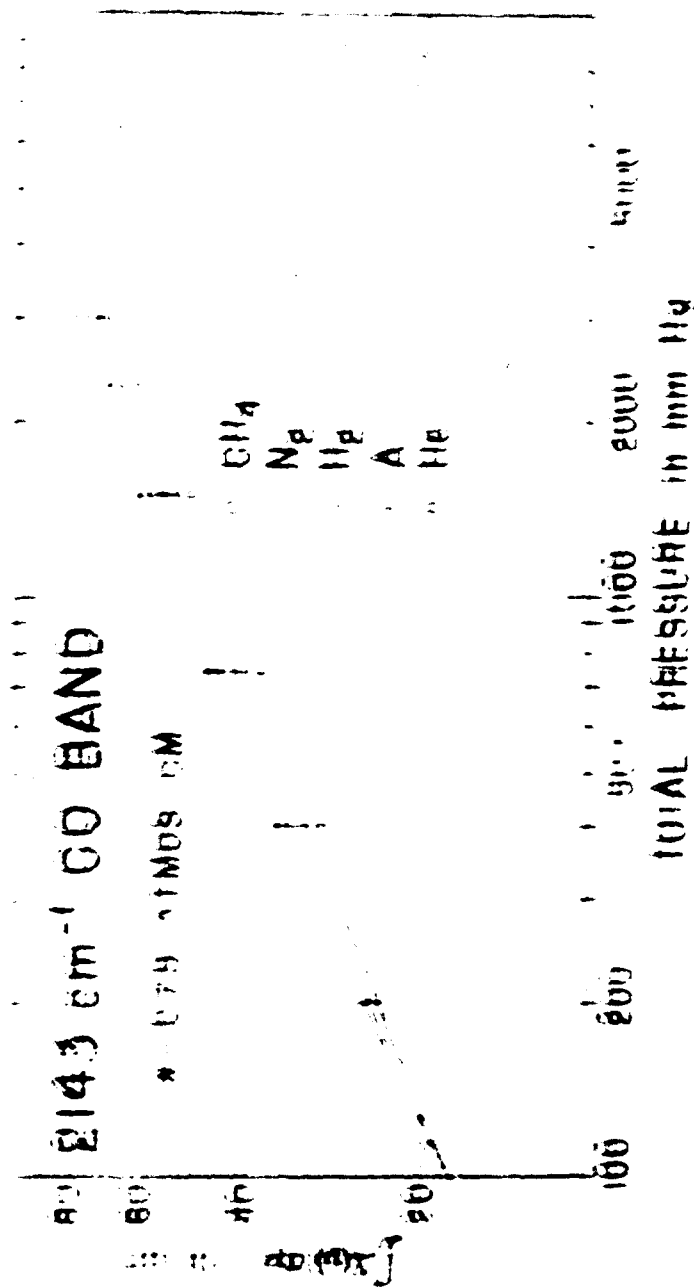
⁺8 was not measured for 1550 cm^{-1} band; 1.58 was used in analysis of the band.

have suggested that the value of B should increase with fractional absorption. This phenomenon arises from the fact that the spectral lines do not have a true Lorentzian shape, and that a self-broadened line absorbs more in the wings than does a foreign-broadened line of the same half-width. Since the line centers are virtually opaque in the case of large fractional absorption, the only growth with increasing pressure results from the wings of the lines, where the self-broadened lines are stronger and the effective value of B is increased. It was not possible to observe any increase in B with increasing total absorption in the present investigation of H_2O , possibly because of the limited values of v and p which were obtained. Although, according to Benedict and Palmer¹⁰, the value of B at a given frequency in an H_2O band might vary from approximately 6 for small fractional absorption to 11 for large fractional absorption, one might expect that the effective value for measuring total absorption of an entire band might not deviate appreciably from 6 since the major portion of the growth of the band occurs at frequencies for which the fractional absorption is not large. This result, which is based on theoretical calculations involving the shapes of individual lines, has been confirmed by Benedict,¹⁵ to a large extent by calculations based on the results of total absorption measurements of H_2O bands reported by HSW. Benedict found that the HSW data yielded a value of B equal to approximately 5 the same as the value determined in the present investigation. It is noted that HSW used a "weighted" pressure (P_w) for the H_2O bands; this corresponds to $B=2$, a value which is believed to be too low in view of the more recent experiments and theoretical calculations.

Values of self-broadening coefficients for individual H_2O lines have been determined by two different sets of workers using different methods. Vasilovsky and Neporant¹¹, by considering the total absorption of a single line, found the broadening ability of H_2O relative to that of N_2 to be such as to correspond to $B=6$. Isatt¹² found the measured half-width of four self-broadened H_2O lines in the 500-600 cm^{-1} region to be approximately 3.6 - 5.5 times the calculated half-width of N_2 -broadened lines; this result corresponds to a value of B varying over approximately the same range, 3.6 - 5.5.

Foreign-Gas Broadening

The relative broadening abilities of two inert gases can be found by comparing the partial pressures of each gas which is required to produce the same total absorption when added to equal samples of an absorbing gas. The method used in the present investigation can best be described by referring to Fig. 5. A sample of CO having a partial pressure of 100 mm Hg was introduced into a 6.35 cm cell, and the total absorption of the 2143 cm^{-1} CO band was measured. The measured value of total absorption was plotted at the lower end of the curves of Fig. 5. One of the foreign gases, He, for example, was then added to the cell to total pressures of approximately 200, 400, 760, 1500, 2200, and 3000 mm Hg; the total absorption was measured at each pressure and the results formed the points for the lower curve of Fig. 5.



Best Available Copy

This procedure was then repeated for each of the other broadening gases; care was always taken to start with, as nearly as possible, the same amount of CO for each set of samples. The total absorption of each sample of CO alone was measured before adding the broadening gas; the consistency of this value of total absorption provided some indication of how nearly equal were the values of absorber concentration for each set of samples.

From the curves of Fig. 5, it can be seen that a total pressure of 960 mm Hg is required to produce a total absorption of 50 cm^{-1} with H_2 used as the broadening gas; a total pressure of 1450 mm Hg is required to produce the same total absorption with He used as the broadening gas. Since the partial pressure of CO is 100 mm Hg in both cases, it is concluded that 1350 mm Hg of He are required to produce the same broadening as 860 mm Hg of H_2 .

A quantity called the foreign-broadening coefficient F of an inert gas b was defined by

$$F = p_{\text{H}_2}/p_b, \quad (11)$$

where p_b is the partial pressure of gas b required to produce the same line broadening as a partial pressure p_{H_2} of H_2 . Thus, from the example above, the foreign-broadening coefficient of He is $860/1350 = 0.64$. Unless otherwise stated, all values of foreign-broadening coefficients F , as well as self-broadening coefficients S , listed in this report are relative to the broadening ability of H_2 .

Values of F were determined in a similar manner for the other broadening gases included in Fig. 5. Calculations were made at several different values of total absorption for each gas; and it was found that there was no significant dependence of F upon the total absorption, which, of course, increased with total pressure. One, therefore, concludes that an unambiguous value of F can be found for each broadening gas for a given absorption band, and that its value has at most a slight dependence on total absorption or pressure for the ranges of pressure included in the present study.

Several other absorption bands, the 2250 cm^{-1} and 1285 cm^{-1} H_2O bands, the 2500 cm^{-1} CO_2 , the 3000 cm^{-1} C_2H_2 , and the 3000 cm^{-1} CH_4 bands, were used to determine the foreign-broadening coefficients for various inert gases. The results of these measurements are listed in Table 2, which also includes the partial pressure of the absorbing gas and the range of total pressures over which calculations of F were made. Also included in Table 2 are values of p_b/p_{H_2} which can be shown from Eq. (1), and the information following it, to be related to F , the foreign-broadening coefficient of gas b , by

$$\frac{p_{b,0}}{p_{\text{H}_2}} = F^{1/2} \left[\frac{(2S + M_b) M_b}{(2S + M_{\text{H}_2}) 2S} \right]^{1/2}, \quad (12)$$

where $2S$ is the molecular weight of H_2 .

Table 2. Foreign-Broadening Coefficients and Relative Molecular Cross Sections

Absorber and Band	Partial Pressure of Absorber* (mm Hg)	Total Pressure Range (mm Hg)	Broadener b	P** (mean)	$\frac{D_{a,b}}{D_{a,H_2}}$ (mean)
H ₂ O 2224 cm ⁻¹	10	25-1000	H ₂	0.73	0.58
			O ₂	0.83	0.93
			A	0.78	0.73
			H ₂	1.23	0.64
			CH ₄	1.08	0.92
H ₂ O 1385 cm ⁻¹	100	180-1000	H ₂	0.70	0.57
			H ₂	1.21	0.64
			A	0.83	0.96
			O ₂	0.72	0.67
			CO ₂	1.17	1.14
			CO	0.97	0.99
CO 2143 cm ⁻¹	100	200-3000	H ₂	0.64	0.56
			A	0.78	0.92
			H ₂	0.83	0.56
			CH ₄	1.12	0.48
CO ₂ 2350 cm ⁻¹	50	80-700	H ₂	0.99	0.52
			O ₂	0.81	0.92
			H ₂	1.17	0.62
			A	0.78	0.93
C ₂ H ₆ 3000 cm ⁻¹ Band 1	10	50-1000	H ₂	0.52	0.51
CH ₄ 3020 cm ⁻¹	10	100-2500	H ₂	0.56	0.56
			A	0.82	0.93
			CO ₂	1.23	1.15

*Cell length = 4.35 cm

**Tabulated values of P are believed accurate to less than 10%.

Since both the self-broadening coefficients B and the foreign-broadening coefficients F are based on the broadening ability of H_2 , it follows that Eq. (5) could be generalized for a sample containing several inert broadening gases b_i to yield

$$P_e = P_g + P_{H_2} + \sum_i F_i P_{b_i} \quad (13)$$

where P_e is the equivalent pressure, p is the partial pressure of the absorbing gas, and F_i is the foreign-broadening coefficient of the i -th gas whose partial pressure is P_{b_i} .

Some of the present results on the measurement of collision cross section ratios can be compared with the results of previous workers. Cross and Daniels⁸ determined values of the ratios for a few of the same inert gases as were used in the present study by observing the fractional absorption at a given frequency in the 2143 cm^{-1} CO band and the 2224 cm^{-1} H_2O band. This method is in contrast to the method of measuring total absorption which was used in the present study. The results of Cross and Daniels are compared with the present results in Table 3.

Table 3. Comparison of Ratios of Collision Cross Sections With Results of Cross and Daniels⁸

b	$D_a, b/D_a, H_2$			$D_a, b/D_a, H_2$		
	$a = H_2O$ 2224 cm^{-1} Band		$\%$ Diff.	$a = CO$ 2143 cm^{-1} Band		$\%$ Diff.
	Cross and Daniels	Present Study		Cross and Daniels	Present Study	
He	0.65	0.58	2.0	0.64	0.6	12.7
H_2	0.70	0.64	6.7	0.68	0.50	11.5
O_2	0.97	0.93	4.1	0.94		
A	0.98	0.93	5.6		0.92	
CH_4					0.96	
C_2H_6	1.09			1.09		

Benesch and Elder¹⁴ used a high-resolution spectrometer to observe a quantity proportional to the line width of an individual rotation line. The results of these workers, which were based on the $J = 4 \rightarrow 5$ line of the 3020 cm⁻¹ CH₄ band, are compared as far as is applicable in Table 4 with the present results based on the total absorption of this same CH₄ band.

Table 4. Comparison of Broadening Abilities and Collision Cross Sections with Results of Benesch and Elder¹⁴

Absorber: CH ₄ 3020 cm ⁻¹ Band				
b	Broadening Ability*		Collision Cross-Sections**	
	Benesch and Elder	Present Study	Benesch and Elder	Present Study
He	1.00	1.00	2.00	2.00
Ar	1.39	1.44	3.24	3.31
O ₂	1.47		3.62	
N ₂	1.73		2.82	
H ₂	1.60	1.70	3.82	3.96
CO	1.73		3.51	
CO ₂	1.79	1.91	3.7	4.11

*Broadening ability of He normalized to 1.00.

**Collision cross section normalized to D_{0,He} = 2.00.

Experimental Results for the H₂O Bands at
2563, 2461, 1285, 1167, 692 and 539 cm⁻¹

Absorption data were obtained for the 2563, 2461, 1285, 1167, 692, and 539 cm⁻¹ H₂O bands, by use of a Perkin-Elmer Model 21 double-beam spectrometer; an NaCl prism interchange unit was used for all but the latter two bands, for which a KBr unit was used. As in previous reports, the data are presented in tabular form and by showing representative absorption curves; and the observed values of total absorption are related to the two parameters, absorber concentration y and equivalent pressure P_e , by the use of curves. Values of equivalent pressure were calculated for each sample by the following equation:

$$P_e = p + 0.12 p, \quad (14)$$

where P is the total pressure due to H₂O at partial pressure p and to the H₂ in the sample.

In Fig. 6 are shown representative absorption curves of the 2563 and 2461 cm⁻¹ bands; the values of y and P_e corresponding to each curve are indicated. The absorption data for these two bands are listed in Table 5.

In the left-hand portion of Fig. 7 the total absorption of the 2563 cm⁻¹ H₂O band is plotted against P_e , with each curve corresponding to a constant value of y . The general features of curves similar to those presented in this report were discussed in considerable detail in Report 1 and will not be repeated. Values of total absorption were taken from the curves in the left-hand portion and replotted against y in the right-hand portion for the different values of P_e indicated. It is believed that the "smoothed" curves in the right-hand portion of Fig. 7 can be used to predict the total absorption of a known H₂O sample to a 3%, except for values of total absorption less than approximately 30 cm⁻¹ for which the error is somewhat greater.

A similar set of curves were drawn for the 2461 cm⁻¹ H₂O band in Fig. 8.

Representative absorption curves of 1285 and 1167 cm⁻¹ H₂O bands are shown in Fig. 9; and the data for these two bands are listed in Table 6. Results of the total absorption measurements of the 1285 cm⁻¹ H₂O band are presented in Figs. 10 and 11 in the same manner as the results of the 2563 cm⁻¹ were presented in Fig. 7. The results for the 1167 cm⁻¹ H₂O band are also shown in Figs. 12 and 13.

Smith and Smith have studied total absorption of the 1285 and 1167 cm⁻¹ H₂O bands in a manner similar to that used in the present study. It is rather difficult to compare the findings of these workers with the present results since theirs were not tabulated. Two figures, which were similar to Figs. 10 and 11, were presented to relate the total

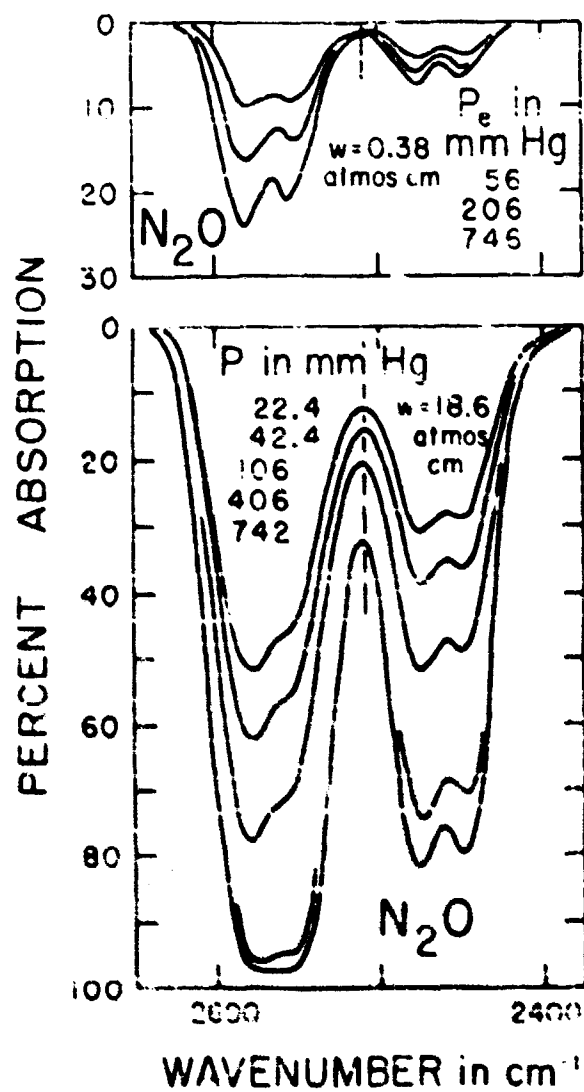


Fig. 6. Absorption curves for the 2465 cm⁻¹ and 2401 cm⁻¹ N₂O bands. The vertical line at 2410 cm⁻¹ represents the frequency at which the bands were divided. Spectral slit width equals approximately 20 cm⁻¹.

Table 5. Data for the 2563 and
2461 cm^{-1} H_2O Bands*

Sample No	P mm Hg	P mm Hg	P ₀ mm Hg	v atmos cm	$\int A(v)dv$ in cm^{-1} 2563 cm^{-1} Band	$\int A(v)dv$ in cm^{-1} 2461 cm^{-1} Band
<u>Path Length = 6.35 cm</u>						
1	10	740	741	0.075	3.2	0.80
2	50	50	50	0.38	5.8	2.38
3	10	200	206	0.38	9.7	3.22
4	50	740	746	0.38	13.8	4.03
5	100	100	112	0.75	11.6	5.0
6	100	400	412	0.75	16.7	5.9
7	100	740	752	0.75	19.1	6.0
8	200	200	224	1.5	21.8	9.4
9	200	740	764	1.5	31.6	12.0
<u>Path Length = 400 cm</u>						
10	12.4	12.4	13.9	5.9	17.3	9.4
11	12.4	23.2	26.7	5.9	21.4	12.0
12	12.4	65.0	64.7	5.9	29.5	15.2
13	12.4	106	106	5.9	43.3	23.0
14	12.4	743	750	5.9	59.8	31.9
<u>Path Length = 300 cm</u>						
15	20	20	22.4	18.6	37.3	21.3
16	20	40	42.4	18.6	44.8	26.7
17	20	104	106	18.6	57.1	37.7
18	20	404	406	18.6	77.6	53.3
19	40	740	742	18.6	81.7	58.0
20	40	50	46	18.6	66.8	47.3
21	40	100	100	18.6	77.4	48.4
22	40	400	406	18.6	87.7	71.9
23	40	740	746	18.6	91.7	76.4
<u>Path Length = 1600 cm</u>						
24	50	40	44.8	76.5	73.9	54.3
25	50	160	168	76.5	88.8	72.8
26	50	206	210	76.5	90.4	77.0

*The absorption bands were observed at 15°C. and 1 atm.

Other uncertainties in observed total absorption is approximately 15 percent for values greater than 30 cm^{-1} , and somewhat greater for smaller values.

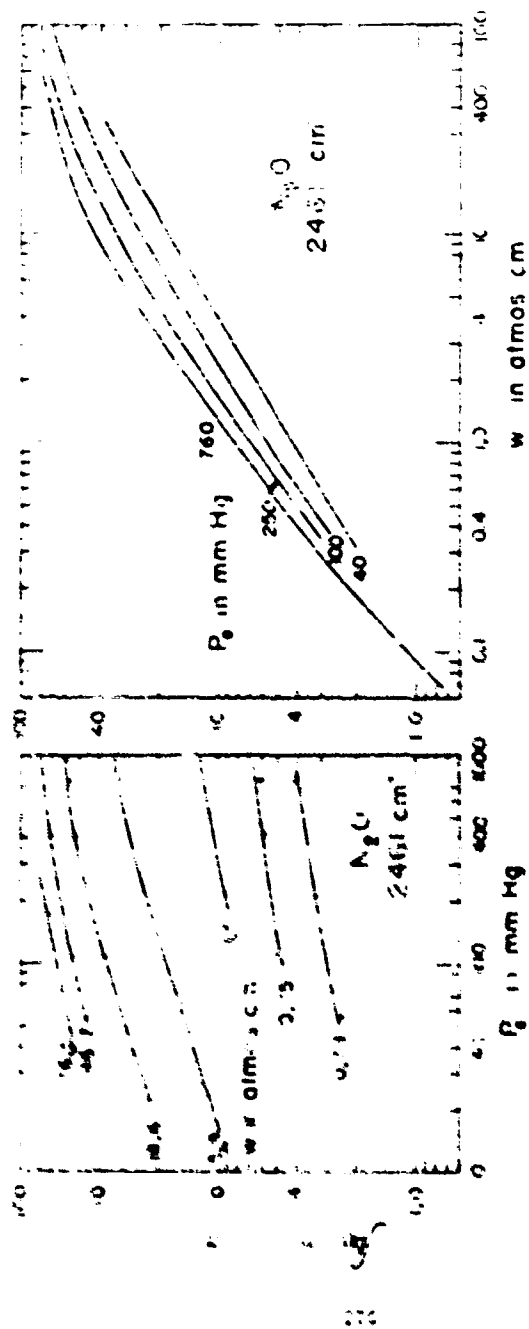


Fig. 1. The total absorption of the 260m μ H_2O band versus P_0 and w . The left-hand portion of the spectrum is the left-hand portion of the spectrum of H_2O and H_2 . The circle points to samples of H_2O and H_2 .

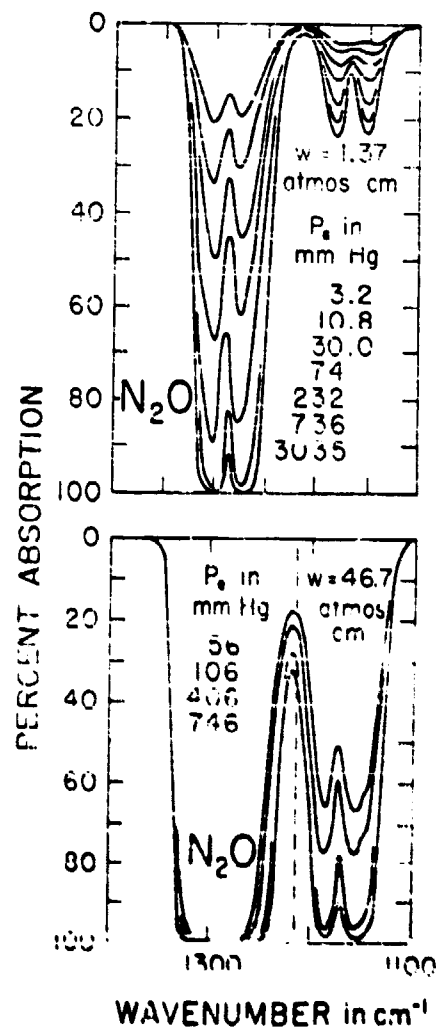


Fig. 9. Absorption curves for the 1265 cm^{-1} and 1167 cm^{-1} N_2O bands. The vertical broken line at 1250 cm^{-1} represents the frequency at which the bands were divided. Spectral slit width equals approximately 10 cm^{-1} .

Table 6. Data for the 1285 and
1167 cm^{-1} H_2O bands*

Sample No.	p mm Hg	P mm Hg	P ₂ mm Hg	v atmos cm	$\int A(v)dv$ in cm^{-1} *	
					1285 cm^{-1}	1167 cm^{-1}
<u>Path Length = 6.35 cm</u>						
1	100	100	112	0.75	36.4	5.4
2	100	200	212	0.75	46.0	6.6
3	100	400	412	0.75	55.5	7.2
4	100	740	752	0.75	61.4	8.2
5	100	140	752	0.75	60.3	7.5
6	100	1475	1485	0.75	64.2	8.0
7	100	2290	2300	0.75	65.4	8.0
8	100	3050	3060	0.75	66.8	8.2
9	100	100	112	0.75	36.7	5.5
10	100	740	752	0.75	60.3	7.6
11	100	1470	1480	0.75	61.7	7.7
12	100	2290	2300	0.75	65.0	7.8
13	100	3050	3060	0.75	65.5	8.2
<u>Path Length = 400 cm</u>						
14	2.9	2.9	3.2	1.37	15.6	3.9
15	2.9	5.9	6.2	1.37	17.0	3.4
16	2.9	10.5	10.6	1.37	20.9	3.6
17	2.9	23.7	24.0	1.37	30.1	3.8
18	2.9	75	75	1.37	40.7	7.4
19	2.9	232	232	1.37	57.5	7.9
20	2.9	756	756	1.37	71.4	11.9
21	2.9	3035	3035	1.37	76.0	12.5
22	5.8	5.8	6.5	2.75	29.1	4.5
23	5.8	12.5	13.2	2.75	31.2	6.0
24	5.8	26.5	26.2	2.75	41.6	6.2
25	5.8	75	75.7	2.75	55.1	12.5
26	5.8	232	232	2.75	70.7	16.3
27	5.8	756	756	2.75	87.2	24.2
28	5.8	3035	3035	2.75	87.8	25.3
29	12.4	12.4	13.9	5.9	44.6	7.8
30	12.4	25.2	26.7	5.9	53.3	12.6
31	12.4	65	64.5	5.9	67.0	17.0
32	12.4	196	196	5.9	82.1	25.6
33	12.4	749	750	5.9	90.5	31.1

Table 6. (Continued)

Sample No.	P mm Hg	P mm Hg	P mm Hg	v cm	$\int A(v)dv$ in cm^{-1} ^a	
					1000 cm ⁻¹	1167 cm ⁻¹
<u>Path Length = 800 cm</u>						
34	10.0	10.0	11.2	9.3	47.2	11.6
35	10.0	20.0	21.2	9.3	57.6	14.8
36	10.0	40.0	41.2	9.3	66.8	18.8
37	10.0	100	101	9.3	80.2	25.0
38	10.0	400	401	9.3	90.2	38.0
39	10.0	740	741	9.3	92.6	43.0
40	10.0	2310	2310	9.3	95.6	48.8
41	20.0	20.0	22.4	9.3	74.2	23.8
42	20.0	40.0	42.4	9.3	81.4	26.6
43	20.0	100	106	9.3	91.0	39.0
44	20.0	400	406	9.3	93.6	55.8
45	20.0	740	742	9.3	95.6	62.4
46	50	50	56	46.7	96.4	46.2
47	50	100	106	46.7	100	55.8
48	50	400	406	46.7	107	73.6
49	50	740	740	46.7	109	78.6
<u>Path Length = 1600 cm</u>						
50	40	40.0	41.8	75.6	101	54.4
51	40	160	168	75.6	110	74.8
52	40	206	211	75.6	111	77.6
53	100	100	112	149	116	84.6
54	100	402	414	149	122	96.4
55	100	500	510	149	122	107.2

^aThe two absorption bands were divided at 1215 cm⁻¹.

^bThe uncertainty in observed total absorption is approximately 25 percent for values greater than 25 cm⁻¹, and somewhat greater for smaller values.

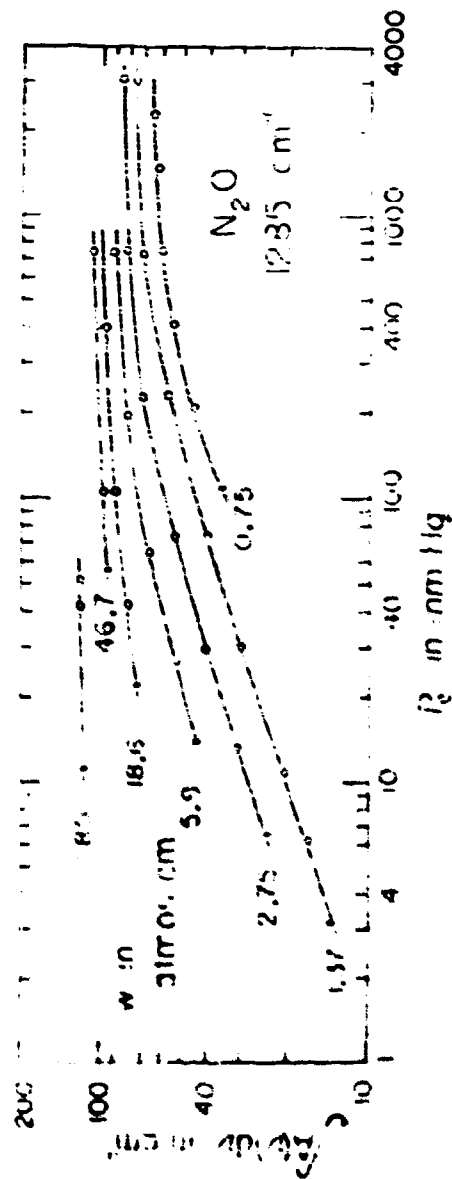


Fig. 10. The total absorption of the 1235 cm⁻¹ H₂O band versus i_0 . The points correspond to samples of H₂O alone, the circles pertain to samples of H₂O and N₂.

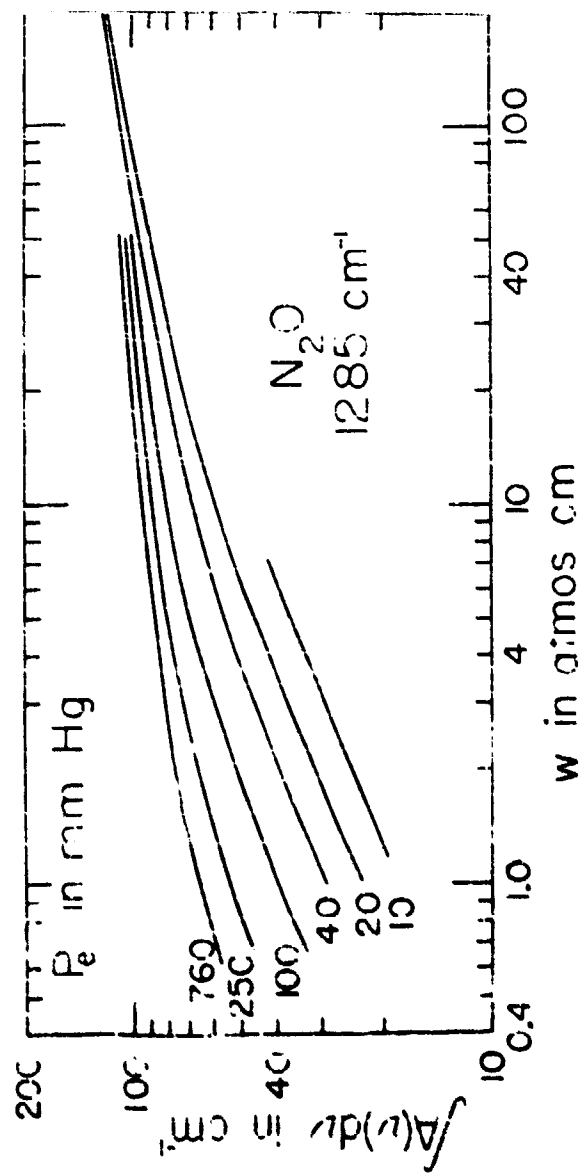


Fig. 11. The total absorption of the 1285 cm^{-1} N_2O band versus w .

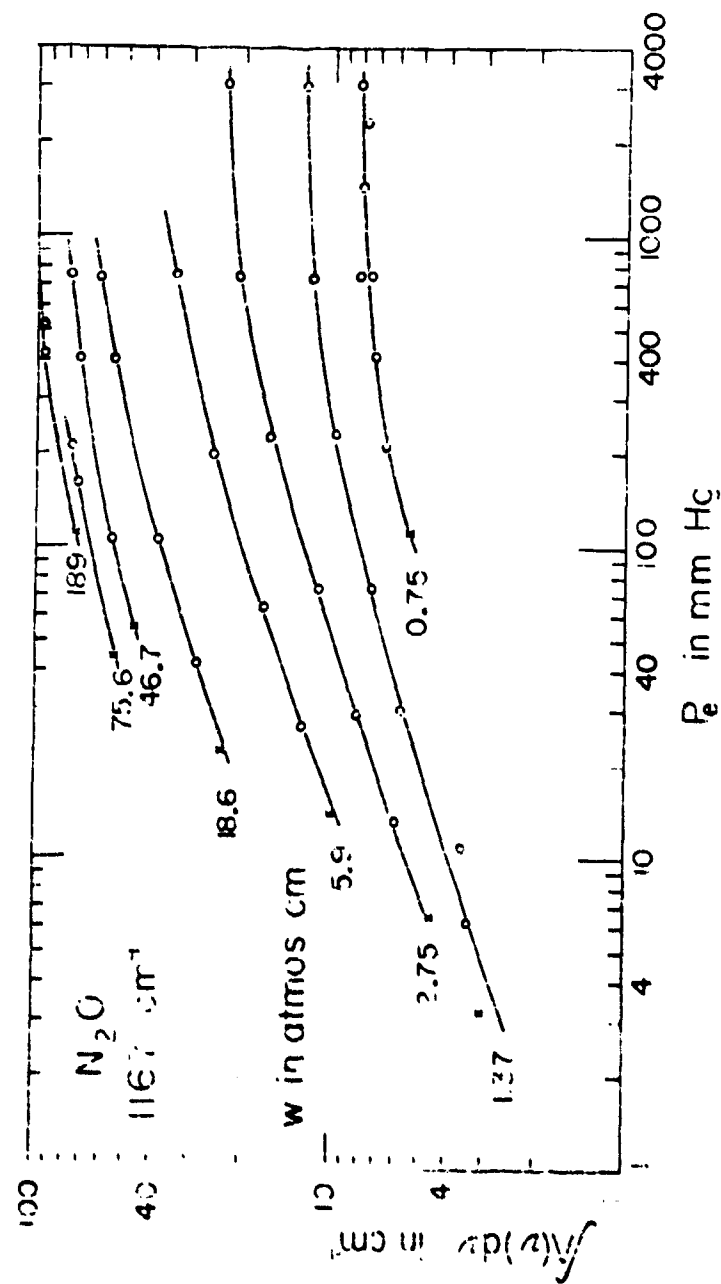


Fig. 12. The total absorptance of the $1167 \text{ cm}^{-1} \text{ H}_2\text{O}$ band versus P_e . The x points correspond to samples of H_2O alone; the circle points to samples of H_2O and N_2 .

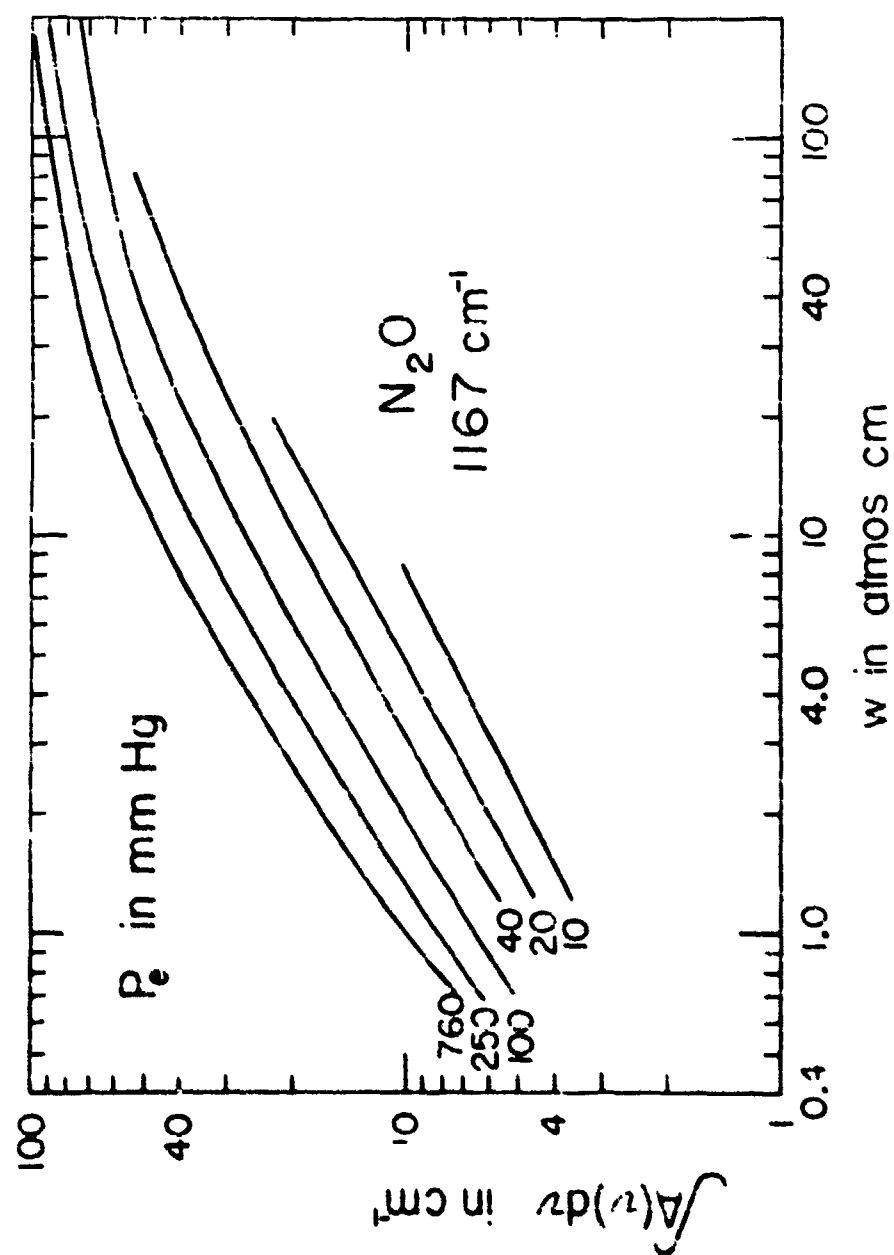


Fig. 13. The total absorption of the 1167 cm^{-1} N_2O band versus w .

absorption of the 1285 cm^{-1} band to equivalent pressure and to a quantity which is proportional to absorber concentration. Values of total absorption were expressed in units of microns instead of cm^{-1} . These figures in the article by Goody and Wornall had been reduced so much that it was difficult to read values of total absorption more closely than approximately $\pm 2\%$. However, the values of total absorption of two different hypothetical samples were predicted by using the curves of Goody and Wornall and by using the curves of Fig. 11. The first sample contained an absorber concentration of 4.01 atm-cm at an equivalent pressure of 100 mm Hg . The curves of Goody and Wornall were used to predict a total absorption of approximately 63 cm^{-1} , while Fig. 11 predicts 65.5 cm^{-1} . Similarly, Goody and Wornall's curves predict a total absorption of approximately 29 cm^{-1} , which can be compared with 33 cm^{-1} predicted by Fig. 11 for a sample of $y = 4.01$ and $P_0 = 10\text{ mm Hg}$. Considering the fact that the curves cannot be read very accurately, one concludes from these two comparisons that the two sets of results are in at least fair agreement.

No curves were presented by Goody and Wornall to relate the total absorption of the 1167 cm^{-1} band to absorber concentration or equivalent pressure; therefore, no comparisons could be made between their results and those of the present investigation. The calculated band intensities from the two investigations are compared below in a subsection on band intensities.

In Fig. 14 are shown representative absorption curves for the 589 and 692 cm^{-1} H_2O bands. The data for these two bands are listed in Table 7; only the samples of relatively large y produced a measurable absorption in the region of the 692 cm^{-1} band. The observed values of total absorption for this band were tabulated, but were not plotted against y or P_0 since only a few values were obtained. The stronger fundamental band was divided at its center, 589 cm^{-1} ; the total absorption of each portion was measured and listed in Table 7 along with the total absorption of the entire band.

A large portion of the 589 cm^{-1} H_2O data were plotted in Fig. 15 with total absorption shown as a function of P_0 . As for the other bands, values were taken from the curves of Fig. 15 to provide points for the smoothed curves of Fig. 16, in which the total absorption was plotted against y for various values of P_0 .

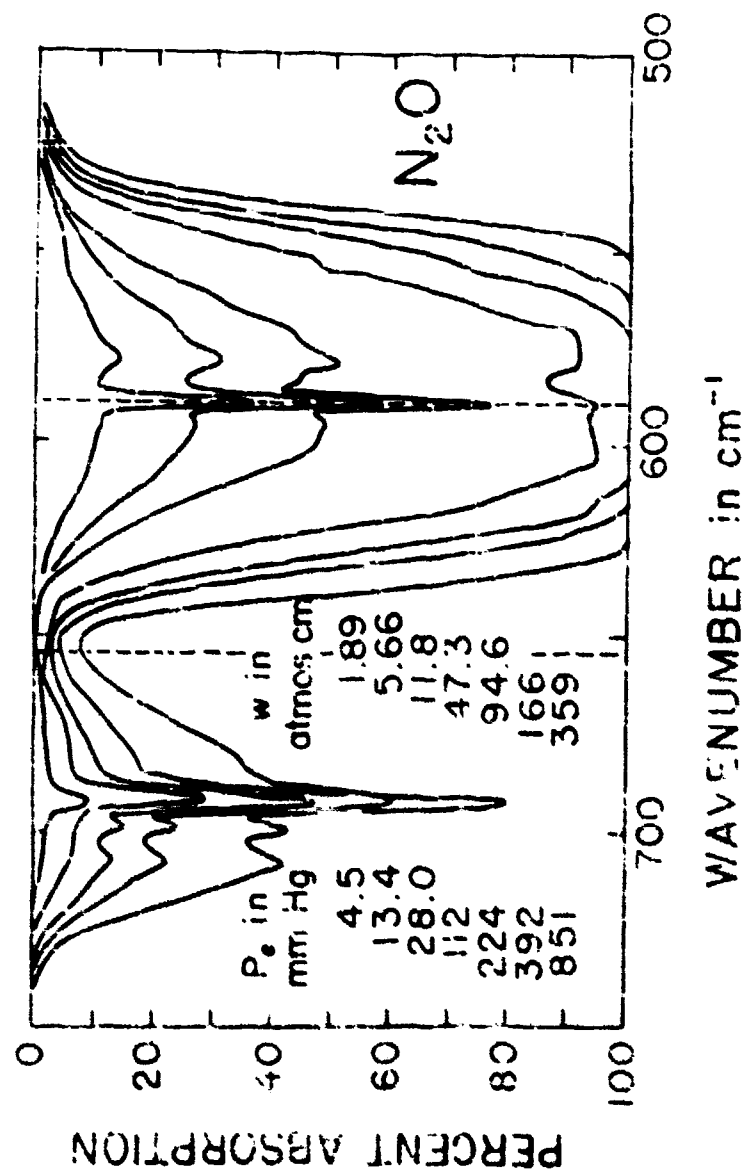


Fig. 14. Absorption curves for the 559 cm^{-1} and 692 cm^{-1} bands. The vertical broken line at 555 cm^{-1} represents the frequency at which the bands were divided. Spectral slit width equals approximately 6 cm^{-1} .

Table 7. Data for the 509 and 692 cm^{-1} H_2O bands

Sample No.	P mm Hg	P mm Hg	P mm Hg	P mm Hg	n	n	$\int A(\nu) d\nu$ in $\text{cm}^{-1} \cdot \text{cm}^2$			
							500-509 cm^{-1}	509-655 cm^{-1}	509 cm^{-1} band	692 cm^{-1} band
Path Length = 6.35 cm										
1	50.1	50.1	50.1	50.1	56.1	0.376	2.75	2.3	5.0	
2	50.1	102	102	102	100	0.376	2.9	2.5	5.4	
3	50.1	251	251	251	260	0.376	3.1	3.0	6.1	
4	50.1	56	56	56	734	0.375	3.6	3.3	6.9	
5	50.1	3075	3075	3075	3085	0.375	4.0	3.6	7.6	
6	15.0	15.0	15.0	15.0	16.8	0.113	1.0	0.9	1.9	
7	15.0	50.1	50.1	50.1	51.9	0.113	1.1	1.3	2.4	
8	15.0	102	102	102	104	0.113	1.2	1.3	2.5	
9	15.0	251	251	251	253	0.113	1.3	1.4	2.7	
10	15.0	56	56	56	715	0.113	1.3	1.5	2.8	
11	15.0	3100	3100	3100	3120	0.113	1.4	1.6	3.0	
12	25.1	300	300	300	308	0.191	2.2	2.4	4.6	
13	25.1	600	600	600	600	0.078	2.1	2.1	4.2	
14	6.1	3000	3000	3000	3000	0.046	0.64	0.76	1.13	
15	6.1	3000	3000	3000	3000	0.030	0.17	0.48	0.85	
16	3.1	3000	3000	3000	3000	0.023	0.41	0.42	0.85	
Path Length = 400 cm										
17	2	2	2	2	2.2	0.34	2.5	1.9	4.4	
18	4	4	4	4	4.5	1.69	4.0	3.4	7.4	
19	8	8	8	8	5.0	3.73	6.9	5.9	12.8	
20	12	12	12	12	13.4	5.66	9.3	8.1	17.4	
21	16	16	16	16	17.9	7.55	11.0	10.5	22.5	
22	25	25	25	25	26.0	11.8	15.6	13.4	29.0	
23	50	50	50	50	46.0	29.7	24.7	23.5	47.5	1.0
24	100	100	100	100	115	67.3	35.4	32.5	65.9	2.3
25	200	200	200	200	224	94.6	41.6	40.7	82.3	4.2
26	350	350	350	350	374	165	45.5	45.8	90.2	3.1
27	700	700	700	700	711	359	50.1	50.5	101	12.6

Table 7 (Continued)

Sample No.	P cm Hg	F cm Hg	P ₀ cm Hg	v cm	$\int A(\nu) d\nu$ in cm ⁻¹			
					580- 550 cm ⁻¹	550- 655 cm ⁻¹	655 cm ⁻¹ band	692 cm ⁻¹ band
23	4	60	20.5	1.09	6.5	5.6	12.5	
29	4	50	50.5	1.09	7.8	7.2	15.0	
30	4	135	195	1.09	9.2	9.6	18.8	
31	4	301	331	1.09	14.5	11.8	26.3	
32	4	760	760	1.09	12.1	14.7	26.8	
33	4	550	1520	1.09	15.4	15.9	29.5	
34	4	1000	3000	1.09	13.1	16.9	32.0	
35	25	50	55	11.8	17.9	18.0	35.9	1.5
36	25	124	127	11.8	22.1	22.4	44.5	1.3
37	25	300	305	11.8	26.5	26.7	53.2	2.3
38	25	752	765	11.8	30.9	31.4	62.3	2.5
39	25	1000	3000	11.8	34.6	34.5	69.1	3.3

*The uncertainty in observed total absorption is approximately ± 5 percent for values greater than 25 cm⁻¹, and somewhat greater for smaller values.

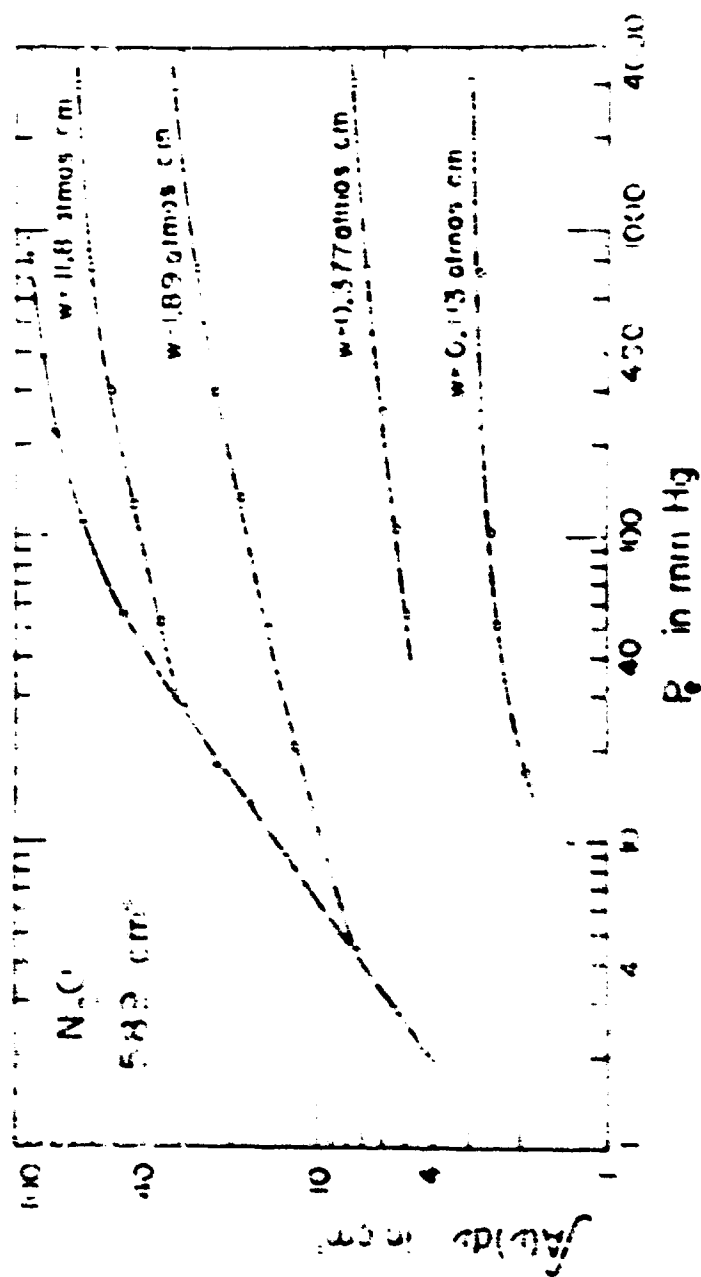
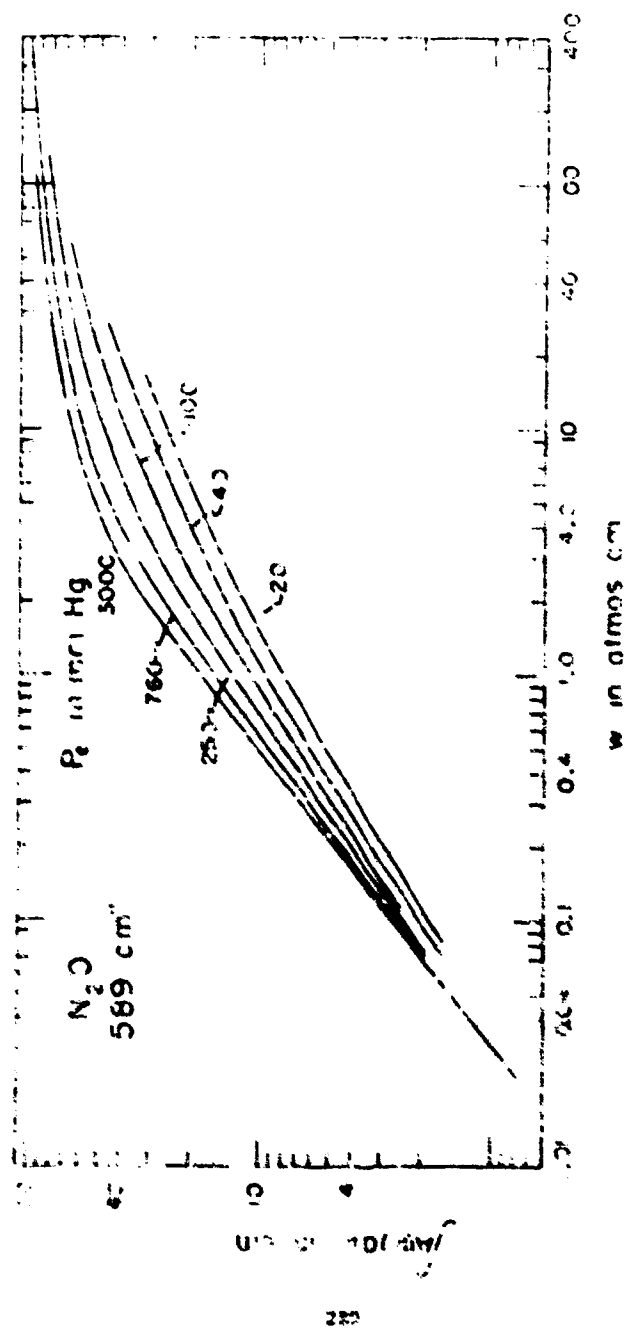


Fig. 1. The total absorption of the 300 cm^{-1} N_2O band versus P_0 . The points correspond to samples of N_2O alone, the circle points to samples of N_2O and H_2 . Both broken curves represent a constant value of y . The solid curve represents samples of N_2O alone for which y is proportional to P_0 .



Band Intensities

It was stated in Report 1 that for samples of sufficient thickness, pressure and low absorber concentration, $k(\nu)\nu \ll 1$ for all frequencies, where $k(\nu)$ is the absorption coefficient, and the band intensity $I(\nu)/\nu$ is related to the total absorption by

$$\int k(\nu) d\nu = \int \frac{I(\nu)}{\nu} d\nu \quad (1)$$

Under the conditions for which Eq. (1) is valid, the total absorption is independent of equivalent thickness and is proportional to ν . The slopes of the curves in the right-hand portions of Figs. 7 and 8 correspond to $P = 7000$ atm. H_2 are seen to increase toward unity at a value approximately equal to unity, a result which indicates that the conditions are satisfied for Eq. (1) to be approximately true. If the most accurate values of band intensity were to be found, it would be essential to obtain more data on the total absorption of samples at high equivalent pressures and low ν ; however, by essentially extrapolating to smaller ν the high-pressure curves of Figs. 7 and 8, as well as the corresponding figures for the other bands, with the slopes increasing to an upper limit of unity, it was possible to estimate the band intensities of four of the H_2O bands reported here. The values obtained are listed in Table 8 along with values of other workers for comparison.

Table 8. H_2O Band Intensities^a

Band	Present Study	Wilson et al. ¹²	Gentry and Herzberg ¹³	Fugère and Gruber ¹⁴
2963 (2-1)	14.1 ± 0.5			
2461	11.5 ± 1.5			
1295		1.0	0.1	1.0
1107	12.0 ± 1.2		1.0	0.1
909	33 ± 4	40		20.0

^aBand intensities in atmos. cm^2 atm.^{-1.}

^bThe smallest values of ν were not sufficiently low to make it possible to measure the intensity of this band.

[illegible][illegible]

2.

...to have ...
...of pose ...
...of an

[illegible]

100

The partial pressure of H_2O , from which y could easily be calculated, was determined by measuring the dew point of the sample in the absorption cell. This was accomplished by the use of a "well" made of a thin piece of "Inconel" tubing, which was closed on one end and was soldered to the wall of the absorption cell, projecting approximately 2 inches into the interior of the cell. Ether was put into the tube and H_2 was bubbled through in order to cool it until condensation formed on the outside wall of the tubing, which could be observed through a window in the absorption cell. A thermometer immersed in the ether was used to determine the temperature at which condensation started.

The accuracy with which the dew point could be determined depended primarily upon how accurately one could tell when condensation started, and also upon how accurately the thermometer read the temperature of the surface on which the H_2O condensed. One would expect that turbulence in the ether, which was caused by the bubbling of the nitrogen, would tend to minimize temperature gradients in the ether; it was found that the reading of the thermometer varied by not more than approximately ± 0.1 to $\pm 0.2^\circ C$ when held at different positions in the ether. It was found that, as the ether was cooled slowly, a temperature was reached at which a very thin film would appear on the surface of the tubing; if this temperature were maintained, no further condensation seemed to occur. However, if the temperature were decreased by approximately $0.2^\circ C$, the condensation increased. In the case of samples of H_2O alone, the partial pressure could be measured with a manometer and compared with the partial pressure determined by use of standard tables relating temperature at which condensation occurred to the partial pressure. It was found that the values of H_2O partial pressure determined by the two methods agreed to approximately ± 2 percent if the temperature used was the one at which condensation would increase, rather than the slightly higher temperature at which a thin film first appeared on the surface of the tubing.

It is believed that the values of y which were determined are accurate to ± 2 or ± 3 percent for samples whose dew-point was greater than $10^\circ C$, and to ± 3 or ± 4 percent for samples having lower dew points. Deviations in y of approximately $1/2$ percent could be observed. H_2O was introduced to the absorption cell by admitting a measured amount of liquid H_2O into a small evacuated bulb which was connected to the absorption cell through a valve and a short piece of copper tubing. The valve and tubing connecting the bulb to the absorption cell were heated gently to avoid condensation in these parts; the valve was then opened and the H_2O allowed to evaporate into the previously evacuated cell. The evaporation could be speeded up by gently heating the liquid H_2O .

By considering the volume of the absorption cell, it was possible to calculate the pressure that would be expected from a known quantity of liquid H_2 if one assumed that all the H_2 were in the vapor phase and none were adsorbed on the cell walls. In most cases it was found that the actual pressure was only approximately 80 to 90 percent as great as the calculated value, a result which indicated that approximately

1/2 the H_2O was adsorbed on the cell walls since care was taken to avoid condensation. If the sample was left in the cell, the pressure was found to decrease gradually for a few hours, thus indicating that more adsorption was occurring.

In the process of obtaining data H_2 was added to the H_2O to produce samples at various values of total pressure less than one atmosphere. The dew point, from which the H_2O partial pressure could be determined, was measured periodically, at least once or twice after adding each sample of H_2 . It was found that the dew point remained essentially constant if the H_2O had been allowed to remain alone in the cell sufficiently long for the adsorption to be complete before H_2 was added. A major portion of the investigation took place during the summer months when the temperature of the absorption cell, which remained near ambient temperature, varied by as much as 6 or 8°C during a given day. As the temperature of the cell increased, a portion of the adsorbed gas apparently was "driven off" the cell walls since the H_2O partial pressure increased at a rate considerably greater than one would predict on the basis of the perfect gas laws. The fact that adsorbed gases are "driven off" solid surfaces by heating is, of course, well known.

Various coatings on the interior of the cell were tried in an attempt to decrease the adsorption; these coatings included automobile lacquer, glyptal varnish, and a film of vacuum pump oil. None of these surface coatings seemed to change significantly the amount of H_2O adsorbed; however, more time was required to "is-gas" the cell by evacuation when one of the above coatings was used. Therefore, the cell was used with the bare steel exposed. Little difference was observed between the adsorption of the steel cell when it was sand-blasted as compared to the cell immediately after it had been sand-blasted. A porcelain coating or glass lining would probably reduce the adsorption, but this would have involved considerable expense and was not considered essential since the H_2O partial pressure could be monitored.

As a result of the investigation of the adsorption of H_2O on the walls of a steel cylinder, it can be concluded that accurate values of γ cannot be determined from a measurement of liquid H_2O introduced into the cell; in general, values determined by this method would be too high. In the work by EDW, values of γ for H_2O samples were determined by measuring the H_2O partial pressure before H_2 was added. It was then assumed that the H_2O partial pressure remained constant as different amounts of H_2 were added and the absorption curves were obtained. On the basis of the investigation of adsorption described above, it can be concluded that the H_2O partial pressure was probably not changed because of H_2 displacing the H_2O which had been adsorbed on the walls of the absorption cell. The greatest causes of variation in the H_2O partial pressure were probably changes in temperature, or further adsorption which might have occurred after the partial pressure was measured. During the major portion of the investigation by EDW the temperature of the absorption cell was nearly constant; therefore, any error in the determination of γ because of temperature variations was probably small.

1/2 the H_2O was adsorbed on the cell walls since care was taken to avoid condensation. If the sample was left in the cell, the pressure was found to decrease gradually for a few hours, thus indicating that more adsorption was occurring.

In the process of obtaining data H_2 was added to the H_2O to produce samples at various values of total pressure less than one atmosphere. The dew point, from which the H_2O partial pressure could be determined, was measured periodically, at least once or twice after adding each sample of H_2 . It was found that the dew point remained essentially constant if the H_2O had been allowed to remain alone in the cell sufficiently long for the adsorption to be complete before H_2 was added. A major portion of the investigation took place during the summer months when the temperature of the absorption cell, which remained near ambient temperature, varied by as much as 6 or 8°C during a given day. As the temperature of the cell increased, a portion of the adsorbed gas apparently was "driven off" the cell walls since the H_2O partial pressure increased at a rate considerably greater than one would predict on the basis of the perfect gas laws. The fact that adsorbed gases are "driven off" solid surfaces by heating is, of course, well known.

Various coatings on the interior of the cell were tried in an attempt to decrease the adsorption; these coatings included automobile lacquer, glyptal varnish, and a film of vacuum pump oil. None of these surface coatings seemed to change significantly the amount of H_2O adsorbed; moreover, more time was required to "is-gas" the cell by evacuation when one of the above coatings was used. Therefore, the cell was used with the bare steel exposed. Little difference was observed between the adsorption of the steel cell when it was somewhat rusty as compared to the cell immediately after it had been sand-blasted. A porcelain coating or glass lining would probably reduce the adsorption, but this would have involved considerable expense and was not considered essential since the H_2O partial pressure could be monitored.

As a result of the investigation of the adsorption of H_2O on the walls of a steel cylinder, it can be concluded that accurate values of y cannot be determined from a measurement of liquid H_2O introduced into the cell; in general, values determined by this method would be too high. In the work by E. V., values of y for H_2O samples were determined by measuring the H_2O partial pressure before H_2 was added. It has been assumed that the H_2O partial pressure remained constant as different amounts of H_2 were added and the absorption curves were obtained. On the basis of the investigation on adsorption described above, it can be concluded that the H_2O partial pressure was probably not changed because of H_2 displacing the H_2O which had been adsorbed on the walls of the absorption cell. The greatest causes of variation in the H_2O partial pressure were probably changes in temperature, or further adsorption which might have occurred after the partial pressure was measured. During the major portion of the investigation by E. V. the temperature of the absorption cell was nearly constant, therefore, any error in the determination of y because of temperature variations was probably small.

Errors arising from further adsorption after the H_2O partial pressure was measured were probably not excessive since investigation of the results shows that the total absorptions of few samples did not change appreciably after having remained in the cell overnight.

Comparison of the present results with those of HBW which covered the same range of values of y and P_0 indicated that the two sets of results agreed within expected experimental error.

Experimental Results

Absorption curves were obtained for the 5332, 5700, and 1595 cm^{-1} H_2O bands by use of a Perkin-Elmer Model 99 spectrometer enclosed in a vacuum tank which is described in Appendix I. A LiF prism was used for the 5332 and 5700 cm^{-1} bands and an NaCl prism for the 1595 cm^{-1} band. The method used to replot the recorded spectra on a linear wavenumber scale and to measure the total absorption is the same as that described by HBW.

The data and results are presented in a manner similar to that described in the previous section for the H_2O bands. Some of the curves which are presented are based on both the present results and the HBW results. Values of equivalent pressure P_0 were calculated for each sample by the following equation:

$$P_0 = P + \Delta p, \quad (16)$$

where P is the total pressure due to H_2O at partial pressure p and to the N_2 in the sample.

In Fig. 17 are shown representative absorption curves of the 5332 cm^{-1} H_2O band; the absorption data for this band are listed in Table 9. The estimated uncertainty of the tabulated values of total absorption is approximately ± 6 to ± 8 percent for values greater than 50 cm^{-1} . The relative uncertainty is somewhat greater for smaller values of total absorption. The accuracy of the tabulated results for the other H_2O bands listed below is approximately the same.

Representative portions of data for the 5332 cm^{-1} band were plotted in Fig. 18 with total absorption versus P_0 , where each curve corresponds to a given value of y . It is noted that in Table 9 the samples are in groups of approximately equal y ; in order to plot the results of these data in Fig. 18, an average value of y was chosen for each group of samples and the observed values of total absorption which are listed in the table were corrected to the average y . The correction was obtained from plots of total absorption versus y where each curve was determined by four points corresponding to the four different path lengths at which each gas mixture was studied.

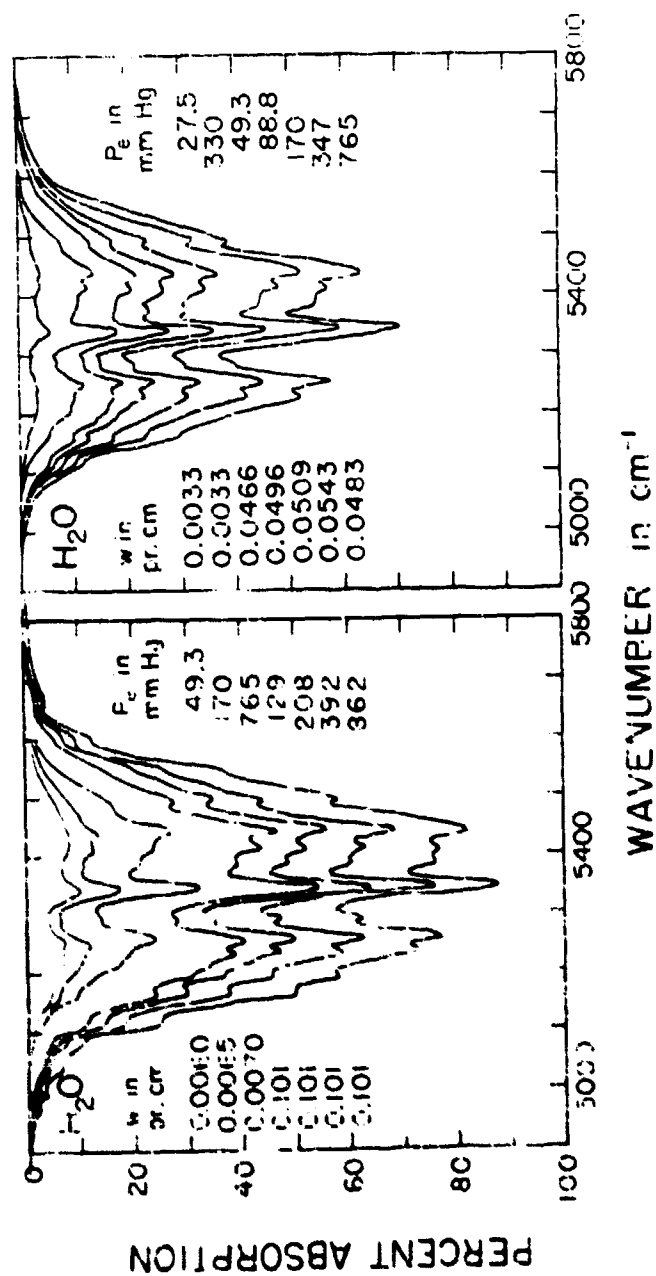


Fig. 27. representative absorption curves of the 5×10^2 cm⁻¹ H₂O band. Spectral slit width equals approximately 20 cm⁻¹.

Table 9. Data for the 5332 cm^{-1} H_2O band

Comp. No.	Temp. $^{\circ}\text{C}$	Path Length cm	P(H_2O) mm Hg	P total mm Hg	P _e mm Hg	ν pr. cm	$\int A(\nu) d\nu$ in cm^{-1} Band
1	-40.0	625	5.5	5.5	27.5	0.0033	11.7
2	29.0	625	5.5	12.0	34.0	0.0033	13.0
3	27.5	625	5.5	21.5	43.5	0.0033	16.1
4	27.5	625	5.5	47.0	69.0	0.0033	19.3
5	29.0	625	5.5	122	144	0.0033	27.0
6	30.0	625	5.5	308	330	0.0033	36.0
7	30.5	625	5.6	760	782	0.0033	51.1
8	25.0	625	9.0	9.9	49.3	0.0060	26.0
9	26.5	625	10.3	24.2	62.2	0.0062	26.0
10	27.5	625	10.3	47.0	88.6	0.0064	33.7
11	28.5	625	10.3	126	170	0.0065	40.3
12	28.5	625	10.6	305	347	0.0070	56.3
13	29.0	625	10.2	724	765	0.0063	74.8
14	28.5	1230	11.6	305	347	0.0137	83.6
15	29.0	1230	10.1	724	765	0.0122	109
16	25.5	2445	9.0	9.9	49.3	0.0234	50.1
17	26.5	2445	10.3	21.2	62.2	0.0244	57.0
18	27.5	2445	10.3	47.0	88.6	0.0243	63.9
19	28.5	2445	10.3	126	170	0.0253	90.3
20	28.5	2445	11.6	305	347	0.0273	116
21	29.0	2445	10.2	724	765	0.0242	147
22	25.5	4375	5.0	9.9	49.3	0.0466	68.6
23	26.5	4375	10.3	21.2	62.2	0.0486	74.1
24	27.5	4375	10.5	47.0	88.6	0.0496	90.1

Table 5. (Continued)

Sample No.	Temp. °C	Path Length cm	$f(\lambda)$ mm Hg	F total mm Hg	P_0 mm Hg	ν pr. cm	$\int A(\nu) d\nu$ in cm^{-1} 5332 cm^{-1} Band
25	28.5	4.875	10.9	126	170	0.0509	120
26	28.5	4.875	11.6	53	5.7	0.0545	164
27	28.0	4.875	10.2	734	765	0.0485	201
28	30.4	4.875	22.5	22.5	113	0.109	151
29	30.7	4.875	21.1	45.0	129	0.101	157
30	31.0	4.875	21.7	122	208	0.101	186
31	31.4	4.875	21.6	507	592	0.101	234
32	31.5	4.875	21.6	775	862	0.101	299
33	25.0	6.25	5.17	5.17	15.9	0.00192	5.9
34	25.0	6.25	6.7	6.7	33.5	0.00405	17.0
35	25.0	6.25	9.2	9.2	45.0	0.00564	27.0
36	25.0	6.25	12.4	12.4	62.0	0.00750	33.7
37	25.0	6.25	14.6	14.6	73.0	0.00850	36.6
38	25.0	4.875	5.17	5.17	15.9	0.0150	20.6
39	25.0	4.875	6.7	6.7	33.5	0.0316	48.5
40	25.0	4.875	9.2	9.2	46.0	0.0436	76.9
41	25.0	4.875	12.4	12.4	62.0	0.0586	88.6
42	25.0	4.875	14.6	14.6	73.0	0.0664	104

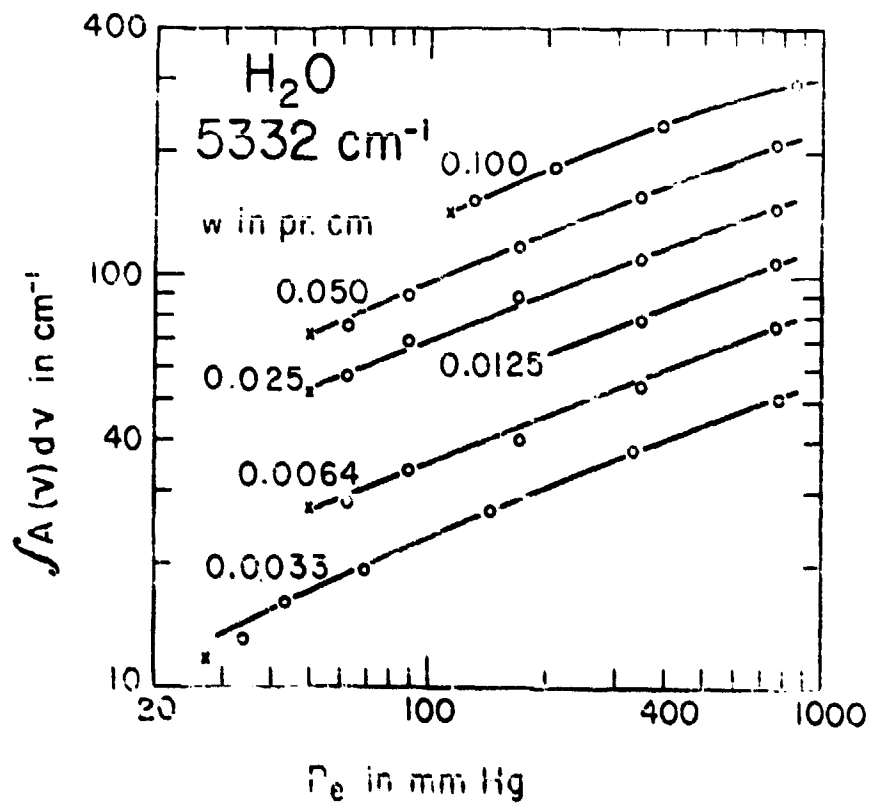


Fig. 10. The total absorption of the $5332 \text{ H}_2\text{O cm}^{-1}$ band versus P_e . The x points correspond to samples of H_2O alone, the circle points to samples of H_2O and N_2 .

The curves of Fig. 19, in which total absorption was plotted against w , were obtained by using both the present results and the HBW results. Values of total absorption were taken from the curves of Fig. 18 and from similar curves which were drawn for the HBW data but are not presented in this report. These values were then used to provide points for the curves of Fig. 19, in which the points were omitted in order to facilitate reading the curves.

Over a small range of values of w the HBW data overlapped the present data and provided a convenient comparison. Curves drawn through each of the two sets of data without consideration for the other set would have agreed to within 5 to 10 percent for most of the different equivalent pressures illustrated in Fig. 19, as well as for the corresponding figures shown below for the other bands. This agreement is good when one considers that the HBW data being compared represented samples of small w for which the accuracy was poorest. Comparison of the present data with those obtained in the early work of Howard and Chapman² was much less favorable; the results of total absorption for similar samples often differed by as much as 25-30 percent.

In view of the improved methods which were described above, the present results were given extra "weight" in determining the positions of the curves of Fig. 19, which are believed to best represent all of the data; and values obtained from these curves are believed to be accurate to ± 6 percent. The same accuracy is estimated for the corresponding curves of other H_2O bands shown below.

Representative absorption curves of the spectral region near 3700 cm^{-1} are shown in Fig. 20. The data are listed in Table 19, which includes the values of the total absorption for the three spectral intervals: 2800-3540 cm^{-1} , 3540-4000 cm^{-1} , and 3800-4300 cm^{-1} . The sum of the total absorptions of the two latter intervals, which together are referred to as the 3700 cm^{-1} band, is also given for each sample. The values of the total absorption for the 2800-3540 cm^{-1} region, which corresponds to the 3.2 μ band in the HBW report, are tabulated for reference by future workers but are not analyzed in the present report.

Figures 21 and 22 contain curves relating the total absorption of the 3700 cm^{-1} band to P_e and w , respectively. These curves were obtained in the same manner as were the corresponding curves for the 5332 cm^{-1} band.

Figures 23 and 24 show representative absorption curves of the 1595 cm^{-1} H_2O band. The data are listed in Table 21, the values of total absorption are included for the 1250-1500 cm^{-1} and 1500-2100 cm^{-1} intervals and for the sum of these two intervals, which is called the 1595 cm^{-1} H_2O band. The data for this band were treated in the same manner as were the data for the 5332 cm^{-1} and 3700 cm^{-1} bands. Figure 25 contains curves relating the total absorption of the present data to P_e for various values of w , and the curves of Fig. 26, which relate total absorption to w for the present data and the HBW data.

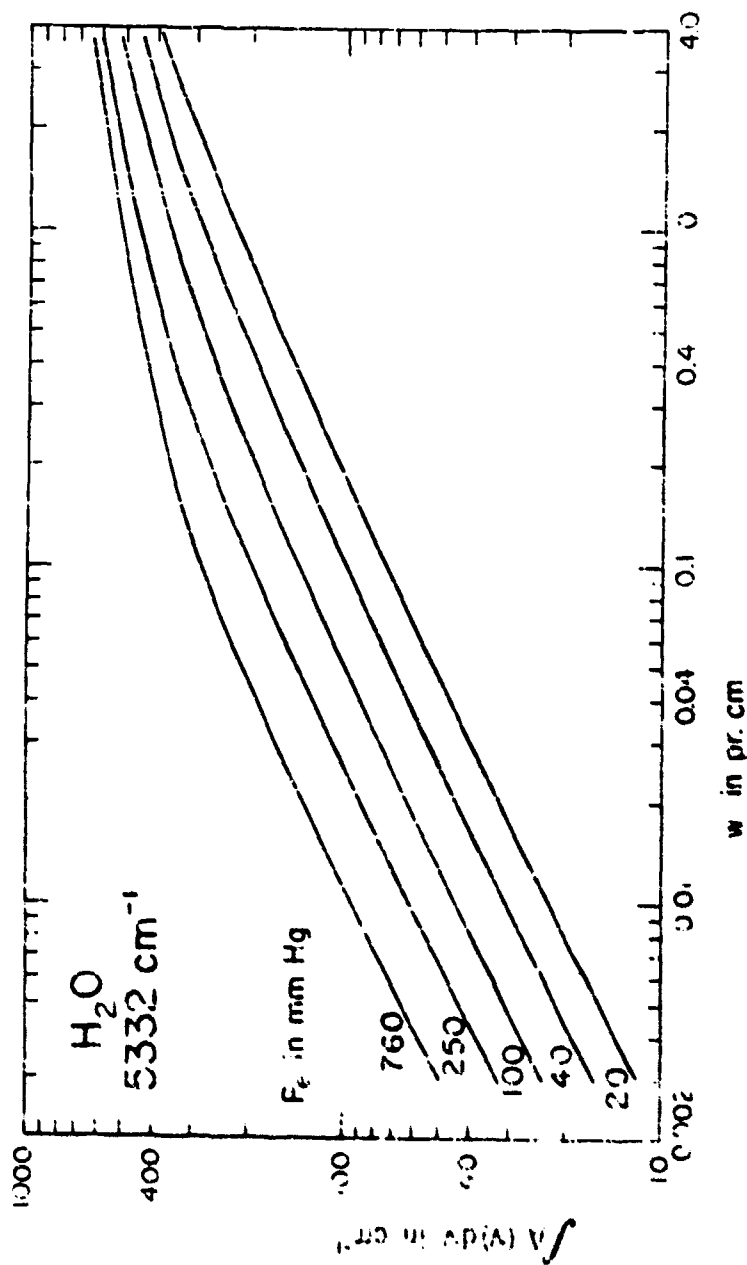


Fig. 19. The total absorption of the $5332 \text{ cm}^{-1} \text{ H}_2\text{O}$ band versus $\bar{\nu}$. The curves are based on RMW data for larger $\bar{\nu}$ and on present data for smaller $\bar{\nu}$.

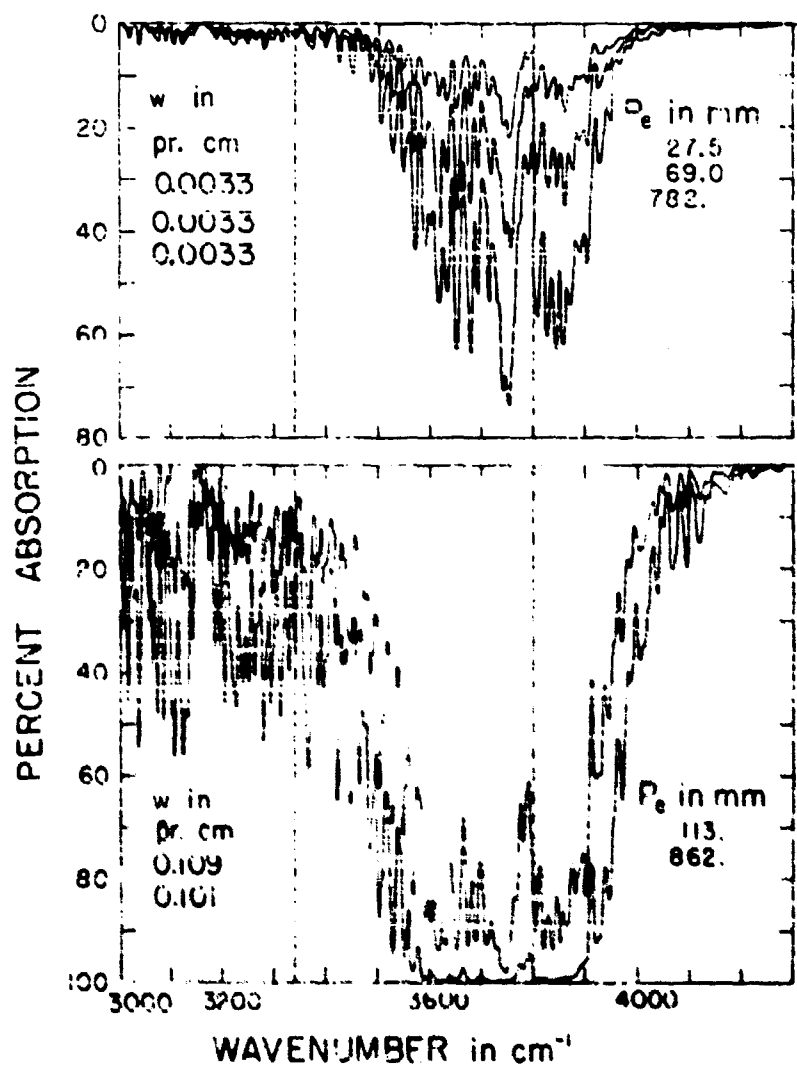


Fig. 1. Representative absorption curves for the 3400 cm^{-1} band. Spectral slit width equals approximately 10 cm^{-1} . The broken vertical lines at 3400 cm^{-1} and 3300 cm^{-1} represent the positions of the peaks in the spectra of pure H_2O and D_2O , respectively.

Table 10. Data for the 3700 cm^{-1} H_2O Band

Sample	Temp., °C	Path length, cm	ρ (H_2O) wt %	P mm Hg	P_0 at Hg	ν cm	$A(\nu)/\nu$ in cm^{-1}	3500- 3540 cm^{-1}	3500- 3530 cm^{-1}	3540- 4500 cm^{-1}
1	20.0	62.5	5.5	5.5	27.5	0.0033	34.7	17.6		52.7
2	20.0	62.5	5.5	11.5	34.0	0.0033	37.7	19.7		57.2
3	20.5	62.5	5.5	21.5	43.5	0.0033	43.5	22.4		64.1
4	21.5	62.5	5.5	37.0	59.0	0.0033	48.1	25.7		76.6
5	22.0	62.5	4.5	128	144	0.0037	64.7	33.0		102
6	22.5	62.5	1.5	348	290	0.0053	93.7	47.7		145
7	23.5	62.5	5.5	750	722	0.0053	108	54.4		155
8	24.0	62.5	11.7	1117	98.5	0.0070	128.1	68.1		181
9	24.5	62.5	12.0	83.5	13.5	0.0071	76.0	39.6		135
10	25.0	62.5	13.5	41.5	87.5	0.0064	79.7	37.7		119
11	25.5	62.5	10.5	126	170	0.0065	119	52		180
12	26.0	62.5	11.5	303	346	0.0067	150	63.2		90
13	26.5	62.5	11.6	761	607	0.0069	172	71.1		164
14	27.0	62.5	11.7	1117	98.5	0.0139	15.0	11.1		142
15	27.5	62.5	12.0	83.5	13.5	0.0140	11.2	10.0		131
16	28.0	62.5	13.5	41.5	87.5	0.0125	10.7	10.1		109
17	28.5	62.5	10.5	126	170	0.0128	13.5	11.6		111
18	29.0	62.5	11.5	303	346	0.0130	21.5	17.8		169
19	29.5	62.5	11.6	761	607	0.0136	24.3	22.5		141
20	30.0	62.5	11.7	1117	98.5	0.0274	22.1	15.0		197
21	30.5	62.5	12.0	83.5	13.5	0.0275	14.4	11.7		120
22	31.0	62.5	10.5	126	170	0.0265	23.0	15.1		226
23	31.5	62.5	13.5	41.5	87.5	0.0251	28.0	18.5		274
24	32.0	62.5	11.5	303	346	0.0262	15.7	11.7		145
25	32.5	62.5	11.6	761	607	0.0270	27.1	13.1		189

Page 1. (Continued)

Sample No.	Temp. °C.	Pole Length, cm.	P ₀ mm Hg	P mm Hg	ΔP/mm Hg	ΔP/Δr cm ⁻¹	ΔP/Δr cm ⁻¹
26	31.0	4675	11.1	11.1	0.000	0.0	33.0
27	31.5	4675	12.0	12.0	0.000	0.0	33.0
28	32.0	4675	13.0	13.0	0.000	0.0	33.0
29	32.5	4675	14.0	14.0	0.000	0.0	33.0
30	33.0	4675	15.0	15.0	0.000	0.0	33.0
31	33.5	4675	16.0	16.0	0.000	0.0	33.0
32	34.0	4675	17.0	17.0	0.000	0.0	33.0
33	34.5	4675	18.0	18.0	0.000	0.0	33.0
34	35.0	4675	19.0	19.0	0.000	0.0	33.0
35	35.5	4675	20.0	20.0	0.000	0.0	33.0
36	36.0	4675	21.0	21.0	0.000	0.0	33.0
37	36.5	4675	22.0	22.0	0.000	0.0	33.0
38	37.0	4675	23.0	23.0	0.000	0.0	33.0
39	37.5	4675	24.0	24.0	0.000	0.0	33.0
40	38.0	4675	25.0	25.0	0.000	0.0	33.0
41	38.5	4675	26.0	26.0	0.000	0.0	33.0
42	39.0	4675	27.0	27.0	0.000	0.0	33.0
43	39.5	4675	28.0	28.0	0.000	0.0	33.0
44	40.0	4675	29.0	29.0	0.000	0.0	33.0

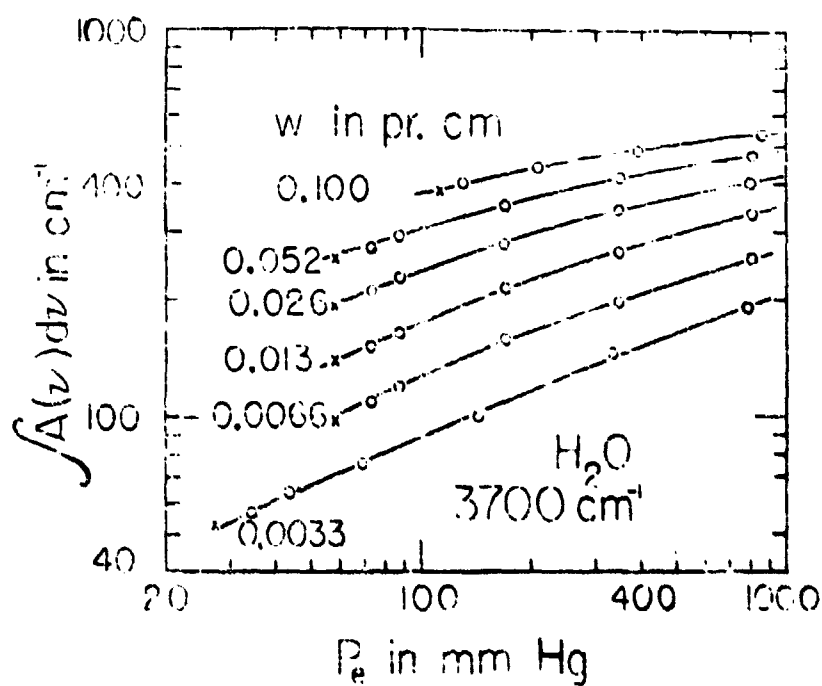


Fig. 21. The total absorption of the 3700 cm⁻¹ H₂O band versus P_e. The X points correspond to samples of H₂O alone, the O points to samples of H₂O and K₂O.

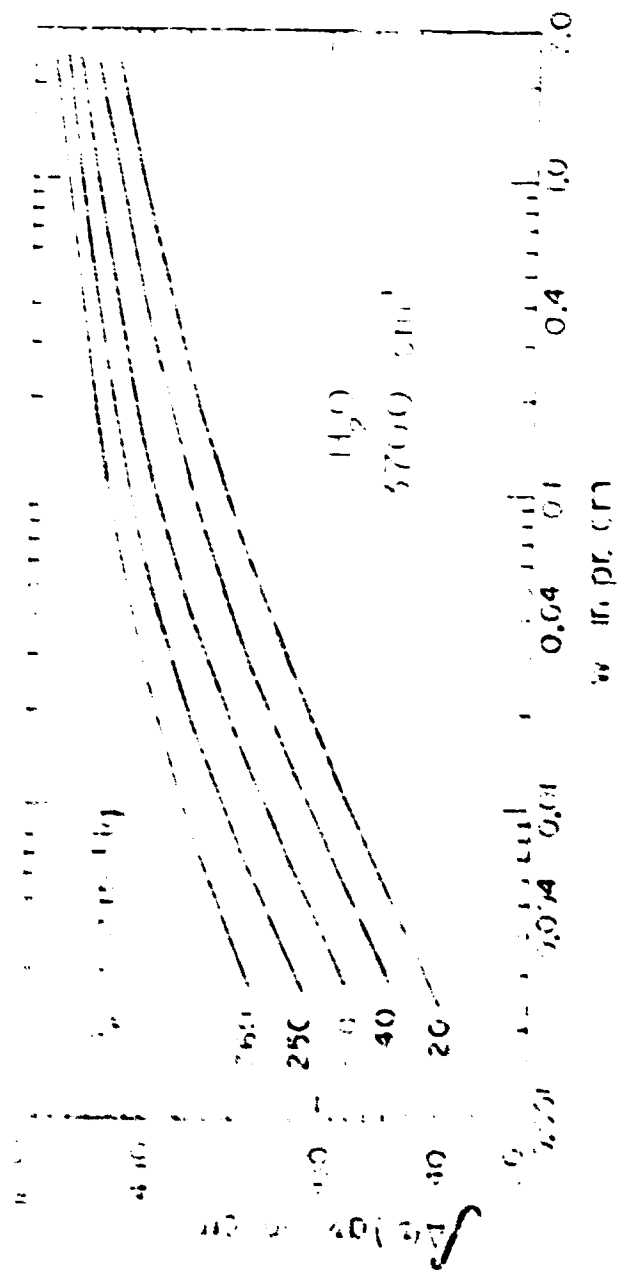


Fig. 1. The total current density of the H_2O and H_2O_2 band versus E . The curves are for H_2O and H_2O_2 for 100% H_2O and 100% H_2O_2 .

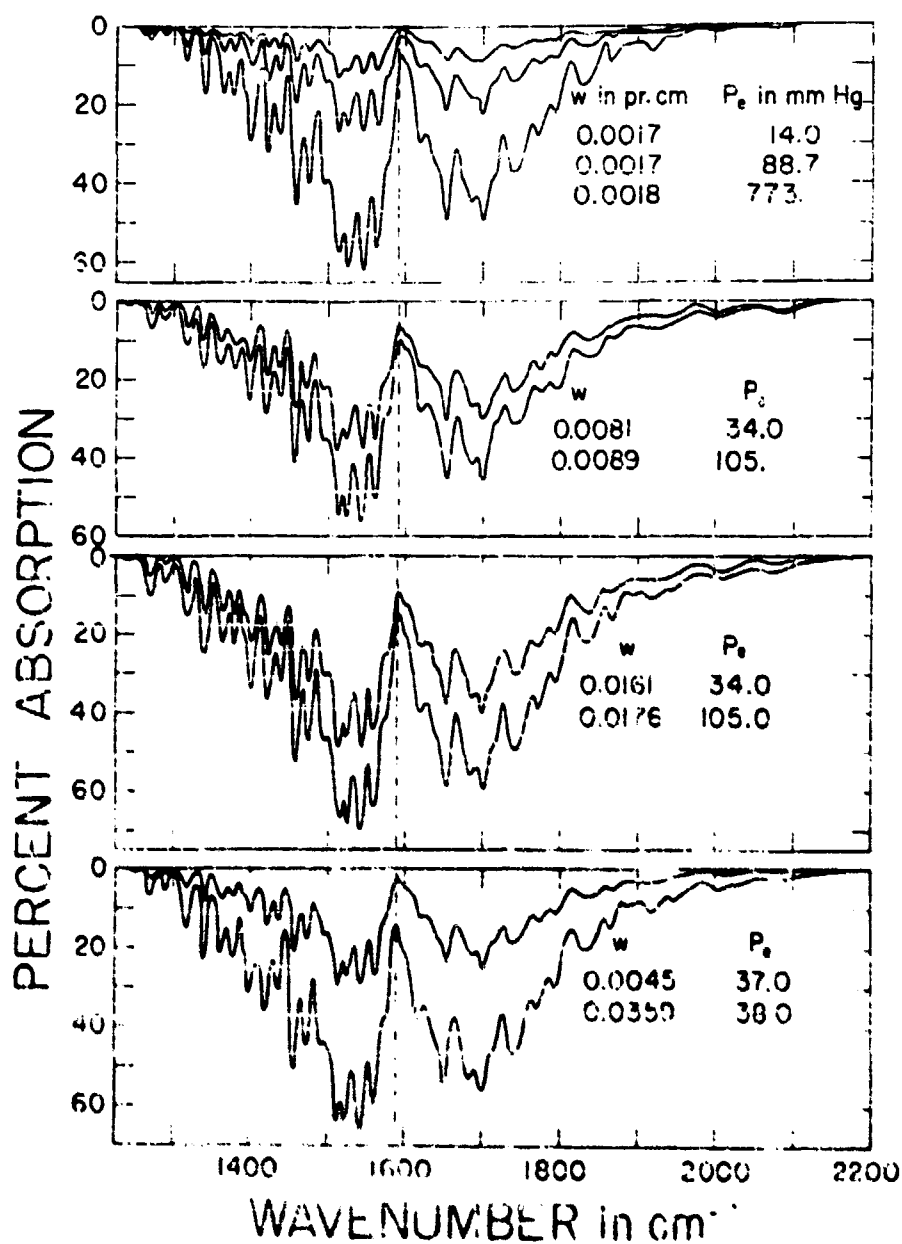


Fig. 23. Successive absorption curves of the 1595 cm^{-1} H_2O band. Spectral slit width equals approximately 1 cm^{-1} .

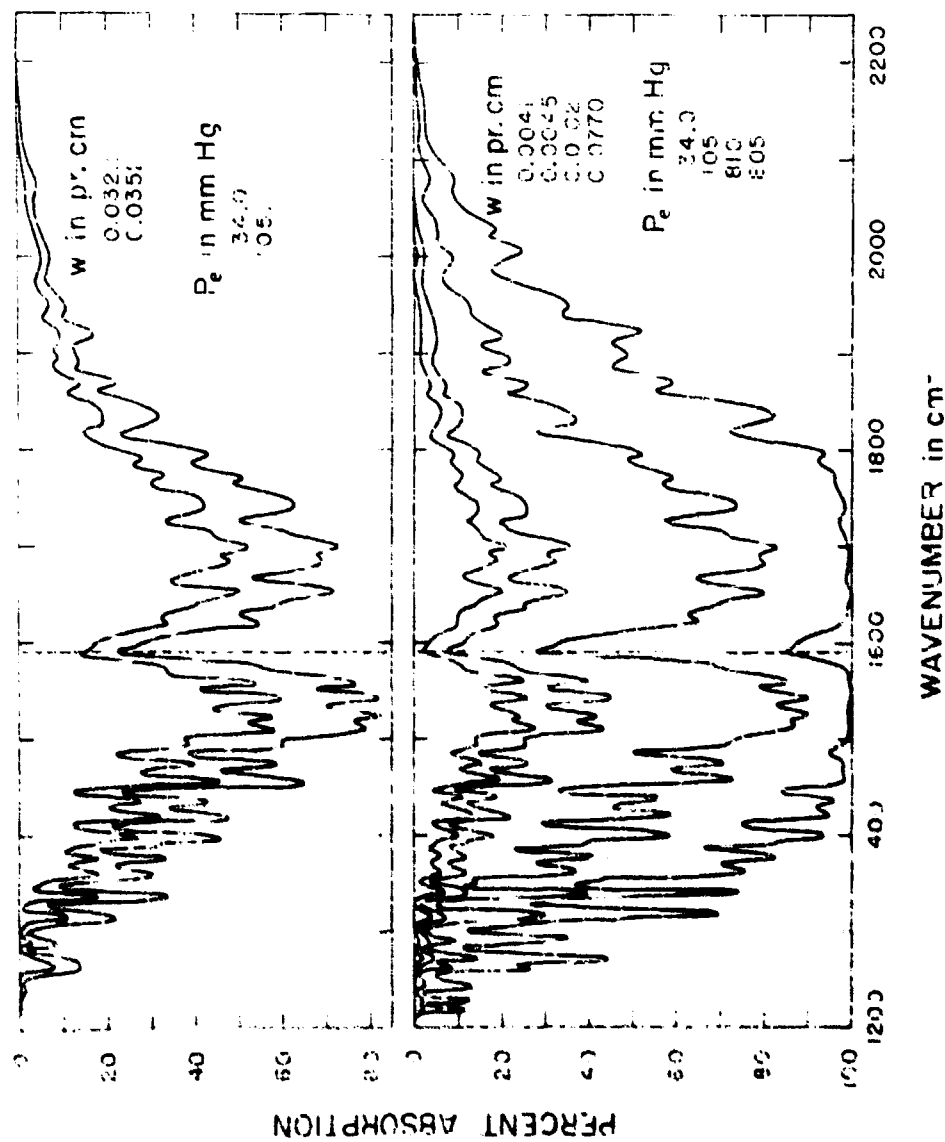


Fig. 2b. Representative absor. for curves of the 165 cm⁻¹ H₂O band. Spectral slit width 0.5 cm⁻¹.

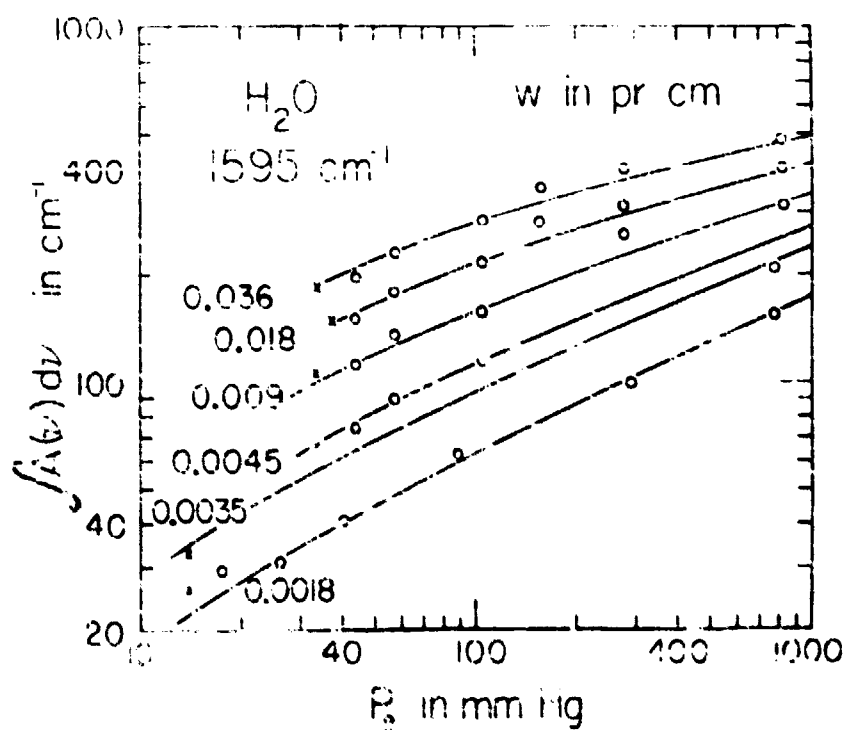


Figure 1. Integral of the first peak of the vapor pressure distribution versus P_g .
 The parameter w corresponds to equation (10) of the text. The circle
 represents the experimental data.

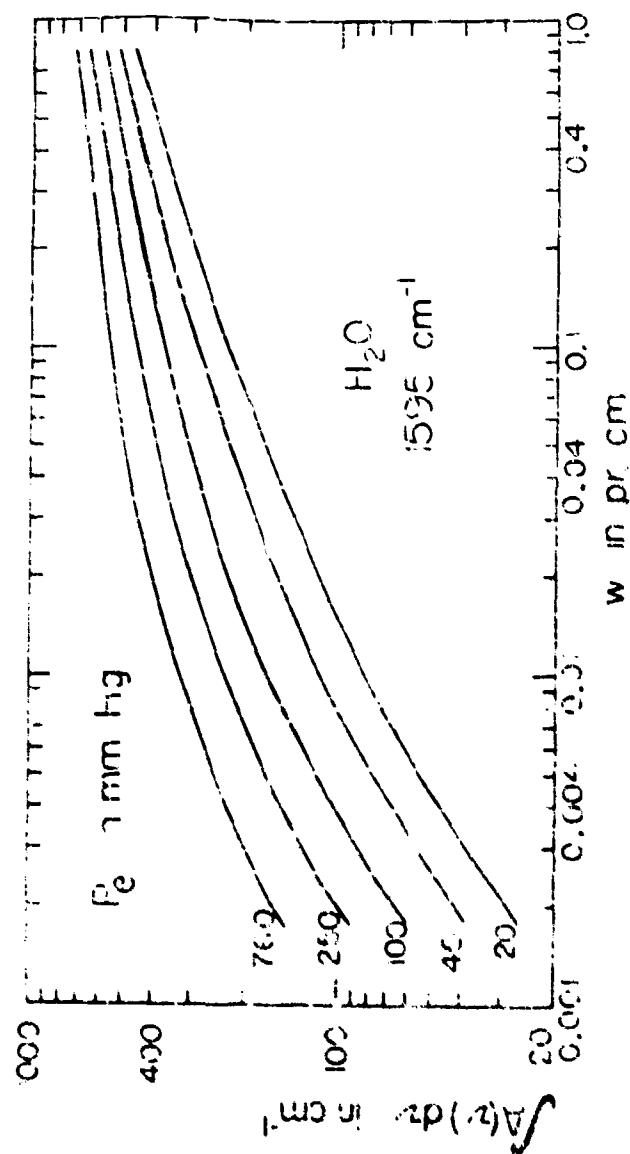


Fig. 10. The total absorption of the 1595 cm^{-1} band versus w . The curves are based on 15 data for 1595 cm^{-1} and on present data for smaller w .

Table I. Data for the 1595 cm^{-1} H_2O Band

Sample	Temp. $^{\circ}\text{C}$	Path Length cm	$p(\text{H}_2\text{O})$ mm Hg	P mm Hg	P_0 mm Hg	V cm	$\frac{A(\nu)_{\text{H}_2\text{O}}}{A(\nu)_{\text{H}_2\text{O}}}$ cm^{-1}	$\frac{A(\nu)_{\text{H}_2\text{O}}}{A(\nu)_{\text{H}_2\text{O}}}$ cm^{-1}
1	23	25	2.30	2.80	14.0	.0017	12.3	12.7
2	24	25	2.50	6.0	17.6	.0018	14.9	14.4
3	27	27	3.20	15.4	26.2	.0019	17.0	16.4
4	26	27	3.20	21.5	40.3	.0019	21.1	22.4
5	24	27	2.80	76.5	88.7	.0017	30.0	30.5
6	25	27	3.05	297.	269.	.0019	50.9	50.9
7	23	25	3.05	704.	713.	.0016	79.4	79.4
8	25	25	2.80	2.80	14.0	.0034	18.2	13.6
9	26	25	3.05	761.	773.	.0036	102.	114.
10	24	25	2.6	6.9	74.0	.0043	30.6	31.3
11	25	27	3.5	13.1	14.1	.0047	38.0	38.2
12	27	27	6.1	25.0	57.4	.0046	45.5	48.8
13	25	27	5.5	75.0	105.	.0045	56.7	59.5
14	24	25	6.6	6.6	34.0	.0031	47.3	53.1
15	25	25	7.8	13.1	44.1	.0092	54.0	59.9
16	27	25	8.1	25.0	57.4	.0095	63.9	69.9
17	25	25	7.5	75.0	105.	.0095	76.6	80.7
18	24	25	6.6	6.6	34.0	.0161	63.7	70.5
19	25	25	7.8	13.1	44.1	.0183	72.1	80.2
20	27	25	8.1	25.0	57.4	.0190	86.6	96.5
21	25	25	7.5	75.0	105.	.0176	100.	117.
22	24	27	6.6	6.6	34.0	.0222	78.9	89.5
23	26	27	7.8	13.1	44.1	.0354	90.4	108.

Table 1. (Continued)

Sample No.	Temp °C	Rurr Length cm	p(H ₂ O)	P		Pe	v	1500-1590		1590-2100		1200-2100
				mm Hg	mm Hg	mm Hg	cm	cm ⁻¹	cm ⁻¹	cm ⁻¹	cm ⁻¹	cm ⁻¹
27	25	.675	8.2	25.0	25.0	57.7	.0378	120	125	125	275	
28	25	.675	7.5	25.0	25.0	55.1	.0352	131	133	133	280	
29	25	.625	7.5	7.5	7.5	57.0	.0045	35.0	38.1	38.1	71.0	
30	25	.625	7.5	7.5	7.5	57.5	.0049	40.1	45.3	45.3	107	
31	26	.645	7.5	7.5	7.5	57.7	.0379	59.1	59.2	59.2	147	
32	26	.675	7.6	7.6	7.6	53.0	.0353	59.0	109	109	202	
33	26.5	.625	16.0	742	742	610	0.0102	133	131	131	390	
34	26.5	.625	16.0	741	741	606	0.0198	190	226	226	516	
35	26.5	.675	16.0	740	740	576	0.0389	280	273	273	493	
36	26.5	.675	16.5	759	759	655	0.0713	286	319	319	575	

SUMMARY

The self-broadening coefficient has been determined for several bands of N_2O , CO , CH_4 , CO_2 , and H_2O ; this coefficient, which is defined in the text, is a measure of the relative broadening ability of the absorbing gas with respect to N_2 . By the use of the experimentally determined self-broadening coefficients it was possible to define an equivalent pressure P_e which served to simplify the analysis of the data by accounting for the broadening by the absorbing gas and by N_2 with the use of a single variable. Values of B used in the analysis of all the bands included in the present research program are summarized in Table 1.

The relative broadening abilities of various inactive gases have been investigated and, where possible, the results have been compared with those of previous workers. The results are shown in Tables 2, 3, and 4.

Absorption curves were obtained from which the total absorption has been determined for the N_2O bands at 2565, 2481, 1285, 1167, 692, and 580 cm^{-1} . The data are listed in Tables 5, 6, and 7, and curves have been drawn to show the functional relationship between total absorption and the two parameters, absorber concentration y and equivalent pressure P_e . Values of the band intensities of part of these bands have been determined and compared in Table 8 with the results reported by other investigators.

Total absorption measurements have also been made for the H_2O bands at 5532, 5700, and 1595 cm^{-1} . The results, which are presented in tabular form and in graphical form with total absorption plotted against y and against P_e , supplement earlier work by Howard, Burch, and Williams¹, and serve as a check against the results of these workers for values of y and P_e included in both. There is good agreement between the earlier results and the present results, which were obtained by improved methods.

REFERENCES

1. Darrell E. Burch and Dudley Williams, Scientific Report 1, Geophysics Research Directorate, Contract No. AF19(604)-2633, Air Research and Development Command, Laurence G. Hanscom Field, Bedford, Massachusetts.
2. Darrell E. Burch, David A. Gryvnak, and Dudley Williams, Scientific Report 2, Geophysics Research Directorate, Contract No. AF19(604)-2633, Air Research and Development Command, Laurence G. Hanscom Field, Bedford, Massachusetts.
3. Edgar B. Singleton, Ph.D. dissertation, The Ohio State University, (1958).
4. Darrell E. Burch, Ph.D. dissertation, The Ohio State University, (1959).
5. J. E. Howard and R. M. Chapman, Engineer Research and Development Laboratories, Contract W44-099-eng-400 with The Ohio State University Research Foundation, Reports 18, 20, 21 (1949); also ERDL-Ohio State Research Foundation, Contract DA-33-099-eng-14, Report No. 1 (1950), and J. Opt. Soc. Am. 42, 423, 856 (1952).
6. J. E. Howard, D. E. Burch, and D. Williams, Geophysical Research Paper No. 40, GRD, Air Force Cambridge Research Laboratories (1955). See also J. Opt. Soc. Am., 46, 186, 237, 242, 334, 432 (1956).
7. R. M. Zoody and T. W. Worrell, Proc. Roy. Soc. A. 209, 178 (1951).
8. P. C. Cross and F. Daniels, J. Chem. Phys. 2, C (1934).
9. D. E. Edwards, J. Opt. Soc. Am. 50, 617 (1960).
10. E. Palmer, J. Opt. Soc. Am. 50, 1222 (1960).
11. K. F. Vasilovsky and R. G. Reporent, Optics and Spectroscopy, Vol. vii, No. 4, 353 (1959).
12. J. Inatt, Ph.D. dissertation, The John Hopkins University, (1960).
13. W. Benedict, (private communication).
14. W. Benesch and T. Elder, Phys. Rev., 91, 308 (1953).
15. A. M. Thorndike, A. J. Wells, and E. B. Wilson, J. Chem. Phys. 15, 157 (1947).
16. D. F. Eggers, Jr., and B. L. Crawford Jr., J. Chem. Phys. 19, 1554 (1951).

APPENDIX I

A VACUUM TANK FOR A PERKIN-ELMER SINGLE-BEAM MONOCHROMATOR

The need for evacuating the optical path of a spectrometer used for investigating strong atmospheric absorption bands was discussed in Report C. Enclosing the Perkin-Elmer Model 21 Double-beam spectrometer in a vacuum tank seemed to be impractical; therefore a vacuum tank was designed and constructed to contain a Perkin-Elmer Model 99 single-beam monochromator which was available in the laboratory. This tank, which is illustrated in Fig. 27, is discussed below.

The tank is featured by its simple and inexpensive construction and by its versatility. The main part of the tank consists of a piece of 22-inch o.d. steel pipe with $3/8$ -inch thick walls, and the end plates are circular pieces of $1/8$ -inch thick steel plate. The monochromator and other components are set on an 18-inch-wide steel plate which is spot-welded inside the tank. A portion of the top of the tank was cut away and the hole covered by a lid of $3/4$ -inch thick plexiglass, which makes it possible to see all the enclosed parts. An endless piece of pure gum rubber cord serves as a gasket between the plexiglass and the steel tank. Rubber channel gaskets provide seals between the cylindrical tank and the flat end plates.

Electrical connections are provided through hermetically sealed porcelain fittings. In order to avoid excessive noise which might arise from a fitting in the circuit between the preamplifier and the amplifier, the cable connecting these two components was put through a hole in the end-plate which could easily be sealed with a putty-like sealing compound. This cable was covered with an air-tight plastic coating; but it was necessary to open the plastic coating and put soft wax around the wires in the cable to prevent leakage through the cable from one end to the other. It should be noted that small leaks can be tolerated since the vacuum pump is left on during operation of the spectrometer.

Mechanical adjustments can be made through one of three "rotating seals" made of a piece of brass stock which was soldered over a hole in the tank and drilled through to accept a piece of $1/8$ -inch drill rod. A circular groove was machined out of the inner surface of the brass piece to hold a small "O" ring to form a seal around the drill rod. These seals were found to be virtually leak proof, and make it possible for adjustments to be made by a rotating motion or by a linear motion by sliding the rod through the "wall". The mechanical connections were used to make minor adjustments of the mirrors, to operate a shutter in front of the entrance slit, to operate a valve on a small absorption cell, to adjust the slits, and to drive the Littrow mirror. The gear box and drive system for the Littrow drive were removed from the



Fig. 20. Drawing of vacuum tank containing a Perlin-Liner Model 3000. The apparatus is described in Appendix I of this report.

and the motor and counter of the monochromator. The external leads were connected to the monochromator through the wall of the vacuum tank. By putting the motor and relay in the outside, it was possible to use a smaller tank, to reduce the size of electrical connections through the tank, and to avoid trouble which might arise from operating the small battery drive motor and the relay in a vacuum.

A small gear-box inside the tank makes it possible to make four separate adjustments with only one dial. A spur gear on the rotating dial can be moved to mesh with any one of four other spur gears which are connected to the various adjusting mechanisms.

The optical diagram above the main portion of Fig. 31 is a convenient arrangement for the use of a shorter absorption cell contained inside the vacuum tank. Gas can be admitted to the cell through a piece of copper tubing which extends through the wall of the tank.

The optical arrangement in the main portion of Fig. 31 is convenient for the use of the 1.5-meter base length, multiple-traversal cell used in obtaining data described previously. The end-plate of the vacuum tank fits against the end-plate of the absorption cell; a 1/2 inch endless gum rubber gasket is held in place between the two end-plates. The end-plate of the vacuum tank is cut away opposite the windows of the absorption cell.

A 3:2 magnified image of the Hertz glow is formed inside the multiple traversal cell. The image size is maintained during the reflections in the cell and then reduced by 2:1 at the entrance slit of the monochromator. The light beam then fills the optics of the monochromator.

No serious difficulties were encountered as a result of operating the monochromator in vacuum. The clapper mechanism apparently needs lubrication more frequently when operated in vacuum, although this was not particularly troublesome. Material tends to sublime from the glow and form thin films on nearby objects; it was therefore necessary either to keep the source several inches from any windows, or to shield these parts from the glow. The two rather minor difficulties described above could probably be avoided by evacuating the tank with the instruments off, and then filling it with N_2 before operating the instrument.

<p>Geophysics Research Directorate Air Force Cambridge Research Laboratories L. G. Hanscom Field, Bedford, Mass. INFRARED ABSORPTION BY MINOR ATMOSPHERIC CONSTITUENTS by Lawrence W. Burch and Dorothy Williams et al. July 1962. 316 pages. illus. AFOSR-62-068.</p> <p>This report presents results of studies concerned with the absorption of infrared radiation by various atmospheric gases. It places particular stress upon previously published instructor reports on (1) absorption by nitrous oxide, carbon monoxide and methane; (2) absorption by carbon dioxide; and (3) absorption by water vapor and nitric oxide.</p>	<p>UNCLASSIFIED</p> <p>1. Infrared Radiation 2. Infrared Research 3. Absorption</p> <p>I. Burch, Dorothy W. II. Francis, Walter L. III. Cevinski, Jay L. IV. Singer, William B. V. Williams, Dorothy</p>	<p>Geophysics Research Directorate Air Force Cambridge Research Laboratories L. G. Hanscom Field, Bedford, Mass. INFRARED ABSORPTION BY MINOR ATMOSPHERIC CONSTITUENTS by Dorothy Williams et al. July 1962. 316 pages. illus. AFOSR-62-068.</p> <p>This report presents results of studies concerned with the absorption of infrared radiation by various atmospheric gases. It places particular stress upon previously published instructor reports on (1) absorption by nitrous oxide, carbon monoxide and methane; (2) absorption by carbon dioxide; and (3) absorption by water vapor and nitric oxide.</p>	<p>UNCLASSIFIED</p> <p>1. Infrared Radiation 2. Infrared Research 3. Absorption</p> <p>I. Burch, Dorothy W. II. Francis, Walter L. III. Cevinski, Jay L. IV. Singer, William B. V. Williams, Dorothy</p>
<p>Geophysics Research Directorate Air Force Cambridge Research Laboratories L. G. Hanscom Field, Bedford, Mass. INFRARED ABSORPTION BY MINOR ATMOSPHERIC CONSTITUENTS by Lawrence W. Burch and Dorothy Williams et al. July 1962. 316 pages. illus. AFOSR-62-068.</p> <p>This report presents results of studies concerned with the absorption of infrared radiation by various atmospheric gases. It places particular stress upon previously published instructor reports on (1) absorption by nitrous oxide, carbon monoxide and methane; (2) absorption by carbon dioxide; and (3) absorption by water vapor and nitric oxide.</p>	<p>UNCLASSIFIED</p> <p>1. Infrared Radiation 2. Infrared Research 3. Absorption</p> <p>I. Burch, Dorothy W. II. Francis, Walter L. III. Cevinski, Jay L. IV. Singer, William B. V. Williams, Dorothy</p>	<p>Geophysics Research Directorate Air Force Cambridge Research Laboratories L. G. Hanscom Field, Bedford, Mass. INFRARED ABSORPTION BY MINOR ATMOSPHERIC CONSTITUENTS by Dorothy Williams et al. July 1962. 316 pages. illus. AFOSR-62-068.</p> <p>This report presents results of studies concerned with the absorption of infrared radiation by various atmospheric gases. It places particular stress upon previously published instructor reports on (1) absorption by nitrous oxide, carbon monoxide and methane; (2) absorption by carbon dioxide; and (3) absorption by water vapor and nitric oxide.</p>	<p>UNCLASSIFIED</p> <p>1. Infrared Radiation 2. Infrared Research 3. Absorption</p> <p>I. Burch, Dorothy W. II. Francis, Walter L. III. Cevinski, Jay L. IV. Singer, William B. V. Williams, Dorothy</p>